

Electronic Thesis and Dissertation Repository

12-8-2014 12:00 AM

Thylakoid Phosphorylation And Cell Morphology In The Antarctic Psychrophile, *Chlamydomonas* sp. UWO241

Beth Szyszka-Mroz
The University of Western Ontario

Supervisor
Dr. Norman Huner
The University of Western Ontario

Graduate Program in Biology

A thesis submitted in partial fulfillment of the requirements for the degree in Doctor of Philosophy

© Beth Szyszka-Mroz 2014

Follow this and additional works at: <https://ir.lib.uwo.ca/etd>



Part of the [Plant Biology Commons](#)

Recommended Citation

Szyszka-Mroz, Beth, "Thylakoid Phosphorylation And Cell Morphology In The Antarctic Psychrophile, *Chlamydomonas* sp. UWO241" (2014). *Electronic Thesis and Dissertation Repository*. 2598.

<https://ir.lib.uwo.ca/etd/2598>

This Dissertation/Thesis is brought to you for free and open access by Scholarship@Western. It has been accepted for inclusion in Electronic Thesis and Dissertation Repository by an authorized administrator of Scholarship@Western. For more information, please contact wlsadmin@uwo.ca.

THYLAKOID MEMBRANE PHOSPHORYLATION AND CELL MORPHOLOGY IN
THE ANTARCTIC PSYCHROPHILE, *CHLAMYDOMONAS SP.* UWO241

(Thesis format: Integrated Article)

by

Beth Szyszka-Mróz

Graduate Program in Biology

A thesis submitted in partial fulfillment
of the requirements for the degree of
Doctor of Philosophy

The School of Graduate and Postdoctoral Studies
The University of Western Ontario
London, Ontario, Canada

© Beth Szyszka-Mróz 2014

Abstract

The unicellular green microalga, *Chlamydomonas sp.* UWO 241, was isolated from perennially, ice-covered Lake Bonney, Antarctica where it has adapted to constant low temperatures and high salinity. A unique characteristic of this algal strain is its inability to undergo state transitions combined with an altered thylakoid protein phosphorylation profile, which suggests the absence of LHCII phosphorylation, and preferential phosphorylation of a set of novel proteins. Examination of the unique phosphoproteins revealed that they are associated with a large pigment-protein supercomplex, which contains components of both photosystem I and the cytochrome *b₆/f* complex and likely functions in cyclic electron flow (CEF). The stability of this photosystem I supercomplex was dependent upon the phosphorylation state of the thylakoid membrane, and the concentration of NaCl. Separation of individual subunits of the supercomplex led to the identification of 2 major phosphorylated proteins, a 17 kDa PsbP-like protein and a 70 kDa ATP-dependent zinc metalloprotease FtsH, which likely play a role in the dynamic switch between linear and cyclic electron flow.

The absence of phosphorylation of light harvesting complex II proteins, associated with state transitions, was also investigated in UWO241. Although it was demonstrated that the Stt7 kinase involved in state transitions is present in the Antarctic psychrophile, minimal phosphorylation of minor LHCII polypeptides occurred due to the absence of phosphorylation sites of Lhcb4 and Lhcb5, believed to play key roles during the transition from state I to state II. Therefore, it appears that UWO241 favours phosphorylation of a PSI-Cyt *b₆/f* supercomplex to regulate PSI CEF rather than regulation of state transitions through the phosphorylation of LHCII proteins.

UWO241 exists either as flagellated, single cells, or as non-motile, multicellular “palmelloids”. Interestingly, growth temperature had a profound effect on cell morphology. UWO241 cultures grown at 11°C exhibited nearly homogenous populations of single cells, while growth at 16°C induced a high ratio of palmelloids to single cells. Thus, a cell filtration technique was established to separate these morphological structures. Compared to single cells, palmelloids exhibited reduced non-photochemical quenching (Φ_{NPQ}) concomitant with greater non-regulated dissipation (Φ_{NO}), a decrease in the abundance of LHCII proteins, with a 2-fold reduction in chlorophyll a/b ratios and carotenoid pools which were 27% lower. Therefore, single cells and palmelloids of UWO241 exhibit structural and functional differences in photosynthetic activity.

Keywords

Cold-adaptation, psychrophile, *Chlamydomonas*, protein phosphorylation, PSI-cytochrome b6/f supercomplex, PsbP-like protein, cyclic electron flow, state transitions, palmelloids

Co-Authorship Statement

Chapter 1: B Szyszka, AG Ivanov, NPA Hüner. Adaptation to low temperature in a photoautotrophic antarctic psychrophile, *Chlamydomonas sp.* UWO241. (Accepted book review chapter)

AG Ivanov – provided critical comments on final manuscript

NPA Hüner – principal investigator, provided suggestions for experimental design and critical comments on final manuscript

Chapter 2: B Szyszka, P Pittock, AG Ivanov, G Lajoie, NPA Hüner. The Antarctic psychrophile, *Chlamydomonas sp.* UWO 241, preferentially phosphorylates a PSI-cytochrome *b₆/f* supercomplex. (Plant Physiology, in revision)

P Pittock and G Lajoie – protein sequencing and analysis, provided critical comments on final manuscript

AG Ivanov – P700 measurements, provided critical comments on final manuscript

NPA Hüner – principal investigator, provided suggestions for experimental design and critical comments on final manuscript

Chapter 3: B Szyszka, M Possmayer, DP Maxwell, NPA Hüner. The psychrophilic state transition variant, *Chlamydomonas sp.* UWO241, exhibits reduced phosphorylation of LHCII subunits and the PSII core complex. (Submitted to Plant Cell)

M Possmayer – creation of the UWO241 cDNA library, assistance with LHCII sequence analyses, assistance with radioactive labeling experiments

DP Maxwell – provided critical comments on final manuscript

NPA Hüner – principal investigator, provided suggestions for experimental design and critical comments on final manuscript

Chapter 4: B Szyszka, A Ivanov, C Trick, NPA Hüner. Palmelloid colonies are photosynthetically distinct from single motile cells in the Antarctic psychrophile, *Chlamydomonas sp.* UWO 241. (Submitted to Journal of Phycology)

A Ivanov – HPLC pigment analysis

C Trick – provided critical comments on final manuscript

NPA Hüner – principal investigator, provided suggestions for experimental design and critical comments on final manuscript

Acknowledgments

Completing my PhD would not have been possible without the support and guidance that I received during my studies, and so I wish to acknowledge the following individuals:

First and foremost, I would like to thank my supervisor and mentor, Dr. Norm Hüner. Norm welcomed me into his lab many years ago to do an undergraduate project, followed by my Master's. His enthusiasm and love for research was contagious, and became the reason I decided to pursue graduate studies. I am grateful for the guidance, support, wisdom and time that he has contributed throughout the years. It has been a pleasure and an honour to be one of Norm's students.

The members of my advisory committee, Dr. Alex Ivanov, Dr. Maxwell and Dr. Charlie Trick, for their time, suggestions and encouragement. Dr. Alex Ivanov and Dr. Marianna Król, for their expertise, technical knowledge and assistance. Alex has been of great help with fluorescence and HPLC measurements. Paula Pittock and Dr. Gilles Lajoie, for their technical assistance in protein sequencing and analysis. The members of the Hüner and Maxwell labs, especially Marc Possmayer for his contribution in creating the UWO241 cDNA library, and Lauren Hollis for her help with experimental techniques. My gratitude is also extended to my colleagues of the 4th floor of NCB, who were not only a source of great advice, but also support and friendships.

And a heartfelt, special thanks to my parents, for their endless love and support throughout my life and experience as a graduate student. For teaching me about hard work and perseverance. I cannot thank them enough for giving me the opportunity and the courage to embark on this journey.

Last, but certainly not least, I would like to thank my wonderful husband, for his friendship, patience and humour throughout the years. And to our son, for being the twinkle in my eye and putting a smile on my face during challenging times. Thank you.

I also gratefully acknowledge the funding I received during my graduate studies, from both NSERC and WGRS.

Table of Contents

Abstract.....	ii
Co-Authorship Statement.....	iv
Acknowledgments.....	v
Table of Contents.....	vi
List of Tables.....	xi
List of Figures.....	xii
List of Appendices.....	xv
List of Abbreviations.....	xvi
Chapter 1.....	1
1 General Introduction.....	1
1.1 Ultrastructure and cell morphology.....	2
1.2 Membrane fatty acid composition.....	3
1.3 Cold-adapted enzymes.....	3
1.4 Energy metabolism.....	4
1.5 Photosynthesis at low temperatures.....	5
1.6 Acclimation to light and low temperature.....	8
1.7 <i>Chlamydomonas sp.</i> UWO241.....	10
1.8 Natural habitat of UWO241.....	11
1.9 Growth of UWO241.....	12
1.9.1 Temperature.....	12
1.9.2 Salt.....	12
1.10 Adaptation of UWO241 to low temperature.....	13
1.11 Photosynthetic electron transport.....	14
1.11.1 Structure of PETC.....	14

1.11.2	Function of PETC	15
1.11.3	Acclimation to temperature and irradiance.....	17
1.11.4	Acclimation to light quality	18
1.11.5	State transitions.....	19
1.11.6	Thylakoid polypeptide phosphorylation profile.....	20
1.12	Objective of the thesis.....	20
1.13	References	21
Chapter 2.....		29
2	The Antarctic psychrophile, <i>Chlamydomonas sp.</i> UWO 241, preferentially phosphorylates a PSI-cytochrome <i>b₆/f</i> supercomplex.....	29
2.1	Introduction.....	29
2.2	Materials and methods	33
2.2.1	Growth conditions.....	33
2.2.2	Blue native PAGE.....	33
2.2.3	SDS-PAGE and immunoblotting.....	34
2.2.4	Sucrose density gradient centrifugation.....	35
2.2.5	Isoelectrofocusing.....	35
2.2.6	Low temperature (77K) fluorescence	36
2.2.7	Measurements of P700 photooxidation	36
2.2.8	Sample preparation for nano-LC-ESI-MS/MS	37
2.2.9	Liquid chromatography nano-tandem mass spectrometry (nano-LC-ESI-MS/MS) analysis.....	37
2.3	Results.....	38
2.3.1	2D-Blue native gel electrophoresis of thylakoid protein complexes	38
2.3.2	Fractionation and purification of thylakoid membrane complexes	43
2.3.3	Stability of the putative PSI ‘supercomplex’	51
2.3.4	Identification of the phosphoproteins of the putative PSI supercomplex .	53

2.3.5	P700-dependent cyclic electron transport.....	58
2.4	Discussion.....	62
2.5	Conclusion.....	68
2.6	References.....	68
2.7	Appendices.....	76
Chapter 3	84
3	Specific Lhcb4 and Lhcb5 phosphorylation sites are absent in the psychrophilic state transition variant, <i>Chlamydomonas sp.</i> UWO241.....	84
3.1	Introduction.....	84
3.2	Materials and methods.....	87
3.2.1	Growth conditions.....	87
3.2.2	Isolation of purified LHCII complexes.....	88
3.2.3	Low temperature (77K) fluorescence.....	88
3.2.4	SDS-PAGE and immunoblotting.....	89
3.2.5	Column chromatography.....	89
3.2.6	Isoelectric focusing.....	90
3.2.7	³³ P labelling.....	90
3.2.8	cDNA library construction.....	91
3.2.9	Cloning of minor LHCII in UWO241.....	92
3.3	Results.....	93
3.3.1	LHCII complexes.....	93
3.3.2	Affinity purification of LHCII phosphorylated polypeptides.....	98
3.3.3	IEF detection of phosphorylated LHCII.....	100
3.3.4	STT7 kinase.....	103
3.3.5	Radioactive ³³ P labelling.....	103
3.3.6	Sequence of monomeric Lhcb4 and Lhcb5.....	108

3.4 Discussion.....	111
3.5 Conclusion	115
3.6 References.....	115
3.7 Appendices.....	120
Chapter 4.....	122
4 Palmelloid colonies are photosynthetically distinct from single motile cells of the Antarctic psychrophile, <i>Chlamydomonas sp.</i> UWO 241	122
4.1 Introduction.....	122
4.2 Materials and methods	125
4.2.1 Growth conditions.....	125
4.2.2 Cell filtration.....	125
4.2.3 Flow cytometry	126
4.2.4 Low temperature (77 K) chlorophyll fluorescence.....	126
4.2.5 Room temperature chlorophyll fluorescence induction.....	127
4.2.6 Pigment analysis and epoxidation states.....	128
4.2.7 SDS-PAGE and immunoblotting.....	128
4.3 Results.....	129
4.3.1 Growth temperature and cell morphology	129
4.3.2 Cell isolation and flow cytometry.....	133
4.3.3 77K fluorescence	136
4.3.4 Chlorophyll a fluorescence induction	138
4.3.5 Pigment composition	141
4.3.6 SDS-PAGE and immunoblotting.....	145
4.4 Discussion.....	145
4.5 Conclusion	148
4.6 References.....	148

4.7 Appendices.....	152
Chapter 5.....	155
5 General discussion and future perspectives	155
5.1 Major contributions.....	155
5.1.1 Phosphoproteins of <i>Chlamydomonas sp.</i> UWO241	155
5.1.2 Reduced PSII phosphorylation in <i>Chlamydomonas sp.</i> UWO241	155
5.1.3 Phosphorylation profile reflects altered function in <i>Chlamydomonas sp.</i> UWO241	156
5.1.4 A model of cyclic electron flow in <i>Chlamydomonas sp.</i> UWO241	156
5.2 Future directions	161
5.3 Conclusions.....	162
5.4 References.....	163
Curriculum Vitae	166

List of Tables

Table 2.1: Chlorophyll <i>a</i> to <i>b</i> ratios (\pm SE) of purified thylakoid membrane complexes	46
Table 2.2: Effects of antimycin A on the far red light induced steady state oxidation of P700 (Δ A820/A820) and half times for P700+ reduction.....	60
Table 2.3: The effects of DCMU on the level of P700 photooxidation under white actinic light excitation	62
Table 3.1: Chlorophyll <i>a/b</i> ratios of purified LHCII complexes from <i>C. reinhardtii</i> 1690, <i>C. raudensis</i> 49.72 and <i>C. sp.</i> UWO241 and 77K fluorescence emission maxima.	96
Table 4.1: Energy partitioning parameters for each cell fraction from Chl fluorescence induction traces.	140

List of Figures

Figure 1.1: Thylakoid membrane components involved in the Z-scheme of linear electron transport.....	7
Figure 1.2: A hypothetical model for state transitions from state I to state II.	9
Figure 1.3: The post-illumination chlorophyll fluorescence transient of the mesophilic SAG 49.72 and psychrophilic UWO 241 <i>Chlamydomonas</i> strains.	17
Figure 2.1: Phosphorylation profile of UWO 241 and SAG 49.72 thylakoid membrane proteins.....	40
Figure 2.2: Blue-native PAGE of thylakoid membrane complexes and subsequent identification of SDS-solubilized complex subunits.....	41
Figure 2.3: BN-PAGE and subsequent analysis of SDS-solubilized complexes from SAG 49.72 and UWO 241.	43
Figure 2.4: Fractionation of major thylakoid membrane complexes of SAG 49.72, UWO 241 and <i>C. reinhardtii</i> 1690.....	45
Figure 2.5: Immunoblot analysis of purified complexes from <i>C. raudensis</i> SAG 49.72, UWO 241 and <i>C. reinhardtii</i> 1690.....	48
Figure 2.6: BN-PAGE of thylakoid membrane complexes and second dimension analysis of the supercomplex fraction from UWO 241.	51
Figure 2.7: Effect of inhibitors of thylakoid protein phosphorylation on the stability of the putative PSI-supercomplex in UWO241..	53
Figure 2.8: Effects of growth salt concentration on phosphorylation.....	55
Figure 2.9: 2D IEF/SDS-PAGE purification of phosphorylated polypeptides from the supercomplex of UWO 241.	56

Figure 2.10: Alignment of the PsbP-like protein from the supercomplex of UWO 241 from spots 1 and 2 with the amino acid sequences of homologous authentic PsbP proteins from three other organisms.....	58
Figure 3.1: 77K chlorophyll fluorescence emission spectra of purified LHCII complexes from <i>C. reinhardtii</i> 1690, <i>C. raudensis</i> 49.72 and <i>C. sp.</i> UWO241 and absorption spectra (B).....	95
Figure 3.2: Purified LHCII complex proteins of <i>C. reinhardtii</i> 1690, <i>C. raudensis</i> 49.72 and <i>C. sp.</i> UWO241 resolved with SDS-PAGE and stained with Coomassie blue	98
Figure 3.3: Affinity purification of LHCII phosphoproteins in <i>C. reinhardtii</i> compared to <i>Chlamydomonas sp.</i> UWO241.....	100
Figure 3.4: Two-dimensional (IEF/SDS-PAGE) separation of purified LHCII in <i>C. reinhardtii</i> treated with inhibitors (NaF and staurosporine) and λ -phosphatase (-/+)	102
Figure 3.5: Two-dimensional (IEF/SDS-PAGE) separation of purified LHCII in <i>Chlamydomonas sp.</i> UWO241.....	103
Figure 3.6: Immunoblot analysis of <i>C. reinhardtii</i> 1690, <i>C. raudensis</i> 49.72 and <i>C. sp.</i> UWO241 thylakoid membranes probed with antibodies specific for the Stt7 kinase.	105
Figure 3.7: Autoradiograph of [γ - ³³ P]ATP-labelled thylakoid proteins in <i>C. reinhardtii</i> 1690 and <i>C. sp.</i> UWO241 following 15 and 30 minutes of light exposure.....	106
Figure 3.8: In vitro [γ - ³³ P]ATP labelling of LHCII proteins in <i>C. reinhardtii</i> and <i>C. sp.</i> UWO241 after 15 minutes of exposure to light (L) were compared to those following 15 minutes of darkness (D) at 8°C and 23°C in both <i>C. reinhardtii</i> and <i>C. sp.</i> UWO241	108
Figure 3.9: Alignment of the monomeric Lhcb4 protein of <i>Chlamydomonas sp.</i> UWO241 with that of <i>Chlamydomonas incerta</i> and the model species, <i>Chlamydomonas reinhardtii</i>	110
Figure 3.10: Alignment of the monomeric Lhcb5 protein of <i>Chlamydomonas sp.</i> UWO241 with that of <i>Chlamydomonas reinhardtii</i> and <i>Volvox carteri</i>	111

Figure 4.1: Light microscope images of <i>Chlamydomonas</i> sp. UWO241 cultures at 100x and 1000x magnification.	131
Figure 4.2: Light microscope images of UWO 241 and SAG 49.72 cells grown under various steady-state temperatures, demonstrating the effects of growth temperature on cell morphology.....	133
Figure 4.3: Membrane filtration procedure carried out for the separation of different sized cell units.....	135
Figure 4.4: Analysis of isolated subpopulations of UWO241 cells using flow cytometry...	136
Figure 4.5: Low temperature (77K) chlorophyll fluorescence emission spectra of UWO241 control cells, LT 5µm cell fraction and 8 µm cell fraction.....	138
Figure 4.6: Chlorophyll fluorescence light response traces of UWO 241 control cells and separated cell fractions: <5 µm and 8-11 µm.....	141
Figure 4.7: Parameters calculated from chlorophyll fluorescence light response traces of UWO 241 control cells and separated cell fractions, measured at increasing actinic light (AL) intensities of 50, 100, 200, 400 and 1000 µmol photons m ⁻² s ⁻¹	143
Figure 4.8: Composition of photosynthetic pigments in control and separated cell fractions based on size	144
Figure 4.9: Coomassie stained SDS-PAGE analysis of thylakoid membrane proteins from control and different-sized cell fractions of UWO 241.	145
Figure 5.1: A model of PSII phosphorylation in <i>C. reinhardtii</i> and <i>C. sp.</i> UWO241.....	156
Figure 5.2: A hypothetical model of linear electron flow and the PSI-Cyt b6/f supercomplex involved in cyclic electron flow in the psychrophilic <i>Chlamydomonas</i> sp. UWO 241.....	160

List of Appendices

Appendix 2S1: Absorption spectra and 77K fluorescence emission analysis of isolated complexes.....	76
Appendix 2S2: Identification of photosystem II phosphoproteins in UWO242.....	77
Appendix 2S3: Heme staining of purified thylakoid membrane complexes of UWO 241....	78
Appendix 2S4: BLAST results for the protein sequence of spots 1 and 2 from a PSI supercomplex of <i>Chlamydomonas sp.</i> UWO 241.....	79
Appendix 2S5: PEAKS results for spot 3 from a PSI supercomplex of <i>Chlamydomonas sp.</i> UWO 241.....	80
Appendix 2S6: PEAKS results for spot 4 from a PSI supercomplex of <i>Chlamydomonas sp.</i> UWO 241.....	81
Appendix 2S7: PEAKS results for a PSI supercomplex of <i>Chlamydomonas sp.</i> UWO 241..	82
Appendix 3S1: Two-dimensional (IEF/SDS-PAGE) separation of purified LHCII in <i>C. reinhardtii</i>	120
Appendix 3S2: Two-dimensional (IEF/SDS-PAGE) separation of purified LHCII in <i>Chlamydomonas sp.</i> UWO241 using narrow pH ranges (pH 4-6, pH 3-5).....	121
Appendix 4S1: Analysis of <i>Chlamydomonas raudensis</i> SAG 49.72 and <i>Chlamydomonas sp.</i> UWO241 cell cultures grown at various temperatures using flow cytometry.....	152
Appendix 4S2: Light microscope images of <i>Chlamydomonas reinhardtii</i> (1690) grown at 12°C and 28°C.....	153
Appendix 4S3: Typical chlorophyll fluorescence emission spectra of UWO 241 control cells and separated cell fractions based on size.....	154

List of Abbreviations

AA	antimycin A
ADP	adenosine diphosphate
ATP	adenosine 5'-triphosphate
BLAST	basic local alignment search tool
CEF	cyclic electron flow
Chl	chlorophyll
CP43	chlorophyll binding protein of PSII
Cyt b_6	cytochrome b_6 of the cytochrome b_6f complex
Cyt f	cytochrome f of the cytochrome b_6f complex
D1/D2	reaction center proteins of PSII
DCMU	3-(3,4-dichlorophenyl)-1,1-dimethylurea
β -DDM	β -dodecyl maltoside
ETR	electron transport rate
Fd	ferredoxin
FeS	a Rieske iron-sulphur protein of the cytochrome b_6f complex
Fm	maximal fluorescence of dark adapted cells
Fm'	maximal fluorescence during actinic light illumination
Fo	minimal fluorescence of dark adapted cells
Fo'	minimal fluorescence during actinic light illumination
Fs	steady state fluorescence

FtSH	filamentous temperature sensitive H
Fv/Fm	maximum PSII photochemical efficiency in the dark adapted state
IEF	isoelectric focusing
LC-ESI-MS	liquid chromatography-electrospray ionization-tandem mass spectrometry
LEF	linear electron flow
LHC	light harvesting complex
Lhca	PSI light harvesting complex
Lhcb	PSII light harvesting complex
NADP ⁺	nicotinamide adenine dinucleotide phosphate (oxidized form)
NADPH	nicotinamide adenine dinucleotide phosphate (reduced form)
NPQ	non-photochemical quenching
OEC	oxygen evolving complex
PCR	polymerase chain reaction
PETC	photosynthetic electron transport chain
PSI	photosystem I
PSII	photosystem II
P680	reaction center Chl a of of PSII (reduced form)
P680 ⁺	reaction center Chl a of of PSII (oxidized form)
P700	reaction center Chl a of PSI (reduced form)
P700 ⁺	reaction center Chl a of PSI (oxidized form)

PAGE	polyacrylamide gel electrophoresis
PQ	plastoquinone (oxidized form)
PQH ₂	plastoquinone (reduced form)
PsaA/B	reaction center proteins of PSI
qP	relative redox state of the primary electron acceptor quinone of PSII
Rubisco	ribulose 1,5-bisphosphate carboxylase/oxygenase
SC	supercomplex
SDS	sodium dodecyl sulphate

Chapter 1

1 General Introduction

The majority of the Earth's biosphere is characterized by cold ecosystems, which for the most part, remain largely unexplored. These permanently cold environments consist of polar and alpine habitats, as well as the ocean depths, where 90% of the volume is below 5°C (Feller and Gerday 2003). In addition, constant low temperatures of these habitats are frequently accompanied by additional abiotic stresses, including desiccation, osmotic stress, as well as immense fluctuations in salinity, irradiance, photoperiod and nutrient availability (Eicken 1992). Consequently, while plants and animals exhibit a rather limited diversity in such extreme environments, microorganisms contribute to the majority of the ecosystem biomass, including bacteria, yeasts, fungi, *Archaea*, protists and cyanobacteria (Feller and Gerday 2003). These microorganisms are often "polyextremophiles", which are able to tolerate several extreme conditions simultaneously. Despite the large, low-temperature coverage of the Earth, relatively little is known about the microorganisms that colonize these areas.

Cold-adapted microorganisms which have successfully inhabited low temperature regions are classified as being either "psychrophilic" or "psychrotrophic". Psychrophiles are defined as organisms having an optimal growth temperature below 15°C but do not grow and survive above temperatures of 20°C (Feller and Gerday 2003). Alternatively, psychrotrophic, or cold-tolerant organisms, do not share this cold requirement, and although they are capable of growth and survival temperatures below 15°C, their optimal growth temperatures are generally above 18°C. Thus, psychrophilic or "cold-loving" organisms are considered to be truly adapted to grow only at low temperatures, whereas psychrotolerant organisms are usually "eurythermal", meaning they are able to grow over a wide range of temperatures.

Organisms can respond to their specific low-temperature environments by either using short-term mechanisms of acclimation or long-term adaptation. Adaptation refers to the combined genetic traits that have been altered by natural selective pressures, which are

heritable and maintained over many generations. In contrast, acclimation describes short-term adjustments to phenotypic and physiological traits which occur within a single lifetime (Hüner et al. 1998). Survival in cold environments necessitates that cellular metabolic rates are balanced with growth and maintenance requirements, and therefore, the energy produced must be sufficient to fulfill all energy demands. Habitats characterized by decreased temperatures pose several major challenges to microbial metabolism, growth and survival, including decreased membrane fluidity, reduced biochemical activity and cold-denaturation of proteins. Therefore, psychrophilic microorganisms exhibit a complex array of mechanisms to compensate for the metabolic challenges associated with cold environments. Remarkably, psychrophiles have evolved to not only survive, but to thrive at temperatures as low as -20°C (Thomas and Dieckmann 2002, D'Amico et al. 2006). Adaptive mechanisms employed by these organisms have been observed on many organizational levels which range from modifications in cell morphology, to membrane lipid and fatty acid composition to alterations in the structure and function of enzymes.

1.1 Ultrastructure and cell morphology

During short periods of cold acclimation, several temperate/mesophilic green algal species exhibit an increase in the number and individual size of both starch grains and oil droplets (Hatano et al. 1982, Nagao et al. 2008). In addition, short-term cold-acclimation induces an increase in the cytoplasmic volume of algal cells, with a concomitant decrease in the vacuole size (Nagao et al. 2008). These structural characteristics have also been observed among cold-adapted algae permanently inhabiting Antarctica (Pocock et al. 2004, Hu et al. 2008, Chen et al. 2012a, Chen et al. 2012b). Another common trait of Antarctic algal species is that they exhibit thicker cell walls, and are often described to exist in multi-cellular structures, surrounded by a mucilaginous sheath (Pocock et al. 2004, Hu et al. 2008, Chen et al. 2012b). It is not clear whether these groups of cells represent temporarily aggregated, cohering cells or reproductive structures involved in sexual or asexual reproduction.

Although some green algae exhibit morphological variability under certain growth conditions, relatively few studies have investigated this phenomenon. Therefore, little is

known about the potential advantage of membrane-bound multicellular structures, over motile unicells. However, at low temperatures, Antarctic bacteria are known to produce large amounts of extracellular exopolysaccharides (Mancuso et al. 2004). These polysaccharides prevent intracellular freezing, provide protection against cold-denaturation of extracellular enzymes, aid in nutrient trapping, and alter adhesive properties of cells (Mancuso et al. 2004). Thus, formation of mucus-embedded multicellular structures in Antarctic algae may provide a more favourable microenvironment under low temperature conditions.

1.2 Membrane fatty acid composition

Biological membranes function as physical barriers, regulate the movement of solutes and ions, and provide a matrix for protein complexes as well as signal transduction pathways (Hazel 1995). As temperatures decline, membrane lipid molecules become packed more tightly, and membranes become increasingly rigid. Such reduction of membrane fluidity can have adverse effects on the physical properties and the overall membrane function (Sinesky 1974, Hazel 1995, Los et al. 2013). Psychrophilic and psychrotolerant organisms can regulate the degree of membrane fluidity by adjusting fatty acid composition of their membrane lipids (Los and Murata 2004, Morgan-Kiss et al. 2006, Los et al. 2013). Biosynthesis of unsaturated fatty acids in response to low temperature in order to modulate membrane fluidity is called “homeoviscous acclimation” (Sinesky 1974). Fatty acid desaturases (FADs) regulate the biosynthesis of unsaturated fatty acids and have been shown to be cold-inducible in a wide range of heterotrophic as well as photoautotrophic organisms (Chen and Thelen 2013, Los et al. 2013).

1.3 Cold-adapted enzymes

Temperature reflects the kinetic energy of molecules – the higher the temperature the higher the kinetic energy of molecules. Biology is characterized by specialized proteins called enzymes that catalyze biochemical reactions within cells. In general, the ability of enzymes to catalyze high rates of chemical bond formation to convert reactants to products is the ability of enzymes to reduce the activation energy for this conversion. To

lower the activation energy, most biochemical reactions require a conformational change in the enzyme catalyzing the reaction to optimize the structure of active site for maximal reaction rates. This is considered to be the rate limiting step for most biochemical reactions and is very temperature sensitive (Hochachka and Somero 2002). Consequently, low temperature imposes a thermodynamic constraint on the rate of enzyme catalyzed reactions. Furthermore, the increased medium viscosity at low temperatures further contributes to reducing biochemical reaction rates (Demechenko et al. 1989). Thus, cold-adapted organisms must compensate for both of these temperature-dependent thermodynamic constraints in order to maintain metabolic homeostasis at low temperature.

Catalytic performance is traditionally measured as k_{cat} , the rate that substrate is converted to product per active site of enzyme ($k_{cat} = \text{rate of reaction} / [\text{enzyme}]$, assuming one active site per enzyme molecule). To maintain appropriate enzyme reaction rates at low temperatures, psychrophiles are characterized by cold-adapted enzymes which can exhibit k_{cat} that can be 5- to 10-fold higher at low temperature than the same enzyme from mesophilic and thermophilic organisms (Hochachka and Somero 2002, Feller and Gerday 2003, Van den Burg 2003). This enhanced catalytic performance of cold adapted enzymes at low temperature is achieved through enhanced protein flexibility especially near the active site (Thomas 2002, Hochachka and Somero 2002, Feller and Gerday 2003). Increased protein flexibility of cold adapted enzymes reflects changes in the primary structure which is consistent with a general lower thermal stability and higher heat sensitivity than the same enzymes from mesophilic species (Feller and Gerday 2003, Van den Burg 2003). However, the increased protein flexibility exhibited by cold adapted enzymes reduces the activation energy for enzyme catalysis which leads to increased k_{cat} at low temperature (Hochachka and Somero 2002).

1.4 Energy metabolism

As described above, rigidification of membranes and decreased reaction rates represent challenges to the management of biochemical processes at low temperatures. However, under low physiological growth temperatures where biological processes for most microorganisms become non-functional, psychrophiles must generate adequate energy

levels to maintain metabolic homeostasis. Photosynthesis and respiration represent the two primary processes involved in energy metabolism in photoautotrophic psychrophiles. These two metabolic processes are coupled since light energy is converted into reductant and ATP for the biosynthesis of triose-P intermediates, via the Calvin-Benson Cycle, that are subsequently exported from the chloroplast to the cytosol either for conversion into sucrose or oxidation via glycolysis and aerobic respiration in the matrix of the mitochondria (Hopkins and Hüner 2009). Hydrolysis of ATP by mitochondria in the cytoplasm is the major energy source for metabolism, growth and development. Thus, cellular concentrations of ATP and adenylates provide information on cellular metabolic states (Bott and Kaplan 1985). Cold-adapted organisms generally exhibit elevated concentrations of adenylate compounds – key molecules of energy metabolism, compared to mesophilic species (Napolitano and Shain 2004).

In both mesophilic and thermophilic organisms, growth rates and ATP levels decline with decreasing temperatures. Therefore, at higher growth temperatures, higher growth rates correspond to increased energy supply, as measured by total adenylate levels (Napolitano and Shain 2004, Napolitano and Shain 2005). In contrast, psychrophilic microorganisms exhibit an inverse relationship between adenylate pool size and growth temperature (Napolitano and Shain 2004, Napolitano and Shain 2005). Therefore, the presence of high levels of ATP and total adenylate pool size at low temperature may represent an additional adaptive mechanism utilized by psychrophiles to offset decreased rates of biochemical reactions at low temperatures (Napolitano and Shain 2004, Napolitano and Shain 2005). It has been suggested that this adaptation likely results from adjustments to components involved in ATP synthesis, either due to structural modifications or alterations in the cellular environment (e.g. pH) (Pörtner et al. 1999).

1.5 Photosynthesis at low temperatures

In addition to low temperature, phototautotrophs must deal with a unique and critical challenge to survival at low temperature that is not faced by heterotrophs. Photosynthetic organisms transform absorbed visible electromagnetic radiation into electrons (NADPH) and chemical energy (ATP) as their primary energy source for all subsequent cellular processes necessary for the establishment of metabolic homeostasis, growth and

development (Fig. 1.1). Photosynthetic organisms must, therefore, maintain a balance between the primary, photophysical and photochemical processes involved in light absorption, energy transfer within light harvesting complexes and charge separation in the reaction centers that generate electrons and the biochemical processes that utilize these electrons for the reduction of C, N and S (Hüner and Grodzinski 2011). The photophysical and photochemical processes are temperature-insensitive, in contrast to downstream metabolic reactions that consume photochemically formed energy products (NADPH and ATP), which are temperature-dependent (Hüner and Grodzinski 2011). Since the rate of PSI photo-oxidation-reduction is not considered limiting during steady-state photosynthesis, the rate of PSII photochemistry is considered to be significantly slower than PSI, in part, due to the diffusion limited oxidation of plastoquinol by the Cyt *b₆/f* complex (Haehnel 1984, Mitchell et al. 1990). A balance between the photophysical and photochemical processes (energy source) and the biochemical processes (energy sinks) that utilize the energy is termed photostasis (Hüner et al. 2003). Photostasis may be represented by the following equation (Falkowski and Chen 2003):

$$\sigma_{\text{PSII}} \times E_k = \tau^{-1}$$

where σ_{PSII} is the effective cross section area of photosystem II, E_k is the irradiance (I) at which the maximum photochemical yield of PSII balances photosynthetic capacity, and τ^{-1} is the rate at which photosynthetic electrons are consumed by downstream metabolic sinks (Falkowski and Chen 2003).

Thus, an imbalance in energy budget occurs whenever the rate of energy absorbed through PSII and the rate of electron flux into photosynthetic electron transport exceeds the metabolic sink capacity, ie. whenever $\sigma_{\text{PSII}} \times E_k > \tau^{-1}$. This may occur as a consequence of increased growth irradiance to exceed E_k , or lowering growth temperature, which causes a decrease in τ^{-1} (Hüner et al. 1998, Hüner et al. 2003, Hüner et al. 2013). Exposure to excess light may lead to a reduced ability to utilize the increased energy trapped by photochemistry, whereas exposure to low temperatures results in the downregulation of metabolic processes downstream of photochemistry (Hüner et al. 1998). Therefore, conditions of high light and cold temperatures result in increased

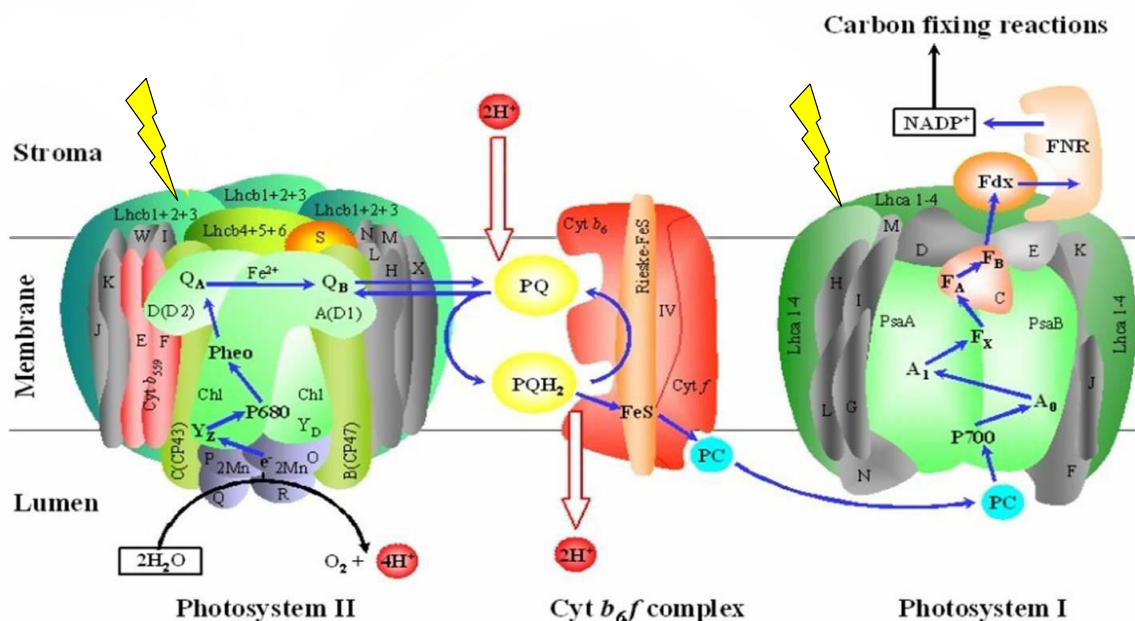


Figure 1.1: Thylakoid membrane components involved in the Z-scheme of linear electron transport. Following resonance energy transfer in the light harvesting complexes (LHC), charge separation occurs in the reaction centers of PSII and PSI. The resulting high energy electron from PSII is transferred to the cytochrome (Cyt) b_6f complex via a plastoquinone (PQ) molecule, and then through plastocyanin (PC) to replace the electron lost by charge separation of PSI. Charge separation at PSI ultimately results in the reduction of NADP^+ to NADPH. Electron transfer from PSII to PSI is coupled to the movement of protons from the stromal side of the thylakoid membrane into the lumen. The generation of a proton gradient is required for the production of ATP by the ATPase complex (not shown) (Adapted from Hüner et al. 2002).

energy input or decreased energy utilization, respectively, which leads to increased excitation pressure (Hüner et al. 1998, Hüner et al. 2003). High excitation pressure occurs when components of the photosynthetic electron transport chain, and the plastoquinone pool (PQ) become over-reduced, as electrons are generated faster by PSII than they can be consumed by the metabolic sinks (Hüner et al. 1998). In turn, a balance can be restored either by increasing the rate of energy utilization and storage (τ^{-1}) by the metabolic sinks or by decreasing the energy input ($\sigma_{\text{PSII}} \times I$), by reducing either the physical size and/or the effective, functional absorption cross section of PSII (Hüner et al. 2003, Hüner et al. 2013).

1.6 Acclimation to light and low temperature

To maintain photostasis, photosynthetic organisms integrate a variety of short-term and long-term acclimation mechanisms (Anderson and Chow 1995). On a short time scale of minutes, organisms can reduce the efficiency of energy transfer to PSII by diverting energy away from PSII in favour of PSI through state transitions (Fig. 1.2) (Kargul and Barber 2008, Rochaix 2011). During exposure to conditions that cause an over-reduction of the plastoquinone (PQ) pool, plastoquinol (PQH₂) binds to the Q(o) site of the cytochrome *b₆/f* complex. Upon docking of plastoquinol, a membrane bound protein kinase, *Stt7* in *Chlamydomonas reinhardtii*, is activated, which phosphorylates LHCII proteins. Recently, it was reported that the STN8 protein kinase appears to be the primary thylakoid protein kinase that regulates the phosphorylation of the PSII core proteins whereas STN7 governs the phosphorylation of Lhcb1, Lhcb2 and Lhcb4 in *Arabidopsis thaliana* (Bonardi et al. 2005, Tikkanen et al. 2008, Fristedt et al. 2009, Rochaix 2011, Tikkanen et al. 2012, Wunder et al. 2013). The orthologous thylakoid protein kinases in *Chlamydomonas reinhardtii* are Stl1 and Stt7 (Fig. 1.2) (Depege et al. 2003, Vener 2006, Rochaix 2011).

Upon phosphorylation, major LHCII trimers dissociate from photosystem II and physically migrate to couple with photosystem I (state II) (Finazzi and Forti 2004). Therefore, this transition to state II results in an increase of PSI antenna size at the

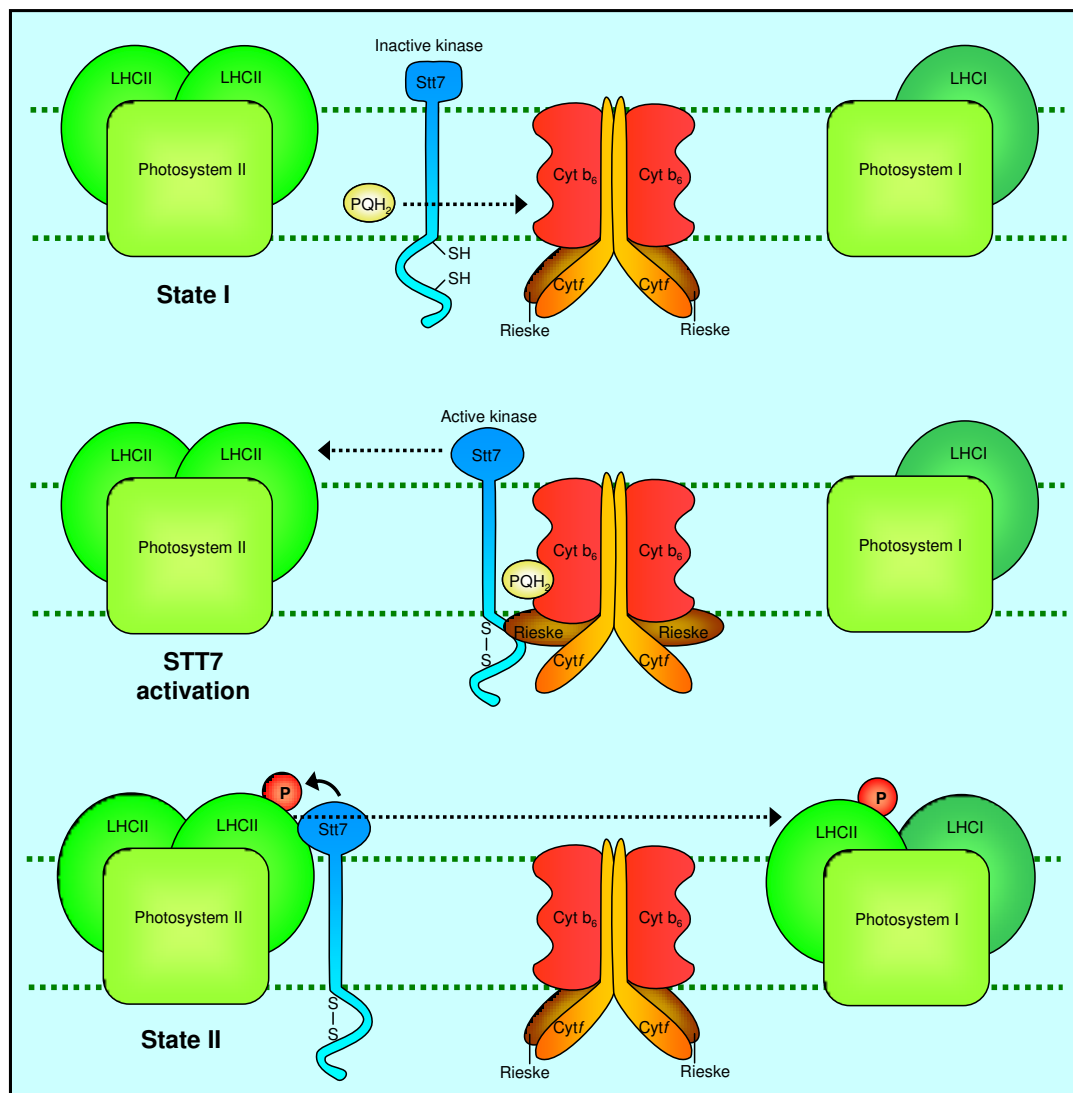


Figure 1.2: A hypothetical model for state transitions from state I to state II. Transition from state I to state II occurs when the redox state of the plastoquinone (PQ) pool is reduced. Docking of a plastoquinol (PQH₂) to the Q(o) site of Cyt b₆ causes the Rieske protein to shift from a distal to proximal position, relative to the thylakoid membrane. This movement results in the interaction of Rieske with the Stt7 kinase, and its subsequent activation. The active Stt7 kinase interacts with PSII, leading to the phosphorylation of LHCII proteins. Phosphorylated LHCII proteins dissociate from PSII and physically migrate to dock with PSI. The transition from state II to state I occurs upon LHCII dephosphorylation by a phosphatase, resulting in LHCII detachment from PSI and re-association w PSII (not shown).

expense of the PSII antenna (Finazzi and Forti 2004). In contrast, when the plastoquinone pool becomes increasingly oxidized, thylakoid phosphatases such as PPH1/TAP38 remove the phosphate group, and the mobile fraction of the PSII antenna becomes associated with PSII (state I) (Rochaix 2011). Alternatively, the photosynthetic apparatus can be protected from excess absorbed light by dissipation of the excess energy as heat by non-photochemical quenching (NPQ) via the xanthophyll cycle (Demmig-Adams et al. 1999, Hüner et al. 2003, Horton et al. 2008, Li et al. 2009). Both state transitions and NPQ are rapid and require no de novo biosynthesis of either new metabolites or proteins and can be activated by either a change in irradiance or temperature (Adams et al. 1995, Kröhl et al. 1999). Since both processes are regulated by the redox state of the plastoquinone pool, state transitions and NPQ are governed by excitation pressure (Wilson and Hüner 2000, Wilson et al. 2006, Rochaix 2011).

Long-term acclimatory responses include alterations in light-harvesting antenna size and adjustments of PSI:PSII stoichiometry to balance the excitation light energy absorbed by the two photosystems (Melis et al. 1996; Yamazaki et al. 2005). Alternatively, photosynthetic organisms may acclimate to enhance the capacity of electron consumption by increasing levels of Calvin cycle components (Hüner et al. 1998). Acclimation may also occur on a greater scale, as some marine phytoplankton avoid exposure to excess light by changing their vertical position in the water column (Falkowski 1983).

1.7 *Chlamydomonas sp.* UWO241

Although cold acclimation, low temperature stress and freezing tolerance have been studied in myriad mesophilic photoautotrophs, we know relatively little about adaptation of true psychrophilic photoautotrophs to cold environments (Hüner et al. 1993). For the past two decades, *Chlamydomonas sp.* UWO241 has been the most studied psychrophilic green alga to date, and consequently can be considered the model organism for the study of psychrophily in photoautotrophs (Morgan-Kiss et al. 2006).

1.8 Natural habitat of UWO241

Chlamydomonas sp. UWO241 originates from the east lobe of Lake Bonney in Taylor Valley, Antarctica – one of the coldest and driest deserts of our planet – with annual air temperatures average of -20°C , and annual precipitation is lower than 10 cm (Neale and Priscu 1995, Priscu 1998). Psychrophilic UWO241 was isolated from the deepest trophic zone, situated at 17 meters below the permanent ice-cover of this unique lake. The presence of a thick (3-4.5 meter) ice cover limits gas exchange between lake water and the atmosphere and prevents vertical mixing within the water column, due to the absence of wind turbulence (Spigel and Priscu 1996). Mixing occurs predominantly via molecular diffusion and the vertical mixing time for Lake Bonney is estimated to be approximately 50,000 years (Moorhead et al. 1999).

Vertical stratification in Lake Bonney results from strong salinity gradients, reaching levels up to 10 times that of seawater at maximum lake depths (Spigel and Priscu 1996, Priscu et al. 1998). Stable salinities of approximately 700 mM are characteristic at the depth where UWO241 was isolated, which is above that of seawater (545 mM) (Priscu 1998). The light environment at the depth where UWO241 naturally exists is characterized by low light ($<50 \mu\text{mol photons m}^{-2} \text{s}^{-1}$) during austral summer and a light spectral distribution that is heavily biased to the blue region of the visible spectrum (450-550 nm) (Lizotte and Priscu 1994, Lizotte et al. 1996).

A recent study of the distribution of microbial eukaryotes using 18S rRNA libraries revealed that Lake Bonney is dominated by photosynthetic protists, with the majority being related to flagellated strains (Bielewicz et al. 2011). Both lobes of the lake were vertically stratified with dominating populations of a cryptophyte at shallow depths (6-10 m), a haptophyte at mid-depths (13 m) and various chlorophytes, including UWO241 residing in the deepest photic zone (15-20 m) (Bielewicz et al. 2011). Thus, UWO241 is a psychrophile that has adapted to an extreme but stable growth regime that is characterized by low temperatures, high salinity and extreme shade in a narrow spectral range distribution.

1.9 Growth of UWO241

1.9.1 Temperature

Cultures of UWO241 exhibit an optimal growth temperature of 8°C and exponential growth up to temperatures of 16°C. However, at 20°C or higher, growth of UWO241 is inhibited which confirms that UWO241 is an obligate psychrophile adapted to growth at low temperatures (Morgan et al. 1998). To address the inability UWO241 to grow at temperatures above 16°C, a recent study examined the effects of supra-optimal temperatures on the physiology of UWO241 (Possmayer et al. 2011). Using the membrane impermeable SYTOX green assay to stain cellular DNA, it was determined that exposure of UWO241 cells to 24°C, results in cell death with a half-time of 34.9 h (Possmayer et al. 2011). Surprisingly, cell death occurred independently of light, as dark incubation of cells showed a comparable half-time of 43.7 h (Possmayer et al. 2011). This suggests that absorption of excess light and formation of reactive oxygen species in the chloroplast of UWO241 play relatively minor roles in cell death (Possmayer et al. 2011). A twelve hour shift of UWO241 from 10°C to 24°C caused reductions in light-saturated rates of photosynthesis and respiration and stimulated excitation pressure and altered energy partitioning. This was associated with a decrease in transcript abundances for LHCII polypeptides and ferredoxin but dramatic increases in the transcript abundance for heat shock proteins (HSPs) (Possmayer et al. 2011). All of these effects were reversible within 24-48 hours of recovery at 10°C, indicating that UWO241 exhibits significant physiological plasticity at a temperature that is lethal to this psychrophile (Possmayer et al. 2011). However, this molecular and physiological plasticity is time dependent at supra-optimal temperatures.

1.9.2 Salt

Although UWO241 has adapted to a salinity of 700 mM, it has been demonstrated that UWO241 is not halophilic, but halotolerant (Pocock et al. 2011). This psychrophilic strain exhibits the ability to grow under a wider salinity range of 10 mM to its upper critical salinity limit of 1300 mM at 8°C, compared to a mesophilic strain that was unable to grow at salt concentrations above 100 mM at 24°C (Pocock et al. 2011). However,

UWO241 exhibited decreased growth rates as salinity increased, with a 35% reduction in growth rate at 700 mM compared to 10 mM NaCl (Pocock et al. 2011). Therefore, despite the hypersaline environment of Lake Bonney, high salt is not an absolute requirement for growth of UWO241, but rather a condition that is tolerated by this psychrophile.

1.10 Adaptation of UWO241 to low temperature

Detailed microscopy studies (Pocock et al. 2004) revealed that *Chlamydomonas sp.* UWO241 cells exist as motile, biflagellate single cells of approximately 10 to 15 μm in length, as well as non-motile membrane-bound palmelloids, consisting of 16 to 32 cells that measure approximately 30 μm . It is not clear if these palmelloids are a product of mitosis or whether they represent meiotic reproductive structures. Similar to other Antarctic algae, UWO241 cells secrete ice-binding proteins (IBPs), which function extracellularly to alter the structure of surrounding ice and increase freezing tolerance (Raymond and Morgan-Kiss 2013).

Analysis of the membrane lipid composition in UWO241 exhibited significantly higher levels of unsaturated fatty acids compared to the mesophilic model organism, *Chlamydomonas reinhardtii*, with an unsaturation index of 2.74, compared to 1.90, respectively (Morgan-Kiss et al. 2002). In addition, UWO241 membranes revealed the presence of several unique polyunsaturated fatty acids, with altered unsaturated bond positions that occurred close to the lipid head group (Morgan-Kiss et al. 2002, Morgan-Kiss et al. 2006). As chloroplasts comprise more than 80% of the total cell membranes, the majority of these fatty acids represent galactolipids (MGDG, DGDG, SQDG and PG) of the photosynthetic thylakoid membranes (Morgan-Kiss et al. 2002, Morgan-Kiss et al. 2006).

In a mechanism used to overcome reduced catalytic efficiency at low temperatures, UWO241 exhibits high concentrations of the large unit of Rubisco, compared to a mesophilic control, *C. raudensis* SAG 49.72 (Dolhi et al. 2013). However, despite these increased levels, Rubisco activity was 30% lower in UWO241 compared to a mesophile, when cells were grown under their optimal growth temperatures of 8°C and 29°C (Dolhi

et al. 2013). However, the *in vitro* results for Rubisco activity are inconsistent with the temperature dependence for light and CO₂ saturated rates of photosynthetic gas exchange which indicate that photosynthetic rates for UWO241 are maximum at the optimal low growth temperature and minimum at non-permissive, high temperatures (Pocock et al. 2007). Furthermore, *in vivo* photosynthetic rates for UWO241 at its optimal growth temperature (8°C) were comparable to those of the mesophile, *Chlamydomonas reinhardtii*, at its optimal growth temperature (29°C) (Pocock et al. 2007).

In addition, growth under similar optimal conditions showed that UWO241 significantly increased concentrations of two major (α and β) subunits of the CF₁ complex of the chloroplast ATP synthase compared to the mesophilic control, *C. reinhardtii* (Morgan et al. 1998). An increase in chloroplast ATP synthase is likely an adaptive strategy to maintain elevated adenylate pools, which are required for ATP-dependent biochemical reactions occurring at low temperatures (Napolitano and Shain 2004, Napolitano and Shain 2005). Increased levels of ATP in UWO241 may also be necessary to actively pump sodium across cell membranes in hypersaline growth environments, as observed for the halotolerant model, *Dunaliella salina* (Liska et al. 2004).

1.11 Photosynthetic electron transport

1.11.1 Structure of PETC

Adaptation of *C. raudensis* UWO241 to its unique environment has resulted in the evolution of distinct structural features in its photosynthetic apparatus. Previous studies have revealed that this Antarctic psychrophile exhibits altered overall stoichiometry of PSII/PSI (Morgan et al. 1998, Szyszka et al. 2007). This reflects the reduced abundance of both PSI and LHCI, resulting in a smaller functional absorptive cross section of this photosystem (σ_{PSI}), compared to *C. reinhardtii* (Morgan et al. 1998). Conversely, the absorptive cross section of PSII (σ_{PSII}) was larger compared to *C. reinhardtii* and a higher proportion of LHCII proteins were found in an oligomeric, rather than a monomeric state (Morgan et al. 1998). As chlorophyll b is present exclusively bound to light harvesting complex (LHC) proteins, high levels of LHCII also result in characteristically low chlorophyll a/b ratios (~1.8-2.0) in UWO241, compared to typical values of ~3.0 in *C.*

reinhardtii (Morgan et al. 1998, Pocock et al. 2004). Relatively high levels of PSII, LHCII and increased PSII cross section most likely allow for more efficient use of light and reflect an adaptation of extreme shade conditions (Neale and Priscu 1995, Morgan et al. 1998).

In addition to altered stoichiometry of photosystems, UWO241 shows higher levels of the cytochrome *b₆/f* complex compared to mesophilic algae under the same growth conditions (Morgan et al. 1998, Szyszka et al. 2007). Based on SDS-PAGE, the cytochrome *f* protein of UWO241 has a 7-kDa lower apparent molecular mass (34 kDa) compared to that of *C. reinhardtii* (41 kDa) (Morgan-Kiss et al. 2002). This mass difference does not affect the ability of the psychrophilic cytochrome *f* to bind the heme factor; however, this covalently bound heme is significantly less stable to high temperature than that of *C. reinhardtii*, which likely reflects an adaptive protein modification towards cold environments (Gudynaite-Savitch et al. 2006). The amino acid sequence of the *petA* gene, encoding the UWO241 cytochrome *f* protein was found to be 79% identical to that of *C. reinhardtii*, with a similar calculated molecular mass, despite the observed apparent molecular mass variance based on SDS-PAGE (Gudynaite-Savitch et al. 2006). Notably, the UWO241 cytochrome *f* sequence revealed the presence of three cysteine residues (C21, C24, and C261), compared to the two cysteine residues (C21 and C24) that are usually observed in other photosynthetic organisms and involved in heme binding (Gudynaite-Savitch et al. 2006). The additional C261 residue of UWO241 cytochrome *f* originates from a transmembrane helix and is not implicated in heme binding (Gudynaite-Savitch et al. 2006). The role of C261 remains to be elucidated.

1.11.2 Function of PETC

In addition to structural differences, the photosynthetic electron transport chain of UWO241 reveals major functional changes (Szyszka et al. 2007, Morgan-Kiss et al. 2005). Two inhibitors of electron transport, DCMU (3-(3,4-dichlorophenyl)-1,1-dimethylurea) and DBMIB (2,5-dibromo-3-methyl-6-isopropyl-p-benzoquinone) were used to examine the redox state of the photosynthetic electron transport chain of UWO241. DCMU competes for the plastoquinone binding site of PSII, blocking the transfer of electrons from PSII to the PQ pool, while DBMIB occupies the Q(o) site of

the cytochrome b_6/f complex, thereby preventing the oxidation of PQ (Trebst 1980). Spectroscopic studies assessing the rates of intersystem electron transport through the light dependent reduction of P_{700}^+ revealed that intersystem electron transport in UWO241 appears to be less sensitive to the presence of DCMU and DBMIB than that of *C. reinhardtii*. These results are consistent with the fact that UWO241 is locked in state I and is unable to undergo a state transition. Thus, it appears that the redox status of the intersystem electron transport of UWO241 is predisposed to favour the oxidized state compared to that of *C. reinhardtii* (Morgan-Kiss et al. 2002).

In addition to production of both ATP plus NADPH through linear electron flow (LEF) between PSII and PSI, cyclic electron flow (CEF) recycles photosynthetic electrons solely around PSI to produce ATP, with no net production of NADPH (Finazzi et al. 1999, Eberhard et al. 2008, Cardol et al. 2011). This pathway functions to adjust the appropriate ratio of ATP/NADPH needed for carbon fixation as well as other cellular processes which require ATP (Lucker and Kramer 2013). An increase in the ratio of CEF/LEF has been observed under environmental conditions associated with increased ATP demand, including, low temperatures (Clarke and Johnson 2001), low CO_2 (Golding and Johnson 2003, Lucker and Kramer 2013), drought (Golding and Johnson 2003) and high light (Munekage et al. 2004). Several reports have suggested that CEF is activated by state I-II transitions (Wollman 2001, Iwai et al. 2010). However, recent studies demonstrated that CEF occurs independently of state transitions and that the kinetics of state transitions are considerably slower than the rapid kinetics observed for CEF activation (Lucker and Kramer 2013, Takahashi et al. 2013). *Chlamydomonas sp.* UWO241 is locked in state I (Morgan-Kiss et al. 2002, Gudynaite-Savitch et al. 2006, Takizawa et al. 2009) and maintains rates of cyclic electron flow that are up to 2-fold greater than that observed for the mesophiles, *C. reinhardtii* and *C. raudensis* SAG 49.72 (Fig. 1.3) (Morgan-Kiss et al. 2002).

Cyclic electron flow also plays a role in photoprotection through dissipation of excess excitation energy and the down regulation of photosystem II (Heber and Walker 1992, Munekage et al. 2002, Golding and Johnson 2003). CEF-dependent generation of a pH gradient (ΔpH) across the thylakoid membrane results from electron transfer from PSII to

the Cyt b_6/f complex. Acidification of the thylakoid lumen increases non-photochemical quenching (NPQ), thereby reducing the efficiency of PSII, PSII photodamage, and electron transfer from PSII to PSI (Heber and Walker 1992, Golding and Johnson 2003). Therefore, CEF may exert regulatory control over PSII activity and electron transport rates through the associated changes in luminal pH. This is called photosynthetic control (Foyer et al. 2012).

A comparison of energy partitioning of UWO241 with the mesophile *C. raudensis* SAG 49.72 at their optimal growth temperatures of 8 °C and 28 °C, respectively, showed that the psychrophile exhibits a 30% reduction in the efficiency of PSII with a nearly 2-fold higher level of non-photochemical quenching (Szyszka et al. 2007). Consistently, UWO241 maintains lower epoxidation states of xanthophyll pigments (violaxanthin, antheraxanthin and zeaxanthin) compared to the mesophilic species, *C. raudensis* SAG 49.72 (Szyszka et al. 2007), which are known to play an important role in energy dissipation and photoprotection under conditions of high light. Higher levels of NPQ and lower epoxidation states could be associated with higher rates of cyclic electron flow in UWO241, since this electron pathway results in the generation of a proton gradient.

As a consequence of the differences in both structure and function of the photosynthetic apparatus, UWO241 maintains comparable photosynthetic capacity, PSII excitation pressure and thus, energy balance to that of mesophilic algae when grown under their respective optimal growth conditions (Morgan et al. 1998, Szyszka et al. 2007).

1.11.3 Acclimation to temperature and irradiance

Recently, the capacity of UWO241 to acclimate to different steady state temperature and light growth regimes was examined and compared to that of the mesophile, *C. raudensis* SAG 49.72 (Szyszka et al. 2007). Although the psychrophile retained the capacity to acclimate to these various conditions, the mechanism employed to maintain photostasis appears to be quite different. UWO241 exhibits alterations in the partitioning of excess excitation energy in response to both elevated growth temperatures and increased growth irradiance (Szyszka et al. 2007). While *C. raudensis* SAG 49.72 favoured energy partitioning through typical down regulatory processes associated with the xanthophyll

cycle and antenna quenching, UWO241 favoured energy partitioning through other constitutive processes involved in energy dissipation, which most likely reflect PSII reaction centre quenching (Szyszka et al. 2007).

Although the xanthophyll cycle does not appear to be the primary process employed for dissipation of excess light energy in UWO241 at low temperature, this psychrophile does maintain a fully functional xanthophyll cycle, and exhibits adjustments of epoxidation states in response to changes in irradiance and temperature (Pocock et al. 2007, Szyszka et al. 2007). Despite the adaptation of UWO241 to a cold environment, surprisingly, this Antarctic psychrophile exhibits greater susceptibility to low temperature photoinhibition of PSII compared to the mesophilic *C. reinhardtii* (Pocock et al. 2007). However, to compensate for this sensitivity to low temperature-induced photoinhibition, UWO241 displays an unusually rapid rate of recovery from photoinhibition at 8°C, as a result of a unique D1 repair cycle that operates maximally at low temperatures (Pocock et al. 2007).

1.11.4 Acclimation to light quality

Adjustments of PSII:PSI stoichiometry are controlled by the redox state of the PQ pool and represents a mechanism for maintaining maximum efficiency of photosynthetic electron transport during long-term acclimation to light intensity and light quality (Falkowski et al. 1981, Melis et al. 1996, Fujita 1997, Miskiewicz et al. 2002, Yamazaki et al. 2005). Under blue light, PSII is preferentially excited and the intersystem electron transport components are mostly reduced, whereas under conditions enriched in red light absorbed mainly by PSI, the components of the intersystem electron pool are mostly in an oxidized state (Melis et al. 1996). Studies with UWO241 have demonstrated that UWO241 is able to adjust photosystem stoichiometry in response to growth temperature, irradiance and light quality (Szyszka et al. 2007, Morgan-Kiss et al. 2005). However, *Chlamydomonas sp.* UWO241 is unable to grow under red light illumination exclusively even though the light is absorbed by Chl a and Chl b. Exposure to such a light environment inhibits growth and photosynthetic rates and results in a 4-fold increase in excitation pressure with concomitant increases in nonphotochemical quenching (Morgan-Kiss et al. 2005).

1.11.5 State transitions

Despite the ability of UWO241 to adjust photosystem stoichiometry, one of the most striking characteristics of UWO241 is that this psychrophile lacks the capacity to redistribute light energy among photosystem I and photosystem II through a process called state transitions (Morgan-Kiss et al. 2005). Thus, *Chlamydomonas sp.* UWO241 is the first natural variant deficient in the state transition response (Morgan-Kiss et al. 2005). Consequently, the ability to undergo state transitions is not an absolute requirement for survival in green algae.

Activation of the Stt7 kinase is initiated by its interaction with the Cyt b_6/f complex, which occurs due to a rotation of the Rieske Fe-S protein from a distal to proximal position upon binding of plastoquinol to the Q(o) site of cytochrome b_6 (Fig. 1.2) (Zito et al. 1999, Finazzi et al. 2001, Wollman 2001). Since Stt7 kinase activation depends on the structure of the Cyt b_6/f complex, the observed 7 kDa difference in apparent molecular mass of cytochrome f in UWO241 compared to that of *C. reinhardtii*, and its possible impairment of state transitions were assessed (Gudynaite-Savitch et al. 2006). The substitution of cytochrome f in a *petA* deletion mutant of the mesophilic *C. reinhardtii* with the *petA* from UWO241 clearly showed that the altered structure of psychrophilic cytochrome f is not responsible for the inability of UWO241 to undergo state transitions (Gudynaite-Savitch et al. 2006).

Another requirement for state transitions has been established by Zer *et al.* (1999) who demonstrated that in order for phosphorylation to occur, LCHII polypeptides must undergo a light-induced conformational change in order to expose the phosphorylation site to the Stt7 kinase (Zer et al. 1999). Although it is not known whether LHCII proteins of the Antarctic psychrophile have the capacity to undergo such conformational changes, nondenaturing and SDS-PAGE analyses have revealed differences in both the structure of LHCII complexes, as well as variation in the apparent molecular masses of several individual LHCII proteins, compared to *C. reinhardtii* and *C. raudensis* SAG 49.72 (Morgan et al. 1998, Szyszka et al. 2007).

1.11.6 Thylakoid polypeptide phosphorylation profile

Phosphorylation of light harvesting complex II (LHCII) polypeptides is essential in the regulation of state transitions (Fig. 1.1) (Finazzi et al. 1999, Zer et al. 1999, Depege et al. 2003). Consistent with the inability to perform state transitions, UWO241 does not phosphorylate LHCII proteins (25-40 kDa) in response to either growth temperature, irradiance or light quality (Morgan-Kiss et al. 2002, Morgan-Kiss et al. 2005, Szyszka et al. 2007). In contrast to the typical phosphorylation patterns observed for photosynthetic organisms, UWO241 exhibits a light dependent phosphorylation of high molecular mass polypeptides (70 kDa, >115 kDa), as well as a small 17 kDa protein (Morgan-Kiss et al. 2002, Szyszka et al. 2007).

1.12 Objective of the thesis

The objective of my Ph.D. thesis is to test the following hypotheses.

Well-studied photosynthetic organisms, including the model green alga, *Chlamydomonas reinhardtii*, exhibit strong phosphorylation of PSII-associated proteins, within the range of 20-45 kDa, which regulate the activity and structure of this photosystem. This leads to the question: what are the unique phosphorylated proteins exhibited by *Chlamydomonas sp.* UWO241 and their potential role(s) in the thylakoid membrane? I hypothesize that in UWO241, the phosphorylated high-molecular mass complex is associated with photosystem I, rather than photosystem II. Similarly to PSII, I hypothesize that the unique phosphoprotein(s) are involved in the regulation of PSI structure and/or the function of photosystem I.

In striking contrast to other photosynthetic organisms, the natural state transition variant, *Chlamydomonas sp.* UWO241 does not appear to exhibit the capacity to phosphorylate LHCII polypeptides. This leads to the question: does phosphorylation of LHCII occur in the Antarctic psychrophile? I hypothesize that the STT7 kinase may be absent in UWO241. Alternatively, UWO241 may exhibit the absence of specific LHCII phosphorylation sites involved in state transitions, resulting in the lack of a State I – State II response.

Chlamydomonas sp. UWO241 cells exist as free-swimming, single cells, as well as non-motile, membrane-bound, palmelloids, which are commonly observed among Antarctic algal species. This leads to the question: are single cells of UWO241 photosynthetically distinct from multi-cellular units? I hypothesize that compared to single cells, multi-cellular structures exhibit photosynthetic differences, associated with a “self-shading” effect. Therefore, palmelloids should exhibit decreased carotenoid concentrations, increased LHClI cross-sectional areas and lower chlorophyll a/b ratios compared to single cells.

1.13 References

- Adams III WW, Hoehn A, Demmig-Adams B.** (1995) Chilling temperatures and the xanthophyll cycle. A comparison of warm-grown and overwintering spinach. *Aust J Plant Physiol* **22**:75-85
- Anderson JM, Chow WS, Park YI.** (1995) The grand design of photosynthesis: acclimation of the photosynthetic apparatus to environmental cues. *Photosyn Res* **46**:129-39
- Bielewicz S, Bell EM, Kong W, Friedberg I, Priscu JC, Morgan-Kiss RM.** (2011) Protist diversity in a permanently ice-covered Antarctic lake during polar night transition. *ISME J* **5**:1559-64
- Bonardi V, Pesaresi P, Becker T, Schleiff E, Wagner R, Pfannschmidt T, Jahns P, Leister D.** (2005) Photosystem II core phosphorylation and photosynthetic acclimation require two different protein kinases. *Nature* **437**:1179-82
- Bott TL, Kaplan LA.** (1985) Bacterial biomass, metabolic state, and activity in stream sediments: relation to environmental variables and multiple assay comparisons. *Appl Environ Microbiol* **50**:508-22
- Cardol P, Forti G, Finazzi G.** (2011) Regulation of electron transport in microalgae. *Biochim Biophys Acta* **1807**:912-18
- Chen Z, HE C, Hu H.** (2012b) Temperature responses of growth, photosynthesis, fatty acid and nitrate reductase in Antarctic and temperate *Stichococcus*. *Extremophiles* **16**:127-33
- Chen Z, Gong Y, Fang X, Hu H.** (2012a) *Scenedesmus sp.* NJ-1 isolated from Antarctica: a suitable renewable lipid source for biodiesel production. *World J Microbiol Biotechnol* **28**:3219-25
- Chen M, Thelen JJ.** (2013) Acyl-lipid desaturase 2 is required for chilling and freezing tolerance in *Arabidopsis*. *Plant Cell* **25**:1430-44
- Clarke JE, Johnson GN.** (2001) In vivo temperature dependence of cyclic and pseudocyclic electron transport in barley. *Planta* **212**:808-16

- D'Amico S, Collins T, Marx JC, Feller G, Gerday C.** (2006) Psychrophilic microorganisms: challenges for life. *EMBO Rep* **7**:385-9
- Demchenko AP, Ruskyn OI, Saburova EA.** (1989) Kinetics of the lactate dehydrogenase reaction in high-viscosity media. *Biochim Biophys Acta* **998**:196-203
- Demmig-Adams B, Adams WW, Ebbert V, Logan BA.** (1999) Ecophysiology of the xanthophyll cycle. In: Frank HA, Young AJ, Britton G, Cogdell RJ, Eds. *Advances in Photosynthesis. The Photochemistry of Carotenoids*. Dordrecht, Kluwer Academic, pp. 245-69
- Depège N, Bellafiore S, Rochaix JD.** (2003) Role of chloroplast protein kinase Stt7 in LHCII phosphorylation and state transition in *Chlamydomonas*. *Science* **299**:1572-5
- Dolhi JM, Maxwell DP, Morgan-Kiss RM.** (2013) Review: the Antarctic *Chlamydomonas raudensis*: an emerging model for cold adaptation of photosynthesis. *Extremophiles* **17**:711-22
- Eberhard S, Finazzi G, Wollman FA.** (2008) The dynamics of photosynthesis. *Ann Rev Genet* **42**:463-15
- Eicken H.** (1992) The role of sea ice in structuring Antarctic ecosystems. *Polar Bio* **12**:3-13
- Falkowski PG.** (1983) Light-shade adaptation and vertical mixing of marine phytoplankton: a comparative field study. *J Mar Res* **41**:215-37
- Falkowski PG, Chen YB.** (2003) Photoacclimation of light harvesting systems in eukaryotic algae. In: Green BR, Parson WW, Eds. *Advances in photosynthesis and respiration. Light harvesting antennas in photosynthesis*. Dordrecht, Kluwer Academic, pp. 423-47
- Falkowski PG, Owens TG, Ley AC, Mauzerall DC.** (1981) Effects of 'growth irradiance levels on the ratio of reaction centers in two species of marine phytoplankton. *Plant Physiol* **68**:969-73
- Feller G, Gerday C.** (2003) Psychrophilic enzymes: hot topics in cold adaptation. *Nat Rev Microbiol* **1**:200-208
- Finazzi G, Forti G.** (2004) Metabolic flexibility of the green alga *C. reinhardtii* as revealed by the link between state transitions and cyclic electron flow. *Photosynth Res* **82**:327-38
- Finazzi G, Furia A, Barbagallo RP, Forti G.** (1999) State transitions, cyclic and linear electron transport and photophosphorylation in *Chlamydomonas reinhardtii*. *Biochim Biophys Acta* **1413**:117-29
- Finazzi G, Zito F, Barbagallo RP, Wollman FA.** (2001) Contrasted effects of inhibitors of cyt b₆/f complex on state transitions in *Chlamydomonas reinhardtii*: the role of Qo site occupancy in LHCII kinase activation. *J Biol Chem* **276**:9770-4

- Foyer CH, Neukermans J, Queval G, Noctor G, Harbinson J.** (2012) Photosynthetic control of electron transport and the regulation of gene expression. *J Exp Bot* **63**:1637-61
- Fristedt R, Willig A, Granath P, Crevecoeur M, Rochaix JD, Vener AV.** (2009) Phosphorylation of photosystem II controls functional macroscopic folding of photosynthetic membranes in *Arabidopsis*. *Plant Cell* **21**:3950-64
- Fujita Y.** (1997) A study on the dynamic features of photosystem stoichiometry - accomplishments and problems for future studies. *Photosyn Res* **53**:83-93
- Golding AJ, Johnson GN.** (2003) Down-regulation of linear and activation of cyclic electron transport during drought. *Planta* **218**:107-14
- Gudynaite-Savitch L, Gretes M, Morgan-Kiss R, Savitch LV, Simmonds J, Kohalmi SE, Hüner NPA.** (2006) Cytochrome f from the Antarctic psychrophile, *Chlamydomonas raudensis* UWO 241: structure, sequence, and complementation in the mesophile, *Chlamydomonas reinhardtii*. *Mol Genet Genomics* **275**:387-98
- Haehnel W.** (1984) Photosynthetic electron transport in higher plants. *Ann Rev Plant Physiol* **35**: 659-93
- Hatano S, Kabata K, Yoshimoto M, Sadakane H.** (1982) Accumulation of free fatty acids during hardening of *Chlorella ellipsoidea*. *Plant Physiol* **70**:1173-7
- Hazel JR.** (1995) Thermal adaptation in biological membranes: is homeoviscous adaptation the explanation? *Annu Rev Physiol* **57**:19-42
- Heber U, Walker D.** (1992) Concerning a dual function of coupled cyclic electron transport in leaves. *Plant Physiol* **100**:1621-6
- Hochachka PW, Somero GN.** (2002) Ed. *Biochemical Adaptation. Mechanisms and process in physiological evolution.* New York: Oxford University Press Inc, pp. 290-450
- Hopkins WG, Hüner NPA.** (2009) Ed. *Introduction to Plant Physiology*, 4th edition. New York: Wiley and Sons, pp. 77-90
- Horton P, Johnson MP, Perez-Bueno ML, Kiss AZ, Ruban AV.** (2008) Photosynthetic acclimation: does the dynamic structure and macro-organisation of photosystem II in higher plant grana membranes regulate light harvesting states? *FEBS J* **275**:1069-79
- Hu H, Li H, Xu X.** (2008) Alternative cold response modes in *Chlorella* (Chlorophyta, Trebouxiophyceae) from Antarctica. *Phycologia* **47**:28-34
- Hüner NPA, Bode R, Dahal K, Busch FA, Possmayer M, Szyszka B, Rosso D, Ensminger I, Krol M, Ivanov AG, Maxwell DP.** (2013) Shedding some light on cold acclimation, cold adaptation, and phenotypic plasticity. *Botany* **91**: 127-36
- Hüner NPA, Grodzinski B.** (2011) Photosynthesis and photoautotrophy. In: Murray Moo-Young, Ed. *Comprehensive Biotechnology* (second edition) Amsterdam, Elsevier, pp. 315-22

- Hüner NPA, Öquist G, Hurry VM, Krol M, Falk S, Griffith M.** (1993) Photosynthesis, photoinhibition and low temperature acclimation in cold tolerant plants. *Photosyn Res* **37**:19-39
- Hüner NPA, Öquist G, Melis A.** (2003) Photostasis in plants, green algae and cyanobacteria: the role of light harvesting antenna complexes. In: Green BR, Parson WW, Eds. *Advances in photosynthesis and respiration. Light harvesting antennas in photosynthesis.* Dordrecht, Kluwer Academic, pp. 401-21
- Hüner NPA, Öquist G, Sarhan F.** (1998) Energy balance and acclimation to light and cold. *Trends Plant Sci* **3**:224-30
- Iwai M, Takizawa K, Tokutsu R, Okamuro A, Takahashi Y, Minagawa J.** (2010) Isolation of the elusive supercomplex that drives cyclic electron flow in photosynthesis. *Nature* **464**:1210-13
- Kargul J, Barber J.** (2008) Photosynthetic acclimation: structural reorganisation of light harvesting antenna; role of redox-dependent phosphorylation of major and minor chlorophyll a/b binding proteins. *FEBS J* **275**:1056-68
- Krol M, Ivanov AG, Jansson S, Kloppstech K, Hüner NPA.** (1999) Greening under high light or cold temperature affects the level of xanthophyll-cycle pigments, early light-inducible proteins, and light-harvesting polypeptides in wild-type barley and the chlorina f2 mutant. *Plant Physiol* **120**:193-04
- Li Z, Ahn TK, Avenson TJ, Ballottari M, Cruz JA, Kramer DM, Bassi R, Fleming GR, Keasling JD, Niyogi KK.** (2009) Lutein accumulation in the absence of zeaxanthin restores nonphotochemical quenching in the *Arabidopsis thaliana* npq1 mutant. *Plant Cell* **21**:1798-12
- Liska AJ, Shevchenko A, Pick U, Katz A.** (2004) Enhanced photosynthesis and redox energy production contribute to salinity tolerance in *Dunaliella* as revealed by homology-based proteomics. *Plant Physiol* **136**:2806-17
- Lizotte MP, Priscu JC.** (1994) Natural fluorescence and quantum yields in vertically stationary phytoplankton from perennially ice-covered lakes. *Limnol Oceanogr* **39**:1399-410
- Lizotte MP, Sharp TR, Priscu JC.** (1996) Phytoplankton dynamics in the stratified water column of Lake Bonney, Antarctica: biomass and productivity during the winter-spring transition. *Polar Biol* **16**:155-162
- Los D, Mironov K, Allakhverdiev S.** (2013) Regulatory role of membrane fluidity in gene expression and physiological functions. *Photosynth Res* **116**:489-09
- Los DA, Murata N.** (2002) Sensing and responses to low temperature in cyanobacteria. In: Storey KB, Storey JM, Eds. *Sensing, Signalling and Cell Adaptation.* Amsterdam, Elsevier Science BV, pp. 139-53
- Los DA, Murata N.** (2004) Membrane fluidity and its roles in the perception of environmental signals. *Biochim Biophys Acta* **1666**:142-57
- Lucker B, Kramer D.** (2013) Regulation of cyclic electron flow in *Chlamydomonas reinhardtii* under fluctuating carbon availability. *Photosyn Res* **117**:449-59

- Mancuso Nichols CA, Garon S, Bowman JP, Raguénès G, Guézennec J.** (2004) Production of exopolysaccharides by Antarctic marine bacterial isolates. *J Appl Microbiol* **96**: 1057-66
- Melis A, Murakami A, Nemson JA, Aizawa K, Ohki K, Fujita Y.** (1996) Chromatic regulation in *Chlamydomonas reinhardtii* alters photosystem stoichiometry and improves the quantum efficiency of photosynthesis. *Photosyn Res* **47**:253-65
- Miskiewicz E, Ivanov AG, Hüner NPA.** (2002) Stoichiometry of the photosynthetic apparatus and phycobilisome structure of the cyanobacterium *Plectonema boryanum* UTEX 485 are regulated by both light and temperature. *Plant Physiol* **130**:1414-25
- Mitchell R, Spillmann A, Haehnel W.** (1990) Plastoquinol diffusion in linear photosynthetic electron transport. *Biophys J* **58**:1011-24
- Moorhead DL, Doran PT, Fountain AG, Lyons WB, McKnight DM, Prisco JC, Virginia RA, Wall DH.** (1999) Ecological legacies: impacts on ecosystems of the McMurdo Dry Valleys. *BioScience* **49**:1009-19
- Morgan RM, Ivanov AG, Prisco JC, Maxwell DP, Hüner NPA.** (1998) Structure and composition of the photochemical apparatus of the Antarctic green alga, *Chlamydomonas subcaudata*. *Photosyn Res* **56**:303-14
- Morgan-Kiss RM, Ivanov AG, Hüner NPA.** (2002) The Antarctic psychrophile, *Chlamydomonas subcaudata*, is deficient in state I-state II transitions. *Planta* **214**:435-45
- Morgan-Kiss R, Ivanov AG, Williams J, Khan M, Hüner NPA.** (2002) Differential thermal effects on the energy distribution between photosystem II and photosystem I in thylakoid membranes of a psychrophilic and a mesophilic alga. *Biochim Biophys Acta* **1561**:251-65
- Morgan-Kiss RM, Ivanov AG, Pockock T, Krol M, Gudynaite-Savitch L, Hüner NPA.** (2005) The Antarctic psychrophile, *Chlamydomonas raudensis* Ettl (UWO241) (Chlorophyceae, Chlorophyta) exhibits a limited capacity to photoacclimate to red light. *J Phycol* **41**:791-800
- Morgan-Kiss R, Prisco JC, Pockock T, Gudynaite-Savitch L, Hüner NPA.** (2006) Adaptation and acclimation of photosynthetic microorganisms to permanently cold environments. *Microbiol Mol Biol Rev* **70**:222-52
- Munekage Y, Hojo M, Meurer J, Endo T, Tasaka M, Shikanai T.** (2002) PGR5 is involved in cyclic electron flow around photosystem I and is essential for photoprotection in *Arabidopsis*. *Cell* **110**:361-71
- Munekage Y, Hashimoto M, Miyake C, Tomizawa K, Endo T, Tasaka M, Shikanai T.** (2004) Cyclic electron flow around photosystem I is essential for photosynthesis. *Nature* **429**:579-82
- Murata N, Los DA.** (1997) Membrane fluidity and temperature perception. *Plant Physiol* **115**:875-9

- Nagao M, Matsui K, Uemura M.** (2008) *Klebsormidium flaccidum*, a charophycean green alga, exhibits cold acclimation that is closely associated with compatible solute accumulation and ultrastructural changes. *Plant Cell Environ* **31**:872-85
- Napolitano MJ, Shain DH.** (2004) Four kingdoms on glacier ice: convergent energetic processes boost energy levels as temperatures fall. *Proc Biol Sci* **271**:S273-6
- Napolitano MJ, Shain DH.** (2005) Distinctions in adenylate metabolism among organisms inhabiting temperature extremes. *Extremophiles* **9**:93-8
- Neale PJ, Pricu JC.** (1995) The photosynthetic apparatus of phytoplankton from a perennially ice-covered Antarctic lake: acclimation to an extreme shade environment. *Plant Cell Physiol* **36**: 253-63
- Nishida I, Murata N.** (1996) Chilling sensitivity in plants and cyanobacteria: the crucial contribution of membrane lipids. *Ann Rev Plant Physiol Plant Mol Biol* **47**:541-68
- Pocock TH, Koziak A, Rosso D, Falk S, Hüner NPA.** (2007) *Chlamydomonas raudensis* (UWO241), chlorophyceae, exhibits the capacity for rapid d1 repair in response to chronic photoinhibition at low temperature. *J Phycol* **43**:924-36
- Pocock T, Lachance MA, Pröschold T, Priscu JC, Kim SS, Hüner NPA.** (2004) Identification of a psychrophilic green alga from Lake Bonney Antarctica: *Chlamydomonas raudensis* Ettl. (UWO 241) Chlorophyceae. *J Phycol* **40**:1138-48
- Pocock T, Vetterli A, Falk S.** (2011) Evidence for phenotypic plasticity in the Antarctic extremophile *Chlamydomonas raudensis* Ettl. UWO 241. *J Exp Bot.* **62**:1169-77
- Possmayer M, Berardi G, Beall BFN, Trick CG, Hüner NPA, Maxwell DP.** (2011) Plasticity of the psychrophilic green alga *Chlamydomonas raudensis* (UWO 241) (Chlorophyta) to supraoptimal temperature stress. *J Phycol* **47**:1098-09
- Pörtner HO, Peck LS, Zielinski S, Conway LZ.** (1999) Intracellular pH and energy metabolism in the highly stenothermal Antarctic bivalve *Limopsis marionensis* as a function of ambient temperature. *Polar Biol* **22**:17-30
- Priscu JC.** (1998) Ed. *Ecosystem Dynamics in a Polar Desert: The McMurdo Dry Valleys, Antarctica*. Vol. 72, Antarctic Research Series. Washington: AGU Press
- Priscu JC, Fritsen CH, Adams EE, Giovannoni SJ, Paerl HW, McKay CP, Doran PT, Gordon DA, Lanoil BD, Pinckney JL.** (1998) Perennial Antarctic lake ice: an oasis for life in a polar desert. *Science* **280**:2095-98
- Raymond JA, Morgan-Kiss R.** (2013) Separate origins of ice-binding proteins in Antarctic *Chlamydomonas* species. *PLoS One* **8**:e59186
- Rochaix JD.** (2011) Regulation of photosynthetic electron transport. *Biochim Biophys Acta* **1807**: 375-83
- Sinensky M.** (1974) Homeoviscous adaptation—a homeostatic process that regulates the viscosity of membrane lipids in *Escherichia coli*. *Proc Natl Acad Sci USA.* **71**:522-25

- Spigel RH, Priscu JC.** (1996) Evolution of temperature and salt structure of Lake Bonney, a chemically stratified Antarctic lake. *Hydrobiologia* **321**:177-90
- Szyszkka B, Ivanov AG, Hüner NPA.** (2007) Psychrophily is associated with differential energy partitioning, photosystem stoichiometry and polypeptide phosphorylation in *Chlamydomonas raudensis*. *Biochim Biophys Acta* **1767**:789-00
- Takahashi H, Clowez S, Wollman FA, Vallon O, Rappaport F.** (2013) Cyclic electron flow is redox-controlled but independent of state transition. *Nat Commun* **4**:1954
- Takizawa K, Takahashi S, Hüner NPA, Minagawa J.** (2009) Salinity affects the photoacclimation of *Chlamydomonas raudensis* Ettl UWO241. *Photosynth Res* **99**:195-03
- Thomas DN, Dieckmann GS.** (2002) Antarctic sea ice – a habitat for extremophiles. *Science* **295**:641-44
- Tikkanen M, Gollan P, Suorsa M, Kangasjarvi S, Aro EM.** (2012) STN7 operates in retrograde signalling through controlling redox balance in the electron transfer chain. *Front Plant Sci* **3**:277
- Trebst A.** (1980) Inhibitors in electron flow: tools for the functional and structural localization of carriers and energy conservation sites. *Methods Enzymol* **69**:675-15
- Tikkanen M, Nurmi M, Kangasjarvi S, Aro E-M.** (2008) Core protein phosphorylation facilitates the repair of photodamaged photosystem II at high light. *Biochim Biophys Acta* **1777**:1432-7
- Van den Burg B.** (2003) Extremophiles as a source for novel enzymes. *Curr Opin Microbiol* **6**:213-8
- Vener AV.** (2006) Phosphorylation of thylakoid proteins. In: Demmig-Adams B, Adams III, WW, Mattoo AK, Eds. *Advances in Photosynthesis and Respiration. Photoprotection, Photoinhibition, Gene Regulation and Environment*. Dordrecht, Kluwer Academic, pp. 107-126
- Wilson KE, Hüner NPA.** (2000) The role of growth rate, redox-state of the plastoquinone pool and the trans-thylakoid Delta pH in photoacclimation of *Chlorella vulgaris* to growth irradiance and temperature. *Planta* **212**:93-02
- Wilson KE, Ivanov AG, Öquist G, Grodzinski B, Sarhan F, Hüner NPA.** (2006) Energy balance, organellar redox status and acclimation to environmental stress. *Can J Bot* **84**:1355-70
- Wollman FA.** (2001) State transitions reveal the dynamics and flexibility of the photosynthetic apparatus. *EMBO J* **20**:3623-30
- Wada H, Gombos Z, Sakamoto T, Murata N.** (1993) Role of lipids in low temperature adaptation. In: Yamamoto HY, Smith CM, Eds. *Current Topics in Plant Physiology: Photosynthetic Responses to the Environment*. Amer Soc Plant Physiol **8**:78-87
- Wunder T, Liu Q, Aseeva E, Bonardi V, Leister D, Pribil M.** (2013) Control of STN7 transcript abundance and transient STN7 dimerisation are involved in the regulation of STN7 activity. *Planta* **237**:541-58

- Yamazaki JY, Suzuki T, Maruta E, Kamimura Y.** (2005) The stoichiometry and antenna size of the two photosystems in marine green algae, *Bryopsis maxima* and *Ulva pertusa*, in relation to the light environment of their natural habitat. *J Exp Bot* **56**:1517–23
- Zer H, Vink M, Keren N, Dilly-Hartwig HG, Paulsen H, Herrmann RG, Andersson B, Ohad I.** (1999) Regulation of thylakoid protein phosphorylation at the substrate level: reversible light-induced conformational changes expose the phosphorylation site of LHCII. *FEBS J* **96**:8277-82
- Zito F, Finazzi G, Delosme R, Nitschke W, Picot D, Wollman FA.** (1999) The Qo site of cytochrome b₆/f complexes controls the activation of the LHCII kinase. *EMBO J* **18**:2961-69

Chapter 2

2 The Antarctic psychrophile, *Chlamydomonas sp.* UWO 241, preferentially phosphorylates a PSI-cytochrome b₆/f supercomplex

2.1 Introduction

The Antarctic psychrophilic green alga, *Chlamydomonas sp.* UWO 241, originates from the lowest trophic zone of lake Bonney, which is characterized by an extremely stable environment of low temperatures (4°C to 6°C), low irradiance (<50 $\mu\text{mol photons m}^{-2} \text{s}^{-1}$), high salt concentrations (700 mM) and a narrow spectral distribution enriched in the blue-green region (Lizotte and Priscu 1992; Morgan-Kiss et al. 2006). Adaptation of UWO 241 to this unique natural aquatic environment has resulted in the evolution of a structurally and functionally distinct photosynthetic apparatus relative to the mesophilic strains *C. raudensis* SAG 49.72 (Pocock et al. 2004) and the model green alga, *C. reinhardtii* (Morgan et al. 1998; Morgan-Kiss et al. 2006). UWO 241 is a halo-tolerant psychrophile (Morgan-Kiss et al. 2006; Takizawa et al. 2009), which dies at temperatures of 20°C or higher (Possmayer et al. 2011). This is consistent with the fact that temperature response curves for light saturated rates of CO₂-saturated O₂ evolution indicate that UWO 241 photosynthesizes maximally at 8°C at rates that are comparable to rates of the mesophile, *C. reinhardtii*, grown and measured at 29°C (Pocock et al. 2007). Although UWO 241 exhibits a low quantum requirement for photoinhibition and the degradation of the PSII reaction center polypeptide D1 (PsbA), this is complemented by a rapid, light-dependent recovery of PSII photochemistry associated with the *de novo* biosynthesis of D1 at low temperature (Pocock et al. 2007). Thus, this psychrophile appears to be photosynthetically adapted to growth at low temperature (Pocock et al. 2007).

UWO 241, exhibits significantly enhanced fatty acid unsaturation associated with all of the major thylakoid lipid classes (MGDG, DGDG, SQDG and PG) as well as a 2- to 10-fold increase in the unique, unsaturated fatty acid, 16:4, depending on the specific thylakoid lipid species (Morgan-Kiss et al. 2002b). Consequently, biophysical

determination of the critical temperature (T_{crit}) for thylakoid membrane destabilization for UWO 241 (40°C) was significantly lower than that for *C. reinhardtii* (50°C) which is consistent with the adaptation of UWO 241 to low temperature (Morgan-Kiss et al. 2002b).

Biochemical analyses of the Chl-protein complexes coupled with immunoblots of their constituent polypeptides indicate that UWO 241 exhibits abundant PSII light harvesting complex associated with a low Chl a/b ratio (1.8-2.0) relative to the mesophiles, SAG 49.72 and *C. reinhardtii* (Chl a/b = 3.0). In addition, UWO 241 exhibits an unusually low level of PSI such that the stoichiometry of PSI/PSII was estimated to be about 0.5 in UWO 241 whereas the mesophiles, SAG 49.72 and *C. reinhardtii*, exhibited a PSI/PSII of about 1.0 grown under optimal growth conditions. These biochemical data were confirmed by measurements of P700 photo-oxidation (Morgan-Kiss et al. 2002a; Szyszka et al. 2007) which indicated that UWO 241 exhibits high rates of PSI cyclic electron flow (CEF) (Morgan-Kiss et al. 2002a).

Recently, we reported that acclimation of UWO 241 to low temperature and low growth irradiance results in alterations in the partitioning of excess excitation energy to maintain cellular energy balance compared to the mesophile, *Chlamydomonas raudensis* SAG 49.72 (Szyszka et al. 2007). While SAG 49.72 favours energy partitioning for photoprotection through the induction of the xanthophyll cycle, the psychrophilic strain, UWO 241, favours energy partitioning for photoprotection through constitutive quenching processes involved in energy dissipation even though UWO 241 exhibits an active xanthophyll cycle (Szyszka et al. 2007; Pocock et al. 2007). Although the molecular basis of the constitutive quenching process for photoprotection has not been elucidated unequivocally, it has been suggested that PSII reaction center quenching through charge recombination may contribute to this non-radiative, energy dissipative pathway (Hüner et al. 2006; Sane et al. 2012). One consequence of this enhanced energy quenching capacity of UWO 241 is that the psychrophile does not exhibit any pigment change in response to photoacclimation (Morgan-Kiss et al. 2006) typically observed for other mesophilic green algae such as *C. reinhardtii*, *D. tertiolecta* (Escoubas et al. 1995), *D. salina* (Smith et al. 1990; Maxwell et al. 1995b) and *Chlorella vulgaris* (Maxwell et

al. 1995a; Wilson et al. 2003). In addition, maximum growth rates of UWO 241 are sensitive to light quality since rates of growth and photosynthesis are inhibited under red light which result in increased excitation pressure in the psychrophile (Morgan-Kiss et al. 2005).

However, the most unusual feature of UWO 241 is that it represents a natural variant that is deficient in state transitions (Morgan-Kiss et al. 2002a; Takizawa et al. 2009). State transitions have been well documented as a short-term mechanism for photoacclimation employed by algae and plants to balance light excitation between PSII and PSI (Allen et al. 1981; Allen 2003; Eberhard et al. 2008; Rochaix 2011). Over-excitation of PSII relative to PSI results in the phosphorylation of several peripheral chlorophyll a/b-binding LHCII proteins, which causes their dissociation from the photosystem II core and subsequent association with photosystem I (Eberhard et al. 2008; Rochaix et al. 2011). As a result, excitation energy is redistributed in favour of PSI at the expense of PSII. Phosphorylation of light harvesting complex II polypeptides is essential in the regulation of state transitions and energy distribution between the two photosystems (Allen 2003; Eberhard et al. 2008; Kargul and Barber 2008; Rochaix 2011). LHCII phosphorylation is initiated by modulation of the redox state of the PQ pool which is sensed through the preferential binding of plastoquinol to the Q_o site of the Cyt b₆/f complex. As a consequence, the thylakoid protein kinases STT7 in *Chlamydomonas reinhardtii* and its orthologue, STN7, in *Arabidopsis thaliana* are activated and LHCII is phosphorylated (Rochaix 2011; Wunder et al. 2013). Similar to all other photosynthetic organisms, the LHCII polypeptides represent the major phosphorylated polypeptides detected in thylakoids of the mesophile, SAG 49.72 (Szyszka et al. 2007). Consistent with a deficiency in state transitions, UWO 241 does not phosphorylate the major LHCII polypeptides in response to changes in either growth irradiance or growth temperature (Morgan-Kiss et al. 2002; Szyszka et al. 2007; Takizawa et al. 2009). In fact, UWO 241 exhibits a unique thylakoid membrane phosphorylation profile compared to either SAG 49.72 or *C. reinhardtii* (Morgan-Kiss et al. 2005; Szyszka et al. 2007; Takizawa et al. 2009). Rather than phosphorylation of LHCII polypeptides, UWO 241 preferentially phosphorylates several novel high molecular mass polypeptides (>70 kDa) (Morgan-Kiss et al. 2002a; Szyszka et al. 2007).

The Cyt b_6/f complex of the photosynthetic intersystem electron transport chain is essential in the regulation of state transitions and activation of the STT7 kinase (Rochaix 2011). The Cyt b_6/f complex of UWO 241 exhibits a unique Cyt f that is 7kD smaller than the expected molecular mass of 41 kD exhibited by *C. reinhardtii* based on SDS-PAGE (Morgan-Kiss et al. 2006; Gudynaite-Savitch et al. 2006; 2007). No other differences in the structure and composition of the Cyt b_6/f complex are apparent. Sequencing of the entire *petA* from UWO 241 indicated that amino acid sequence of the Cyt f from UWO 241 exhibited 79% identity to that of *C. reinhardtii*. Through domain swapping between *petA* of UWO 241 and that of *C. reinhardtii* and subsequent transformation of a $\Delta petA$ mutant of *C. reinhardtii* with the chimeric gene constructs, we reported that the apparent differences in molecular masses observed for *petA* in UWO 241 are due to differences in the amino acid sequences of the small domain of Cyt f . However, complementation of the $\Delta petA$ mutant of *C. reinhardtii* with the entire *petA* from either UWO 241 or *C. reinhardtii* completely restored the capacity for state transitions in the $\Delta petA$ mutant. Thus, we concluded that the changes in the amino acid sequence of the small domain of Cyt f of UWO 241 can not account for inability of UWO 241 to undergo state transitions (Gudynaite-Savitch et al. 2006; 2007).

Since state transitions are inhibited in UWO 241, I hypothesized that the unique protein phosphorylation pattern observed in UWO 241 reflects an alternative mechanism to regulate energy flow within the photosynthetic apparatus of this Antarctic psychrophile. Thus, the objective of the present research was to identify and characterize the high molecular mass polypeptides phosphorylated in the psychrophile, UWO 241. We report that *Chlamydomonas sp.* UWO 241 preferentially phosphorylates specific polypeptides associated with a PSI-Cyt b_6/f supercomplex. The role of the PSI-Cyt b_6/f supercomplex and its phosphorylation status in the regulation of PSI cyclic electron transport in UWO 241 is discussed. We suggest that adaptation of *Chlamydomonas sp.* UWO 241 to its unique low temperature and low light environment favours phosphorylation of a PSI-Cyt b_6/f supercomplex to regulate PSI cyclic electron transport rather than regulation of state transitions through the phosphorylation of LHCII proteins.

2.2 Materials and methods

2.2.1 Growth conditions

Chlamydomonas raudensis SAG 49.72 and *Chlamydomonas reinhardtii* 1690 were grown axenically in Bold's basal medium (BBM) at 24°C, whereas the psychrophilic strain *C. raudensis* UWO 241 was grown in BBM supplemented with 0.7 M NaCl at 5°C. All cell cultures were aerated continuously under ambient CO₂ conditions in 4L glass Pyrex bottles and grown under an irradiance of 250 μmol photons m⁻² s⁻¹ which was generated by fluorescent tubes (Sylvania CW-40). To assess the effects salt concentration on the structure and organization of PSI, *C. raudensis* UWO 241 cells were grown in BBM media supplemented with either 70 mM or 700 mM NaCl. Mid-log phase cells were used in all experiments.

2.2.2 Blue native PAGE

Cells were disrupted by passing the suspension through a chilled French press at 6000 lb/in², twice. Thylakoid membranes were purified through a sucrose step gradient centrifugation procedure as described previously (Chua and Bennoun 1975). Isolated thylakoid membranes were diluted in dH₂O at a chlorophyll concentration of 2.0 mg/mL and solubilized with 2% (w/v) β-DDM (Sigma) on ice for 30 min and centrifuged at 20000 g for 30 min to remove unsolubilized material. The supernatant was supplemented with 0.25 volume of sample buffer (50 mM BisTris-HCl, pH 7.2, 50 mM NaCl, 10% (w/v) glycerol, 0.001% (w/v) Ponceau S and 0.1 volume of a solution containing 5% (w/v) Serva Blue G and 750 mM ε-aminocaproic acid and subjected to BN-PAGE using 4-16% (w/v) acrylamide gradient gels (Invitrogen). Electrophoresis was performed at 4°C at 15 mA for 1.5 hours. For protein separation in the second dimension, the lanes were excised and incubated with 1% (v/v) β-mercaptoethanol and 1% (w/v) SDS for 10 minutes at room temperature, rinsed with dH₂O and subjected to SDS-PAGE as described below. NaF was present at a final concentration of 20 mM throughout the thylakoid isolation and purification procedure, except where noted, to inhibit any phosphatase activity and to ensure maximum protein phosphorylation.

2.2.3 SDS-PAGE and immunoblotting

Thylakoids were isolated as described in (Morgan-Kiss et al. 2005). Total thylakoid preparations from all three *Chlamydomonas* strains were solubilized in a 60 mM Tris (pH 7.8) buffer containing 1 mM EDTA, 12% (w/v) sucrose, 1% (w/v) DTT and 2% (w/v) SDS to attain an SDS:Chl ratio of 20:1. Total thylakoid samples were loaded on an equal chlorophyll basis. Purified complex fractions isolated by sucrose density centrifugation were solubilized with 1% (w/v) SDS and 1% (v/v) β -mercaptoethanol, and loaded on a chlorophyll basis with the following content : thylakoids 1.4 μ g; LHCII 0.6 μ g; PSII 0.5 μ g; PSI 1.1 μ g; 'SC' 0.9 μ g Chl per lane. These concentrations were used to achieve optimal detection of complex subunits and were calculated based on chlorophyll/protein ratios and estimated protein number/complex values.

Electrophoresis was performed using a Mini-Protean II apparatus (Bio-Rad) with a 12% (w/v) polyacrylamide resolving gel, containing 6 M Urea, 0.66 M Tris (pH 8.8) and 8% (w/v) polyacrylamide stacking gel, containing 0.125 M Tris (pH 6.8) using the Laemmli buffer system (Laemmli 1970). In-gel heme staining was detected by peroxidase activity in the presence of 3,3',5,5'-tetramethylbenzidine (TMBZ) as described previously (Thomas et al. 1976). Proteins separated by SDS-PAGE were stained with Coomassie blue or transferred electrophoretically to nitrocellulose membranes (Bio-Rad, 0.2 μ m pore size) at 100 V for 1 h at 5°C. The membranes were pre-blocked with a Tris-buffered salt (20 mM Tris, pH 7.5; 150 mM NaCl) containing 5% (w/v) skim milk powder and 0.01% (v/v) Tween 20. Membranes were probed with various antibodies as indicated in the figures at the following dilutions: PsaA at 1:2000; PsaD at 1:5000; PsaC 1:2000; Lhca1 at 1:2000; PsaL at 1:5000; D1 at 1:5000; Cyt *f* 1:2000; Lhcb 3 at 1:2000; CP43 at 1:2000. Polyclonal phosphothreonine (Ph-Thr) antibody (Zymed Laboratories Inc.) was used at 1:500 dilution to immunodetect thylakoid phosphoproteins. After incubation with secondary antibodies conjugated with horseradish peroxidase (Sigma), the antibody-protein complexes were visualized using ECL chemiluminescent detection reagents (GE Healthcare).

2.2.4 Sucrose density gradient centrifugation

Cells were disrupted using a French press as described above. Thylakoid membranes were purified through a sucrose step gradient centrifugation procedure as described in (Chua and Bennoun 1975). Purified thylakoid membranes were resuspended in dH₂O at a chlorophyll concentration of 0.9 mg/mL and solubilized with 1% (w/v) β -DDM on ice for 25 min and centrifuged to remove unsolubilized material. Purified thylakoid membranes were loaded on a continuous 1.3-0.1 M sucrose density gradient and ultracentrifuged as previously described in (Takahashi et al. 1991). All buffers for both thylakoid isolation and complex purification were supplemented with either 20 mM NaF or 0.2 μ M staurosporine. Separated bands containing each complex were fractionated. Complexes were diluted 3 times with 20 mM Hepes, pH 7.5 and pelleted by centrifugation at 150 000g for 8 hours.

2.2.5 Isoelectrofocusing

Concentrated fractions of the PSI-supercomplex (SC) were precipitated with 4 volumes of 100% acetone for 1 hour at -20°C. The samples were centrifuged and the pellet was resuspended in 80% (v/v) acetone and 10 mM DTT. Samples were recentrifuged and the final pellets were dried with N₂. Isoelectric focusing was performed in a vertical mini-gel format as described by Anderson and Peck (2008). Samples were solubilized in IEF sample buffer (7 M urea, 2 M thiourea, 2% (w/v) CHAPS, 0.8% (v/v) ampholytes pH 3-10, 50 mM DTT, 4% (v/v) glycerol and a trace of bromophenol blue for one hour and centrifuged to remove insoluble material. IEF gels (9 M urea, 1% (w/v) CHAPS, 6% (v/v) polyacrylamide) were cast with 0.4% (v/v) broad range ampholytes (pH 3-10) and subjected to electrophoresis using a Mini-Protean II apparatus (Bio-Rad) with 25 mM Tris and 10 mM phosphoric acid in the upper and lower chambers, respectively. For separation of proteins in the second dimension, single lanes were excised from the focused gels and incubated with equilibration buffer (60 mM Tris pH 6.8, 2% (w/v) SDS, 0.1 M DTT and 10% (v/v) glycerol) for 10 minutes. Gel pieces were placed across 12% (w/v) SDS-PAGE gels and over-layed with equilibration buffer supplemented with 1% (w/v) agarose and a trace of bromophenol blue. Second dimension gels were incubated with 12% (v/v) TCA and stained with a modified Coomassie stain (27% (v/v) ethanol,

10% (v/v) acetic acid, 0.08% (w/v) Coomassie R-250, 0.5% (w/v) CuSO₄) to reduce background staining of ampholytes or immunoblotted as described above.

2.2.6 Low temperature (77K) fluorescence

Samples of purified thylakoids and complex fractions were pipetted into NMR tubes, frozen in liquid nitrogen and excited at 436 nm (QuantaMaster, Photon Technology International Canada, London, Ontario) and emission spectra were collected between 650 and 800 nm using a 814 Photomultiplier Detection System fluorometer (PTI Canada), with Felix32 Analysis Module (V1.2) software (PTI Canada). A slit width of 4 nm was used for both excitation and emission. Chlorophyll concentration ranged from 5-12 µg/mL and spectra were normalized to a maximum signal value of 1.0 for comparison. All spectra were corrected for the wavelength dependence of the detector.

2.2.7 Measurements of P700 photooxidation

Far-red light induced photooxidation of P700 in SAG4972 and UWO241 *Chlamydomonas* strains was estimated as a change in absorbance around 820 nm ($\Delta A_{820-860}$) using a PAM-101 chlorophyll fluorescence measuring system equipped with a dual wavelength emitter-detector ED-P700DW and PAM-102 units (Heinz Walz GmbH, Effeltrich, Germany) as described in detail earlier (Klughammer and Schreiber 1991; Ivanov et al. 2000). Samples were prepared as described by Herbert et al. (1995). The relative redox state of P700 was determined *in vivo* under ambient CO₂ conditions at the corresponding growth temperature of 5°C (UWO241) or 25°C (SAG4972). Far red light (FR; λ_{\max} = 715 nm, 10 W m⁻², Schott filter RG 715) was provided by a FL-101 light source. After reaching a steady state level of P700⁺ in the presence of FR background, ST (half peak width 14 µs) and MT (50 ms) pulses of AL were applied with a XMT-103 and XST-103 power/control units, respectively, via a multibranching fibre optic system connected to the emitter-detector unit and the cuvette.

Alternatively, the P700 photo-oxidation was monitored in the presence of white actinic light (AL) exciting both PSI and PSII as described in Ivanov et al. 2012. White AL (150 µmol photons m⁻²s⁻¹) was provided by a Schott lamp (KL 1500, Schott Glaswerke, Mainz, Germany) and controlled from a Walz PAM-103 Trigger Control Unit.

The P700 transients were measured in the absence and presence of the following inhibitors of electron transport: 40 μM DCMU and 20 μM Antimycin A (AA). Freshly prepared stock solutions of DCMU and AA in 95% (v/v) ethanol were added to the cell suspension to a final solvent concentration of 0.5% (v/v). Samples were pre-incubated for 15 min in the dark at the corresponding growth temperatures in either the presence or absence of DCMU and AA prior to the measurement. Data analysis was performed using a MicrocalTM OriginTM Version 7.0 software package (Microcal Software Inc., Northampton, MA, USA).

2.2.8 Sample preparation for nano-LC-ESI-MS/MS

In-gel digestion was performed using a MassPREP automated digester station (PerkinElmer). Gel pieces were Coomassie destained using 50 mM ammonium bicarbonate and 50% (v/v) acetonitrile which was followed by protein reduction using 10 mM dithiothreitol (DTT), alkylation using 55 mM iodoacetamide (IAA), and tryptic digestion. Peptides were extracted using a solution of 1% (v/v) formic acid and 2% (v/v) acetonitrile and lyophilized. Prior to mass spectrometric analysis, dried peptide samples were re-dissolved in water and 0.1% (v/v) formic acid for LC-MS/MS analysis.

2.2.9 Liquid chromatography nano-tandem mass spectrometry (nano-LC-ESI-MS/MS) analysis

Between 50% and 100% of each original sample was injected on a NanoAcquity UPLC (ultra performance liquid chromatography) (Waters) equipped with a 25 cm \times 75 μm C18 reverse phase column employing a 60-min LC gradient [5–40% (v/v) ACN, 0.1% (v/v) formic acid] and detected in a data-dependent acquisition mode by tandem MS (Q-ToF Ultima; Waters). The MS was directed to use the following data-dependent acquisition parameters: survey scans range 300 or 400–1800 m/z , 1 s scans, 1–4 precursors selected based on charge state (+2, +3 and, +4 ions). MS/MS fragmentation was then performed on the ions using the charge-state collision energy profile function. Raw data were converted to .pkl format using PLGS 2.2.5 (Protein Lynx Global Server, Waters Corp). The resulting .pkl file was processed by Peaks (BSI) for deNovo sequencing, and homology searching against NCBI green plants. The following settings were used: mass

error of 0.15 Da, fixed mod for Carbamidomethyl Cysteine, Variable mod for oxyM, Phospho STY, Iodo Y.

2.3 Results

2.3.1 2D-Blue native gel electrophoresis of thylakoid protein complexes

Fig. 2.1A (arrow) indicates that the mesophile, *Chlamydomonas raudensis* SAG 49.72, and the psychrophile, *Chlamydomonas sp.* UWO 241, exhibited comparable levels of LCHII polypeptides. Consistent with previous published data (Szyszka et al. 2007), SAG 49.72 exhibited the expected phosphorylation of LHCII, the core PSII complex CP43 as well as the reaction centre polypeptide, D1 (Fig. 2.1B). In contrast, the psychrophile, UWO 241 exhibited minimal phosphorylation of these PSII and LHCII polypeptides but rather exhibited major thylakoid protein phosphorylation bands at a molecular mass greater than 130 kD as well as a polypeptide of about 17 kD (Fig. 2.1B, arrows). As an initial step in the identification and characterization of these novel phosphorylated thylakoid protein(s) in UWO 241, we used 2D-non-denaturing blue-native polyacrylamide gel electrophoresis (2D-BN-PAGE) which allowed for the separation of more than 50 different polypeptide subunits which represent components of thylakoid multi-subunit complexes (Kugler et al. 1997).

Thylakoid membranes from SAG 49.72 (Fig. 2.2A, lanes 1 and 2) and UWO 241 (Fig. 2.2A, lanes 3 and 4) were solubilized in the presence of β -dodecyl maltoside, and the resultant intact protein complexes separated in the first dimension on a blue-native gel according to their molecular mass. Although both the SAG 49.72 and UWO 241 exhibited the presence of 9 thylakoid protein complexes of molecular masses that varied between 150 and 750 kD, the relative abundances of these protein complexes varied dramatically (Fig. 2.2A). To identify these protein complexes, the first dimension was subjected to SDS-PAGE (Fig. 2.2B) and subsequently probed with specific antibodies to major thylakoid protein complexes (Fig. 2.2C) which allowed us to identify most of the major complexes separated in the first dimension (Fig. 2.2A). Separation of thylakoid complexes by blue native gel electrophoresis revealed several differences between the

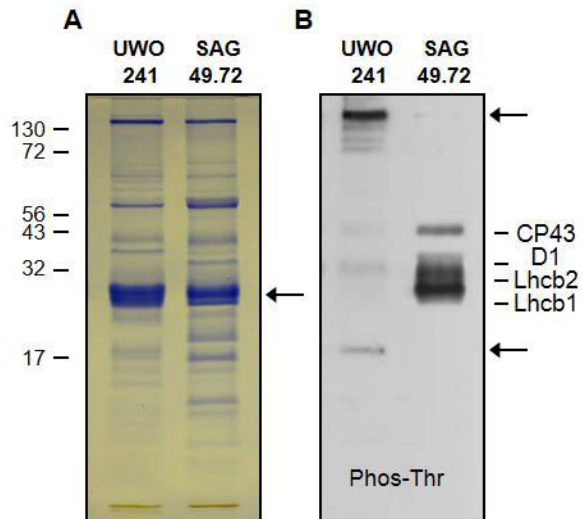


Figure 2.1: Phosphorylation profile of UWO 241 and SAG 49.72. Thylakoid membrane proteins (arrow indicates major LHCII polypeptides) were isolated in the presence of 20 mM NaF and separated by SDS-PAGE, stained with Coomassie (A). Corresponding membranes were probed with antibodies specific for phospho-threonine (B). Arrow indicates the novel, high molecular mass protein phosphorylated band in UWO 241. Apparent molecular masses are indicated on the left (kDa).

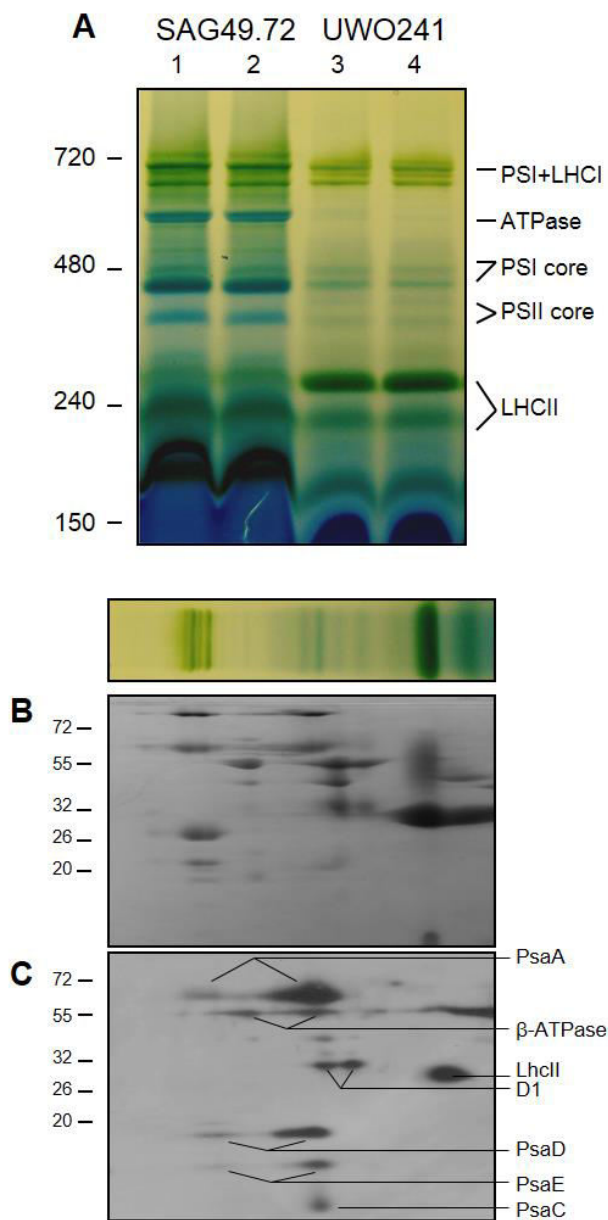


Figure 2.2: Blue-native PAGE of thylakoid membrane complexes and subsequent identification of SDS-solubilized complex subunits. Pure thylakoids of SAG 49.72 and UWO 241 were solubilized with 1% (w/v) n-dodecyl- β -maltoside, loaded on an equal chlorophyll (50 μ g) basis and separated on a 3-16% gradient native gel (A). Separated complexes of UWO 241 were denatured and the resulting subunits were run on SDS-PAGE. Second dimension gels of UWO 241 were stained with Coomassie (B) and immunoblotted with specific antibodies for subunits of each thylakoid membrane complex (C). Molecular masses are indicated on the left (kDa).

major thylakoid membrane complexes of SAG 49.72 and UWO 241. Consistent with previous results (Morgan et al. 1998), UWO 241 exhibited a decreased abundance of PSI+LHCI complexes, which migrate at ~700 kDa (Fig. 2.2A). The majority of the LHCII complexes from the mesophilic strain migrated as a band of lower apparent molecular mass of ~240 kDa, compared to the major LHCII band of the psychrophile, LHCII structure and/or protein conformation. In addition, the ATPase, PSI and PSII core complexes in UWO 241 exhibited reduced G_{250} stain binding relative to those present in SAG 49.72 (Fig. 2.2A).

The second dimension SDS-PAGE gels indicated qualitative as well as quantitative differences in the polypeptide complement of the various thylakoid protein complexes present in SAG 49.72 (Fig. 2.3A) compared to UWO 241 (Fig. 2.3B). Subsequently, phosphothreonine antibodies were used to detect the phosphorylated polypeptides present in the intact membrane protein complexes of SAG 49.72 (Fig. 2.3C) and UWO 241 (Fig. 2.3D) separated in the first dimension. Immunoblot analysis of the second dimension indicated that SAG 49.72 exhibited a major phosphorylated polypeptide of 28-30 kDa associated with LHCII and hence, a component of the PSII complex (Fig. 2.3C, spot 3). In addition, two phosphorylated polypeptides of 43 and 32 kDa, respectively (Fig. 2.3C, spot 1 and 2) were identified as the PSII reaction core antenna polypeptide, CP43 (PsbC) and D1 (psbA), respectively. However, no phosphorylated polypeptides of molecular mass of 130 kDa or greater were detected in SAG 49.72 thylakoid membranes (Fig. 2.3C). Thus, as expected, the major sites of thylakoid protein phosphorylation in SAG 49.72 were the subunits of the PSII-LHCII supercomplex.

Even though UWO 241 exhibited significant levels of the PSII subunits D1, CP43 and LHCII, the psychrophile exhibited minimal phosphorylation of any of these PSII subunits, which is consistent with the results presented in Fig. 2.1. Instead, we detected the phosphorylation of a high molecular mass (>130 kDa) complex in UWO 241 (Fig. 2.3D, spot 1). These phospho-protein(s) originated from a large complex that migrated with an apparent molecular mass of ~1000 kDa, which is slightly larger than that of the PSI+LHCI antenna complex (~700 kDa) (Fig. 2.3B). In addition, the second phospho-

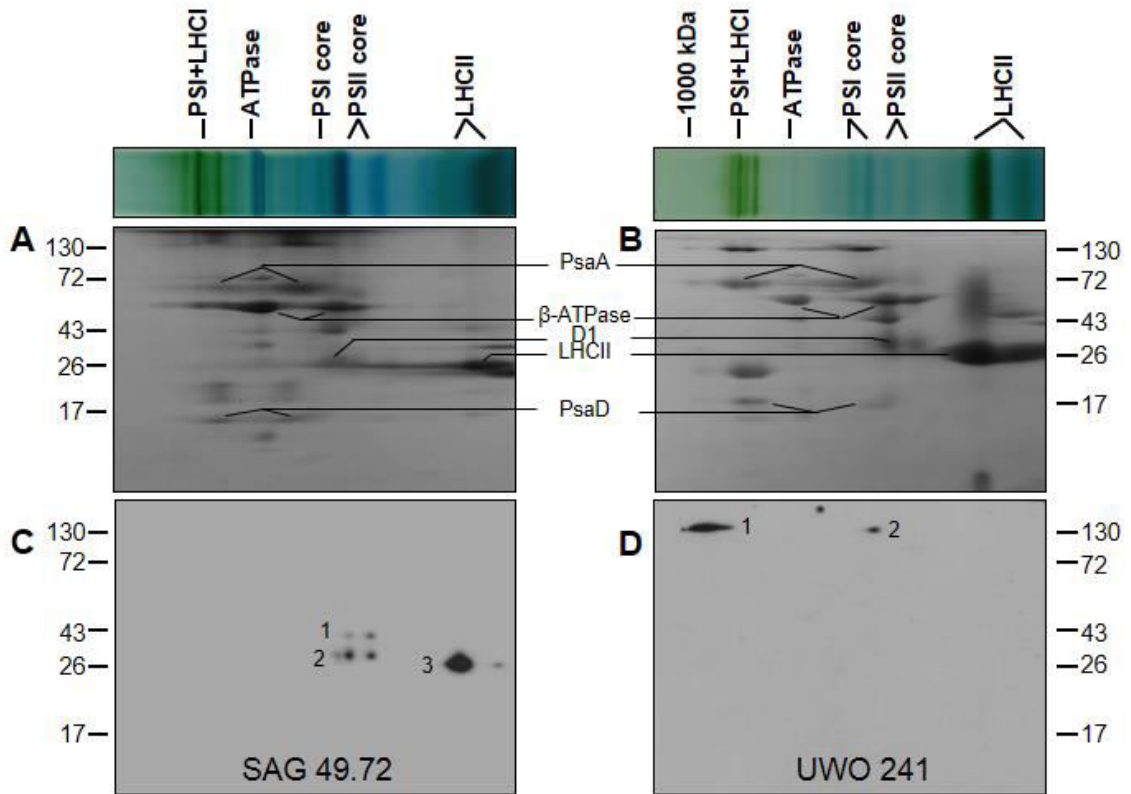


Figure 2.3: BN-PAGE and subsequent analysis of SDS-solubilized complexes. BN-PAGE gel strips from SAG 49.72 and UWO 241 were treated with 1% (w/v) SDS and β -mercaptoethanol and denatured subunits were separated using SDS-PAGE. (A) and (B), second dimension gels were stained with Coomassie blue. (C) and (D) represent corresponding membranes immunoblotted with phospho-threonine antibodies. Molecular masses are indicated (kDa).

protein migrated together with the PSI core complex (Fig. 2.3D, spot 2). Thus, phosphorylation in the mesophilic SAG 49.72 strain appeared to be associated with the PSII core complex and LHCII, while the psychrophile, UWO 241, exhibited phosphorylation of high molecular mass polypeptides (≥ 130 kDa). We hypothesized that the phosphoproteins detected in UWO 241 were components of a PSI-associated pigment-protein complex.

2.3.2 Fractionation and purification of thylakoid membrane complexes

To identify the specific subunits associated with the high molecular mass protein complex, that undergo phosphorylation in UWO 241, sucrose gradient centrifugation was performed in order to fractionate, isolate and purify the major pigment-protein complexes from thylakoid membranes of the psychrophile, UWO 241, and the mesophile, SAG 49.72 (Fig. 2.4A). The model green alga, *Chlamydomonas reinhardtii* strain 1690 was used as an additional internal control for comparison (Fig. 2.4A, 1690). Sucrose density ultracentrifugation of purified thylakoid membranes treated with n-dodecyl- β -D-maltoside (DDM) resulted in the separation of 4 distinct but comparable green bands in the mesophiles, SAG 49.72 and 1690 (Fig. 2.4A). Although UWO 241 also generated 4 distinct green bands, the densities and the relative proportions of the green bands in UWO 241 differed significantly from those observed in either SAG 49.72 or 1690 (Fig. 2.4A).

In all cases, band 1 was the major complex separated on the sucrose gradient based on Chl concentration. The absorption spectra (Fig. 2.4B) and Chl *a/b* ratios (Table 2.1) indicated that band 1 was a Chl *a/b* pigment protein complex in UWO 241 as well as in SAG 49.72 and 1690 (Appendix 2S1, A and B). The 77K fluorescence emission spectra for band 1 exhibited a single emission maximum between 678 and 681 nm (Fig. 2.4D, Appendix 2S1, E and F) which is consistent with the identification of band 1 as LHCII in all three samples (Krause and Weis 1991). Band 2 exhibited a Chl *a/b* ratio of between 6.99 and 8.57 (Table 2.1) and absorption spectra consistent with a Chl *a* pigment protein complex in SAG 49.72, 1690 (Appendix 2S1, A and B) as well as UWO 241 (Fig. 2.4B). The 77K fluorescence emission spectra of band 2 exhibited an emission maximum at 685

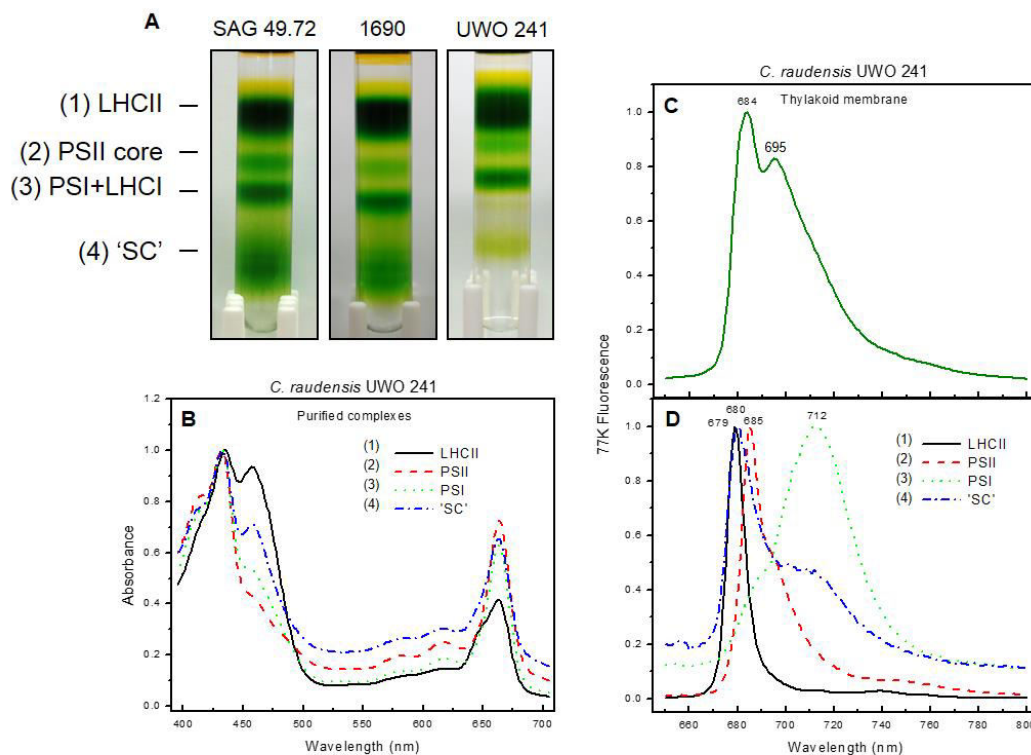


Figure 2.4: Fractionation of major thylakoid membrane complexes of SAG 49.72, UWO 241 and *C. reinhardtii* 1690. Thylakoid membranes were purified in the presence of NaF, solubilized with 1% (w/v) β -DDM, loaded on a continuous sucrose density gradient (1.3M-0.1M) and ultracentrifuged (A). 'SC' represents a band of high density 'supercomplexes'. Absorption spectra of fractionated complexes (B) following sucrose density centrifugation. 77K fluorescence emission spectra (C) of intact thylakoid membranes of UWO 241 and subsequent purified fractions of LHCII, PSII, PSI and 'SC' (D). Emission peak maxima are indicated above each peak (nm).

Table 2.1: Chlorophyll *a* to *b* ratios (\pm SE) of purified thylakoid membrane complexes from each algal strain. Individual complexes were isolated using sucrose gradient fractionation. Values followed by different letters are significantly different, as determined by ANOVA and Tukey's test ($p < 0.01$).

	Complex	<i>C. reinhardtii</i> 1690	<i>C. raudensis</i> SAG 49.72	<i>C. sp.</i> UWO 241
Chlorophyll a/b ratio	Band 1	1.50 \pm 0.04f	1.94 \pm 0.03e	1.32 \pm 0.12g
	Band 2	8.48 \pm 0.09a	8.57 \pm 0.40a	6.99 \pm 0.56b
	Band 3	7.33 \pm 0.52b	8.43 \pm 0.91ab	5.29 \pm 0.39c
	Band 4	4.98 \pm 0.45c	8.05 \pm 2.09ab	2.58 \pm 0.33d

nm and a shoulder at 695 nm which is consistent with the identification of band 2 as the PSII core complex (Krause and Weis 1991) (Fig. 2.4D, Appendix 2S1; E and F). Band 3 also exhibited a Chl *a/b* ratio of 5.29 to 8.43 (Table 2.1), and absorption spectra consistent with a Chl *a* pigment-protein complex in all three strains examined (Fig. 2.4B, Appendix 2S1; A and B). However, band 3 exhibited a single 77K fluorescence emission maximum between 712-715 nm, which is consistent with the tentative identification of this band as a PSI complex in both SAG 49.72 and 1690 as well as the psychrophile (Krause and Weis 1991) (Fig. 2.4D; Appendix 2S1, E and F). We note with interest that, as expected, a major PSI emission band between 706-708 nm was detected in purified thylakoids from SAG 49.72 and 1690 (Appendix 2S1, C and D). However, no major PSI emission band at 707 nm was detected in purified thylakoids from UWO 241 (Fig. 2.4C) even though purified PSI exhibited a 77K fluorescence emission maximum between 712-715 nm (Fig. 2.4D).

Band 4 exhibited a Chl *a/b* ratio of between 4.98 and 8.05 in the two mesophilic strains, SAG 49.72 and 1690 (Table 2.1) and absorption spectra consistent with a Chl *a* pigment-protein complex (Appendix 2S1, A and B). This complex exhibited an unusual 77K fluorescence emission spectrum with a prominent emission maximum at 715 nm and an emission maximum of lower intensity between 680-683 nm in both SAG 49.72 and 1690 (Appendix 2S1; E and F). In contrast, band 4 from UWO 241 exhibited a much lower Chl *a/b* ratio (2.58) than either SAG 49.72 or 1690 (Table 1) and a major 77K emission maximum at 680 nm with a shoulder at 712 nm (Fig. 2.4D).

To confirm the tentative identification of the individual Chl-protein complexes separated by sucrose density centrifugation based on spectral analyses, we examined the polypeptide composition of each green band by SDS-PAGE for SAG 49.72 (Fig. 2.5A); 1690 (Fig. 2.5B) and UWO 241 (Fig. 2.5C) coupled with immunoblotting (Fig. 2.5G). Fig. 2.5A, B and C indicates that band 1 consists of major polypeptides of about 24 kDa which react positively with Lhcb3 antibodies (Fig. 2.5G). The spectral data combined with the polypeptide analyses and immunoblots are consistent with the identification of band 1 as the major Chl *a/b* light harvesting complex of PSII in all three strains. SDS-PAGE of band 2 indicated that it contained 3 major polypeptides in the molecular mass

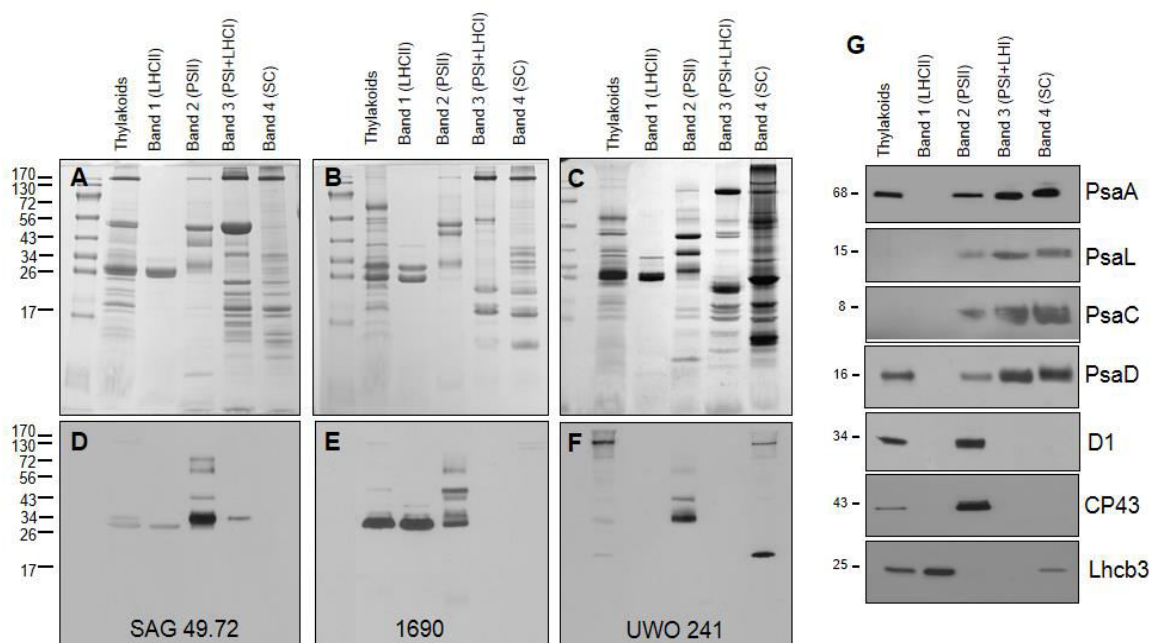


Figure 2.5: Immunoblot analysis of purified complexes from *C. raudensis* SAG 49.72, UWO 241 and *C. reinhardtii* 1690. Thylakoid membrane proteins and fractions isolated by sucrose density centrifugation from SAG 49.72 (A), 1690 (B) and UWO 241 (C) were Coomassie stained. Corresponding membranes from each of the strains were immunoblotted with phospho-threonine antibodies (D-F). (G), Corresponding membranes containing purified complexes from UWO 241 were probed with antibodies specific for various polypeptides, as indicated on the right. Molecular masses are indicated on the left (kDa), lane numbers are shown in brackets.

range of 32 to 47 kDa in all three strains (Fig. 2.5A,B,C). The immunoblots indicated that the major polypeptides of the pigment-protein complex associated with band 2 are the 32 kDa D1 (PsbA) and CP43 (Fig. 2.5G). The spectral data combined with the polypeptide analyses and immunoblots are consistent with the identification of band 2 as the PSII core-reaction centre complex. However, band 2 also exhibited minor levels of the PSI subunits psaA, PsaL, PsaC and PsaD but no detectable levels of Lhcb3 (Fig. 2.5G).

The major polypeptides associated with band 3 exhibited molecular masses in the 21 kDa range, the 50-60kDa range as well as a major, high molecular mass polypeptide >100 kDa (Fig. 2.5A,B,C). The immunoblots confirmed that this Chl-protein complex consisted of the major PSI reaction polypeptide, psaA, and the PSI subunits PsaL, PsaC and PsaD but no PSII subunits (D1, CP43) or Lhcb3 were detected in this fraction. The spectral data combined with the polypeptide analyses and immunoblots are consistent with the identification of band 3 as the PSI core-reaction centre-LHCI complex.

Similar to band 3, band 4 was a multi-subunit Chl *a* pigment-protein complex in all three strains examined (Fig. 2.5A,B,C) containing the PSI-associated subunits (psaA, psaL, psaC and psaD) but neither D1 nor CP43 associated with PSII (Fig. 2.5G). Since the 77K emission spectrum of band 4 was distinct from that of band 3, we suggest that band 4 represents a PSI pigment-protein complex distinct from the PSI core-reaction centre complex. Given that band 4 represents the highest density complex separated on the sucrose gradient, we suggest that band 4 may represent a putative PSI 'supercomplex' based on our spectral and polypeptide analyses.

For all 3 algal strains tested, purified pigment-protein complexes were subjected to denaturation by SDS-PAGE (Fig. 2.5, A-C) followed by immunodetection with phosphothreonine antibodies to detect the phosphorylated subunits in each complex (Fig. 2.5, D-F). We detected no major phosphorylated polypeptides associated with the PSI core complexes from either SAG 49.72 (Fig. 2.5D, Band 3), 1690 (Fig. 2.5E, Band 3) or UWO 241 (Fig. 2.5F, Band 3). However, phosphorylation of threonine residues in SAG 49.72 (Fig. 2.5D) and *C. reinhardtii* (Fig. 2.5E) were detectable for the major Lhcb polypeptides of LHCI (Fig. 2.5, D and E, Band 1) as well as the PSII core complex

polypeptides, D1 and CP43 (Fig. 2.5, D and E, Band 2). Although the PSII core complex polypeptides D1 and CP43 (Appendix 2S2, B and C) were phosphorylated in UWO 241 (Fig. 2.5F, Band 2; Appendix 2S2, A), no phosphorylated LHCII polypeptides were detected in UWO 241, even in the purified LHCII complex (Fig. 2.5F, Band 1). However, in contrast to either SAG 49.72 or 1690, UWO 241 exhibited two novel phosphorylated polypeptides (Fig. 2.5F, Band 4), associated with the high molecular mass putative 'supercomplex' – one high molecular mass band (>130 kDa), and one low molecular mass band of ~17 kDa which was also detected in the thylakoid fraction (Fig. 2.5F).

BN-PAGE was repeated in order to compare the molecular mass and composition of the putative PSI 'supercomplex' to the other sucrose gradient purified complexes isolated from UWO 241 (Fig. 2.6A). LHCII, PSII and the PSI + LHCI core complex exhibited the expected molecular masses of ~240, ~450 and ~700 kDa, respectively (Fig. 2.6A, Band 1, 2 and 3 respectively). However, BN-PAGE confirmed that the putative PSI 'supercomplex' was distinguishable from the PSI + LHCI complex (Fig. 2.6A, Band 4). The PSI + LHCI complex remained largely intact as a single pigment-protein complex with a molecular mass of ~700 kDa and only a small fraction present as a ~460 kDa complex (Fig. 2.6A, Band 3). In contrast, the putative PSI 'supercomplex' (Fig. 2.6A, Band 4) exhibited a major component of a molecular mass complex of ~460 kDa with the presence of two other smaller chlorophyll-protein subcomplexes of ~250 and 160 kDa respectively that were absent from the PSI + LHCI complex (Fig. 2.6A, Band 3). This further supports our suggestion that this unique complex (Fig. 2.6A, Band 4) is indeed a modified photosystem I complex.

To examine the polypeptide composition of the two smaller chlorophyll-containing subcomplexes observed in Fig. 2.6A (Band 4), the purified putative PSI 'supercomplex' was solubilized with SDS and separated in the second dimension by SDS-PAGE (Fig. 2.6B). Immunoblots confirmed the presence of PsaA (Fig. 2.6C) and PsaD (Fig. 2.6D) in the 460 kDa pigment-protein complex and a 17 kDa phosphorylated polypeptide (Fig. 2.6E). In addition, immunoblots of the polypeptides associated with the two smaller (~250 and 160 kDa) subcomplexes exhibited the presence of the cytochrome *f*

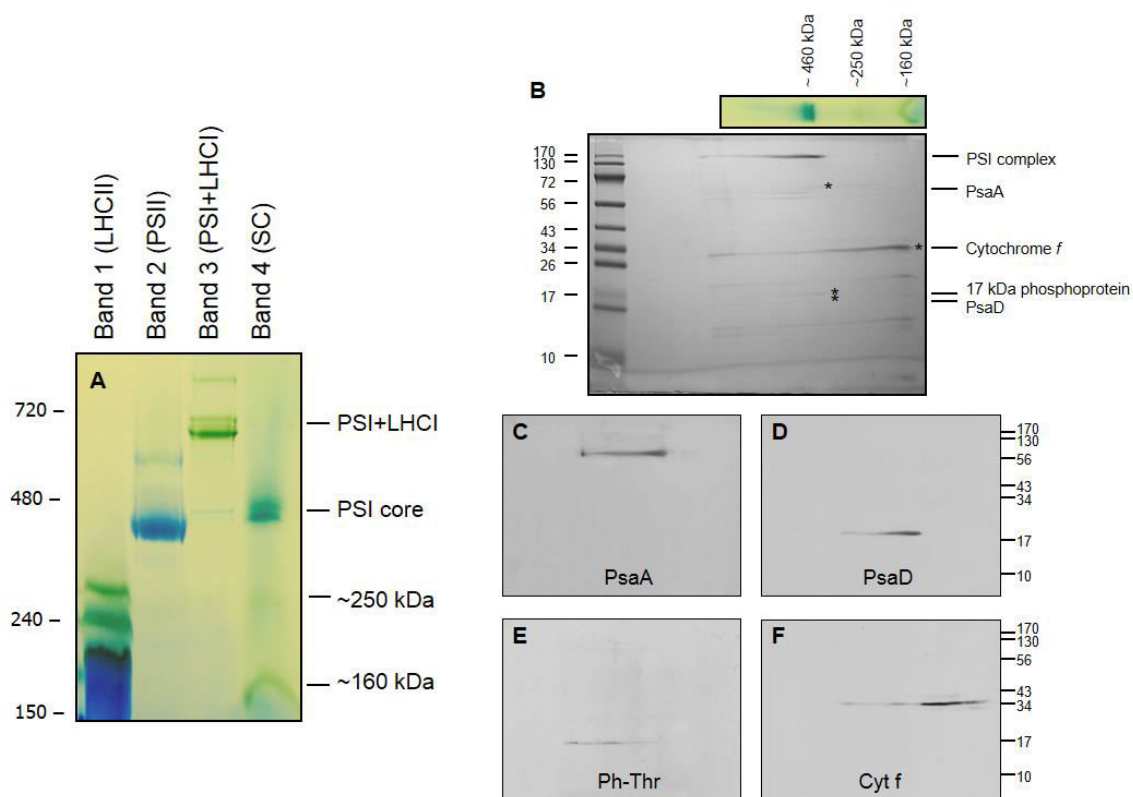


Figure 2.6: BN-PAGE of thylakoid membrane complexes and second dimension analysis of the supercomplex fraction from UWO 241. (A) UWO 241 complexes purified by sucrose density centrifugation were separated on a 3-16% gradient native gel. Following separation of the SC by BN-PAGE, the resulting gel strip was solubilized with SDS and individual subunits were separated using SDS-PAGE and stained with Coomassie blue (B). Corresponding membranes immunoblotted with various specific antibodies as indicated (C-F). (C), PsaA. (D), PsaD. (E), phospho-threonine. (F), cytochrome *f*. Location of these proteins is represented by asterisks (B) in the stained supercomplex 2-D gel. Apparent molecular masses are indicated on the sides (kDa).

polypeptide (Fig. 2.6F). The 34 kDa polypeptide identified as cytochrome *f* by immunoblotting (Fig. 2.6F) matched the 34 kDa polypeptide present in the Coomassie blue gel (Fig. 2.6B, asterisk). The presence of cytochrome *f* within this purified PSI supercomplex was also confirmed by heme staining, which indicated a heme structure associated with a 34 kDa subunit as well as the large (>130 kDa) band (Appendix 2S3). Consequently, the cytochrome *b₆/f* complex appears to be a component of the putative PSI supercomplex of UWO 241.

2.3.3 Stability of the putative PSI ‘supercomplex’

To test the sensitivity of the putative PSI ‘supercomplex’ to thylakoid protein phosphorylation status, the effects of the phosphatase inhibitor, NaF, and the kinase inhibitor, staurosporine (Staur), on the stability of pigment-protein complexes separated by sucrose density centrifugation were examined (Fig. 2.7A). UWO 241 pigment-protein complexes isolated in the presence of NaF resulted in the separation of four distinct bands including a high density band of supercomplexes: LHCII, PSII core, PSI+LHCI, and the putative PSI-supercomplex (SC) (Fig. 2.7A). In contrast, the SC band was absent when thylakoid complexes were isolated in the presence of staurosporine although the major chlorophyll-protein complexes associated with LHCII, PSII, and PSI+LHCI were still observed (Fig. 2.7A). Fig. 2.7B confirms that staurosporine inhibits the phosphorylation of the specific polypeptides associated with the putative PSI supercomplex (polypeptides >130 kDa plus the 17 kDa polypeptide) as well as the PSII subunits, CP43 and as well as the 32 kDa D1 polypeptide. These results indicate that the phosphorylation state of the thylakoid membrane proteins affect the stability of the putative PSI supercomplex of UWO 241.

Fractionation of the sucrose gradients containing thylakoids from UWO 241 treated with either NaF (Fig. 2.7C) or staurosporine (Fig. 2.7D) indicated that the phosphorylation state of the thylakoid membranes altered the migration patterns for both PsaA (Fig. 2.7E and 2.7F) as well as Cyt *f* (Fig. 2.7G and H). Consistent with the formation of the putative PSI supercomplex consisting of both PSI and Cyt *b₆/f* components in the presence of NaF, both *psaA* and cytochrome *f* were detected in the high density fractions 4-7, coincident with the band for the putative PSI supercomplex on the sucrose gradient

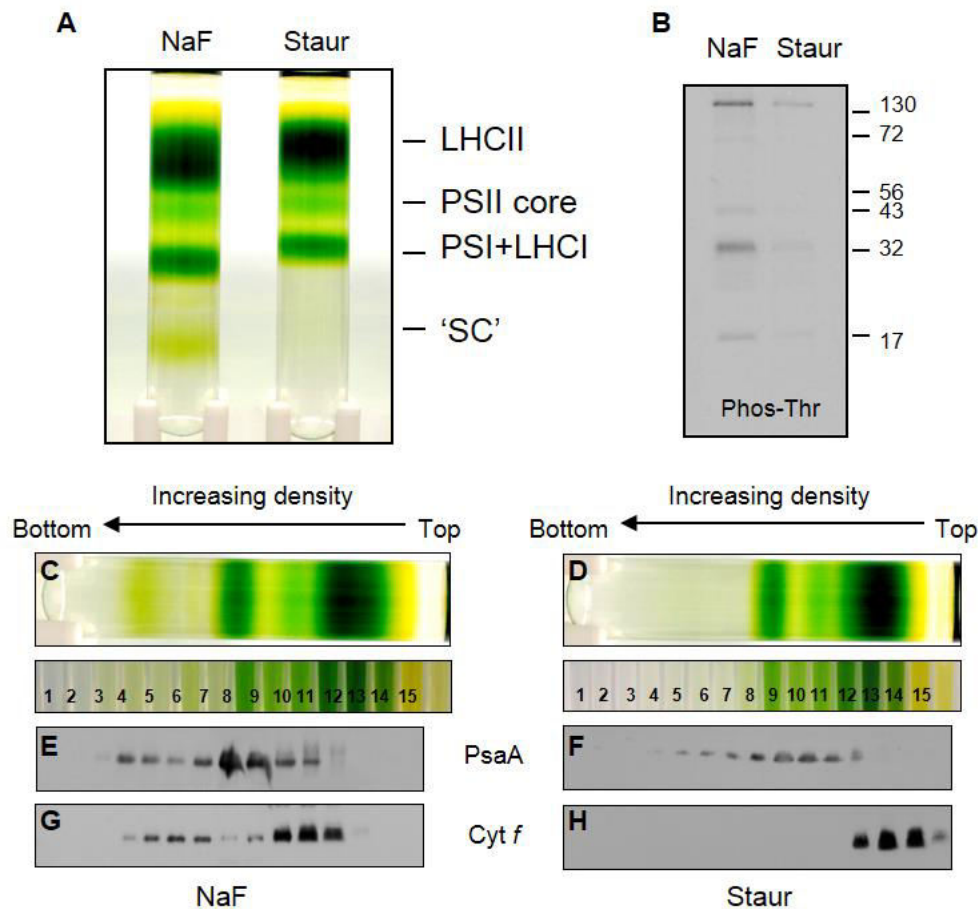


Figure 2.7: Effect of inhibitors of thylakoid protein phosphorylation on the stability of the putative PSI-supercomplex (SC) in UWO241. Thylakoid membranes were either treated with the phosphatase inhibitor, NaF or with the kinase inhibitor, staurosporine (A). Under these conditions, thylakoid membrane proteins separated on SDS-PAGE were probed with antibodies specific for phospho-threonine. Thylakoid membranes treated with either NaF (C) or staurosporine (D) were fractionated into 15 fractions of equal volume (0.8 ml), solubilized with SDS, and 20 μ l of each fraction was separated by SDS-PAGE. (E-H), corresponding membranes were immunoblotted with antibodies specific for PsaA and Cyt *f*, as indicated.

(Fig. 2.7E, G). However, the primary fractions containing the highest levels of *psaA* and *Cyt f* were detected in the lower density fractions 7-10 and 10-12 respectively in the presence of NaF. In contrast, in the presence of staurosporine, the pigment band associated with the putative PSI supercomplex (Fig. 2.7A) was not detectable and minimal levels of *psaA* and *Cyt f* were detected in the high density fractions 4-7 (Fig. 2.7F, H). Furthermore, *psaA* and *Cyt f* were detected only in the lower density fractions 7-11 and 12-15 respectively (Fig. 2.7F, H). We note with interest that the fractions containing *Cyt f* shifted to lower densities in the presence of staurosporine (Fig. 2.7G, H).

UWO 241 is not only a psychrophile, but, it is also halotolerant (Takizawa et al. 2009). SDS-PAGE indicated that salt concentration had minimal effects on the thylakoid polypeptide complement of UWO 241 (Fig. 2.8A). However, phospho-threonine immunoblot analysis of total SDS-solubilized thylakoid membrane proteins indicated that growth at low salt (70 mM) resulted in a marked reduction in the phosphorylation status of both the 17 kDa band and the large >130 kDa protein complex, compared to cells grown in high salt (700 mM) (Fig. 2.8B). Furthermore, sucrose gradient purification of the thylakoid pigment-protein complexes from low salt grown cells resulted in an 86% reduction of the putative PSI 'supercomplex', based on Chl content, compared to that of high salt grown cells (Fig. 2.8, C and D). Regardless of the salt concentration under which UWO 241 was grown, phosphorylation of the major LHCII was not detected which is consistent with previous results (Takizawa et al. 2009).

2.3.4 Identification of the phosphoproteins of the putative PSI supercomplex

The purified putative PSI 'supercomplex' of UWO 241 was subjected to 2D isoelectric focusing (IEF)-SDS-PAGE to isolate and purify the phosphorylated protein subunit(s) in preparation for sequencing by mass spectrometry (Fig. 2.9). IEF indicated the presence of at least 4 major phosphoproteins detected with phospho-threonine antibodies in the purified putative PSI supercomplex of UWO 241 (Fig. 2.9B, spots 1-4). Phosphoprotein 1 (pI = 8.5) and 2 (pI = 7.2) exhibited comparable molecular masses (17 kDa) but different isoelectric points. Phosphoprotein 3 (70 kD) and 4 (>130 kD) differed in molecular mass as well as isoelectric points (4.9 and 6.9 respectively).

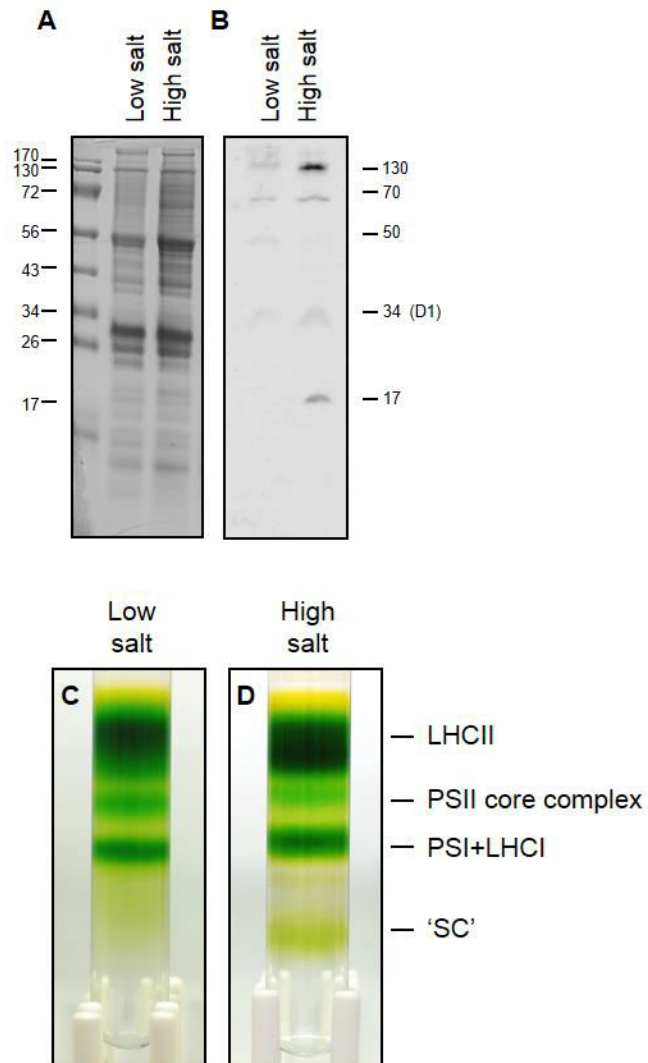


Figure 2.8: Effects of growth salt concentration on phosphorylation. Total thylakoid membrane proteins of UWO 241 grown with high (700 mM) and low (70 mM) NaCl were loaded on an equal chlorophyll basis and separated by SDS-PAGE. (A) gel stained with Coomassie blue. (B), corresponding membrane probed with antibodies specific for phospho-threonine. Subsequently, complexes of UWO 241 grown in either 70 mM (C) or 700 mM NaCl (D) were fractionated by sucrose density centrifugation. Apparent molecular masses are indicated (kDa).

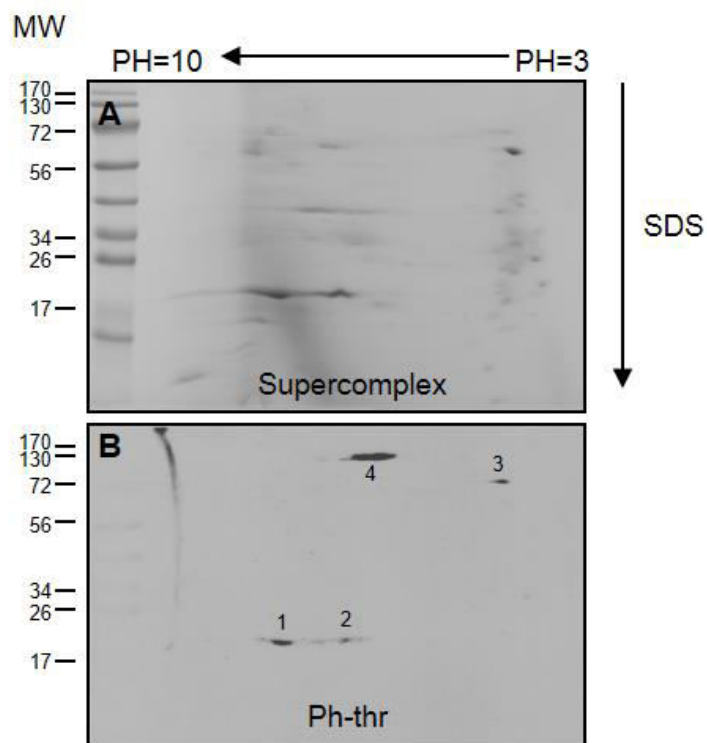


Figure 2.9: 2D IEF/SDS-PAGE purification of phosphorylated polypeptides from the supercomplex of UWO 241. Isoelectric focusing (broad range, pI 3-10) was used to separate SC subunits based on isoelectric points in the first dimension. Resultant gel strips were equilibrated and separated on a 12% SDS-PAGE gel and stained with Coomassie (A) or immunoblotted with phospho-threonine antibodies (B). Apparent molecular masses are indicated on the left (kDa).

Phosphoproteins 1-4 were excised from the gel, digested and analyzed by nano-LC-ESI-MS/MS. For identification, the resultant peptide ions generated by nano-LC-ESI-MS/MS were searched against NCBI databases using Peaks (homology) Sequencing of the peptides originating from phosphoproteins 1 and 2, and revealed that these two phosphoproteins were the same protein since the peptide sequences exhibited 94.0 % identity. A database protein BLAST search of these peptide sequences revealed that these polypeptides belonged to the PsbP superfamily of proteins, and is hereafter referred to as a “PsbP-like” protein. Spots 1 and 2 showed significant sequence matches to a number of authentic PsbP proteins, which are summarized in Appendix 2S4. Among these, PsbP (OEE2/OEC23) from *Chlamydomonas reinhardtii* showed the highest sequence similarity with 70.6 % of the amino acids being identical to the PsbP-like protein. Fig. 2.10 shows the alignment of phosphoproteins 1 and 2 with amino acid sequences of authentic PsbP from *C. reinhardtii*, *Arabidopsis thaliana* and spinach.

Nano-LC-ESI-MS/MS analysis of the 70 kDa phosphoprotein 3 revealed the presence of 2 polypeptides. Since these proteins had the same apparent molecular mass of 72 kDa and isoelectric points of 4.9, they could not be separated by isoelectric focussing. However, based on sequence analyses, the two polypeptides were identified as an ATP-dependent zinc metalloprotease FtsH from *Medicago sativa* (summarized in Appendix 2S5) and a heat shock cognate 70 kDa protein as determined by the matching of five peptides from *Arabidopsis thaliana* (Appendix 2S5). Although the Peaks programme had identified potential phosphorylation modifications sites for all 3 proteins (PsbP-like, HSP, FtsH), the ion scores of individual peptides were insufficient to confirm the specific phosphorylated threonine residues detected by immunoblotting.

Phosphoprotein 4 contained several different proteins, with 14 and 9 peptide matches to PsaA and PsaB, respectively (Appendix 2S6). Phosphoprotein 4 also showed the presence of an ATP-dependent FtsH metalloprotease, with 3 sequence matches, 2 of which were identical to those found in the 70 kDa phosphoprotein 3. Therefore, the 70 kDa phosphoprotein 3 is probably an FtsH metalloprotease which was also present in the large (>130 kDa) protein complex and may be responsible for the positive phosphorylation signal associated with phosphoprotein 4.

```

Spot 1      1 -----
Spot 2      1 -----
C.reinhardtii 1 -----MATALCNKAFAAAPVARPASRRSAVVVRASGSDVSRR
A.thaliana   1 MAYSACFLHQSAALASSAARSSSSSSSSSRHVLSLSPVQIICKRAQQSHED----DNSAVSRR
S.oleracea   1 MASTACFLHHAHAISSPAAGRGSAAQRYQAVSIKPNQIVCKRAQKQDDNEANVLNSGVSRR

          ↓
Spot 1      1 -----APAYGDCANVFGKVTNKSQFLPYVGDGFVQLPCKWNPSKE
Spot 2      1 -----AYGDCANVFGKVTNKSQFLPYVGDGFVQLP-----CKE
C.reinhardtii 38 AALAGFAGAAAL-VSSSPANAAAYGDCANVFGKVTNKSQFLPYVAGDGFALLLPAKWNPSKE
A.thaliana   57 LALTLVLIQAAAAGVSKVSPADAAYGEANVFGKPKTNTDFLPYNGDGFQVQVPAKWNPSKE
S.oleracea   61 LALTVLIQAAAAGVSKVSPADAAYGEANVFGKPKKNTDFLPYNGDGFQVQVPAKWNPSKE

          ↓
Spot 1      42 QDFPGVQLRYEDNCDVNNFVLLKLS-----DFGDQKAFLNVSYSYLLGKQAYSGETAK
Spot 2      35 QDFPGVQLRYEDNCDVNNFVLLKFTF-----SDFGTQKAFLNVSYSYLLGKQSFSGESK-
C.reinhardtii 97 NDFPGVQLRYEDNCDVNNFVLLAQDTRKATADFGSQDRFLESYSYLLGKQAYSGETQ-
A.thaliana   117 IEYFGVQLRYEDNCDVNNFVLLVMTPTDKKSLTDYGSPEEFLSQVNYLLGKQAYFGETA-
S.oleracea   121 KEFPGVQLRYEDNCDVNNFVLLVQPTDKKSLTDYGSPEEFLSQVNYLLGKQAYFGETA-

          ↓
Spot 1      95 SEGGFAPNRVSAASLLDLSEVTDKK--TYYTYELLTR--DGDEGGKHQLIGA-----
Spot 2      89 SEGGFAPNRVSAASLLDLSEVTDKK--TYYTYELLTR--DGDEGGKHQLIGA-----
C.reinhardtii 156 SEGGFAPNRVSAASLLDVSTTDDKKGKTYTYELLVRSADGDEGGKHQLIGATVGS DNKL
A.thaliana   176 SEGGFDNNAVATANLLESSSQEVGG-KPYYYLSVLTRADGDEGGKHQLIGATVN-GKRL
S.oleracea   180 SEGGFDSGVVASANVLESSTPVVDG-KQYYSITVLRTRADGDEGGKHQVIGATVVK-DCKL

          ↓
Spot 1      -----
Spot 2      -----
C.reinhardtii 216 YIICKRAQAGDKRWFKGAKKFEAMGAFDSTTVV
A.thaliana   234 YIICKRAQAGDKRWFKGAKKFEVESAATSFVA
S.oleracea   238 YIICKRAQAGDKRWFKGAKKFEVESAATSFVA

```

Figure 2.10: Alignment of the PsbP-like protein from the supercomplex of UWO 241 from spots 1 and 2 with the amino acid sequences of homologous authentic PsbP proteins from three other organisms. The alignment was performed using CLUSTALW program. The GenBank accession numbers are: *Chlamydomonas reinhardtii*, P11471.1; *Arabidopsis thaliana*, NP172153.1; *Spinacia oleracea*, P12302.1. Multiple phosphorylation sites (S73, S133, S140, S151, T154, S156, S166, S169, S174, T175, T176, T177, S241, T243) that have been recently identified are indicated for PsbP1 (arrows) and PsbP4 (S142, asterisk) in *Chlamydomonas reinhardtii* (Wang et al. 2014)

The presence of the individual polypeptides associated with the specific protein spots isolated by IEF (Fig. 2.9B) was confirmed by nano-LC-ESI-MS/MS analysis of the complete, PSI supercomplex purified by sucrose gradient centrifugation (Appendix 2S7). In addition to the polypeptides associated with phosphoprotein spots 1-4 (Fig. 2.9B) in the complete, purified complex, we also detected an ADP-ribosylation factor associated with the ARF family of GTPases, RF4, a PSI assembly protein associated with the Ycf4 superfamily in *Chlamydomonas*, an adenine nucleotide translocator as well as the expected Cyt *f* from *Chlamydomonas sp.* UWO 241 and the PsbP subunits.

2.3.5 P700-dependent cyclic electron transport

Far-red (FR) light-induced absorbance changes at 820 nm ($\Delta A_{820-860}$) were used as an estimate of the extent of P₇₀₀ photooxidation in vivo (Asada et al. 1993; Mi et al. 1992; Ivanov et al. 2000; Morgan-Kiss et al. 2002). Illumination of the algal cells with FR light caused an increase in $A_{820-860}$ signal, which indicated the oxidation of P₇₀₀ to the P₇₀₀⁺ radical. Thus, steady state FR light induced absorbance changes ($\Delta A_{820-860}$) were used to express the steady state level of P₇₀₀ photooxidation. Under control conditions, the mesophilic strain SAG49.72 exhibited almost a 2-fold higher steady-state value of $\Delta A_{820-860}$ than UWO241 cells (Table 2.2), which is in agreement with previous results (Morgan-Kiss et al. 2002a, b).

Since under FR illumination PSI is the primary photosystem that is operational, the kinetics of P₇₀₀⁺ reduction when the FR light is turned off is presumed to reflect primarily the rates of cyclic electron flow (CEF) around PSI (Maxwell and Biggins 1976, Ravenel et al. 1994) and/or the interaction of stromal components with the intersystem electron transport chain (Asada et al. 1992). The rates of P₇₀₀⁺ reduction in the dark ($t_{1/2}^{\text{red}}$) were 3-fold faster in UWO 241 (1.1 s) compared to SAG 49.72 (3.4 s) (Table 2.2), indicating an increased capacity for CEF around PSI and/or increased interaction between stromal electron donors and intersystem electron transport in UWO 241 compared to the mesophilic SAG 49.72 strain. To confirm this, antimycin A (AA) was used as an effective inhibitor of the AA-sensitive FQR-dependent pathway for CEF (Moss and Bendall 1984; Shikanai 2007; Antal et al. 2013). Although blocking the FQR-dependent

Table 2.2: Effects of antimycin A (AA, 20 μ M) on the far red (FR) light induced steady state oxidation of P700 ($\Delta A_{820/A820}$) and half times for P700+ reduction after turning off the FR light in a mesophilic (SAG 49.72) and psychrophilic (UWO 241) strains of the green alga *Chlamydomonas* cultivated at different growth temperatures and either high (HS, 700 mM) or low salt (LS) concentrations (70 mM). All data represent mean values (\pm SE) from 4 – 11 measurements. All measurements were performed at the corresponding growth temperatures of 5°C (SAG 49.72) and 25°C (UWO 241), or at the same growth temperature of 16°C. Values followed by different letters are significantly different, as determined by ANOVA and Tukey's test ($p < 0.01$) for both P700 oxidation (lower case) and P700+ half times (upper case).

Strains/Treatments	$\Delta A_{820-860} (P_{700}^+) (mV)$			$t_{1/2}^{red} (P_{700}^+) (s)$		
	Control	+ AA	% of control	Control	+ AA	% of control
SAG 49.72(25°C)	14.2 \pm 1.7(8)	26.3 \pm 1.6(5)	185.1b	3.4 \pm 1.2(7)	9.0 \pm 0.4(7)	266.7B
SAG 49.72(16°C)	15.7 \pm 1.7(9)	47.7 \pm 8.1(4)	303.8a	10.1 \pm 0.9(9)	19.2 \pm 3.5(4)	190.1C
UWO 241(5°C) (HS)	7.1 \pm 1.4(6)	21.9 \pm 2.4(10)	310.0a	1.1 \pm 0.2(6)	8.2 \pm 0.8(10)	747.7A
UWO 241(16°C)	50.0 \pm 7.6(10)	82.2 \pm 11.2(5)	164.4b	7.9 \pm 0.8(10)	9.3 \pm 0.9(5)	117.7D
UWO 241(5°C) (LS)	29.9 \pm 3.5(11)	38.2 \pm 3.4(5)	127.7c	2.7 \pm 0.5(11)	2.1 \pm 0.1(5)	77.8E

CEF pathway with AA resulted in a comparable level in $\Delta A_{820-860}$, the presence of AA inhibited the $t_{1/2}^{\text{red}}$ 7.5-fold in UWO 241 but only 2.7-fold in SAG 49.72 (Table 2.2), thus confirming the significantly greater stimulation of CEF in UWO 241 relative to SAG 49.72 cells. Since, under control conditions, the steady state level of P_{700}^+ UWO 241 was twice lower compared to SAG 49.72, preventing the influx of electrons to the intersystem electron transport chain by blocking the CEF with AA caused a differential increase in P_{700} photo-oxidation in UWO 241 (3-fold) versus SAG 49.72 (2-fold) such that $\Delta A_{820-860}$ was comparable in UWO 241 and SAG 49.72 at their optimal growth temperature of 25° and 5°C (Table 2.2).

While the oxidation of P_{700} under FR almost exclusively reflects the excitation of PSI, the extent of P_{700} photooxidation under white actinic light (AL) is affected by the excitation of both PSII and PSI (Asada et al. 1993). The contribution of linear electron transport from PSII to P_{700}^+ was estimated by measuring the extent of steady-state P_{700} photooxidation induced by white actinic light (AL) in the absence or presence of DCMU (Table 2.3). Under white AL excitation in the absence of DCMU (P_{700}^+ control), electrons derived from PSII continuously reduced P_{700}^+ and generated a $\Delta A_{820-860}$ that was 18% greater in UWO 241 than in SAG 49.75 (Table 2.3). Preventing the electron flow from PSII to P_{700}^+ in the presence of the PSII inhibitor, DCMU, caused a 47% increase of the steady-state level of P_{700}^+ (Table 2.3) in SAG 49.72, suggesting that electrons available for P_{700}^+ reduction originated from PSII and were delivered to P_{700}^+ via intersystem electron transport. In contrast, UWO 241 cells exhibited only 12% increase of P_{700}^+ in the presence of DCMU (Table 2.3). This indicates that a greater fraction of electrons available for P_{700}^+ reduction must have been derived from sources other than PSII and that the contribution of PSII and intersystem electron transport to the reduction of P_{700}^+ was limited in the psychrophile, UWO 241, compared to the mesophile, SAG 49.72.

Since the stability of PSI supercomplex of UWO 241 was more stable when cells were grown under high salt rather than low salt (Fig. 2.8), we examined the effect of salt concentration on the P_{700} photo-oxidation signal ($\Delta A_{820}/A_{820}$) and the dark relaxation kinetics of P_{700}^+ in UWO 241. The results in Table 2 show that in UWO 241 grown at 5°C and high salt (HS), the $t_{1/2}^{\text{red}}$ was 2.4-fold greater than that for UWO 241 grown at

Table 2.3: The effects of DCMU on the level of P700 photooxidation (P700+) under white actinic light (AL, 150 2 s-1) excitation of in the mesophilic (SAG 49.72) and psychrophilic (UWO 241) strains of the green alga *Chlamydomonas*. The extent of the P700 photooxidation level was estimated by the AL-induced absorbance changes at 820 nm in the absence and presence of 40 μ M DCMU to inhibit the electron flow from PSII. All values represent means \pm SE from 9 – 13 measurements in 3 independent experiments. All measurements were performed at the corresponding growth temperatures for UWO 241 (5°C) and SAG 49.72 (25°C). Values followed by different letters are significantly different, as determined by ANOVA and Tukey's test ($p < 0.01$).

Strains	$\Delta A_{820-860} (P_{700}^+) (mV)$		
	P700 ⁺ _{control}	P700 ⁺ _{DCMU}	$\Delta A_{DCMU} / \Delta A_{control}$
SAG 49.72	84.09 \pm 3.89(9)	124.16 \pm 3.08(13)	1.47a
UWO 241	99.75 \pm 2.66(11)	111.75 \pm 4.35(11)	1.12b

5°C but low salt (LS). Thus, growth of UWO 241 at low salt inhibited the rate of PSI CEF.

2.4 Discussion

Photosynthetic organisms typically display a characteristic phosphorylation profile of specific thylakoid membrane polypeptides the majority of which are associated with photosystem II (Owens and Ohad 1982). First, phosphorylated polypeptides associated with the PSII core reaction centre complex which undergo phosphorylation include the D1/D2 reaction center polypeptides as well as the 43-kDa chlorophyll a-binding protein (CP43) (Hansson and Vener 2003; Turkina et al. 2006; Vener 2006; 2007; Yokthongwattana and Melis 2006; Edleman and Mattoo 2008). Phosphorylation of D1/D2 and CP43 is associated with the disassembly, degradation and resynthesis of the D1 protein during PSII repair cycle in response to PSII chronic photoinhibition (Yokthongwattana and Melis 2006; Edelman and Mattoo 2008; Tikkanen et al. 2008; Fristedt et al. 2009). Several proteins of the PSII light harvesting antenna are also important sites of thylakoid protein phosphorylation that regulate energy distribution between PSII and PSI through state transitions in plants and green algae (Rochaix 2011) and also serves to protect PSI under fluctuating irradiance (Grieco et al. 2012). These polypeptides include the LHCII complex components, Lhcbm1 and Lhcbm10, and a minor LHCII antennae subunit CP29 (Lhcb4) during state transitions in *Chlamydomonas reinhardtii* (Kargul et al. 2005; Turkina et al. 2006; Vener 2007) and Lhcb1, Lhcb2 and Lhcb4 in terrestrial plants (Bergantino et al. 1995; Bergantino et al. 1998; Tikkanen et al. 2006). In addition, Lhcbm4, Lhcbm6, Lhcbm9, Lhcbm11, CP29 (Lhcb4) and CP26 (Lhcb5) have also been shown to undergo phosphorylation during high light exposure in *C. reinhardtii* (Turkina et al. 2006; Vener 2007). Although phosphorylation of PSI polypeptides appears to be quite rare (Vener 2006; 2007), PsaD, an extrinsic stroma-exposed protein, was recently reported as the first phosphorylated photosystem I subunit in *Arabidopsis*, along with another phosphoprotein, PSI-P, which has been characterized as a novel subunit of plant photosystem I (Hansson and Vener 2003).

STN8 appears to be the primary thylakoid protein kinase that regulates the phosphorylation of the PSII core proteins whereas STN7 is involved in the

phosphorylation of Lhcb1, Lhcb2 and Lhcb4 in *Arabidopsis thaliana* (Bonardi et al. 2005; Tikkanen et al. 2008; Fristedt et al. 2009; Rochaix 2011). The orthologous thylakoid protein kinases in *Chlamydomonas reinhardtii* are STT8 and STT7 (Depege et al. 2003; Vener 2006; Rochaix 2011). The activity of these thylakoid protein kinases are light dependent and regulated via the redox state of the intersystem photosynthetic electron transport chain (Bonardi et al., 2005; Vener 2006; Tikkanen et al. 2006; Tikkanen et al. 2008; Rochaix 2011; Tikkanen et al. 2012).

Consistent with other mesophilic photosynthetic organisms such as *C. reinhardtii* 1690 and *C. raudensis* SAG 49.72, UWO 241 exhibits phosphorylation of the two PSII core proteins, CP43 and D1. This is in agreement with previous studies that show that UWO 241 exhibits a rapid rate of D1 repair and recovery from photoinhibition at low temperatures (Pocock et al. 2007). Consequently, it appears that STT8 is present and active in UWO 241. However, in contrast to other photosynthetic organisms, UWO 241 does not display phosphorylation of PSII-associated LHCI polypeptides which is consistent with our previous reports that UWO 241 is a natural, green algal variant that does not exhibit the capacity to undergo state transitions and appears to be locked in state I (Morgan-Kiss et al. 2001; Gudynaite-Savitch et al. 2006; Gudynaite-Savitch et al. 2007; Szyszka et al. 2007; Takizawa et al. 2009). We report here, for the first time, that this Antarctic psychrophile preferentially phosphorylates a pigment-protein supercomplex with a molecular mass of about 1000 kDa rather than LHCI components. Absorption spectroscopy, 77K fluorescence emission spectroscopy, immunoblot and nano-LC-ESI-MS/MS analyses are consistent with the identification of this pigment-protein complex as a PSI supercomplex. The PSI-supercomplex from UWO 241 consists of components of both photosystem I and the cytochrome *b₆/f* complex. We were able to detect and identify four specific phosphorylated polypeptides associated with this PSI supercomplex: two phosphorylated polypeptides with a comparable molecular mass of 17 kD but different isoelectric points were identified by nano-LC-ESI-MS/MS to be PsbP-like proteins. The third phosphorylated polypeptide was identified as a putative ATP-dependent zinc metalloprotease FtsH.

The phosphorylation state of thylakoid membranes is the net effect of the combined rates of protein phosphorylation by thylakoid kinases such as the STT7/STT8 kinases versus the rates of dephosphorylation by thylakoid protein phosphatases such as PPH1/TAP38 (Rochaix 2011). The stability of the PSI-supercomplex in UWO 241 appears to be sensitive to the phosphorylation state of the phosphoprotein subunits since the abundance of this complex is greatest when purified in the presence of NaF which maximizes thylakoid polypeptide phosphorylation by inhibiting thylakoid phosphatases. Conversely, the abundance of the PSI-supercomplex is minimal when it is purified in the presence of the kinase inhibitor, staurosporine (Fig. 2.7). Thus, phosphorylation of the PSI-supercomplex in UWO 241 may potentially play a role in providing structural stability to this pigment-protein complex. This is consistent with our previous report which indicated that the phosphorylation status of the high molecular polypeptide complex of UWO 241 thylakoids is light dependent (Szyszka et al. 2007). In addition to polypeptide phosphorylation status, maximum stability of the PSI supercomplex was also dependent upon the salt concentration under which UWO 241 cells were grown: high salt stabilized whereas low salt de-stabilized the PSI supercomplex. The latter is consistent with the fact that UWO 241 is not only a psychrophile but it is also adapted to high salt concentrations present in Lake Bonney, Antarctica from which it was isolated (Morgan-Kiss et al. 2006; Takizawa et al. 2009).

Several recent reports involving thylakoid membrane complex isolation have revealed the existence of PSI supercomplexes. Peng et al. (2008) reported a novel NDH-PSI supercomplex with a molecular mass of >1000 kDa in *Arabidopsis thaliana* which was composed almost exclusively of the PSI subunits as well as NDH subunits. Takahashi et al. (2006) used sucrose density centrifugation to isolate PSI-LHCI supercomplexes from *Chlamydomonas reinhardtii* cells locked in either state I or state II, and observed the reorganization of several LHCII subunits among the two photosystems during state transitions. Lemeille et al. (2009) examined the role of the STT7 kinase during state transitions in *Chlamydomonas reinhardtii* and reported STT7 was associated with a large molecular weight complex which co-fractionated with subunits of both the cytochrome *b₆f* complex and PSI, but not with subunits of PSII. Iwai et al. (2010) identified a supercomplex in *Chlamydomonas reinhardtii* that governs cyclic electron flow. This

complex is composed of PSI-LHCI, LHCII, the cytochrome b_6/f complex, ferredoxin-NADPH oxidoreductase (FNR), and the PGRL1 protein (Iwai et al. 2010) and was isolated as a high density band following sucrose density gradient centrifugation of thylakoid membranes treated with n-tridecyl- β -D-maltoside (TM) (Iwai et al. 2010). However, the PSI supercomplex of UWO 241 is phosphorylated and we identified the three specific phosphorylated subunits of the PSI supercomplex to be an ATP-dependent zinc metalloprotease FtsH, and two PsbP-like polypeptides (Appendix 2S4, 2S5; Fig. 2.10). We are unaware of any previous reports which indicate that PSI supercomplexes are regulated by protein phosphorylation.

A unique feature of the polypeptide composition of the PSI supercomplex in UWO 241 is the presence of two PsbP-like proteins which are reversibly phosphorylated. However, Yang et al. (2003) reported that the oxygen-evolving enhancer protein 2 (OEE2) is phosphorylated via the cytoplasmic kinase domain of WAK1, a member of the WAK family of cell wall associated receptor kinases in *Arabidopsis thaliana*. Authentic PsbP and PsbQ proteins typically are luminal PSII subunits of the oxygen-evolving complex (OEC) and play a role in stabilizing the Mn-cluster (Ghanotakis et al. 1984; Miyao and Murata 1985; Ifuku et al. 2008). PsbP (OEC23) has also been shown to be required for PSII core assembly, stability and function (Ifuku et al. 2005; Yi et al. 2007). In addition to the authentic *PsbP* genes, recent genomic and proteomic studies have demonstrated the existence of many PsbP in the chloroplast of higher plants (Ishihara et al. 2008; Ifuku et al. 2010). In *Arabidopsis thaliana*, there are eight PsbP homologs, all of which contain a thylakoid lumen-targeting signal (Ishihara et al. 2007; Ifuku et al. 2008; Ishihara et al. 2008; Ifuku et al. 2010). Based on similarity to the PsbP1 sequence (near 40% similarity), two PsbP homologs have been referred to as PsbP-like (PPL) proteins, and the other PsbP homologs have been named PsbP domain (PPD) proteins (Ishihara et al. 2007; Ishihara et al. 2008). Alignment of amino acid sequences with that of cyanoP protein revealed that both PPL homologs, and PPD1 show significant homology to cyanoP (>40% similarity) indicating that they are most likely of cyanobacterial origin (Ishihara et al. 2008).

However, recently, the PsbP-domain protein 1 (PPD1) was shown to be essential for photosystem I assembly in *Arabidopsis thaliana* (Liu et al. 2012), a function unrelated to

that of authentic PsbP proteins, which are components of PSII. Yeast two-hybrid assays revealed that PPD1 interacts specifically with PsaA and PsaB of PSI and acts at the post-translational level (Liu et al. 2012). Furthermore, an *Arabidopsis* mutant of the PsbP-domain 5 protein (PPD5) exhibited decreased levels of NADPH dehydrogenase (NDH) activity (Roose et al. 2011). The function of PPD6 is not unknown, but it is unique compared to other PsbP homologs, as it contains an intramolecular disulfide bond which may indicate sensitivity to redox regulation (Hall et al. 2012).

The molecular function of two PsbP-like homologs, PPL1 and PPL2, was also recently examined and compared with that of PsbP (Ishihara et al. 2007). Although both PPL proteins were involved in maintaining primary electron flow during plant stress responses, their functions were found to be diverse (Ishihara et al. 2007). Unexpectedly, PPL2 was shown to be the first subunit required for the accumulation of the chloroplast NDH complex in the thylakoid lumen (Ishihara et al. 2007). In addition, the function of either PPL1 or PPL2 did not overlap with that of authentic PsbPs, and neither protein was tightly associated with PSII (Ishihara et al. 2007). More recent studies have also confirmed that PPL2 (17 kDa) is a novel subunit associated with the NDH complex in *Arabidopsis* (Peng et al. 2009; Suorsa et al. 2009). In addition, several PsbQ-like (PQL) proteins (including PsbQ-F1 and PsbQ-F2, both 17 kDa) have been shown to be necessary for the function of the NDH complex in *Arabidopsis* (Majeran et al. 2008; Peng et al. 2009; Suorsa et al. 2009; Yabuta et al. 2010). Furthermore, PQL1 and PQL2 were found to be tightly associated with the NDH-PS I supercomplex (Suorsa et al. 2010; Yabuta et al. 2010). Thus, it appears that the majority of PPL and PQL polypeptides are required for the accumulation, stabilization and activity of the NDH complex (Ishihara et al. 2008; Yabuta et al. 2010) as well as PSI (Liu et al. 2012). In contrast to authentic PsbP subunits, PPLs and PQLs are not associated with PSII. Thus, we suggest that the identified PsbP-like phosphoproteins of UWO 241 may share a similar function in stabilizing the PSI-supercomplex of UWO 241. However, our nano-LC-ESI-MS/MS analyses did not detect the presence of an NDH complex associated with the PSI supercomplex of UWO 241.

Linear electron flow (LEF) produces NADPH plus ATP whereas CEF recycles photosynthetic electrons around photosystem I to generate ATP only (Finazzi et al. 1999; Eberhard et al. 2008; Cardol et al. 2011). Two CEF pathways have been proposed: (1) the NAD(P)H dehydrogenase (NDH)-dependent pathway and (2) a ferredoxin (Fd)-PQ reductase (FQR) pathway (Shikanai 2007; Eberhard et al. 2008; Johnson 2011; Cardol et al. 2011). The NDH pathway appears to be important in plants where a chloroplastic, type I Ndh complex (NDH) similar to that found in plant mitochondria participates in CEF in combination with the Cyt *b₆/f* complex. However, the chloroplast genome of green algae lack the genes that encode the chloroplastic Ndh complex (Maul et al. 2002; Oudot-Le Secq et al. 2007) and thus, it has been suggested that in green algae CEF does not proceed through such a complex (Peltier and Cournac 2002). However, non-photochemical reduction of the plastoquinone pool is observed in green algae (Mus et al. 2005) which may be regulated by a type II NAD(P)H dehydrogenase (Nda2) in *Chlamydomonas reinhardtii* (Jans et al. 2008; Cardol et al. 2011). The FQR pathway, unlike the NDH pathway, is sensitive to antimycin A but the precise nature of FQR remains unknown. However, it has been suggested that *PGR5* and *PGRL1* first identified in *Arabidopsis thaliana* (Shikanai 2007) and present in the *Chlamydomonas reinhardtii* genome (Merchant et al. 2007) may encode regulatory components of CEF in green algae (Cardol et al. 2011). Based on spectroscopic assessments (Fig. 2.4; Appendix 2S1), polypeptide composition (Fig. 2.3), and immunoblots (Fig. 2.5) and BN-PAGE (Fig. 2.6) and nano-LC-ESI-MS/MS of the high-density, pigment protein complex purified by sucrose density centrifugation, we conclude that the Antarctic psychrophile exhibits a novel PSI-Cyt *b₆/f* supercomplex that represents the primary site of thylakoid protein phosphorylation and whose stability is dependent upon the thylakoid protein phosphorylation status as well as salt concentration. What is the functional role of the PSI supercomplex in UWO 241? Based on the P700 measurements (Table 2.2, Table 2.3), we conclude that the presence of the novel PSI-Cyt *b₆/f* supercomplex contributes to enhanced CEF in UWO 241. We suggest that the presence of this PSI supercomplex in UWO 241 coupled with high rates of CEF reflects an adaptation to low temperature and high salt conditions which compensates for the fact that this psychrophile is locked in state I and lacks the ability to undergo state transitions.

2.5 Conclusion

In conclusion, we suggest that the reversible phosphorylation of the PSI-Cyt b_6/f supercomplex in the Antarctic psychrophile, *Chlamydomonas sp.* UWO 241 plays a role in the dynamic modulation between linear and cyclic electron transport which is dependent upon the phosphorylation status of the specific phosphoproteins subunits (two PsbP-like polypeptides, and an ATP-dependent zinc metalloprotease FtsH) of the PSI-supercomplex as well as the presence of high salt concentrations. The CEF pathway in the psychrophile may be used to balance the excitation energy of the two photosystems and provide a constant supply of ATP, just as state transitions balance excitation energy during linear electron flow. Therefore, due to adaptation to its unique Antarctic environment of low temperature combined with low irradiance but high salt, we suggest that *Chlamydomonas sp.* UWO 241 favours regulation of CEF through phosphorylation of a PSI-supercomplex rather than through the regulation of state transitions through phosphorylation of PSII-associated LHCII proteins.

2.6 References

- Allen JF** (2003) State transitions – a question of balance. *Science* **299**: 1530–1532
- Allen JF, Bennett J, Steinback KE, Arntzen CJ** (1981) Chloroplast protein phosphorylation couples plastoquinone redox state to distribution of excitation energy between photosystems. *Nature* **291**: 21–25
- Anderson JC, Peck SC** (2008) A simple and rapid technique for detecting protein phosphorylation using one-dimensional isoelectric focusing gels and immunoblot analysis. *Plant J* **55**: 881–885
- Antal TK, Kukarskikh GP, Bulychev AA, Tyystjärvi E, Krendeleva T** (2013) Antimycin A effect on the electron transport in chloroplasts of two *Chlamydomonas reinhardtii* strains. *Planta* **237**: 1241–1250
- Asada K, Heber U, Schreiber U** (1992) Pool size of electrons that can be donated to P700+, as determined in intact leaves: donation to P700+ from stromal components via the intersystem chain. *Plant Cell Physiol* **33**: 927–932
- Asada K, Heber U, Schreiber U** (1993) Electron flow to the intersystem chain from stromal components and cyclic electron flow in maize chloroplasts, as determined in intact leaves by monitoring redox change of P700 and chlorophyll fluorescence. *Plant Cell Physiol* **34**: 39–50
- Bergantino E, Dainese P, Cerovic Z, Sechi S, Bassi R** (1995) A Post-translational modification of the Photosystem II subunit CP29 protects maize from cold stress. *J Biol Chem* **270**: 8474–8481

- Bergantino E, Sandona D, Cugini D, Bassi R** (1998) The Photosystem II subunit CP29 can be phosphorylated in both C3 C4 plants as suggested by sequence analysis. *Plant Mol Biol* **36**: 11-22
- Bonardi V, Pesaresi P, Becker T, Schleiff E, Wagner R, Pfannschmidt T, Jahns P, Leister D** (2005) Photosystem II core phosphorylation and photosynthetic acclimation require two different protein kinases. *Nature* **437**: 1179-1182
- Cardol P, Forti G, Finazzi G** (2011) Regulation of electron transport in microalgae. *Biochim Biophys Acta* **1807**: 912-918
- Chua NH, Bennoun P** (1975) Thylakoid membrane polypeptides of *Chlamydomonas reinhardtii*: wild-type and mutant strains deficient in photosystem II reaction center. *Proc Natl Acad Sci USA* **72**: 2175–2179
- Depege N, Bellafiore S, Rochaix JD** (2003) Role of chloroplast protein kinase Stt7 in LHCII phosphorylation and state transition in *Chlamydomonas*. *Science* **299**: 1572-1575
- Edelman M, Mattoo AK** (2008) D1-protein dynamics in photosystem II: the lingering enigma. *Photosynth Res* **98**: 609-620
- Eberhard S, Finazzi G, Wollman FA** (2008) The dynamics of photosynthesis. *Annu Rev Genet* **42**: 463-515
- Escoubas JM, Lomas M, LaRoche J, Falkowski PG** (1995) Light intensity regulates cab gene transcription via the redox state of the plastoquinone pool in the green alga, *Dunaliella tertiolecta*. *Proc Nat Acad Sci USA* **92**: 10237-10241
- Finazzi G, Furia A, Barbagallo RP, Forti G** (1999) State transitions, cyclic and linear electron transport and photophosphorylation in *Chlamydomonas reinhardtii*. *Biochim Biophys Acta* **1413**: 117–129
- Fristedt R, Willig A, Granath P, Crevecoeur M, Rochaix JD, Vener AV** (2009) Phosphorylation of photosystem II controls functional macroscopic folding of photosynthetic membranes in *Arabidopsis*. *Plant Cell* **21**: 3950-3964
- Ghanotakis DF, Topper JN, Babcock GT, Yocum CF** (1984) Water-soluble 17 and 23 kDa polypeptides restore oxygen evolution by creating a high-affinity site for Ca²⁺ on the oxidizing side of photosystem II. *FEBS Lett* **170**: 169–173
- Grieco M, Tikkanen M, Paakkarinen V, Kangasjarvi S, Aro EM** (2012) Steady-state phosphorylation of light-harvesting complex II proteins preserves photosystem I under fluctuating white light. *Plant Physiol* **160**: 1896-1910
- Gudynaite-Savitch L, Gretes M, Morgan-Kiss R, Savitch LV, Simmonds J, Kohalmi SE, Hüner NPA** (2006) Cytochrome f from the Antarctic psychrophile, *Chlamydomonas raudensis* UWO 241: structure, sequence, and complementation in the mesophile, *Chlamydomonas reinhardtii*. *Mol Genet Genomics* **275**: 387-98
- Gudynaite-Savitch L, Loiselay C, Savitch LV, Simmonds J, Kohalmi S, Choquet Y, Hüner NPA** (2007) The small domain of cytochrome f from the psychrophile,

Chlamydomonas raudensis UWO 241, modulates the apparent molecular mass and decreases the accumulation of cytochrome f in the mesophile, *Chlamydomonas reinhardtii*. *Biochem Cell Biol* **85**: 616-627

- Hall M, Kieselbach T, Sauer UH, Schröder WP** (2012) Purification, crystallization and preliminary X-ray analysis of PPD6, a PsbP-domain protein from *Arabidopsis thaliana*. *Acta Cryst* **F68**: 278–280
- Hansson M, Vener AV** (2003) Identification of three previously unknown *in vivo* protein phosphorylation sites in thylakoid membranes of *Arabidopsis thaliana*. *Mol Cell Proteomics* **2**: 550–559
- Herbert SK, Martin RE, Fork DC** (1995) Light adaptation of cyclic electron transport through photosystem I in the cyanobacterium *Synechococcus* sp. PCC 7942. *Photosyn Res* **46**: 277-285
- Hüner NPA, Ivanov AG, Sane PV, Pockock T, Krol M, Balseris A, Rosso D, Savitch LV, Hurry VM, Öquist G** (2006) Photoprotection of Photosystem II: Reaction centre quenching versus antenna quenching. In B Demmig-Adams, WW Adams, AK Mattoo, eds, *Advances in Photosynthesis and Respiration. Photoprotection, Gene Regulation and Environment*, Vol 21. Dordrecht, Springer, pp 155–173
- Ifuku K, Ishihara S, Sato F** (2010) Molecular functions of oxygen-evolving complex family proteins in photosynthetic electron flow. *J Integr Plant Biol* **52**: 723–734
- Ifuku K, Ishihara S, Shimamoto R, Ido K, Sato F** (2008) Structure, function, and evolution of the PsbP protein family in higher plants. *Photosynth Res* **98**: 427–37
- Ifuku K, Yamamoto Y, Ono T, Ishihara S, Sato F** (2005) PsbP protein, but not PsbQ protein, is essential for the regulation and stabilization of Photosystem II in higher plants. *Plant Physiol* **139**: 1175-1184
- Ishihara S, Takabayashi A, Endo T, Ifuku K, Sato F** (2008) Functional analysis of two PsbP-Like (PPL) proteins in I. In JF Allen, E Gantt, JH Golbeck, B Osmond, eds, *Photosynthesis. Energy from the sun: 14th international congress on photosynthesis*. Springer, Heidelberg, pp 1085–1088
- Ishihara S, Takabayashi A, Ido K, Endo T, Ifuku K, Sato F** (2007) Distinct functions for the two PsbP-like proteins PPL1 and PPL2 in the chloroplast thylakoid lumen of *Arabidopsis*. *Plant Physiol* **145**: 668–679
- Ivanov AG, Park YI, Miskiewicz E, Raven JA, Hüner NPA, Öquist G** (2000) Iron stress restricts photosynthetic intersystem electron transport in *Synechococcus* sp. PCC 7942. *FEBS Lett* **485**: 173-177
- Ivanov AG, Sane PV, Simidjiev I, Park YI, Hüner NPA, Öquist G** (2012) Restricted capacity for PSI-dependent cyclic electron flow in *ΔpetE* mutant compromises the ability for acclimation to iron stress in *Synechococcus* sp. PCC 7942 cells. *Biochim Biophys Acta* **1817**: 1277-1284
- Iwai M, Takizawa K, Tokustu R, Okamuro A, Takahashi Y** (2010) Isolation of the elusive supercomplex that drives cyclic electron flow in photosynthesis. *Nature* **464**: 1210–1213

- Jans F, Mignolet E, Houyoux PA, Cardol P, Ghysels B, Cuiné S, Cournac L, Peltier G, Remacle C, Franck F** (2008) A type II NAD(P)H dehydrogenase mediates light-independent plastoquinone reduction in the chloroplast of *Chlamydomonas*. *Proc Natl Acad Sci USA* **105**: 20546–20551
- Johnson GN** (2011) Physiology of PSI cyclic electron transport in higher plants. *Biochim Biophys Acta* **1807**: 906-911
- Kargul J, Barber J** (2008) Photosynthetic acclimation: Structural reorganisation of light harvesting antenna: role of redox-dependent phosphorylation of major and minor chlorophyll a/b binding proteins. *FEBS J* **275**: 1056-1068
- Kargul J, Nield J, Benson S, Vener AV, Barber J** (2005) Light-harvesting complex II protein CP29 binds to photosystem I of *Chlamydomonas reinhardtii* under State 2 conditions. *FEBS J* **272**: 4797-4806
- Klughammer C, Schreiber U** (1991) Analysis of light-induced absorbency changes in the near-infrared spectral region. 1. Characterization of various components in isolated chloroplasts. *Z Naturforsch C* **46**: 233-244
- Krause GH, Weis E** (1991). Chlorophyll fluorescence and photosynthesis: the basics. *Annu Rev Plant Phys Plant Mol Biol* **42**: 313-349
- Kugler M, Jansch L, Kruft V, Schmitz UK, Braun HP** (1997) Analysis of the chloroplast protein complexes by BN-PAGE. *Photosynth Res* **53**: 35–44
- Laemmli UK** (1970) Cleavage of structural proteins during the head of bacteriophage T4. *Nature* **227**: 680–685
- Lemeille S, Willig A, Depège-Fargeix N, Delessert C, Bassi R, Rochaix JD** (2009) Analysis of the chloroplast protein kinase Stt7 during state transitions. *PLoS Biol* **7**: e45
- Liu J, Yang H, Lu Q, Wen X, Chen F, Peng L, Zhang L, Lu C** (2012) PSBP-DOMAIN PROTEIN1, a nuclear-encoded thylakoid lumenal protein, is essential for photosystem I assembly in *Arabidopsis*. *Plant Cell* **24**: 4992–5006
- Lizotte MP, Priscu JC** (1992) Spectral irradiance and bio-optical properties in perennially ice covered lakes of the dry valleys (Antarctica). *Antarc Res Ser* **57**: 1–14
- Majeran W, Zybailov B, Ytterberg AJ, Dunsmore J, Sun Q, van Wijk KJ** (2008) Consequences of C4 differentiation for chloroplast membrane proteomes in maize mesophyll and bundle sheath cells. *Mol Cell Proteomics* **7**: 1609–1638
- Maul JE, Lilly JW, Cui L, dePamphilis CW, Miller W, Harris EH, Stern DB** (2002) The *Chlamydomonas reinhardtii* plastid chromosome islands of genes in a sea of repeats. *Plant Cell* **14**: 2659-2679
- Maxwell PC, Biggins J** (1976) Role of cyclic electron transport in photosynthesis as measured by the photoinduced turnover of P700 in vivo. *Biochemistry* **15**: 3975–3981

- Maxwell DP, Laudenbach DE, Hüner NPA** (1995) Redox regulation of light-harvesting complex II and *cab* mRNA abundance in *Dunaliella salina*. *Plant Physiol* **109**: 787-795
- Merchant SS, Prochnik SE, Vallon O, Harris EH, Karpowicz SJ, Witman GB, Terry A, Salamov A, Fritz-Laylin LK, Marechal-Drouard L, Marshall WF, Qu LH, Nelson DR, Sanderfoot AA, Spalding MH, Kapitonov VV, Ren Q, Ferris P, Lindquist E, Shapiro H, Lucas SM, Grimwood J, Schmutz J, Cardol P, Cerutti H, Chanfreau G, Chen CL, Cognat V, Croft MT, Dent R, Dutcher S, Fernandez E, Fukuzawa H, Gonzalez-Ballester D, Gonzalez-Halphen D, Hallmann A, Hanikenne M, Hippler M, Inwood W, Jabbari K, Kalanon M, Kuras R, Lefebvre PA, Lemaire SD, Lobanov AV, Lohr M, Manuell A, Meier I, Mets L, Mittag M, Mittelmeier T, Moroney JV, Moseley J, Napoli C, Nedelcu AM, Niyogi K, Novoselov SV, Paulsen IT, Pazour G, Purton S, Ral J-P, Riano-Pachon DM, Riekhof W, Rymarquis L, Schroda M, Stern D, Umen J, Willows R, Wilson N, Zimmer SL, Allmer J, Balk J, Bisova K, Chen CJ, Elias M, Gendler K, Hauser C, Lamb MR, Ledford H, Long JC, Minagawa J, Page MD, Pan J, Pootakham W, Roje S, Rose A, Stahlberg E, Terauchi AM, Yang P, Ball S, Bowler C, Dieckmann CL, Gladyshev VN, Green P, Jorgensen R, Mayfield S, Mueller-Roeber B, Rajamani S, Sayre RT, Brokstein P, Dubchak I, Goodstein D, Hornick L, Huang YW, Jhaveri J, Luo Y, Martinez D, Ngau WCA, Otilar B, Poliakov A, Porter A, Szajkowski L, Werner G, Zhou K, Grigoriev IV, Rokhsar DS, Grossman AR** (2007) The *Chlamydomonas* genome reveals the evolution of key animal and plant functions. *Science* **318**: 245-250
- Mi H, Endo T, Schreiber U, Asada K** (1992) Donation of electrons to the intersystem chain in the cyanobacterium *Synechococcus* sp. PCC 7002 as determined by the reduction of P700⁺. *Plant Cell Physiol* **33**: 1099–1105
- Miyao M, Murata N** (1985) The Cl⁻ effect on photosynthetic oxygen evolution: interaction of Cl⁻ with 18-kDa, 24-kDa and 33-kDa proteins. *FEBS Lett* **180**: 330–308
- Morgan RM, Ivanov AG, Prisco JC, Maxwell DP, Hüner NPA** (1998) Structure and composition of the photochemical apparatus of the antarctic green alga, *Chlamydomonas subcaudata*. *Photosyn Res* **56**: 303-14
- Morgan-Kiss RM, Ivanov AG, Hüner NPA** (2002a) The Antarctic psychrophile, *Chlamydomonas subcaudata*, is deficient in state I state II transitions. *Planta* **214**: 435–445
- Morgan-Kiss RM, Ivanov AG, Pockock T, Krol M, Gudynaite-Savitch L, Hüner NPA** (2005) The Antarctic psychrophile, *Chlamydomonas raudensis* Ettl. (UWO241) (Chlorophyceae, Chlorophyta) exhibits a limited capacity to photoacclimate to red light. *J Phycol* **41**: 791-00
- Morgan-Kiss R, Ivanov AG, Williams J, Khan M, Hüner NPA** (2002b) Differential thermal effects on the energy distribution between photosystem II and

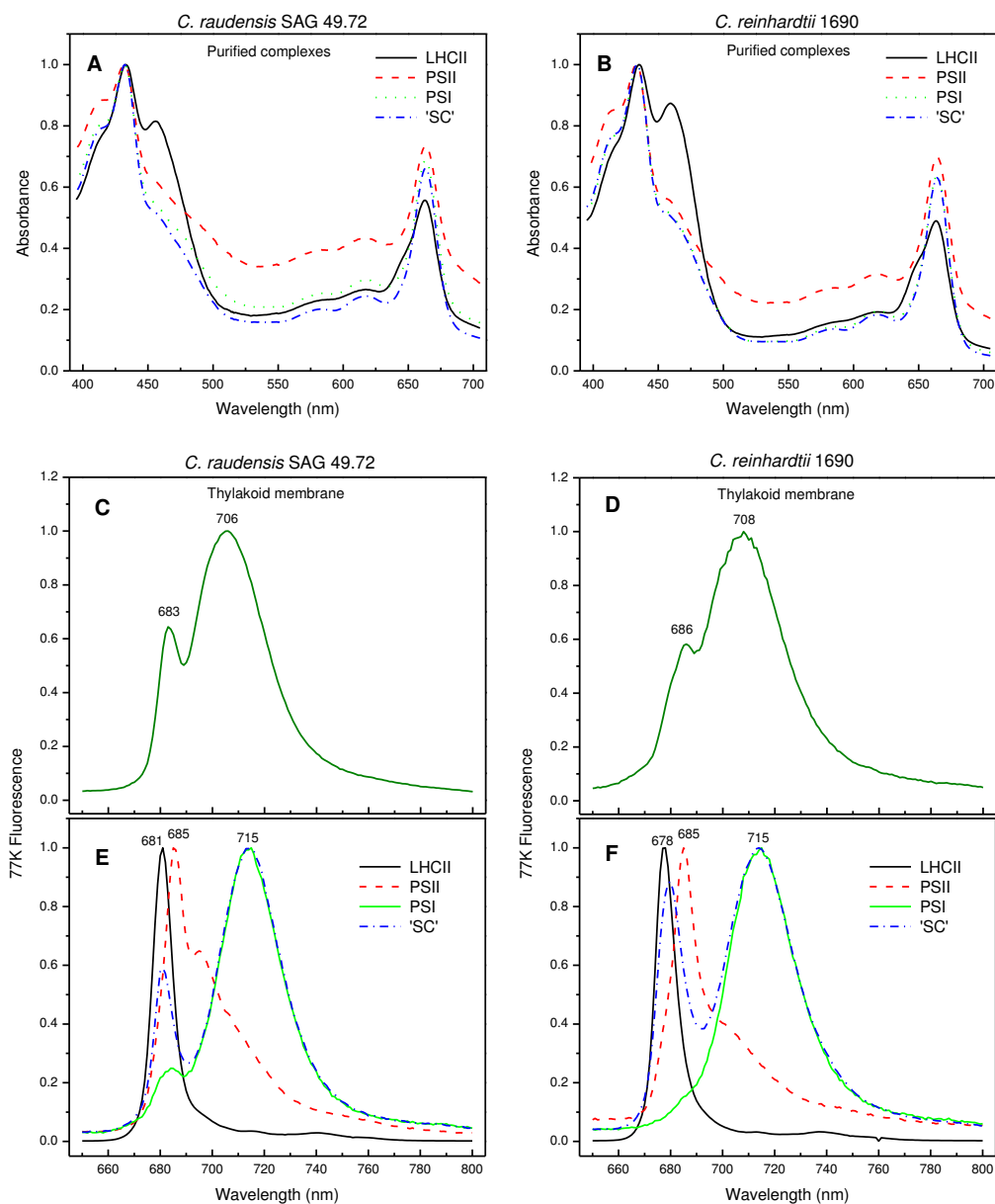
photosystem I in thylakoid membranes of a psychrophilic and a mesophilic alga. *Biochim Biophys Acta* **1561**: 251-265

- Morgan-Kiss RM, Priscu JC, Pockock T, Gudynaite-Savitch L, Hüner NP** (2006) Adaptation and acclimation of photosynthetic microorganisms to permanently cold environments. *Microbiol Mol Biol Res* **70**: 222-52
- Moss DA, Bendall DS** (1984) Cyclic electron transport in chloroplasts: the Q-cycle and the site of action of antimycin. *Biochim Biophys Acta* **767**: 389-395
- Mus F, Cournac L, Cardettini V, Caruana A, Peltier G** (2005) Inhibitor studies on non-photochemical plastoquinone reduction and H₂ photoproduction in *Chlamydomonas reinhardtii*. *Biochim Biophys Acta* **1708**: 322–332
- Oudot-Le Secq MP, Grimwood J, Shapiro H, Armburst EV, Bowler C, Green BR** (2007) Chloroplast genomes of the diatoms *Phaeodactylum tricornutum* and *Thalassiosira pseudonana*: comparison with other plastid genomes of the red lineage. *Mol Genet Genomics* **277**: 427-439
- Owens GC, Ohad I** (1982) Phosphorylation of *Chlamydomonas reinhardtii* chloroplast membrane proteins *in vivo* and *in vitro*. *J Cell Biol* **93**: 712–718
- Peltier G, Cournac L** (2002) Chlororespiration. *Annu Rev Plant Biol* **53**: 523–550
- Peng L, Fukao Y, Fujiwara M, Takami T, Shikanai T** (2009) Efficient operation of NAD(P)H dehydrogenase requires supercomplex formation with photosystem I via minor LHCI in *Arabidopsis*. *Plant Cell* **21**: 3623–3640
- Peng L, Shimizu H, Shikanai T** (2008) The chloroplast NAD(P)H dehydrogenase complex interacts with photosystem I in *Arabidopsis*. *J Biol Chem* **283**: 34873–34879
- Pockock TH, Koziak A, Rosso D, Falk S, Hüner NPA** (2007) *Chlamydomonas raudensis* (UWO241), chlorophyceae, exhibits the capacity for rapid d1 repair in response to chronic photoinhibition at low temperature. *J Phycol* **43**: 924-936
- Pockock T, Lachance MA, Pröschold T, Priscu JC, Kim SS, Hüner NPA** (2004) Identification of a psychrophilic green alga from Lake Bonney Antarctica: *Chlamydomonas raudensis* Ettl. (UWO 241) *Chlorophyceae*. *J Phycol* **40**: 1138-1148
- Possmayer M, Berardi G, Beall BFN, Trick CG, Hüner NPA, Maxwell DP** (2011) Plasticity of the psychrophilic green alga *Chlamydomonas raudensis* (UWO 241) (Chlorophyta) to supraoptimal temperature stress. *J Phycol* **47**: 1098-09
- Ravenel J, Peltier G, Havaux M** (1994) The cyclic electron pathways around photosystem I in *Chlamydomonas reinhardtii* as determined *in vivo* by photoacoustic measurements of energy storage. *Planta* **193**: 251–259
- Rochaix JD** (2011) Regulation of photosynthetic electron transport. *Biochim Biophys Acta* **1807**: 878-886
- Roose JL, Frankel LK, Bricker TM** (2011) Developmental defects in mutants of the PsbP domain protein 5 in *Arabidopsis thaliana*. *PLoS One* **6**: e28624

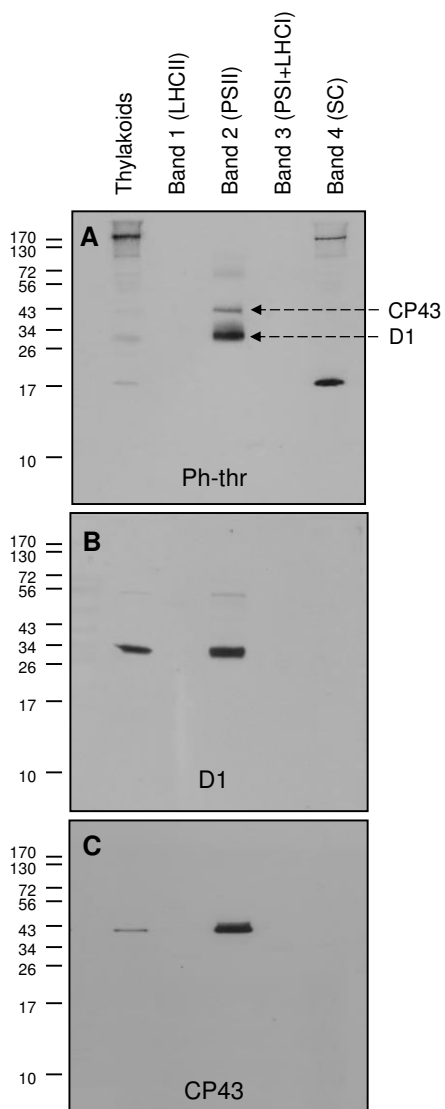
- Sane PV, Ivanov AG, Öquist G, Hüner NPA** (2012) Thermoluminescence. In JJ Eaton-Rye, BC Tripathy, TD Sharkey, eds, *Advances in Photosynthesis and Respiration. Photosynthesis: Plastid Biology, Energy Conversion and Carbon Assimilation*, Vol 34. Springer Science, pp 445-474
- Shikanai T** (2007) Cyclic electron transport around photosystem I: genetic approaches. *Annu Rev Plant Biol* **58**:199–217
- Smith BM, Morrissey PJ, Guenther JE, Nemson JA, Harrison MA, Allen JF, Melis A** (1990) Response of the photosynthetic apparatus in *Dunaliella salina* (green alga) to irradiance stress. *Plant Physiol* **93**: 1433-1440
- Suorsa M, Sirpiö S, Aro EM** (2009) Towards characterization of the chloroplast NAD(P)H dehydrogenase. *Mol Plant* **2**: 1127–1140
- Suorsa M, Sirpiö S, Paakkarinen V, Kumari N, Holmström M, Aro EM** (2010) Two proteins homologous to PsbQ are novel subunits of the chloroplast NAD(P)H dehydrogenase. *Plant Cell Physiol* **51**: 877–883
- Szyszkla B, Ivanov AG, Hüner NPA** (2007) Psychrophily is associated with differential energy partitioning, photosystem stoichiometry and polypeptide phosphorylation in *Chlamydomonas raudensis*. *Biochim Biophys Acta* **1767**: 789-00
- Takahashi Y, Goldschmidt-Clermont M, Soen SY, Franzén LG, Rochaix JD** (1991) Directed chloroplast transformation in *Chlamydomonas reinhardtii*: insertional inactivation of the *psaC* gene encoding the iron sulfur protein destabilizes photosystem I. *EMBO J* **10**: 2033–2040
- Takahashi H, Iwai M, Takahashi Y, Minagawa J** (2006) Identification of the mobile light-harvesting complex II polypeptides for state transitions in *Chlamydomonas reinhardtii*. *Proc Natl Acad Sci USA* **103**: 477–482
- Takizawa K, Takahashi S, Hüner NPA, Minagawa J** (2009) Salinity affects the photoacclimation of *Chlamydomonas raudensis* Ettl. UWO241. *Photosynth Res* **99**: 195-203
- Thomas P, Ryan D, Levine W** (1976) An improved staining procedure for the detection of peroxidase activity of cytochrome f-450 on sodium dodecyl sulphate polyacrylamide gels. *Anal Biochem* **75**: 168–176
- Tikkanen M, Gollan P, Suorsa M, Kangasjarvi S, Aro EM** (2012) STN7 operates in retrograde signalling through controlling redox balance in the electron transfer chain. *Frontiers Plant Physiol* **3**: article 277
- Tikkanen M, Nurmi M, Kangasjarvi S, Aro EM** (2008) Core protein phosphorylation facilitates the repair of photodamaged photosystem II at high light. *Biochim Biophys Acta* **1777**: 1432-1437
- Tikkanen M, Piippo M, Suorsa M, Sirpio S, Mulo P, Vainonen JP, Vener AV, Allahverdiyeva Y, Aro EM** (2006) State transitions revisited - a buffering system for dynamic low light acclimation of *Arabidopsis*. *Plant Mol Biol* **62**: 779-793

- Turkina MV, Kargul J, Blanco-Rivero A, Villarejo A, Barber J, Vener AV** (2006) Environmentally modulated phosphoproteome of photosynthetic membranes in the green alga *C. reinhardtii*. *Mol Cell Proteomics* **5**: 1412–1425
- Vener AV** (2006) Phosphorylation of thylakoid proteins. In B Demmig-Adams, WW Adams, AK Mattoo, eds, *Advances in Photosynthesis and Respiration. Photoprotection, Gene Regulation and Environment*, Vol 21. Dordrecht, Kluwer Academic Publishers, pp.107-126
- Vener AV** (2007) Environmentally modulated phosphorylation and dynamics of proteins in photosynthetic membranes. *BBA - Bioenergetics* **1767**: 449-457
- Wang H, Gau B, Slade WO, Juergens M, Li P, Hicks LM.** (2014) The global phosphoproteome of *Chlamydomonas reinhardtii* reveals complex organellar phosphorylation in the flagella and thylakoid membrane. *Mol Cell Proteomics* **13**(9): 2337-53
- Wilson KE, Krol M, Hüner NPA** (2003) Temperature-induced greening of *Chlorella vulgaris*. The role of the cellular energy balance and zeaxanthin-dependent nonphotochemical quenching. *Planta* **217**: 616-627
- Wunder T, Liu Q, Aseeva E, Bonardi V, Leister D, Pribil M** (2013) Control of STN7 transcript abundance and transient STN7 dimerisation are involved in the regulation of STN7 activity. *Planta* **237**: 541-558
- Yabuta S, Ifuku K, Takabayashi A, Ishihara S, Ido K, Ishikawa N, Endo T, Sato F** (2010) Three PsbQ-like proteins are required for the function of the chloroplast NAD(P)H dehydrogenase. *Plant Cell Physiol* **51**: 866–876
- Yang EJ, Oh YA, Lee ES, Park AR, Cho SK, Yoo YJ, Park OK** (2003) Oxygen-evolving enhancer protein 2 phosphorylated by glycine-rich protein 3/wall associated kinase 1 in *Arabidopsis*. *Biochem Biophys Res Commun* **305**: 862-868
- Yi X, Hargett SR, Liu H, Frankel LK, Bricker TM** (2007) The PsbP protein is required for photosystem II complex assembly/stability and photoautotrophy in *Arabidopsis thaliana*. *J Biol Chem* **282**: 24833-24841
- Yokthongwattana K, Melis A** (2006) Photoinhibition and recovery in oxygenic photosynthesis: mechanism of a photosystem II damage and repair cycle. In B Demmig-Adams, WW Adams, AK Mattoo, eds, *Advances in Photosynthesis and Respiration. Photoprotection, Gene Regulation and Environment*, Vol 21. Dordrecht, Springer Science, pp 175-191

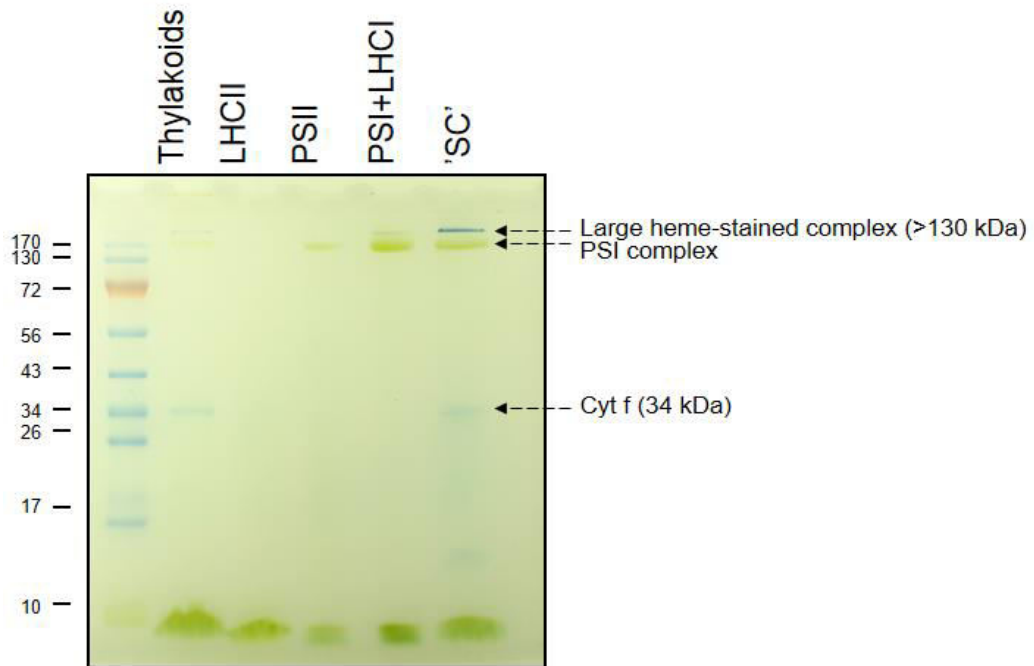
2.7 Appendices



Appendix 2S1: Absorption spectra and 77K fluorescence emission analysis of isolated complexes. Absorption spectra of fractionated complexes from *C. raudensis* SAG 49.72 and *C. reinhardtii* 1690 (A and B). Corresponding 77K emission spectra (C and D) of thylakoid membranes and (EF), subsequent purified fractions of LHCII, PSII and PSI, following mild solubilization with β -DDM and sucrose density centrifugation. Emission peak maxima are indicated above each peak (nm).



Appendix 2S2: Identification of photosystem II phosphoproteins. (A), Phosphorylation profile of purified complex fractions from UWO 241. Immunoblots probed with specific antibodies for the D1 protein (B) and CP43 (C) of photosystem II, as indicated.



Appendix 2S3: Heme staining of purified thylakoid membrane complexes of UWO 241. Complexes were solubilized and separated on a 12% SDS-PAGE gel. The presence of heme was detected at 34 kDa and a large (>130 kDa) band in the lanes containing total thylakoid membrane proteins and the supercomplex fraction.

Appendix 2S4: BLAST results for the protein sequence of spots 1 and 2 from a PSI supercomplex of *Chlamydomonas sp.* UWO 241. A BLAST search of non-redundant databases using the amino acid sequence obtained for spot 1 revealed 90 hits with *E* values of <1.0 (www.ncbi.nlm.nih.gov/BLAST/). The best twenty-five matches are listed.

Accession	Organism	Protein	Coverage (%)	E-value
P11471.1	<i>Chlamydomonas reinhardtii</i>	oxygen-evolving enhancer protein 2	98	8e-69
XP_001694126.1	<i>Chlamydomonas reinhardtii</i>	oxygen-evolving enhancer protein 2	98	8e-69
XP_002956365.1	<i>Volvox carteri</i>	oxygen-evolving enhancer protein 2	98	2e-59
XP_002505689.1	<i>Micromonas sp. FCC299</i>	oxygen-evolving complex 23 kDa protein	97	1e-47
XP_003060004.1	<i>Micromonas pusilla</i>	oxygen-evolving complex 23 kDa protein	98	2e-47
ABK22374.1	<i>Picea sitchensis</i>	unknown	98	1e-45
ABK26108.1	<i>Picea sitchensis</i>	unknown	98	3e-45
O49080.1	<i>Fritillaria agrestis</i>	oxygen-evolving enhancer protein 2	98	7e-45
XP_002521576.1	<i>Ricinus communis</i>	oxygen-evolving enhancer protein 2	98	9e-45
ABR16937.1	<i>Picea sitchensis</i>	unknown	98	1e-44
ABK21284.1	<i>Picea sitchensis</i>	unknown	98	3e-44
XP_001422601.1	<i>Ostreococcus lucimarinus</i>	oxygen evolving enhancer protein 2	98	1e-43
XP_002889614.1	<i>Arabidopsis lyrata</i>	oxygen-evolving enhancer protein 2	98	1e-43
P12302.1	<i>Spinacia oleracea</i>	oxygen-evolving enhancer protein 2	98	2e-43
XP_002881132.1	<i>Arabidopsis lyrata</i>	oxygen-evolving enhancer protein 2	98	2e-43
NP_172153.1	<i>Arabidopsis thaliana</i>	oxygen-evolving enhancer protein 2-1	98	6e-43
XP_001763729.1	<i>Physcomitrella patens</i>	predicted protein	98	1e-42
Q9SLQ8.1	<i>Cucumis sativus</i>	oxygen-evolving enhancer protein 2	98	2e-42
P16059.1	<i>Pisum sativum</i>	precursor for 23-kDa protein of PSII	98	2e-42
P93566.1	<i>Solanum tuberosum</i>	23 kDa oxygen evolving protein of PSII	98	3e-42
ACJ84745.1	<i>Medicago truncatula</i>	unknown	98	3e-42
XP_001753947.1	<i>Physcomitrella patens</i>	predicted protein	98	4e-42
ADQ00373.1	<i>Sequoia sempervirens</i>	oxygen-evolving enhancer protein 2	98	6e-42
BAE71271.1	<i>Trifolium pratense</i>	putative PSII-P (PsbP) protein	98	1e-41
XP_001771262.1	<i>Physcomitrella patens</i>	predicted protein	98	2e-41

Appendix 2S5: PEAKS results for spot 3 from a PSI supercomplex of *Chlamydomonas* sp. UWO 241. Data analysis suggests the presence of two proteins identified in this spot.

Accession (homologous organism)	Protein identity	Theoretical Mass (kDa)	Matched sequences	Peaks score (%)	Coverage (%)
gi 17865463 (<i>Medicago sativa</i>)	ATP-dependent zinc metalloprotease FTSH	75.7	KEISKDEIADALERI KAPCIVFIDEIDAVGRQ RLESGLYSRS KLELQEVVDFLKN RGQAGGLTFFAPSEERL CIVFIDEIDAVGRQ KGCLLVGPPGTGKT	99.1	15.30
gi 15232682 (<i>Arabidopsis thaliana</i>)	Heat shock cognate 70 kDa protein 3 (HSC70-3)	71.1	RVEIANDQGNRT RIINEPTAAAIAYGLDKK RFEELNIDLFRK NAVVTVPAYFNDSQRQ RTTPSYVAFTDSERL	99.0	9.86

Appendix 2S6: PEAKS results for spot 4 from a PSI supercomplex of *Chlamydomonas* sp. UWO 241. Data analysis suggests the presence of several proteins identified in this spot. Proteins with the highest scores and a minimum of 3 matching peptides are shown.

Accession (homologous organism)	Protein identity	Theoretical Mass (kDa)	Matched sequences	Peaks score (%)	Coverage (%)
gi 41179070 (<i>Chlamydomonas reinhardtii</i>)	Photosystem I P700 chlorophyll a apoprotein A1 (PsaA)	83.0	RDYDPTNNYNLLDRV KIAVDRNPVETSFEKW RAIMADLYPSFAKG FFTLNWSEYSDFLTFKG DPTNNYNLLDRV RNSMADLYPSFAKG KIAVNRPVETSFEKW IAVDRNPVETSFEKW RFPCDGPGRG RNPVETTFEKW WAKPGHFSRT IPDKANLGFRF NPVETSFEKW KLLDAGVDPKE	99.2	12
gi 548601 (<i>Chlamydomonas moewusii</i>)	Photosystem I P700 chlorophyll a apoprotein A2 (PsaB)	81.7	KDEPVALSIVQARL KTPLANIVYWKD KDKPVALSIVQARL KDFGYSFPCEGPGRG YDPEANKGNVLARI SFPCDGPGRG DPEANKGNVLARI KQILVQPVFAQWQSAQGKT RDYDPEANKGNVLARI	98.8	9
gi 115470052 (<i>Oryza sativa</i>)	ATP-dependent zinc metalloprotease FTSH1	72.7	KLELQEVVDFLKN* KAPCIVFIDEIDAVGRQ* RYSEFLSAVKDGKV	84.3	6

*Note: marked peptides of FTSH are exact matches of those found in the 70 kDa protein spot number 3.

Appendix 2S7: PEAKS results for a purified PSI-Cyt *b₆* supercomplex of *Chlamydomonas* sp. UWO 241. Proteins with the highest scores, false discovery rate of 1% and a minimum of 3 matching peptides are shown, and listed in order of $-10\log P$ values.

Accession (homologous organism)	Protein identity	Matched sequences	Peaks score (%)	Coverage (%)
gi 41179070 (<i>Chlamydomonas reinhardtii</i>)	Photosystem I P700 chlorophyll a apoprotein A1 (PsaA)	FFTLNWSEYSDFLTFKG KIAVDRNPVETSFEKW RDYDPTNNYNNLLDRV RAIMADLYPSFAKG RFPCDGPGRG IPDKANLGFRF RALSITQGRA	99.2	11
gi 238013200 (<i>Zea mays</i>)	ADP-ribosylation factor (ARF family GTPase)	KLGEIVTTIPTIGFNVETVEYKN KNISFTVWDVGGQDKI KQDLPNAMNAEITDKL RILMVGLDAAGKT RDAVLLVFANKQ RMLNEDELRD RDAVLLVFANKQ	99.1	52
gi 41179066 (<i>Chlamydomonas reinhardtii</i>)	Photosystem I subunit VII (PsaC)	KIYDTCIGCTQCVRA RACPLDVLEMVPWDGCKA KDYDTCIGCTQCVRA RCETACPTDFLSVRV RVYLGSESTRS KIYDTCIGCTQCVRA RACPLDVLEMVPWDGCKA	98.9	63
gi 331268127 (<i>Chlorella variabilis</i>)	Cytochrome <i>b₆</i>	RLEIQAIADISSKY YSLPWDQIGYWAVKI KVYDWFEEERL RVYLTGGFKK	98.7	20
gi 159479282 (<i>Chlamydomonas reinhardtii</i>)	Photosystem I reaction center subunit II (PsaD)	KEQIFEMPTGGAAIMRQ KKEQIFEMPTGGAAIMRQ KKEQCLALTTQLRN	90.6	16
gi 145341034 (<i>Ostreococcus lucimarinus</i>)	FtsH Metalloprotease	KENAPCIIFVDEIDAVGRS RADILDPELLRPGRF KGCLLVGPPGTGKT RIADEAYEVALKQIRD	98.8	9
gi 27734238 (<i>Chlamydomonas raudensis</i>)	Cytochrome <i>f</i>	AYPIFAQQNYENPRE KIPGGPEVIVKE KYPIYVGNRG KSNNTVYNSPVSQTITEILKL	98.7	16
gi 302833183 (<i>Volvox carteri</i>)	Hypothetical protein	KIQFALGLLPAIIFGQKY KMAFLDGAPPERL RFDFPDIPAPWNGIVAILRN	97.4	8
gi 156619331 (<i>Chlamydomonas moewusii</i>)	Photosystem I assembly protein RF4 (Ycf4 superfamily)	REIPLTGIGQPLTLKD KQASELANFLQVSLEGL RIDLSYSLKD	95.4	19

Continued on next page

Accession (homologous organism)	Protein identity	Matched sequences	Peaks score (%)	Coverage (%)
gi 159471964 (<i>Chlamydomonas reinhardtii</i>)	Oxygen-evolving enhancer protein 2 (PsbP)	AAYGDSANVFGKV QSEGGFAPNRVSAASLLDVSTTTDKK RVSAASLLDVSTTTDKKG AIADFGSQDKFLNSVSYLLGKQAYSGETQS QSEGGFAPNRV	96.6	23
gi 307135850 (<i>Cucumis melo</i>)	Adenine nucleotide translocator	KLLIQNQDEMIKS RYFPTQALNFAFKD KEEGFGSLWRG KSSLDAFSQILKN	98.5	11

Chapter 3

3 Specific Lhcb4 and Lhcb5 phosphorylation sites are absent in the psychrophilic state transition variant, *Chlamydomonas sp.* UWO241

3.1 Introduction

Conversion of light energy into chemical energy occurs through two, multisubunit photosystems, photosystem II (PSII) and photosystem I (PSI), which function in parallel to generate an electrochemical gradient of protons across the thylakoid membrane. To optimize photosynthetic rates, a balance must be maintained between absorbed light energy of photosystem II and photosystem I during linear electron flow. State transitions are a mechanism to balance light excitation energy distribution between the two photosystems in plant and green algae, during short-term acclimation to changes in light conditions (Rochaix 2011, Mingawa 2011). The transition from state I to state II is regulated by reversible phosphorylation of light harvesting proteins (LHC) associated with photosystem II (LHCII). Preferential excitation of PSII leads to the activation of a thylakoid membrane kinase which phosphorylates subunits of LHCII (Rochaix et al. 2012). Upon phosphorylation, LHCII proteins disassociate from PSII and migrate to dock with PSI (state II). This process is reversible upon preferential excitation of PSI, which inactivates the kinase, allowing dephosphorylation of LHCII proteins and their return to PSII (state I). Therefore, state transitions operate to adjust the relative absorptive cross sections of PSI and PSII, a process which optimizes photosynthetic efficiency under fluctuating light conditions.

Phosphorylation of PSII-associated light harvesting proteins was observed more than three decades ago (Bennett 1977, Allen 1992). Since then, many studies have revealed that LHCII phosphorylation is an extremely complex event, dependent on multiple factors (Vener 2008). Phosphorylation of LHCII proteins is dependent on the redox state of the plastoquinone (PQ) pool (Allen et al. 1981). The transition from state I to state II

occurs when the PQ pool is reduced and a plastoquinol (PQH₂) binds to the Q(o) site of cytochrome b₆ in the cytochrome b₆/f complex (Vener et al. 1995, Vener et al. 1997). Upon docking of plastoquinol, the Rieske Fe-S protein of the Cyt b₆/f complex undergoes a conformational change, affecting its interaction with, and subsequent activation of the protein kinase, Stt7, which phosphorylates LHCII proteins of *Chlamydomonas reinhardtii* (Depège et al. 2003, Lemeille et al. 2009). However, it is not known whether Stt7 directly phosphorylates LHCII proteins or whether it is part of a kinase cascade involved in state transition signalling. The orthologous protein in *Arabidopsis* is the STN7 kinase (Bellafiore et al. 2005). Dephosphorylation of LHCII proteins requires a phosphatase, which was recently identified as TAP38/PPH1, in *Arabidopsis* (Pribil et al. 2010, Shapiguzov et al. 2010).

Previous studies have shown that exposure to high irradiance levels drastically reduces LHCII phosphorylation status (Rintamäki et al. 1997). It is proposed that inhibition of LHCII phosphorylation results from reduction of the thiol groups of the LHCII kinase, thereby inactivating it through the ferredoxin-thioredoxin system in the stroma (Rintamäki et al. 1997). Two cysteine residues on the luminal, N-terminal end are conserved among all Stt7/STN7 kinases which are critical for Stt7 activity and may represent targets of this redox mechanism (Lemeille et al. 2009, Lemeille and Rochaix 2010). Therefore, in addition to redox control by plastoquinone and components of the cytochrome b₆/f complex, activity of the Stt7/STN7 kinase is regulated by the ferredoxin-thioredoxin system (Rintamäki et al. 1997). Control of Stt7 activity has also been suggested to occur at the level of protein accumulation. Compared to state II, Stt7 exhibits significantly lower abundance under prolonged state I conditions and following exposure to high light (Lemeille et al. 2009). Therefore, Stt7 becomes less stable and has been proposed to degrade under conditions which promote its inactivity (Lemeille et al. 2009). Furthermore, exposure to low light causes light-induced conformational changes of LHCII proteins which enhance the accessibility of LHCII phosphorylation sites to the kinase, whereas high-light treatment prevents LHCII phosphorylation (Zer et al. 1999).

Chlamydomonas reinhardtii LHCII consists of two minor (monomeric) LHCII, Lhcb4 (CP29) and Lhcb5 (CP26), in addition to ten major (trimeric) Lhcbm proteins (Lhcbm1-

10). In *C. reinhardtii*, the major Lhcbm proteins consist of Type I (Lhcbm3, Lhcbm4, Lhcbm6, Lhcbm8 and Lhcbm9), Type II (Lhcbm5), Type III (Lhcbm2 and Lhcbm7) and Type IV (Lhcbm1 and Lhcbm10) (Mingawa and Takahashi 2004). Major Lhcbm proteins are organized in trimers, which are connected to the PSII core complex through monomeric Lhcb4 and Lhcb5. It has been proposed that both minor LHCII, Lhcb4, Lhcb5 and one major LHCII, Lhcbm5 physically shuttle between PSII and PSI during state transitions and their affinity for either photosystem may depend on phosphorylation state (Takahashi et al. 2006, Kargul and Barber 2008). During state I conditions, these three LHCII proteins may act as linker proteins as they are located at the interface between the PSII core and major LHCII trimers (Kargul and Barber 2008, Tokutsu et al. 2009, Lemeille and Rochaix 2010). Therefore, it is likely that dissociation of Lhcb4, Lhcb5 and Lhcbm5, results in the release of major (trimeric) LHCII (Tokutsu et al. 2009, Lemeille and Rochaix 2010).

Chlamydomonas sp. UWO241, represents the first known natural variant which is deficient in state transitions (Morgan-Kiss et al. 2002). This unique green alga was isolated from Antarctica, where it exists 17 meters below the ice-covered surface of Lake Bonney (Neale and Priscu 1995, Priscu 1998). This depth represents the lake's lowest trophic zone, which is characterized by low light irradiance ($<50 \mu\text{mol photons m}^{-2} \text{s}^{-1}$) enriched in the blue-green region of the visible spectrum (450-550 nm), low temperatures (4-6°C), and high salt concentrations (700 mM) (Lizotte and Priscu 1994, Lizotte et al. 1996, Spiegel and Priscu 1996). In addition to high salt tolerance, UWO241 has an optimal growth temperature of 8°C with an inability to grow at temperatures above 16°C, which classifies this alga as an obligate psychrophile (Lizotte and Priscu 1992, Morgan et al. 1998, Pocock et al. 2011).

Structurally, UWO241 exhibits a low PSI:PSII ratio of about 0.5, contributing to an unusually low chlorophyll a/b ratio (~1.8-2.0), and a cytochrome *b₆f* complex containing a cytochrome *f* subunit that is 7 kDa smaller than that of *C. reinhardtii* (Morgan et al. 1998, Morgan-Kiss et al. 2002, Gudynaite-Savitch et al. 2006, Szyszka et al. 2007). However, transformation of *C. reinhardtii* with *petA* from UWO241 demonstrated that the 7 kDa reduction in apparent molecular mass of Cyt *f* does not contribute to the

inability of UWO241 to undergo state transitions (Gudynaite-Savitch et al. 2006). In addition, it has been demonstrated that UWO241 is unable to grow exclusively under far red light (Morgan-Kiss et al. 2005).

Functionally, UWO241 exhibits differential energy partitioning, greater levels of non-photochemical quenching (NPQ) and significantly higher rates of photosystem I cyclic electron transport compared to mesophilic alga (Morgan-Kiss et al. 2002, Szyszka et al. 2007). Analysis of thylakoid protein phosphorylation using phospho-threonine antibodies revealed that UWO241 exhibits a unique phosphoprotein profile compared to other photosynthetic organisms (Morgan-Kiss et al. 2002, Szyszka et al. 2007). In addition to phosphorylation of the typically observed PSII core complex phosphoproteins, D1 and CP43, UWO241 phosphorylates a 17 kDa PsbP-like protein and a 70 kDa FtsH metalloprotease associated with the formation of a PSI-Cyt *b₆f* complex, which is likely involved in cyclic electron flow (CEF) around PSI (Chapter 2).

The inability of UWO241 to perform a state transition response was demonstrated by the absence of changes in the low-temperature (77K) chlorophyll fluorescence emission maxima at 713 nm (PSI) relative to 690 nm (PSII) in response to either light intensity, light quality or increased temperatures (Morgan-Kiss et al. 2002). Furthermore, in contrast to all other photosynthetic organisms, phosphorylation of light harvesting complex II proteins associated with state transitions, has never been detected in UWO241 using immunoblot analysis with antibodies specific for phospho-threonine (Morgan et al. 1998, Morgan-Kiss et al. 2002, Szyszka et al. 2007, Takizawa et al. 2009). We hypothesized that a state transition deficiency in UWO241 may be a consequence of either the absence of the Stt7 kinase involved in LHCI protein phosphorylation, or alternatively, the absence of the predicted LHCI phosphorylation sites in the psychrophile.

3.2 Materials and methods

3.2.1 Growth conditions

Chlamydomonas reinhardtii 1690 and *Chlamydomonas raudensis* SAG 49.72 were grown axenically in Bold's basal medium (BBM), whereas *C. sp.* UWO 241 was grown

in BBM supplemented with 0.7 M NaCl. All cultures were aerated continuously under ambient CO₂ conditions in 4L glass Pyrex bottles. A growth irradiance of 150 μmol photons m⁻² s⁻¹ was generated by fluorescent tubes (Sylvania CW-40), and measured with a quantum sensor attached to a radiometer (Model LI-189; Li-Cor, Lincoln, Neb., USA). Cultures of *C. reinhardtii* and *C. raudensis* were grown at 23°C, whereas, those of *C. sp.* UWO241 were grown at 5°C. Mid-log phase cells were used in all experiments.

3.2.2 Isolation of purified LHCII complexes

Cells were disrupted by passing a suspension through a chilled French press at 6000 lb/in², twice. Thylakoid membranes were purified through a sucrose step gradient centrifugation procedure as described previously (Chua and Bennoun, 1975). Pure thylakoid membranes were resuspended in dH₂O at a chlorophyll concentration of 0.9 mg/mL and solubilized with 1% (w/v) β-DDM on ice for 25 min and centrifuged to remove unsolubilized material. Pure thylakoid membranes were loaded on a continuous 1.3-0.1 M sucrose density gradient and ultracentrifuged as previously described in (Takahashi et al. 1991). Separated bands containing LHCII were isolated, diluted 3 times with 20 mM Hepes, pH 7.5 and centrifuged at 150 000g for 8 hours. Purified LHCII complexes were stored at -80°C until use.

For inhibitor treatments, cell cultures were divided in half and all buffers for thylakoid/complex purification were supplemented with either 20 mM NaF or 0.2 μM staurosporine. Treatment with λ-phosphatase (New England Biolabs) was performed as described by Anderson Peck (2008).

3.2.3 Low temperature (77K) fluorescence

Samples of purified LHCII complex fractions were resuspended to a chlorophyll concentration between 5-10 μg/ml in the presence of 10% (v/v) glycerol. Samples were frozen in NMR tubes with liquid nitrogen and excited at 436 nm (QuantaMaster, Photon Technology International Canada, London, Ontario. Corrected emission spectra were collected between 650 and 800 nm using a 814 Photomultiplier Detection System fluorometer (PTI Canada), with Felix32 Analysis Module (V1.2) software (PTI Canada).

A slit width of 4 nm was used for both excitation and emission. Spectra were normalized to a maximum signal value of 1.0 for comparison.

3.2.4 SDS-PAGE and immunoblotting

Purified LHCII complex fractions isolated by sucrose density centrifugation were solubilized with 1% (w/v) SDS and 1% (v/v) β -mercaptoethanol, and loaded on an equal chlorophyll basis. Electrophoresis was performed using a Mini-Protean II apparatus (Bio-Rad) with a 18% (w/v) polyacrylamide resolving gel, containing 6 M Urea, 0.66 M Tris (pH 8.8) and 8% (w/v) polyacrylamide stacking gel, containing 0.125 M Tris (pH 6.8) using the Laemmli buffer system (Laemmli 1970). Proteins separated by SDS-PAGE were stained with Coomassie blue or transferred electrophoretically to nitrocellulose membranes (Bio-Rad, 0.2 μ m pore size) at 100 V for 1 h at 5°C. The membranes were pre-blocked with a Tris-buffered salt (20 mM Tris, pH 7.5; 150 mM NaCl) containing 3% (w/v) BSA or 5% (w/v) milk powder and 0.01% (v/v) Tween 20. Membranes were probed with antibodies specific for the Stt7 kinase, D1 protein, or *Chlamydomonas* LHCII antibodies Lhcb4/Lhcb5/Lhcbm5 from Agrisera. Immunodetection of phosphorylation was performed using phosphothreonine, phosphoserine and phosphotyrosine antibodies from Zymed Laboratories Inc. at 1:500 dilution. After incubation with secondary antibodies conjugated with horseradish peroxidase (Sigma), the antibody-protein complexes were visualized using ECL chemiluminescent detection reagents (GE Healthcare) and performed according to the manufacturer's instructions.

3.2.5 Column chromatography

A phosphoprotein purification kit from Qiagen (Valencia, CA) was used according to the manufacturer's instructions, to enrich LHCII phosphoproteins from *C. reinhardtii* and *C. sp.* UWO241. Concentrated pure LHCII complex fractions from both alga were diluted to equal chlorophyll concentrations, and protein concentrations of 0.1 mg/ml, as quantified by the Bradford assay. A total of 25 mL was applied to the phosphoprotein purification column at room temperature and phosphoproteins were eluted with 2 mL of phosphoprotein elution buffer. All buffers and the purification column were provided in the kit by the manufacturer (Qiagen). Flow-through and eluted fractions were acetone

precipitated with 80% (v/v) acetone at -20°C, overnight. Precipitated samples were solubilized with solubilization buffer (60 mM Tris-HCl, 1 mM EDTA, 12% (w/v) sucrose 2% (w/v) SDS and 1% (v/v) β -mercaptoethanol), loaded on an equal protein basis (1 μ g/lane), and resolved by 12.5% (w/v) SDS-PAGE, followed by Coomassie staining or immunoblot analysis, as described above.

3.2.6 Isoelectric focusing

Concentrated LHCII complexes were precipitated with 4 volumes of 80% (v/v) acetone for 1 hour at -20°C. The samples were centrifuged and the pellet was resuspended in 80% (v/v) acetone. Samples were recentrifuged and the final pellets were dried with N₂. Isoelectric focusing was performed in a vertical mini-gel format as described by Anderson and Peck (2008). Samples were solubilized in IEF sample buffer (7 M urea, 2 M thiourea, 2% (w/v) CHAPS, 0.8% (v/v) ampholytes (Biorad) 50 mM DTT, 4% (v/v) glycerol and a trace of bromophenol blue) for one hour and centrifuged to remove insoluble material. IEF gels (9 M urea, 1% (w/v) CHAPS, 6% (v/v) polyacrylamide) were cast with 0.4% (v/v) ampholytes (pH 3-10, 4-6 or 3-5) and subjected to electrophoresis using a Mini-Protean II apparatus (Bio-Rad) with 25 mM Tris (or HEPES for narrow pH ranges) and 10 mM phosphoric acid in the upper and lower chambers, respectively. For separation of proteins in the second dimension, single lanes were excised from the focused gels and incubated with equilibration buffer (60 mM Tris pH 6.8, 2% (w/v) SDS, 0.1 M DTT and 10% (v/v) glycerol) for 10 minutes. Gel pieces were placed across 18% (w/v) SDS-PAGE gels and over-layed with equilibration buffer supplemented with 1% (w/v) agarose and a trace of bromophenol blue. Second dimension gels were incubated with 12% (v/v) TCA and stained with Coomassie blue or immunoblotted as described above.

3.2.7 ³³P labelling

Thylakoid membranes were purified through a sucrose step gradient centrifugation procedure as described above (Chua and Bennoun 1975). Pure thylakoids were resuspended, at a chlorophyll concentration of 0.4 mg/mL, in 25 mM Tricine (pH 7.8), 100 mM sorbitol, 20 mM NaCl and 5 mM MgCl₂ as described in Carlberg et al., 1999.

Membranes were phosphorylated in the presence of 0.25 mM ATP, containing [γ - ^{33}P] (0.02 mCi/mg of chlorophyll). Phosphorylation was measured at either 23°C or 8°C, under an irradiance of either 200 $\mu\text{mol photons m}^{-2} \text{s}^{-1}$ or in darkness. The reaction was terminated by the addition of 50 mM EDTA (pH 8) and 20 mM NaF, followed by rapid centrifugation and resuspension of the membranes in solubilization buffer containing 4% (w/v) SDS and 100 mM DTT. Proteins were resolved on 12.5% (w/v) SDS-PAGE gels, transferred electrophoretically onto nitrocellulose membranes at 100 V for 1 h at 5°C, and exposed to film, as described above. Subsequently, autoradiographs (nitrocellulose membranes) were stained with Ponceau S stain (0.1% (w/v) Ponceau S and 5.0% (w/v) acetic acid) for 30 minutes and rinsed with dH₂O.

3.2.8 cDNA library construction

A modified CTAB protocol (Doyle 1991) was used to extract RNA from liquid-nitrogen-ground *C. raudensis* UWO 241 cells. Briefly, 2x (v/w) CTAB buffer at 60°C was added to tissue, vortexed, and incubated for 10 minutes at 60°C. Following two chloroform extractions, nucleic acids were precipitated with an equal volume of isopropanol. Nucleic acids were re-suspended in DEPC-treated water and RNA was precipitated with an equal volume of 4 M LiCl. Following re-suspension, contaminating polysaccharides were precipitated by adding 1/30th volume 3 M sodium acetate (pH 5.2) and 1/10th volume 100% ethanol, incubated on ice for 30 minutes, and centrifuged for 30 minutes (Asif et al. 2000). The supernatant was transferred to a new tube, and RNA was precipitated with sodium acetate and ethanol, the pellet was washed with 70% (v/v) ethanol, and re-suspended in DEPC-treated water.

Messenger-RNA was isolated from total RNA using the Life Technologies (Burlington, ON) Dynabeads® mRNA Purification Kit, according to the manufacturer's instructions. A cDNA library was constructed with the Agilent (Santa Clara, CA) Lambda Zap Gigapack Gold III cDNA library construction kit according to the manufacturer's instructions. Treatment of mRNA with methylmercury hydroxide was performed prior to reverse transcription.

3.2.9 Cloning of minor LHCII in UWO241

The cDNA library was screened for two minor LHCII proteins, Lhcb4 and Lhcb5. Primers were designed based on known conserved regions within *C. reinhardtii* Lhcb4/Lhcb5 nucleotide sequences available through the NCBI database. Two gene-specific primers were used to isolate the full-length cDNA in combination with two vector-specific, T3/T7 primers for each gene, as indicated below.

Lhcb4

(Forward) 5'-TTCCGCGAGTGGGAGCTGAT-3'

(T7) 5'-TACGACTCACTATAGGGCGAATTG-3'

(Reverse) 5'-AGAACTCAGCGCCACCGACC-3'

(T3a) 5'-TTAACCTCACTAAAGGGAACAAA-3'

Lhcb5

(Forward) 5'-TACTTCGCCGTGCCTTGGGG-3'

(T7) 5'-TACGACTCACTATAGGGCGAATTG-3'

(Reverse) 5'-ATGGCACGGCGAAGTAGT-3'

(T3b) 5'-GCTTCCGGCTCGTATGTTGTGTGG-3'

Taq DNA polymerase (New England BioLabs, Ipswich, MA) was used in PCR reactions to amplify the sequences of Lhcb4 and Lhcb5. Samples were resolved on 1% (w/v) agarose gels, stained with ethidium bromide. Bands were excised from the gel and purified with a gel extraction kit (Quiagen, Hilden, Germany). DNA fragments were submitted for sequencing reactions (Robarts Research Institute, London, ON).

Overlapping, gene sequences were combined using CodonCode Aligner software, and the resulting nucleotide sequences were used to generate Lhcb4 and Lhcb5 amino acid sequences. These were aligned with existing Lhcb4/Lhcb5 protein sequences available through the NCBI database (<http://www.ncbi.nlm.nih.gov>), using the Clustal W program (Larkin et al. 2007).

3.3 Results

3.3.1 LHCII complexes

To examine the photosystem II pigment-protein complexes involved in state transitions, light harvesting complexes from control species, *C. reinhardtii* 1690 and the mesophile, *C. raudensis* SAG 49.72 as well as the psychrophile, *Chlamydomonas* sp. UWO241 were isolated by sucrose density ultra-centrifugation. Purified LHCII from each species was characterized using 77K fluorescence emission and visible absorption spectroscopy (Fig. 3.1). In all three species, the 77K chlorophyll fluorescence spectra exhibited single emission peaks with maxima between 678-681 nm, consistent with the identification of these fractions as purified light harvesting complexes of photosystem II (Krause and Weiss, 1991; Fig. 3.1A). Relative to Chl a absorption at 435 and 663 nm, the characteristic Chl b absorption band at 457 nm and the shoulder at 647 nm was increased in UWO241 LHCII complexes, compared to LHCII of both mesophilic species (Fig. 3.1B). This is consistent with the observed differences in LHCII chlorophyll a/b ratios (Table 3.1). LHCII isolated from UWO241 contained the lowest Chl a/b ratio of 1.30, which was 13-32% lower compared to both mesophilic LHCII complexes (Table 3.1). Therefore, the LHCII complex of UWO241 exhibits different spectral characteristics, compared to those of the control mesophilic species, *C. raudensis* and *C. reinhardtii*.

Native LHCII complexes of *C. reinhardtii*, *C. raudensis* and *C. sp.* UWO241 were solubilized with SDS and fractionated into individual protein subunits using SDS-PAGE (Fig. 3.2). Previous studies have established that LHCII complexes of *C. reinhardtii* contain two minor proteins, Lhcb4 and Lhcb5, as well as ten major Lhcbm proteins (Lhcbm1-10). Major Lhcbm proteins share nearly identical amino acid sequences and molecular masses, which results in co-migration during SDS-PAGE (Lemeille et al. 2010, Bassi and Wollman 1991). As a result, major Lhcbm proteins typically resolve into four bands, designated as p11 (Type I), p13 (Type I), p16 (Type IV) and p17 (Type III), in the range of 25-33 kDa (Lemeille et al. 2010, Bassi and Wollman 1991). Among these major Lhcbm proteins in *C. reinhardtii*, phosphorylation occurs on p11, p13 and p16, but not on p17 (Mingawa and Takahashi 2004). Minor proteins, Lhcb4 and Lhcb5, migrate at

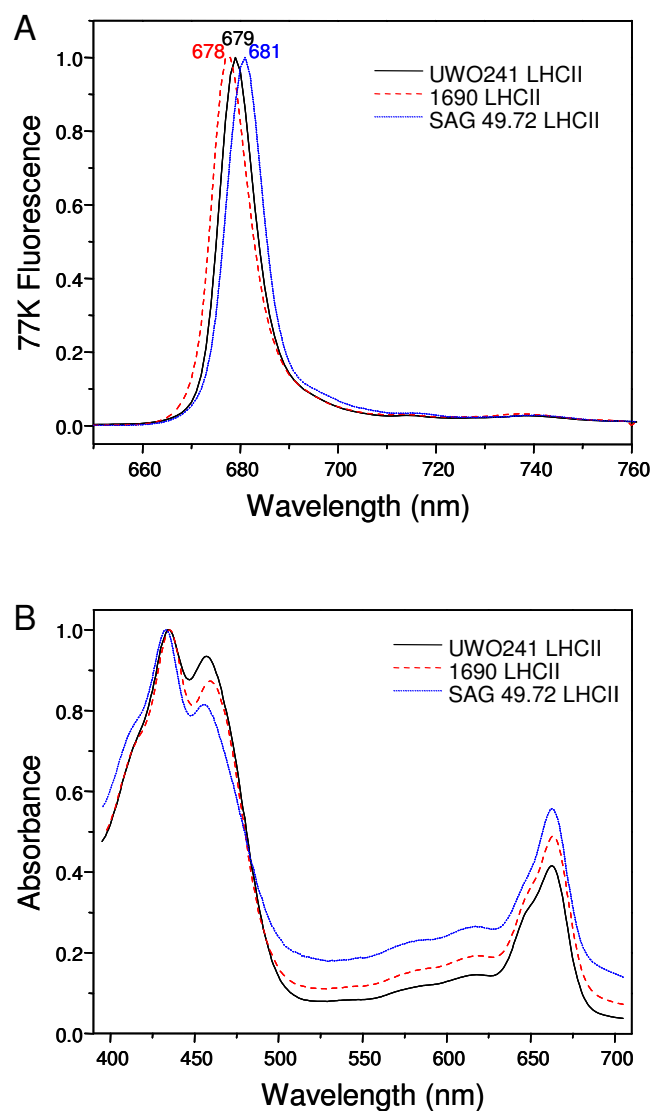


Figure 3.1: 77K chlorophyll fluorescence emission spectra of purified LHCII complexes from *C. reinhardtii* 1690, *C. raudensis* 49.72 and *C. sp.* UWO241 (A) and absorption spectra (B). Emission spectra were obtained for chlorophyll a excitation at 436 nm.

Table 3.1: Chlorophyll a/b ratios of purified LHCII complexes from *C. reinhardtii* 1690, *C. raudensis* 49.72 and *C. sp.* UWO241 and 77K fluorescence emission maxima.

	Chl a/b	77K maxima
1690	1.49 ± 0.05	678 nm
SAG 49.72	1.91 ± 0.06	681 nm
UWO241	1.30 ± 0.08	679 nm

higher apparent molecular masses of 35-39 kDa, as p9 and p10 bands, respectively (Lemeille et al. 2010).

Consistent with previous reports, *C. reinhardtii* LHCII complex proteins separated into three major Lhcbm protein bands p13/11 (31 kDa), p16 (26 kDa), p17 (25 kDa) and one minor LHCII band p9/10 (38 kDa) (Fig. 3.2A). LHCII complexes of *C. raudensis* resolved into three major Lhcbm protein bands, p13/11 (30 kDa), p16 (28 kDa), p17 (27.5 kDa) and one minor LHCII band p9/p10 (35 kDa) (Fig. 3.2A). The apparent molecular mass of each LHCII protein band varied in the psychrophile, compared to *C. reinhardtii*. LHCII subunits of UWO241 resolved into one minor LHCII band, p9/10 (37 kDa), and three lower molecular mass bands, presumed to represent major Lhcbm protein bands, which we designated as pA (30.5 kDa), pB (29 kDa) and pC (27 kDa) (Fig. 3.2A). Therefore, individual subunits of UWO241 LHCII complexes exhibit variation in apparent molecular mass, compared to those of *C. reinhardtii*.

Phosphorylation of LHCII in UWO241 has not been detected when intact, thylakoid membrane fractions are probed with antibodies specific for phosphorylated threonine residues (Morgan-Kiss et al. 2002, Szyszka et al. 2007, Takizawa et al. 2009). We examined whether a positive signal may be obtained when using purified LHCII complexes (Fig. 3.2). Consistent with previous studies, immunoblotting of LHCII with phospho-threonine antibodies revealed three bands, at 38 kDa (p10), 35 kDa and 31 kDa (p13/11) in *C. reinhardtii* and one prominent band at 30 kDa (p11/13) in *C. raudensis* (Fig. 3.2B). In contrast, phos-thre antibodies did not react with any LHCII subunits in UWO241 (Fig. 3.2B). Phospho-serine antibodies reacted weakly with two major LHCII bands in *C. reinhardtii*, at 31 kDa (p13/11), 25-26 kDa (p16/17) and two bands in *C. raudensis*, at 30 kDa (p11/13) and 27 (p16/17) (Fig. 3.2C). Phos-serine antibodies did not react with LHCII in UWO241. Therefore, in contrast to both mesophilic species, LHCII of *Chlamydomonas sp.* UWO241 did not result in a positive signal with either phospho-threonine or phospho-serine antibodies, even in the purified LHCII complex (Fig. 3.2B and C).

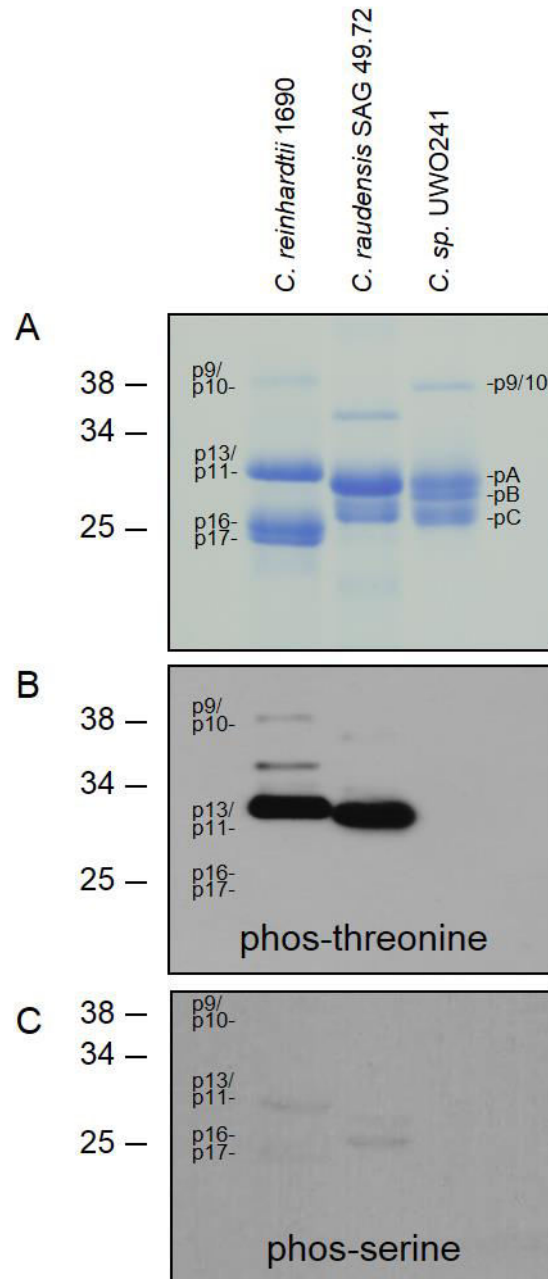


Figure 3.2: Purified LHCII complex proteins of *C. reinhardtii* 1690, *C. raudensis* 49.72 and *C. sp.* UWO241 resolved with SDS-PAGE and stained with Coomassie blue (A). Purified LHCII complex proteins immunoblotted with antibodies specific for phospho-threonine (B) and phospho-serine (C). Molecular masses (kDa) are indicated on the left.

3.3.2 Affinity purification of LHCII phosphorylated polypeptides

To enhance the resolution of the differential pattern for LHCII phosphorylation, purified pigment-protein LHCII complexes of UWO241 and the model green alga, *C. reinhardtii*, were subjected to affinity chromatography using a phospho-protein purification kit in order to separate phosphorylated and unphosphorylated LHCII proteins (Fig. 3.3). The percentage of LHCII proteins bound to the column was estimated from the total chlorophyll content of the eluted, phosphoprotein-enriched fraction relative to the control fraction prior to affinity chromatography (Fig. 3.3A). The *C. reinhardtii* phosphoprotein-enriched, eluted fraction contained 17.8% of the total chlorophyll, compared to only 2.8% of the total chlorophyll in the UWO241 sample (Fig. 3.3A).

Unphosphorylated proteins present in the flow-through fraction and phosphorylated LHCII present in the eluted fractions were acetone precipitated, loaded on an equal protein basis (1 µg/lane) and separated by SDS-PAGE (Fig. 3.3B). Immunoblot analysis with phospho-threonine antibodies confirmed that separation of phosphorylated from non-phosphorylated proteins occurred in *C. reinhardtii*, as the flow-through fraction (-) (Fig. 3.3C, lane 1) exhibited weaker binding of the phospho-threonine antibodies, compared to the signal from the column-bound (+), eluate (Fig. 3.3C, lane 3). In contrast, neither the flow-through (-) or eluate (+) fractions of UWO241 LHCII exhibited a positive signal with phospho-threonine antibodies (Fig. 3.3C, lane 2 & 4). Thus, purified LHCII proteins of UWO241 did not generate a positive signal with phospho-threonine antibodies, even after affinity purification. Although LHCII phosphorylation typically occurs on threonine residues, we were also unable to attain a positive signal using either phospho-serine or phospho-tyrosine antibodies on the column-bound LHCII protein fraction of UWO241 (data not shown). We concluded that phos-thre/ser/tyr antibodies were not able to detect phosphorylation of LHCII proteins in the Antarctic psychrophile, *Chlamydomonas sp.* UWO241.

3.3.3 IEF detection of phosphorylated LHCII

Since phosphorylation of UWO241 LHCII could not be detected with specific phosphorylation antibodies, two-dimensional IEF/SDS-PAGE was used to separate

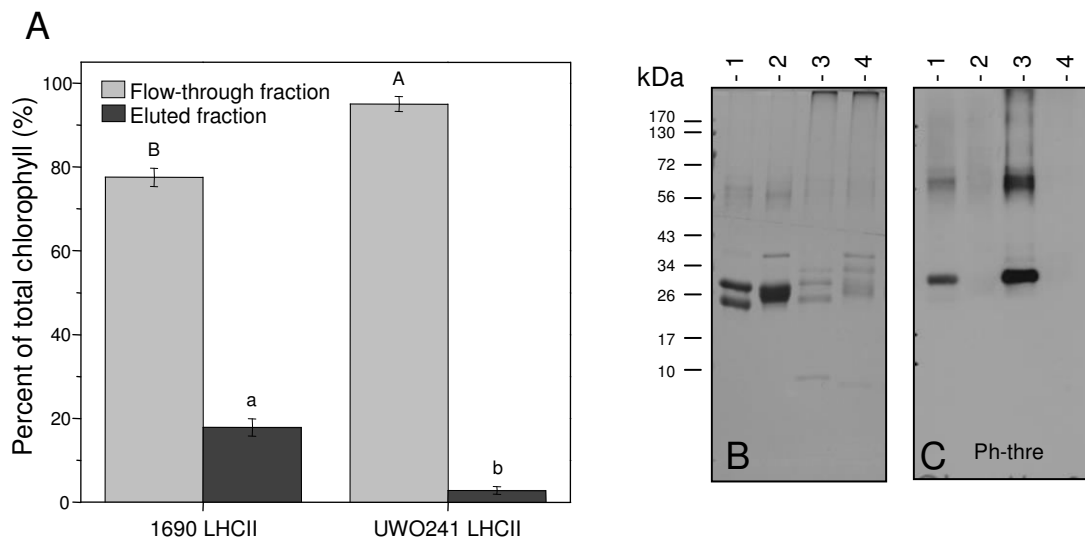


Figure 3.3: Affinity purification of LHCII phosphoproteins. Mean total chlorophyll percentage (\pm SE) of LHCII proteins from the flow-through (unbound) and eluted (column-bound) fractions following affinity purification of phosphoproteins in *C. reinhardtii* compared to *Chlamydomonas sp.* UWO241 (A). Mean percentages were analyzed by an unpaired t-test ($p < 0.001$). Different letters indicate significant difference for $n=3$, as determined by an unpaired t-test ($p < 0.001$) for both percentage of chlorophyll in flow-through fractions (upper case) and percent of chlorophyll in eluted fractions (lower case). Flow-through (non-phosphorylated) and column-eluted (phosphorylated) proteins were loaded on a protein basis (1 μ g/lane) for separation by SDS-PAGE, followed by detection with Coomassie blue (B). A corresponding membrane was immunoblotted with antibodies specific for phospho-threonine (C). Lane numbers are indicated in brackets, molecular masses (kDa) on the left. Lane 1, *C. reinhardtii* flow-through; lane 2, UWO241 flow-through; lane 3, *C. reinhardtii* column-eluate; lane 4, UWO241 column-eluate.

purified LHCII proteins of *C. reinhardtii* and *C. sp.* UWO241. Previous studies have shown that post-translational processing and chemical modification of proteins can be detected using isoelectric focusing (Gianazza 1995; Anderson and Peck 2008). Protein phosphorylation results in a one-charge or two-charge shift in isoelectric point (pI) at pH less than 6 or greater than 7, respectively, associated with the addition of each acidic phosphate group. This can be resolved with IEF (Gianazza 1995; Anderson and Peck 2008).

Two-dimensional IEF/SDS-PAGE protein maps were established to examine migrational shifts in isoelectric points of purified LHCII proteins in both *C. reinhardtii* and *C. sp.* UWO241. Prior to separation, cells were treated with either a phosphatase inhibitor (NaF) or a kinase inhibitor (staurosporine), to induce LHCII phosphorylation and dephosphorylation, respectively. Alternatively, acetone precipitated LHCII proteins isolated in the presence of NaF were treated with a λ -phosphatase to examine the potential for dephosphorylation, by removal of phosphate groups *in vitro*. Figure 3.4 shows the result for *C. reinhardtii* LHCII proteins treated with either NaF/staurosporine (Fig. 3.4A and B) or with λ -phosphatase (Fig. 3.4C and D). Compared to treatment with either staurosporine or λ -phosphatase (Fig. 3.4A, C), the presence of NaF alone resulted in the appearance of four protein spots (Fig. 3.4A, black arrows). These spots corresponded to one minor LHCII spot from band p9/10 (pH 6.1, spot 1), two major LHCII spots from band p13/11 (pH 4.9 and 4.5, spot 2 and 3), and one major LHCII spot from band p16/17 (pH 4.4, spot 4), which is not evident in the presence of either the kinase inhibitor, staurosporine (Fig. 3.4B) or λ -phosphatase (Fig. 3.4D). Thus, treatment with either staurosporine or λ -phosphatase appeared to be effective in removing phosphate groups. Consistently, spots #1, 2 and 3, which correspond to p9/10 and p11/13, reacted positively when probed with phospho-threonine antibodies in *C. reinhardtii* (Appendix 2S1). In contrast, spot #4 (p16/p17) did not produce a signal with phospho-threonine antibodies, consistent with the findings observed in Figure 3.2B.

However, in contrast to *C. reinhardtii*, this technique was unable to detect any changes in LHCII protein migration under phosphorylating and nonphosphorylating conditions in

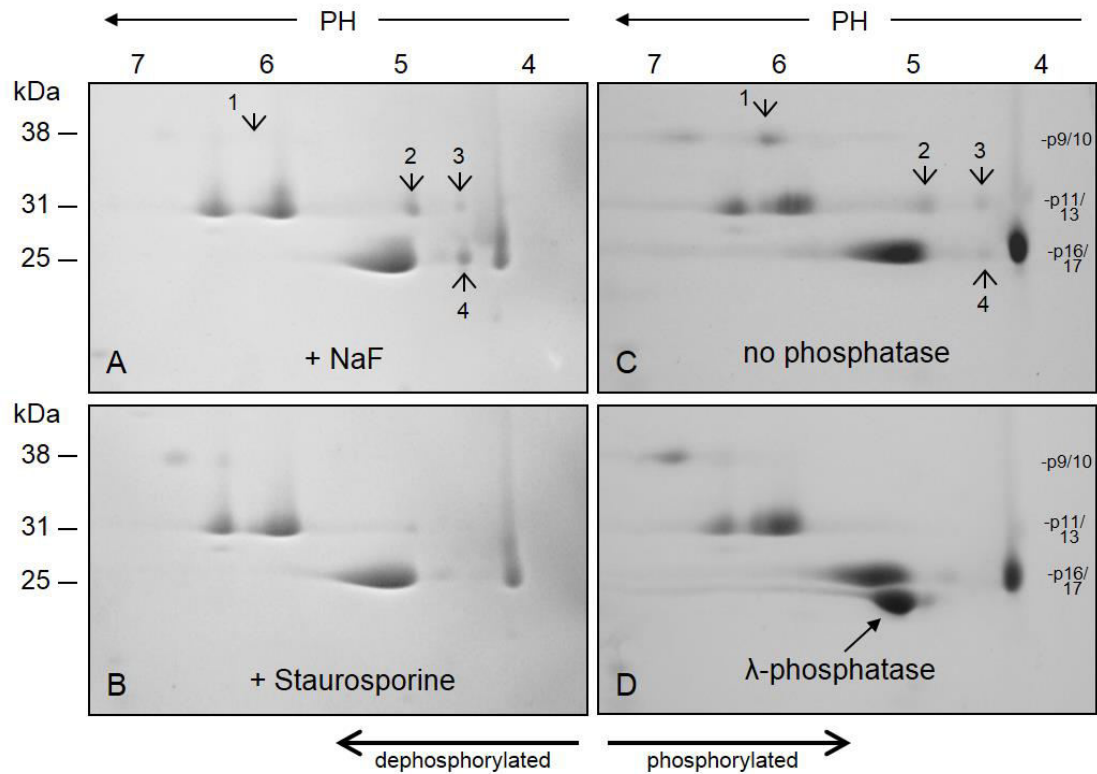


Figure 3.4: Two-dimensional (IEF/SDS-PAGE) separation of purified LHCII in *C. reinhardtii*. Samples were treated with inhibitors (NaF and staurosporine) (A and B) and a λ -phosphatase (-/+ (C and D). Broad range (3-10 pH) IEF was performed in the first dimension, followed by SDS-PAGE. Arrows indicate differences in patterns of protein migration among treatments.

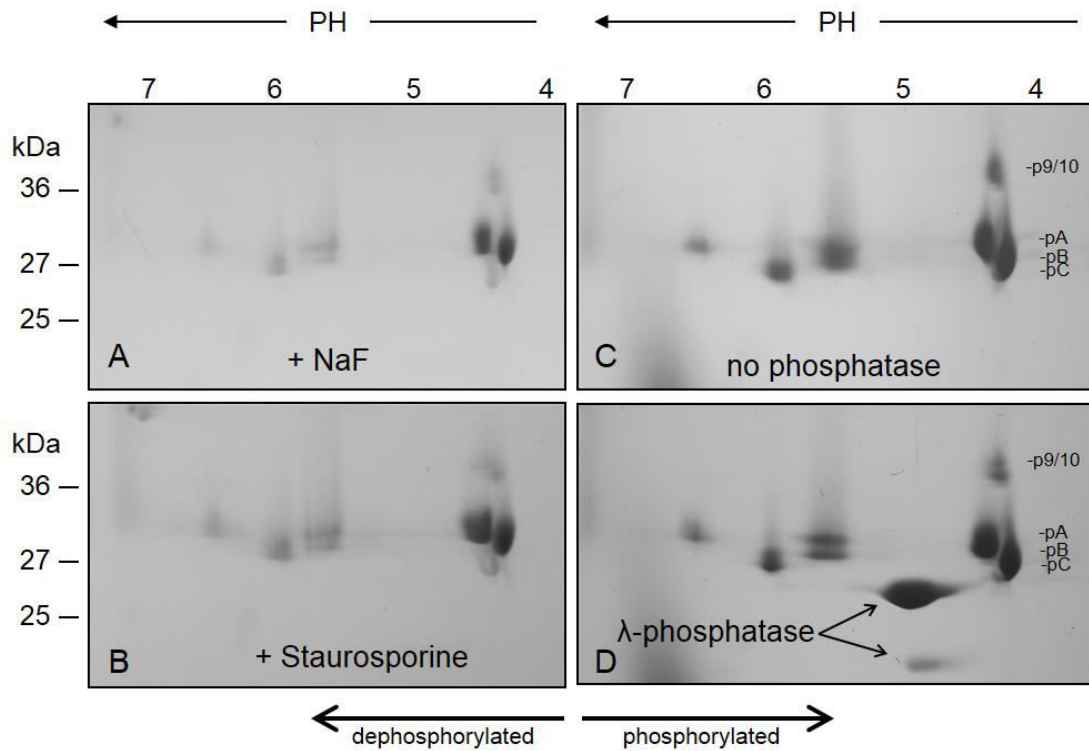


Figure 3.5: Two-dimensional (IEF/SDS-PAGE) separation of purified LHCII in *Chlamydomonas sp.* UWO241. Samples were treated with inhibitors (NaF and staurosporine) (A and B) and a λ -phosphatase (-/+ (C and D). Broad range (3-10 pH) IEF was performed in the first dimension, followed by SDS-PAGE.

the psychrophile, *C. sp.* UWO241 (Fig. 3.5) regardless of the pH range used for IEF dimension (Appendix 2S3).

Therefore, regardless of either the extent of purification or the resolution of the separation technique, phosphorylated LHCII polypeptides were not detected in UWO241 using the phospho-threonine antibody technique.

3.3.4 STT7 kinase

Since no LHCII phosphorylation was detected in UWO241, I hypothesized that, as a consequence of adaptation to its unique environment, the Stt7 kinase required for the phosphorylation of light harvesting complexes (LHCII) during state transitions, may be absent in UWO241. To assess the presence of this kinase, thylakoid membranes from *C. reinhardtii* 1690, *C. raudensis* SAG 49.72 and *Chlamydomonas sp.* UWO241 were probed with antibodies specific for Stt7 (Fig. 3.6). The state-transition deficient Antarctic psychrophile, UWO241, exhibited similar levels of the 70-kDa Stt7 kinase polypeptide compared to both mesophilic species (Fig. 3.6). Furthermore, a second band with an apparent molecular mass of 67 and 62 kDa reacted positively with Stt7 antibodies in *C. reinhardtii* and UWO241, respectively. Thus, it was concluded that the Stt7 kinase required for LHCII polypeptide phosphorylation is present in the Antarctic psychrophile, UWO241.

3.3.5 Radioactive ^{33}P labelling

The most sensitive technique for detection of phosphorylation is radioactive labelling of phosphoproteins with either ^{32}P or ^{33}P (Vener 2008). Therefore, this method was employed to determine whether any LHCII-associated phosphorylation could be detected in the psychrophilic UWO241. Sucrose-gradient purified thylakoid membrane proteins of *C. reinhardtii* and *C. sp.* UWO241 were allowed to phosphorylate *in vitro*, in the presence of [γ - ^{33}P]ATP at temperatures of 23°C and 8°C, respectively following 15 and 30 minutes of light exposure (Fig. 3.7A). The identity of thylakoid protein bands was confirmed using specific antibodies (Fig. 3.7B).

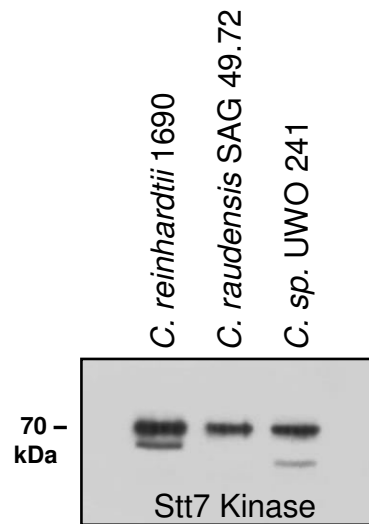


Figure 3.6: Immunoblot analysis of *C. reinhardtii* 1690, *C. raudensis* 49.72 and *C. sp.* UWO241 thylakoid membranes probed with antibodies specific for the Stt7 kinase.

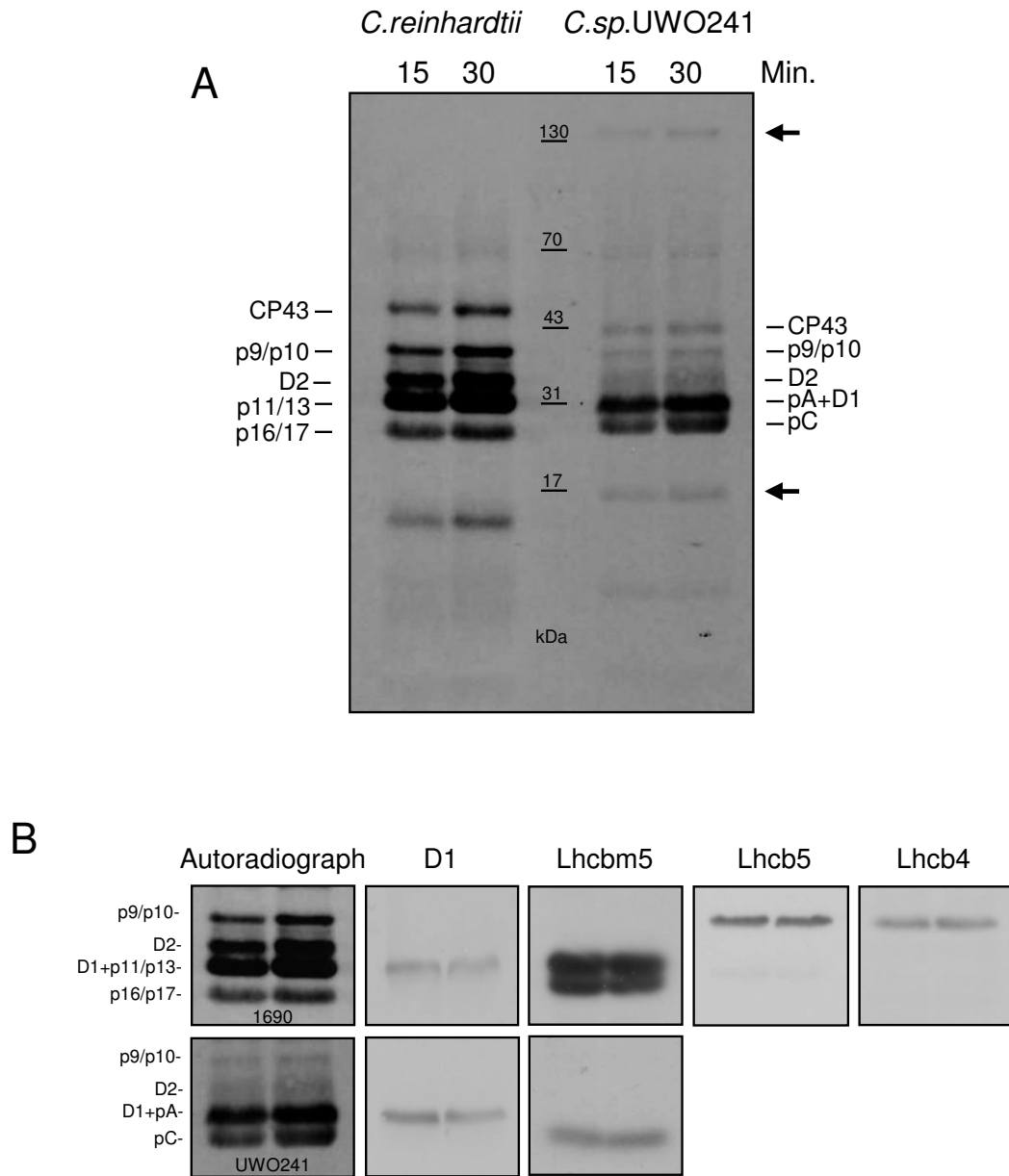


Figure 3.7: Autoradiograph of [γ - 33 P]ATP-labelled thylakoid proteins in *C. reinhardtii* 1690 (left) and *C. sp.* UWO241 (right) following 15 and 30 minutes of light exposure (A). Identification of [γ - 33 P]ATP-labelled phosphoprotein bands in *C. reinhardtii* 1690 (top panels) and *C. sp.* UWO241 (bottom panels) using immunoblotting with antibodies specific for D1, Lhcbm5, Lhcb5, and Lhcb4 (as indicated). The position of the D2 protein was assigned based on previous studies (Lemeille et al. 2010).

In *C. reinhardtii*, high levels phosphorylation were observed for the minor LHCII band (p9/p10 at 36-38 kDa), consisting of Lhcb4 and Lhcb5, and both major LHCII bands (p11/p13 at 31 kDa as well as p16/p17 at 25-26 kDa) (Fig. 3.7A and B). In addition, strong phosphorylation was observed for the PSII core complex proteins, D2 (35 kDa) and CP43 (44 kDa).

Despite negative results obtained with phospho-threonine antibodies, radioactive labelling revealed that LHCII phosphorylation does indeed occur in *C. sp.* UWO241 (Fig. 3.7A). Phosphorylation of the major LHCII protein bands, pA (29 kDa) and pC (27 kDa) was observed in the psychrophile, although the levels of phosphorylation were lower than that of *C. reinhardtii* (Fig. 3.7A, B). However, minimal phosphorylation of minor LHCII band p9/p10 (37 kDa) and the PSII core complex proteins, CP43 (42 kDa) and D2 (35 kDa), was observed in UWO241, compared to *C. reinhardtii* (Fig. 3.7A).

Furthermore, at least two PSII core complex phosphoproteins, D1 and D2, co-migrate with LHCII proteins in the range of 30-35 kDa. D1 co-migrated with the p11/p13 band (31 kDa) in *C. reinhardtii* as well as the pA band (30.5 kDa) of *C. sp.* UWO241 (Fig. 3.7B) and it is not known how much D1 phosphorylation contributes to the signal originating from these bands.

Therefore, based on ^{33}P -labelling, we conclude that UWO241 does phosphorylate LHCII, in contrast to the use of phospho-threonine antibodies (Fig. 3.7A). However, the phosphorylation pattern of UWO241 is distinct from *C. reinhardtii*. Consistent with previous studies (Chapter 2), UWO241 exhibited phosphorylation of a high molecular mass complex (<130 kDa), and a 17 kDa PsbP-like protein, associated with a PSI-Cyt b_6/f supercomplex, in addition to the typically observed D1 (31 kDa) and CP43 (43 kDa) PSII core complex proteins (Fig. 3.7A).

The light-dependence for thylakoid protein phosphorylation in *C. reinhardtii* and *C. sp.* UWO241 was also examined at their optimal growth temperatures (Fig. 3.8A). As expected, levels of [γ - ^{33}P]ATP incorporation were highest under illumination for both minor (36-38 kDa) and major (25-31 kDa) LHCII

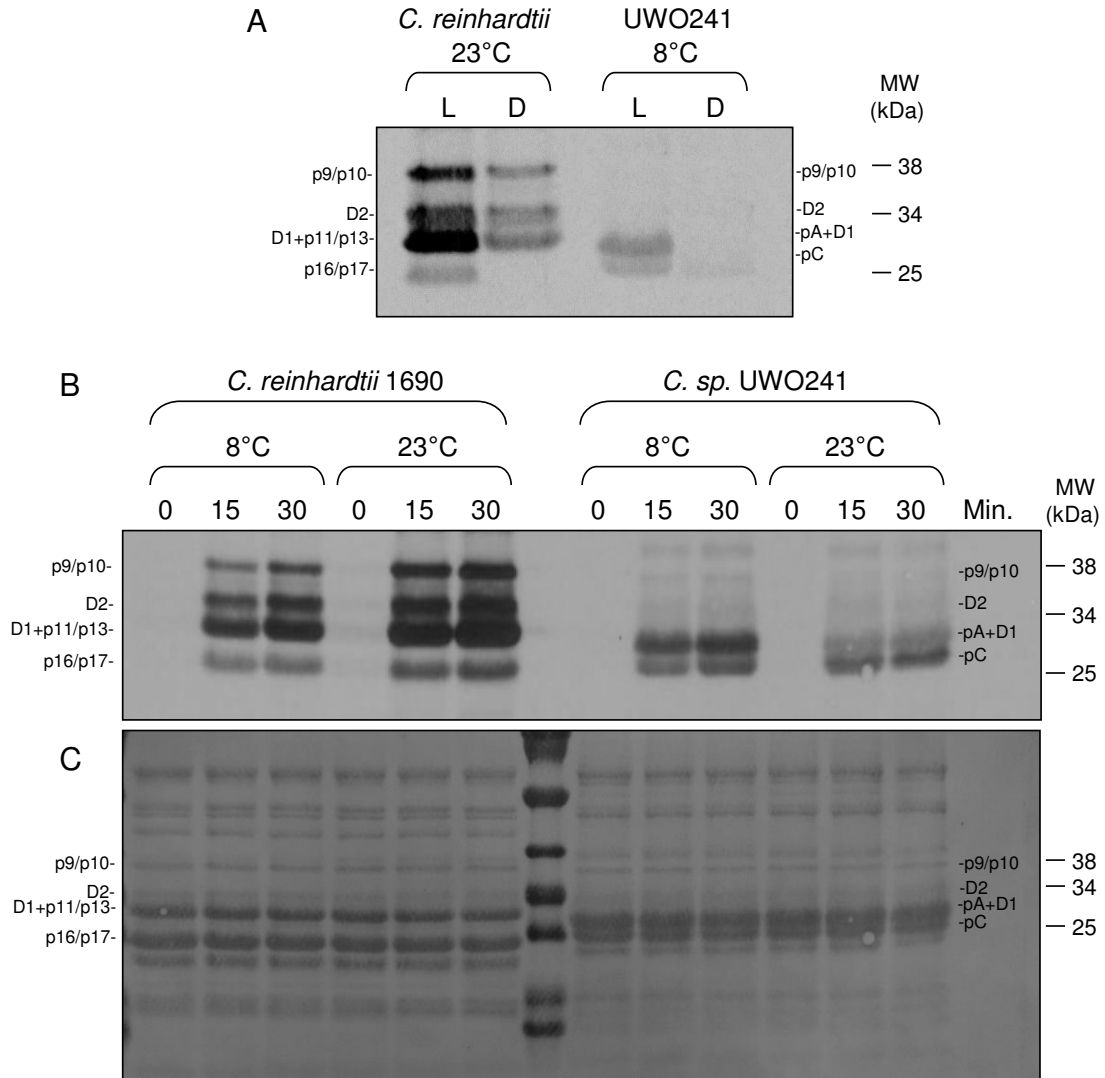


Figure 3.8: In vitro [γ - ^{33}P]ATP labelling of LHCII proteins in *C. reinhardtii* and *C. sp.* UWO241. Levels of thylakoid membrane phosphorylation after 15 minutes of exposure to light (L) were compared to those following 15 minutes of darkness (D), at 8°C and 23°C (as indicated) in both *C. reinhardtii* and *C. sp.* UWO241 (B). Purified thylakoids were phosphorylated at 8°C and 23°C (as indicated) for 0, 15 and 30 minutes, in the presence of light (200 $\mu\text{mol}/\text{m}^2/\text{s}$) (B). The [γ - ^{33}P]ATP-labelled nitrocellulose membrane was stained with Ponceau S to visualize abundance of LHCII compared in part B (C). Levels of phosphorylation after 15 minutes of exposure to light (L) were compared to those following 15 minutes of darkness (D), at 8°C and 23°C (as indicated) in both *C. reinhardtii* and *C. sp.* UWO241 (B).

bands of *C. reinhardtii*, and decreased in the dark (Fig. 3.8A). In contrast to the results for phospho-threonine immunoblots, UWO241 also exhibited light-dependent phosphorylation of pA and D1 polypeptides, albeit at a much lower level than observed for *C. reinhardtii* (Fig. 3.8A). Since optimal growth temperatures for *C. reinhardtii* and UWO241 differ significantly, we examined the effects of temperature on the thylakoid polypeptide phosphorylation status (Fig. 3.8B). As expected, thylakoid polypeptide phosphorylation status was greater at 23°C than 8°C for *C. reinhardtii* (Fig. 3.8C). In contrast, thylakoid polypeptide phosphorylation status was higher at 8°C than 23°C for UWO241 (Fig. 3.8C). However, consistent with the data in Fig. 3.8A, thylakoids from UWO241 never exhibited the phosphorylation status observed for *C. reinhardtii*, regardless of phosphorylating conditions.

In conclusion, [γ -³³P]ATP labelling experiments demonstrated a lower level of LHCII phosphorylation in the psychrophile, UWO241, compared to *C. reinhardtii*, as well as differences in phosphorylation status in response to temperature. A decrease in phosphorylation was specifically observed for the minor LHCII protein band (p9/10), consisting of Lhcb4 and Lhcb5, as well as the PSII core complex.

3.3.6 Sequence of monomeric Lhcb4 and Lhcb5

Since isolated thylakoids from UWO241 exhibited lower levels of PSII-LHCII phosphorylation than *C. reinhardtii*, we hypothesized that phosphorylation sites of LHCII may be absent or altered in the state transition deficient psychrophile, *Chlamydomonas sp.* UWO241. To examine the phosphorylation sites present in monomeric LHCII proteins of *C. sp.* UWO241, *Lhcb4* and *Lhcb5* genes were cloned from a cDNA library. The cDNA derived sequence for *Lhcb4* of UWO241 encoded a 264 amino acid protein, compared to 280 amino acids in *C. reinhardtii* (Fig. 3.9). UWO241 Lhcb4 shared a 66.3% amino acid identity with *C. reinhardtii* and 65.4% identity with *Chlamydomonas incerta*, with low similarity within the first 50 amino acids of the N-terminal end (Fig. 3.9). The multiple phosphorylation sites of Lhcb4 in *C. reinhardtii* have been identified as threonine 7, 11, 17, 18, 33 and serine 103 (Fig. 3.9, red boxes) (Turkina et al. 2006, Lemeille et al. 2010). Compared to *C. reinhardtii* Lhcb4, threonine 7 is absent, threonine 17 is substituted with a proline (P), threonine 33 with a glutamine (Q), and serine 103 is

```

                                     7    11    17 18
C.reinhardtii -----MVFKFP-----TPPGTQK---KAGTTATKPA 23
C.incerta -----MAFKFKLPGSTPAGTTK---KAGTTATKPA 28
V.carteri MQTVLAKSSFMGARPFVGVAGKAKWMDKKLPFSLPSFGLERKSGTVAAKPKAGTATTKPA 60
C.spUWO241 -----MKSLLRTP-----TASRPV 14
C.subellipsoidea -----MVHLSGSFGLSITALAPQ-----NGAKTV 24
                                     :...

                                     33
C.reinhardtii PKATT-KKVAITSTGTRSGGVGYRKYQGDLWLPNTRPEWLDGSLPGDRGFDPGLGSKPS 82
C.incerta PKATTTKKVAVNTGTRSGGVGYRKYQGDLWLPNTARPEWLDGSLPGDRGFDPGLGSKPS 88
V.carteri PKATT-KKVASSSGTRSGGVGYRKYQGDLWLPNTRPEWLDGSLPGDRGFDPGLGSKPS 119
C.spUWO241 AVGAT-KKTTQKTGKRTSAAP--TQDALWLPNTERPEWLDGSLPGDRGFDPGLGSKPG 70
C.subellipsoidea MAATKIVRKAQKAAN-SATRTYKFKFDGDLWLPNTQRPWLDGSLPGDRGFDPLELSPKS 83
      .. : : :... ***** ** ***** :...

                                     103
C.reinhardtii EFVVIGVDENDQNAAKNNKGSVEAIVQATPDEVSSENRLAPYSEVFGARFRECELIHGR 142
C.incerta EFVVIGVDENDQNVGKNNKGTVEAIVQASPDEVSSENRLAPYSEVFGARFRECELIHGR 148
V.carteri EFVVIGVDENDQNAAKNNKGSVEAVVTATPDEVSAENRLAPYSEVFGARFRECELIHGR 179
C.spUWO241 EAVLIGVDDNDINAFAFNKGTVEAIVSKVVDVVEP-TPFAPYSEVFGIQRFRECELIHGR 129
C.subellipsoidea EFLQVDLDQSDINKSVNKAGSIVGKYSSS-KVQATGAALSPYSEVFGARFRECELIHGR 142
* : :...:.* * . * * : . . . :*****: **** *****

C.reinhardtii WAMLACLALVAEATTGVSWVEAGKVELDGASYAGLSLPPFSITQLIWIWIEVILVGGAEFYR 202
C.incerta WAMLACLALVAEATTGVSWVEAGKVELDGASYAGLSLPPFSITQLIWIWIEVILVGGAEFYR 208
V.carteri WAMLACLGLVAEATTGVSWVDAGKVELDGASYAGLSLPPFSITQLIWIWIEVILVGGAEIYR 239
C.spUWO241 WAMLACLGVFVGEATTGVSWVDAGKVELDASTWAGLPLPFIDITQLIWIWIEALLVGGAEVYR 189
C.subellipsoidea WAMLGALGVVIAEATTGVSWVDAGKVELDGTQYLGFSLPPFSISQLIWIWIEVLLVGGAEIYR 202
****..** ..*.******:*****.: : *:.***.:*****.:*****.**

C.reinhardtii NSETNPEKRCYPGGVFDPLKLAS--EDEERAFRLKTAIEKHARLAMVSFFGYGVQA-LST 259
C.incerta NTETDPEKRCYPGGVFDPLKLAS--EDEERAFRLKTAIEKHARLAMVSFFGYG----- 259
V.carteri NTETNPEKRCYPGGFFDPLKLAS--EDEERAFRLKTAIEKHARLAMVSFFGYSVQA-FTT 296
C.spUWO241 NAELDPELRVYPPGGFFDPLGLAGPNADPEKVFALKNAEIKHGRLAMIAFLGFVVQAGVND 249
C.subellipsoidea NRSTDLQERIYPGGLFDPLKLAS--DDSQRTFKLREAEIKHGRLAMVAFLGAQLQS---- 256
* . : : * **** ** * . * :.* * : *****:*****:.*

C.reinhardtii GEGALGSLAKFADGLNNGKGL 280
C.incerta -----
V.carteri GEGALGSLAKFADGLNNGKAL 317
C.spUWO241 GAGALGSAAKFAASL----- 264
C.subellipsoidea -RQSLYERSQWP----- 267

```

Figure 3.9: Alignment of the monomeric Lhcb4 protein of *Chlamydomonas sp.* UWO241 with that of *Chlamydomonas incerta* and the model species, *Chlamydomonas reinhardtii*. The alignment was performed using CLUSTALW program. The GenBank accession numbers are: *C. reinhardtii*, XP_001697193.1; *V. carteri*, XP_002951424.1; *C. incerta*, ABD37915.1; *C. subellipsoidea*, EIE21681.1. Positions of confirmed phosphorylation sites in *Chlamydomonas reinhardtii* are marked with boxes (threonine 7, 11, 17, 18, 33 and serine 103) for each species. An asterisk (*) indicates positions with a fully conserved residue, a colon (:) indicates conservation between groups of strongly similar properties, and a period (.) indicates conservation between groups of weakly similar properties.


```

                                     10
C.reinhardtii -----M Q I Q A L F K K I G A S-----A P A K K 18
C.incerta -----M Q I Q A L F K K I A A S-----A P A K K 18
V.carteri -----M Q I Q A L F K K I A A S-----A P A K K 18
C.subellipsoidea MANALRSEFLGATLKRTEISQTKGAERVQVQAFFNKKITAKKVEKKVEKKVAKVQKTASKT 60
UWO241 -----M Q L K A F S T R S V Q Q-----A G R K 17

C.reinhardtii GTASTKVVVKPSKAGGKATRGWLGG-QGGAADLDKWYGPDRKLFPLPSGLYDRSEIPEYLN 77
C.incerta -----A G G K A T R G W L G G-Q G G A A D L D K W Y G P D R K L F L P S G L Y D R S E I P D Y L N G 47
V.carteri GTSSTKVVVKPS---GKATKGWLGG-QGGAVNLDKWYGPDRVLFPLPSGLYDRSEVPAYLN 74
C.subellipsoidea ASKATKQVKAAS-GKRTKGFGE-AGGAQGLDKWYGPSRALFLPGGLDPSDVPTYL 118
UWO241 AVVASAKPKAKAASGKATKGWGGGKENNEVDLSAWYGPDRKLFPLPGGLDPEDEVPSYLDG 77
** :*: * * .. *. ***** * ***** * :*: * *:

C.reinhardtii ELAGDYGYDPLGLGKDPETVAKYRENE LLHARWAM LAAAGIL IPEGLQANGANIKGGTWF 137
C.incerta ELAGDYGYDPLGLGKDPETVAKYRENE LLHARWAM LAAAGIL IPEGLQANGANIKGGTWF 107
V.carteri ELAGDYGYDPLGLGKDTETVAKYREY ELLHARWAM LAAAGIL IPEGLQANGANIKGGVWF 134
C.subellipsoidea TLAGDYGYDPLGLGKDTATVEKYRAYELI HARWAM LAAAGII IPEGLQANGAAIKGGTWF 178
UWO241 TLAGDYGYDPLGLGKDEEQVEAYRANEL LHARWAM LAAAGII IPEGLASNGANLVGPTWF 137
***** * * * *:*****:***** :* * : * .**

C.reinhardtii ETGAEMLNGGTLNYFAVPWGI VSNPLPLFAVIAIEVGLMGAVEFYRRNGTGPAGYSPGIG 197
C.incerta ETGAEMLNGGTLNYFAVPWGI VSNPLPLFAVIAIEVGLMGAVEFYRRNGSGPAGYSPGIG 167
V.carteri ETGAEMLNGGTLNYFAVPWGI VSNPLPLFAVIAIEVGLMGAVEFYRRNGTGPAGYSPGIG 194
C.subellipsoidea ETGAEMLNGGTLNYFAVPWGI IINNPLPLFLV VVIEVALLGAVER YRQS GEGPPGYSPGVG 238
UWO241 ETGAAMLEGGTLNYFAVPWGI IGNPLPLFLVVAIEVGLMGAVEKYRSEGTGPQGYAKGVG 197
**** *:*****:***** *:*.**.*:**** * * ** *: * *:

C.reinhardtii KFDSSVFDGLDPLYPGGPFDP LGLADDPEV LQELKVKEIKNGR LAMVSVLGF AVQSYVTG 257
C.incerta KFDSSVFDGLDPLYPGGPFDP LGLADDPEV LQELKVKEIKNGR LAMVSVLGF AVQSYVTG 227
V.carteri KFDSSVFEGLD SIYPGGPFDP LGLADDPEV FQELKVKEIKNGR LAMVSVLAF AIQSYVTG 254
C.subellipsoidea KFDSSIFSGLDNLYPGGPFDP LGLADDPE TFAELKVKEIKNGR LALISVLGF AVQSYVTG 298
UWO241 KFEPDVF DGVDPMPYGGPFDP LGLADDPEV LAELKVKEIKNGR LAMVSVLGF AVQGYVTG 257
**.:*.**.* :*****:*****:*****:***.***.***

C.reinhardtii EGPYANWTKHVADPFGYNLLTVLGAERTPTL 289
C.incerta EGPYANWTKHVADPFGYNLLTVLGAERTPTL 259
V.carteri EGPYTNWIKHVQDPFGYNLLTVLGNEDRVPTL 286
C.subellipsoidea EGPYANWSKHVADPFGYNLLTIIGAEDRVPTL 330
UWO241 EGPYANWSKHVADPFGYNLLSVLGAERIATL 289
****:* ** * *****:;* * * .**

```

Figure 3.10: Alignment of the monomeric Lhcb5 protein of *Chlamydomonas sp.* UWO241 with that of *Chlamydomonas reinhardtii* and *Volvox carteri*. The alignment was performed using CLUSTALW program. The GenBank accession numbers are: *C. reinhardtii*, XP_001695927.1; *V. carteri*, XP_002949400.1. Threonine 10, the position of a confirmed phosphorylation site in *Chlamydomonas reinhardtii* is marked with a box. An asterisk (*) indicates positions with a fully conserved residue, a colon (:) indicates conservation between groups of strongly similar properties, and a period (.) indicates conservation between groups of weakly similar properties.

replaced with a threonine (T) residue in UWO241 Lhcb4 (Fig. 3.9). Thus, UWO241 shares only one phosphorylation site, Thr18, out of the six phosphorylation sites identified in Lhcb4 of *C. reinhardtii*. Interestingly, *Coccomyxa subellipsoidea* C-169, an Antarctic unicellular green alga from the division chlorophyta, also shares only one phosphorylation site, Thr7, with *C. reinhardtii* (Fig. 3.9). *C. subellipsoidea* is the first eukaryotic microorganism from a polar environment to have its genome sequenced (Blanc et al. 2012).

Similar to *C. reinhardtii*, the cDNA derived sequence for Lhcb5 in UWO241 predicted to encode a 289 amino acid protein (Fig. 3.10) and exhibited a 72.6% amino acid identity with that of *C. reinhardtii* and 70.6% identity with that of *Volvox carteri*, with low similarity within the first 30 amino acids of the N-terminal end (Fig. 3.10). Only one phosphorylation site has been confirmed in Lhcb5 of *C. reinhardtii*, on threonine 10 (Turkina et al. 2006). However, threonine 10 is substituted with a serine (S) residue in the Lhcb5 sequence of UWO241 (Fig. 3.10). Therefore, UWO241 does not share the only phosphorylation site identified in Lhcb5 of *C. reinhardtii*. Similarly, this site is not conserved in the Antarctic green alga, *C. subellipsoidea* (Fig. 3.10).

3.4 Discussion

State transitions occur through a signaling network comprising the cytochrome b_6/f complex, protein kinases and phosphatases (reviewed in Vener 2008). Our data provide evidence that the Stt7 kinase involved in LHCII phosphorylation is present in the thylakoid membranes of UWO241. At the protein level, UWO241 exhibits similar levels of Stt7 as the model green alga, *C. reinhardtii* (Fig. 3.6). Therefore, we show that a lack of state transitions in UWO241 is not due to the absence of the Stt7 kinase. Instead, our results indicate that the state transition deficiency in the Antarctic psychrophile, *C. sp.* UWO 241 occurs due to a reduced phosphorylation status of both the PSII core complex, and minor LHCII proteins, Lhcb4 and Lhcb5. Differences in N-terminal ends of Lhcb4 and Lhcb5, together with altered number of phosphorylation sites, likely contribute to reduced phosphorylation of these proteins in the Antarctic psychrophile, UWO241 (Fig. 3.9, 3.10). Interestingly, the psychrotolerant Antarctic green alga, *Coccomyxa*

subellipsoidea C-169, also exhibits reduced number of phosphorylation sites and altered amino acid sequences along the N-terminal ends of Lhcb4 and Lhcb5.

Strong evidence exists that these minor LHCII proteins, Lhcb4 and Lhcb5, play an important role in state transitions as they act as linker proteins between major LHCII trimers and the PSII core. Due to this unique position, it is believed that phosphorylated, minor LHCII uncouple from PSII, causing dissociation of the peripheral antenna during State II (Turkina et al. 2006, Iwai et al. 2008). The role of Lhcb4 in state transitions is of particular interest, since this minor LHCII protein is hyperphosphorylated with six phosphorylation sites in *Chlamydomonas reinhardtii* (Turkina et al. 2006, Lemeille et al. 2010). Previous studies have demonstrated that Lhcb4 is essential for state transitions in *C. reinhardtii* (Tokutsu et al. 2009). Although mutants lacking Lhcb4 exhibit a reduction in PSII antenna size during state I-II transitions due to LHCII dissociation, released LHCII proteins fail to dock with PSI (Tokutsu et al. 2009).

The six phosphorylation sites of Lhcb4 have been identified as Thr7, 11, 17, 18, 33, and Ser103 in *Chlamydomonas reinhardtii* (Turkina et al. 2006). However, recent studies have shown that only two phosphorylated residues of Lhcb4 were unique to state II (Thr33, Ser103), and only one, Thr33, was dependent on the activity of the STT7 kinase (Lemeille et al. 2010). Although Thr33 is also phosphorylated in state I, phosphorylation is enhanced under state II conditions, which may promote the dissociation of major LHCII trimers from PSII or the association of Lhcb4 with PSI (Lemeille et al. 2010).

Examination of the Lhcb4 amino acid sequence in the psychrophile revealed that only one of five phosphorylated threonine residues (Thr18) is present in UWO241, compared to *C. reinhardtii* (Fig. 3.9). Thus, UWO241 Lhcb4 exhibits the absence of Thr7, 11, 17, and the Stt7-dependent, Thr33 phosphorylated site (Fig. 3.9). In addition, the only phosphorylated serine (Ser103) of Lhcb4 is substituted with a threonine, compared to *C. reinhardtii* (Fig. 9). Similarly, the only phosphorylated threonine (Thr10) residue of Lhcb5 is replaced with a serine in UWO241 (Fig. 3.10). Therefore, I suggest that the absence of four phosphorylated threonine residues of Lhcb4 and the only phosphorylated threonine residue of Lhcb5, results in reduced monomeric LHCII phosphorylation and

most likely contributes to a lack of state transitions in the Antarctic psychrophile, UWO241.

Consistently, labelling of thylakoid membrane proteins with [γ - ^{33}P]ATP demonstrates a significant reduction in phosphorylation levels of both major and minor LHCII proteins in *C. sp.* UWO241, compared to *C. reinhardtii* (Fig. 3.7, 3.8). *Chlamydomonas reinhardtii* exhibited relatively strong phosphorylation of all major p11/p13, p16/p17 and minor p9/p10 LHCII bands. In contrast, while UWO241 maintains comparable phosphorylation levels of the major pC (27 kDa) band, this psychrophile exhibits reduced phosphorylation of the major pA (30.5 kDa) band and minimal phosphorylation of minor p9/p10 (37 kDa) proteins. It should be noted that the phosphorylated D1 protein co-migrates with pA in UWO241 (Fig. 3.7B), and the extent of contribution by D1 phosphorylation to the D1+pA LHCII band is not known.

The only LHCII band in UWO241 which exhibits comparable levels of phosphorylation to *C. reinhardtii* is the major pC band (Fig. 3.7, 3.8). This 27 kDa band shares a similar apparent molecular mass with the 25-26 kDa p16/p17 band in *C. reinhardtii*, and likely represents related major Lhcbm proteins. While p16 (also known as Type IV) is not phosphorylated in *C. reinhardtii*, recent studies have demonstrated that phosphorylated p17 LHCII (Type III) are not unique to State II, but also occur in State I, suggesting that phosphorylation of p17 Lhcbm proteins may play a role unrelated to state transitions (Mingawa and Takahashi 2004, Iwai et al. 2008). Another major LHCII band of UWO241, pA (30.5 kDa), exhibits reduced phosphorylation compared to the p11/p13 (31 kDa) Lhcbm band in *C. reinhardtii* (Fig. 3.7, 3.8). Recent studies have shown that phosphorylated p11/p13 LHCII (Type I) remain associated with PSII, suggesting that phosphorylation of these major proteins is not enough to induce detachment from PSII during state transitions (Iwai et al. 2008). Therefore, it is possible that phosphorylation of both pA (30.5 kDa) and pC (27 kDa), the major Lhcbm bands of *C. sp.* UWO241, may not be associated with state transitions.

Since CP43 and the D2 protein become strongly phosphorylated under State II conditions, it has been hypothesized that simultaneous phosphorylation of both PSII core

subunits and monomeric, minor LHCII (Lhcb4 and Lhcb5) are required to initiate the dissociation of LHCII by coulombic repulsion (Turkina et al. 2006, Iwai et al. 2008). Interestingly, compared to *C. reinhardtii*, minimal phosphorylation of CP43 and D2 was observed in UWO241, following ^{33}P labelling of thylakoid membrane proteins (Fig. 3.7). Thus, strongly reduced phosphorylation of the PSII core in UWO241 may negatively affect undocking of peripheral antennae and contribute to a state transition deficiency.

Purification of phosphorylated LHCII proteins using affinity chromatography in UWO241, in combination with immunoblotting, demonstrated that LHCII phosphorylation wasn't detected with phospho-threonine antibodies (Fig. 3.3). However, a negative result using immunoblotting to detect phosphorylation sites does not rule out the presence of phosphorylation. The use of phosphothreonine antibodies has been reported to result in limited detection of only four to five major thylakoid phosphoproteins in some higher plants (Aro et al. 2004, Vener 2008). In addition, immunoreactivity with various commercial antibodies differs among phosphoproteins (Rintamäki et al. 1997, Vener 2008). Krol et al (2009) reported that although phosphorylation of the D1 polypeptide of the chlorina f_2 mutant of barley could not be detected using phospho-threonine antibodies, in vitro phosphorylation using $[\gamma\text{-}^{32}\text{P}]\text{ATP}$, did result in labelling of the D1 polypeptide of the barley mutant. Thus, detection of phosphorylation with immunoblotting should be used with caution, and negative results should be confirmed using alternative techniques.

Phosphorylation of LHCII proteins occurs on the surface-exposed, N-terminal regions exposed to the stroma. Zer et al. (1999) demonstrated that LHCII proteins undergo temperature-dependent, light-induced conformational changes that expose phosphorylation sites at the N-terminal domains to protein kinase(s) (Vink et al. 2004). In contrast, light intensities exceeding those required for light saturation of electron flow, result in inaccessibility of the kinase(s) to LHCII phosphorylation sites in both higher plants and *C. reinhardtii* (Zer et al. 1999, Vink et al. 2004). Therefore, alterations in LHCII protein structure may also affect the accessibility or inaccessibility of specific antibodies to the phosphorylation site(s) of LHCII proteins.

3.5 Conclusion

Here, we show that in contrast to other photosynthetic organisms, UWO241 exhibits significantly reduced levels of phosphorylation of the minor LHCII proteins, Lhcb4 and Lhcb5. We suggest that differences in amino acid N-terminal domains, together with altered phosphorylation sites contribute to reduced phosphorylation associated with the minor LHCII proteins, Lhcb4 and Lhcb5. Reduced PSII core complex phosphorylation may negatively affect LHCII dissociation from PSII, whereas reduced phosphorylation of minor LHCII may prevent the association of LHCII with PSI, resulting in the failure to transition to State II and an overall state transition deficiency in the Antarctic psychrophile, *Chlamydomonas sp.* UWO241.

3.6 References

- Allen JF, Bennett J, Steinback KE, Arntzen CJ.** (1981) Chloroplast protein phosphorylation couples plastoquinone redox state to distribution of excitation energy between photosystems. *Nature* **291**: 25–29
- Allen JF.** (1992) Protein phosphorylation in regulation of photosynthesis. *Biochim Biophys Acta* **1098**(3):275-335
- Anderson JC, Peck SC.** (2008) A simple and rapid technique for detecting protein phosphorylation using one-dimensional isoelectric focusing gels and immunoblot analysis. *Plant J* **55**(5):881-5
- Aro EM, Rokka A, Vener AV.** (2004) Determination of phosphoproteins in higher plant thylakoids. *Methods Mol Biol* **274**:271-85
- Asif M, Dhawan P, Nath P.** (2000) A simple procedure for the isolation of high quality RNA from ripening banana fruit. *Plant Mol Biol Rep* **18**:109-15
- Bassi R, Wollman FA.** (1991) The chlorophyll-a/b proteins of photosystem II in *Chlamydomonas reinhardtii*. *Planta* **183**(3):423-33
- Bellafiore S, Barneche F, Peltier G, Rochaix JD.** (2005) State transitions and light adaptation require chloroplast thylakoid protein kinase STN7. *Nature* **433**:892–5
- Bennett J.** (1977) Phosphorylation of chloroplast membrane polypeptides. *Nature* **269**:344–6
- Blanc G, Agarkova I, Grimwood J, Kuo A, Brueggeman A, Dunigan DD, Gurnon J, Ladunga I, Lindquist E, Lucas S, Pangilinan J, Pröschold T, Salamov A, Schmutz J, Weeks D, Yamada T, Lomsadze A, Borodovsky M, Claverie J-M, Grigoriev IV, Van Etten JL.** (2012) The genome of the polar eukaryotic microalga *Coccomyxa subellipsoidea* reveals traits of cold adaptation. *Genome Biol* **13**(5):R39

- Carlberg I, Rintamäki E, Aro EM, Andersson B.** (1999) Thylakoid protein phosphorylation and the thiol redox state. *Biochemistry* **38**(10):3197-204
- Chua NH, Bennoun P.** (1975) Thylakoid membrane polypeptides of *Chlamydomonas reinhardtii*: wild-type and mutant strains deficient in photosystem II reaction center. *Proc Natl Acad Sci USA* **72**:2175–9
- de Bianchi S, Dall'Osto L, Tognon G, Morosinotto T, Bassi R.** (2008) Minor antenna proteins CP24 and CP26 affect the interactions between photosystem II subunits and the electron transport rate in grana membranes of *Arabidopsis*. *Plant Cell* **20**(4):1012-28
- Depège N1, Bellafiore S, Rochaix JD.** (2003) Role of chloroplast protein kinase Stt7 in LHCII phosphorylation and state transition in *Chlamydomonas*. *Science* **299**(5612):1572-5
- Doyle J.** (1991) DNA protocols for plants. In Hewitt, G., Johnston, A. B. & Young, J. P. [Eds.] *Molecular Techniques in Taxonomy*. Springer Berlin Heidelberg, pp. 283-93.
- Gianazza E.** (1995) Isoelectric focusing as a tool for the investigation of post-translational processing and chemical modifications of proteins. *J Chromatogr* **705**:67–87
- Gudynaite-Savitch L, Gretes M, Morgan-Kiss RM, Savitch LV, Simmonds J, Kohalmi SE, Hüner NPA.** (2006) Cytochrome f from the Antarctic psychrophile, *Chlamydomonas raudensis* UWO 241: structure, sequence, and complementation in the mesophile, *Chlamydomonas reinhardtii*. *Mol Genet Genomics* **275**(4):387-98
- Iwai M, Takahashi Y, Minagawa J.** (2008) Molecular remodeling of Photosystem II during state transitions in *Chlamydomonas reinhardtii*. *Plant Cell* **20**(8):2177–89
- Kargul J, Barber J.** (2008) Photosynthetic acclimation: Structural reorganisation of light harvesting antenna - role of redox-dependent phosphorylation of major and minor chlorophyll a/b binding proteins. *FEBS J* **275**:1056-68
- Krause GH, Weiss E.** (1991) Chlorophyll fluorescence and photosynthesis: the basics. *Annu Rev Plant Phys Plant Mol Biol* **42**:313-49
- Krol M, Ivanov AG, Booij-James I, Mattoo AK, Sane PV, Hüner NPA.** (2009) Absence of the major light-harvesting antenna proteins alters the redox properties of photosystem II reaction centres in the chlorina F2 mutant of barley. *Biochem Cell Biol* **87**(4):557-66
- Laemmli UK.** (1970) Cleavage of structural proteins during the head of bacteriophage T4. *Nature* **227**:680–85
- Larkin MA, Blackshields G, Brown NP, Chenna R, McGettigan PA, McWilliam H, Valentin F, Wallace IM, Wilm A, Lopez R, Thompson JD, Gibson TJ, Higgins DG.** (2007) Clustal W and Clustal X version 2.0. *Bioinformatics* **23**:2947-8

- Lemeille S, Willig A, Depège-Fargeix N, Delessert C, Bassi R, Rochaix JD.** (2009) Analysis of the chloroplast protein kinase Stt7 during state transitions. *PLoS Biol* **7**(3):e45
- Lemeille S, Turkina MV, Vener AV, Rochaix JD.** (2010) Stt7-dependent phosphorylation during state transitions in the green alga *Chlamydomonas reinhardtii*. *Mol Cell Proteomics* **9**(6):1281-95
- Lemeille S, Rochaix JD.** (2010) State transitions at the crossroad of thylakoid signalling pathways. *Photosynth Res* **106**(1-2):33-46
- Lizotte MP, Priscu JC.** (1994) Natural fluorescence and quantum yields in vertically stationary phytoplankton from perennially ice-covered lakes. *Limnol Oceanogr* **39**:1399-410
- Lizotte MP, and Priscu JC.** (1992) Spectral irradiance and bio-optical properties in perennially ice covered lakes of the dry valleys (Antarctica). *Antarc Res Ser* **57**:1-14
- Lizotte MP, Sharp TR, Priscu JC.** (1996) Phytoplankton dynamics in the stratified water column of Lake Bonney, Antarctica: biomass and productivity during the winter-spring transition. *Polar Biol* **16**:155-62
- Mingawa J.** (2011) State transitions-the molecular remodelling of photosynthetic supercomplexes that controls energy flow in the chloroplast. *Biochim Biophys Acta* **1807**(8):897-905
- Mingawa J, Takahashi Y.** (2004) Structure, function and assembly of Photosystem II and its light-harvesting proteins. *Photosynth Res* **82**:241-63
- Morgan RM, Ivanov AG, Priscu JC, Maxwell DP, Hüner NPA.** (1998) Structure and composition of the photochemical apparatus of the antarctic green alga, *Chlamydomonas subcaudata*. *Photosynth Res* **56**:303-14
- Morgan-Kiss RM, Ivanov AG, Hüner NPA.** (2002). The Antarctic psychrophile, *Chlamydomonas subcaudata*, is deficient in state I-state II transitions. *Planta* **214**:435-45
- Morgan-Kiss RM, Ivanov AG, Pockock T, Krol M, Gudynaite-Savitch L, Hüner NPA.** (2005) The Antarctic psychrophile, *Chlamydomonas raudensis* Ettl (UWO241) (Chlorophyceae, Chlorophyta) exhibits a limited capacity to photoacclimate to red light. *J Phycol* **41**:791-00
- Neale PJ, Priscu JC.** (1995) The photosynthetic apparatus of phytoplankton from a perennially ice-covered Antarctic lake: acclimation to an extreme shade environment. *Plant Cell Physiol* **36**:253-63
- Pockock T, Vetterli A, Falk S.** (2011) Evidence for phenotypic plasticity in the Antarctic extremophile *Chlamydomonas raudensis* Ettl. UWO 241. *J Exp Bot* **62**:1169-77
- Pribil M, Pesaresi P, Hertle A, Barbato R, Leister D.** (2010) Role of plastid protein phosphatase TAP38 in LHCII dephosphorylation and thylakoid electron flow. *PLoS Biol.* **8**(1):e1000288

- Priscu JC.** (1998) Ed. Ecosystem Dynamics in a Polar Desert: The McMurdo Dry Valleys, Antarctica. Vol. 72, Antarctic Research Series. Washington, AGU Press
- Rintamäki E1, Salonen M, Suoranta UM, Carlberg I, Andersson B, Aro EM.** (1997) Phosphorylation of light-harvesting complex II and photosystem II core proteins shows different irradiance-dependent regulation in vivo. Application of phosphothreonine antibodies to analysis of thylakoid phosphoproteins. *J Biol Chem* **272**(48):30476-82
- Rochaix JD.** (2011) Regulation of photosynthetic electron transport. *Biochim Biophys Acta* **1807**(8):878-86
- Shapiguzov A, Ingelsson B, Samol I, Andres C, Kessler F, Rochaix JD, Vener AV, Goldschmidt-Clermont M.** (2010) The PPH1 phosphatase is specifically involved in LHCII dephosphorylation and state transitions in *Arabidopsis*. *Proc Natl Acad Sci USA* **107**(10):4782–87
- Spigel RH, Priscu JC.** (1996) Evolution of temperature and salt structure of Lake Bonney, a chemically stratified Antarctic lake. *Hydrobiologia* **321**:177-90
- Szyszkka B, Ivanov AG, Hüner NPA.** (2007). Psychrophily is associated with differential energy partitioning, photosystem stoichiometry and polypeptide phosphorylation in *Chlamydomonas raudensis*. *Biochim Biophys Acta* **1767**:789-00.
- Takahashi Y, Goldschmidt-Clermont M, Soen SY, Franzén LG, Rochaix JD.** (1991) Directed chloroplast transformation in *Chlamydomonas reinhardtii*: insertional inactivation of the *psaC* gene encoding the iron sulfur protein destabilizes photosystem I. *EMBO J* **10**:2033–40
- Takahashi H, Iwai M, Takahashi Y, Mingawa J.** (2006). Identification of the mobile light-harvesting complex II polypeptides for state transitions in *Chlamydomonas reinhardtii*. *Proc Natl Acad Sci USA* **103**:477-82
- Takizawa K, Takahashi S, Hüner NPA, Mingawa J.** (2009) Salinity affects the photoacclimation of *Chlamydomonas raudensis* Ettl UWO241. *Photosynth Res* **99**(3):195-203
- Tokutsu R, Iwai M, Minagawa J.** (2009) CP29, a monomeric light-harvesting complex II protein, is essential for state transitions in *Chlamydomonas reinhardtii*. *J Biol Chem* **284**(12):7777-82
- Turkina MV, Kargul J, Blanco-Rivero A, Villarejo A, Barber J, Vener AV.** (2006) Environmentally modulated phosphoproteome of photosynthetic membranes in the green alga *Chlamydomonas reinhardtii*. *Mol and Cell Prot* **5**:1412–25
- Vener AV, Van Kan PJ, Gal A, Andersson B, Ohad I.** (1995) Activation/deactivation cycle of redox-controlled thylakoid protein phosphorylation. Role of plastoquinol bound to the reduced cytochrome *bf* complex. *J Biol Chem* **270**:25225–232
- Vener AV, Van Kan PJ, Rich PR, Ohad I, Andersson B.** (1997) Plastoquinol at the quinol oxidation site of reduced cytochrome *bf* mediates signal transduction

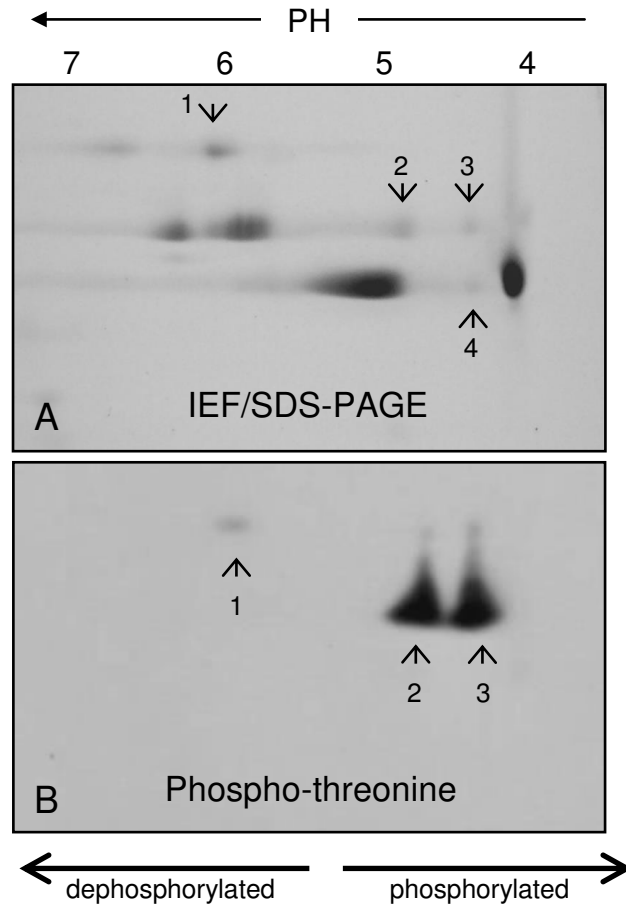
between light and protein phosphorylation: thylakoid protein kinase deactivation by a single turnover flash. *Proc Natl Acad Sci USA*, **94**:1585–90

Vener A. (2008) Phosphorylation of thylakoid proteins. In Demmig-Adams, B., Adams, W., & Mattoo, A. [Eds] *Photoprotection photoinhibition gene regulation and environment*. Springer, Dordrecht, pp.108.

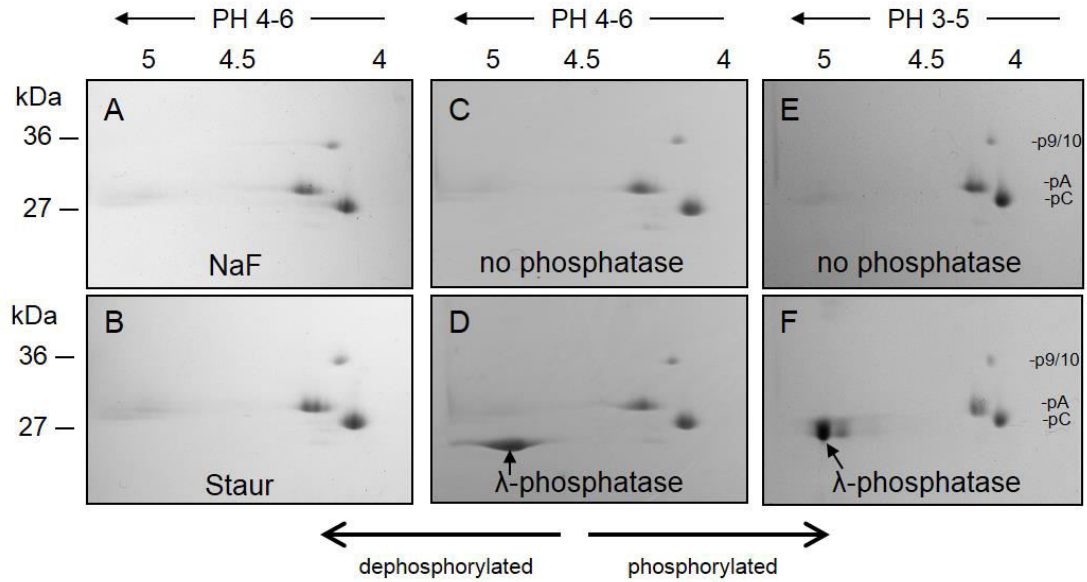
Vink M, Zer H, Alumot N, Gaathon A, Niyogi K, Herrmann RG, Andersson B, Ohad I. (2004) Light-modulated exposure of the light-harvesting complex II (LHCII) to protein kinase(s) and state transition in *Chlamydomonas reinhardtii* xanthophyll mutants. *Biochemistry* **43**(24):7824-33

Zer H, Vink M, Keren N, Dilly-Hartwig HG, Paulsen H, Herrmann RG, Andersson B, Ohad I. (1999) Regulation of thylakoid protein phosphorylation at the substrate level: reversible light-induced conformational changes expose the phosphorylation site of the light-harvesting complex II. *Proc Natl Acad Sci USA* **96**(14):8277-82

3.7 Appendices



Appendix 3S1: Two-dimensional (IEF/SDS-PAGE) separation of purified LHCII in *C. reinhardtii*. Arrows indicate differential migration of proteins associated with phosphorylation. A corresponding immunoblot probed with antibodies specific for phospho-threonine demonstrates a positive reaction with spots 1, 2 and 3 (B).



Appendix 3S2: Two-dimensional (IEF/SDS-PAGE) separation of purified LHCII in *Chlamydomonas sp.* UWO241 using narrow pH ranges (pH 4-6, pH 3-5), combined with either inhibitor treatment (AB) or +/- phosphatase (C-F), did not result in detectable pI changes of LHCB proteins.

Chapter 4

4 Palmelloid colonies are photosynthetically distinct from single motile cells of the Antarctic psychrophile, *Chlamydomonas* sp. UWO 241

4.1 Introduction

Chlamydomonas reinhardtii is a commonly used laboratory species of a unicellular, biflagellate green alga. During asexual reproduction, *C. reinhardtii* protoplasts can divide into 2, 4, 8, or 16 daughter cells from a single mother cell. Prior to the division phase, cells can double several times in size, and the number of cell divisions depends on the size of the mother cell, resulting in the formation of daughter cells that are uniform in size (Craigie and Cavalier-Smith 1982, Oldenhof et al. 2007). Enzymatic degradation of the mother cell (sporangia) wall allows for the release of daughter cells from each sporangium (Schlösser 1966). A glycoprotein serine protease, termed sporangin (vegetative lytic enzyme, VLE) is secreted into the culture medium, which specifically digests the wall of the mother cell, but not that of single vegetative cells (Schlösser 1966, Jaenicke et al. 1987, Matsuda et al. 1995). Recent studies have shown that prior to its release, accumulation of sporangin is localized to the flagella of daughter cells within the sporangial cell wall (Kubo et al. 2009).

Alternatively, during sexual reproduction, fusion of gametes leads to the formation of a zygospore, surrounded by a hard, thick, multilayered cell wall, which is resistant to harsh environmental conditions (Trainor 1985, Harris 2009). Among some species of *Chlamydomonas*, akinete (asexual resting spore) formation has been reported under unfavourable conditions, such as desiccation (reviewed in Coleman 1983). This occurs when the vegetative cell wall thickens, concomitant with the accumulation of carotenoids, starch and lipids (Coleman 1983).

In addition, the presence of “palmelloid” colonies has been observed among species of *Chlamydomonas* to varying degrees (Harris 2009). “Palmelloid” is a broad term that

describes a morphological state characterized by multiple, non-motile, clumped cells. Previous reports indicate that palmelloid formation in *Chlamydomonas* can be induced by the addition of chelating agents, non-metabolizable organic acids, calcium deficiency and high phosphate concentrations (Iwasa and Murakami 1968, Iwasa and Murakami 1969, Harris 2009). Olsen et al. (1983) observed that during growth under phosphate limitation, palmelloids of *C. reinhardtii* became attached to the walls of culture vessels and exhibited lower growth rates of 0.03h^{-1} , compared to 0.21h^{-1} of free-swimming, vegetative cells. Palmelloids had a high ratio of polyphosphate to total phosphorous and showed decreased levels of alkaline phosphatase activity (APA) (Olsen et al. 1983).

The herbicide paraquat also induces palmelloid formation in *C. eugametos* (Franqueira et al. 1999). Paraquat inhibits photosynthetic electron transport at photosystem I (Devine et al. 1993) and results in the generation of superoxide anion, a reactive oxygen species (ROS), which causes lipid peroxidation and damage to cell membranes (Tissut et al. 1987). While chlorophyll content decreases at lower paraquat concentrations ($\leq 0.15\ \mu\text{M}$), carotenoid inhibition only occurred at highest herbicide concentrations ($\geq 0.3\ \mu\text{M}$), concomitant with strong reductions in growth rate and formation of palmelloids (Franqueira et al. 1999).

It is presumed that palmelloids result from a failure of daughter cell to be released from the mother cell, due to either flagellar malfunction or abnormal production of membranes and cell walls (Fritsch 1945, Nakamura et al. 1975, Harris 2009). In *C. eugametos*, the palmelloid condition can be induced by chloroplatinic acid, a compound that blocks cell division and causes incomplete cytokinesis in *E.coli* (Rosenberg et al. 1967, Nakamura et al. 1975). Palmelloids produced this way showed multiple layers of cell wall material, and it was concluded that the inability of palmelloid cells to separate in this case, occurs due to abnormalities in cell wall formation (Nakamura et al. 1975).

In synchronous cultures grown under a 12 h light-12 h dark regime, the *Chlamydomonas reinhardtii* mutant 'ls', exhibited delayed liberation of zoospores which required light (Mergenhagen 1980). It was suggested that this light dependency was due to a deficiency in energy supply in the dark, as it could be overcome by an extended light period or the

addition of acetate (Voigt et al. 1989). Furthermore, this mutant accumulates sporangia under suboptimal aeration conditions and in high-density cultures entering stationary-phase (Voigt et al. 1989). In this case, increasing the light period or addition of a carbon source did not result in the release of zoospores, which did not occur until sporangia were resuspended in fresh culture medium (Voigt et al. 1989). Analyses of sporangia in these cases revealed that they contained abnormal, multilayered sporangial walls, which did not occur under optimal growth conditions (Voigt et al. 1990).

Studies have also suggested that the increased incidence of palmelloids among *Chlamydomonas* cells in the presence of grazers provides protection from predation by rotifers by minimizing the risk of being consumed (Mikheeva and Kruchkova 1980, Lurling and Beekman 2006). Lurling and Beekman (2006) found that despite grazer presence, palmelloids were absent in the dark, suggesting that light and active growth is a requirement for palmelloid formation.

The current study investigates palmelloid formation in the cold-adapted psychrophile, *Chlamydomonas sp.* UWO241. UWO241 was isolated from the permanently ice-covered Lake Bonney in Antarctica, at a depth of 17m. The thick, 3-4.5m layer of ice cover attenuates between 97-99% incident PAR, absorbs wavelengths greater than 600 nm and prevents vertical mixing of the water column (Fritsen and Priscu 1999; Howard-Williams et al. 1998). Consequently, Lake Bonney consists of highly stratified layers of phytoplankton, produced by strong salinity gradients (Spigel and Priscu 1996). The discrete layer where UWO241 exists is thus characterized by low irradiance ($<50 \mu\text{mol photons m}^{-2} \text{s}^{-1}$) in the blue-green range, high salinity and average temperatures between 4-6°C (Lizotte and Priscu 1994).

Chlamydomonas sp. UWO241 is classified as an obligate psychrophile, with an optimal growth temperature of 8°C, and an inability to grow above 16°C (Morgan et al. 1998). Despite the extremely stable environment of UWO241, this shade-adapted psychrophile exhibits the capacity to acclimate to alterations of temperature and light regimes (Morgan et al. 1998, Morgan-Kiss et al. 2002; Szyszka et al. 2007).

Cells of UWO241 are ellipsoidal, or oval-shaped and exists as either free-swimming, single cells or non-motile, membrane-bound palmelloids containing multiple, flagellated cells (Pocock et al. 2004, Fig. 4.1A and B). All previous photosynthetic research on UWO241 has been performed on heterogenous mixtures of motile, single cells and palmelloids which assumed that the single chloroplast within a single UWO241 cell is functionally and compositionally indistinguishable from that with cells of a palmelloid. The purpose of this study was to determine whether palmelloids are photosynthetically distinct from single cells in *Chlamydomonas sp.* UWO 241. It was hypothesized that compared to single cells, palmelloids would exhibit characteristics of shade adaptation resulting from a self-shading effect.

4.2 Materials and methods

4.2.1 Growth conditions

Chlamydomonas reinhardtii (1690) and *Chlamydomonas raudensis* SAG 49.7 were grown axenically in Bold's basal medium (BBM), whereas *Chlamydomonas sp.* UWO 241 was grown in BBM supplemented with 0.7 M NaCl. All cultures were aerated continuously under ambient CO₂ conditions in 250 mL glass Pyrex tubes suspended in temperature-regulated aquaria. Growth irradiance was generated by fluorescent tubes (Sylvania CW-40), and measured with a quantum sensor attached to a radiometer (Model LI-189; Li-Cor, Lincoln, Neb., USA). Control *Chlamydomonas sp.* UWO241 cells were grown at 5°C, whereas growth temperature experiments were performed between 8°C-16°C for UWO241 and 11-28°C for both *Chlamydomonas reinhardtii* and *Chlamydomonas raudensis* SAG 49.72 (as indicated). All cells were grown under an irradiance of 100-150 $\mu\text{mol photons m}^{-2} \text{s}^{-1}$. Mid log phase cells were used in all experiments.

4.2.2 Cell filtration

Using a glass filter holder with fritted glass support (EMD Millipore), approximately 1L of dilute cell culture was passed through 11 μm hydrophilic nylon net filters (EMD Millipore, product #NY1102500) in order to remove any large clumps of cells. During this first step, culture dilution was adjusted so that the cell suspension was able to pass

through the apparatus by gravity flow alone. Cells captured on the filter were discarded and the flow-through filtrate was utilized as the control fraction. This control cell suspension was passed through hydrophilic polycarbonate membrane filters with 8 μm pores (Sterlitech, product #PCT8025100) by drawing fluid with the aid of gentle vacuum aspiration. Cells retained on the filters were washed three times with 4 mls of culture medium to resuspend the cells. Resulting filters were collected in Falcon tubes and suspended with 5 mls of media. The supernatant was centrifuged at 3000 rpm for 5 minutes to concentrate the cells, which were used as the 8-11 μm fraction. The flow-through filtrate was passed through hydrophilic polycarbonate membrane filters with 5 μm pores (Sterlitech, product #PCT5025100) using gentle vacuum aspiration. Cells retained on the filters were washed, resuspended in culture medium and centrifuged as above, and represented the 5-8 μm fraction, whereas, the flow-through filtrate was centrifuged and represented the single cell, <5 μm fraction.

4.2.3 Flow cytometry

Control cells and separated cell fractions were diluted and analyzed using a BD Accuri™ C6 flow cytometer (BD Biosciences, Oxford, UK). Cell sizes were examined through forward scatter (FSC) and red chlorophyll fluorescence (FL3). Analysis of the mean FSC and FL3 values was performed by manual gating to exclude debris at lower scatter intensities. Culture samples were analyzed in triplicate, using a volume of 50 μl , with a minimum of 10 000 events collected for each sample. Results were visualized on FSC and FL3 overlay histograms.

4.2.4 Low temperature (77 K) chlorophyll fluorescence

Low temperature (77K) chlorophyll fluorescence emission spectra of UWO241 cell culture and cell fractions were collected as described previously (Szyszka et al. 2007) using a PTI QM-7/2006 spectrofluorometer (Photon Technology International, South Brunswick, NJ, USA) equipped with double monochromators, R928P red-sensitive photomultiplier tube (Hamamatsu Photonics, Shizuoka-ken, Japan) and a liquid nitrogen cuvette. Cell cultures and cell fractions were frozen in liquid nitrogen in the presence of 30% (v/v) glycerol before the measurements. Corrected fluorescence emission spectra

were excited at 436 nm and recorded from 650 nm to 800 nm using slit width of 2.5 nm for both excitation and emission. The fluorescence difference spectra were obtained as described in (Savitch et al. 2011).

Decomposition analysis of the fluorescence emission spectra in terms of 5 Gaussian bands was carried out by a non-linear least squares algorithm that minimizes the chi-square function (Morgan-Kiss et al. 2002a) using a Microcal Origin Version 6.0 software package (Microcal Software, Northampton, MA, USA). The fitting parameters for the five Gaussian components, that is, position, area and full width at the half-maximum (FWHM), were free-running parameters.

4.2.5 Room temperature chlorophyll fluorescence induction

In vivo, modulated chlorophyll a fluorescence was measured with whole cells using a Xe-PAM system (Heinz-Walz GmbH, Effeltrich, Germany). After 15 minutes of dark adaptation, Chl fluorescence at open PSII reaction centers (F_o) was excited by a non-actinic modulated measuring beam ($0.5 \mu\text{mol m}^{-2} \text{s}^{-1}$), pulsed at 2 Hz. Maximum fluorescence (F_m) at closed PSII reaction centers (F_m) was induced by a saturating white light pulse (800 ms, $2400 \mu\text{mol photons m}^{-2} \text{s}^{-1}$). All measurements were performed at the corresponding growth temperature using a water-jacketed cuvette. Maximum photochemical efficiency (F_v/F_m) was calculated as $F_m - F_o/F_m$, using dark-adapted cells. F_m' was measured under constant actinic light ($100 \mu\text{mol m}^{-2} \text{s}^{-1}$), with saturating light flashes in 30 s intervals. Data acquisition was managed using a PAM-Data Acquisition System PDA-100 and the WinControl software application (Heinz-Walz).

Fluorescence parameters were calculated during steady state photosynthesis using the equations described by Kramer et al. (2004): $\Phi_{\text{PSII}} = (F_m' - F_s)/F_m'$, $\Phi_{\text{NO}} = 1/[NPQ + 1 + qL(F_m/F_o - 1)]$, $\Phi_{\text{NPQ}} = 1 - \Phi_{\text{PSII}} - \Phi_{\text{NO}}$, where Φ_{PSII} is the yield of photochemistry, Φ_{NPQ} is the yield of non-photochemical dissipation by down-regulation through antenna quenching and Φ_{NO} is the yield of all other processes involved in non-photochemical energy losses. The relative PSII electron transport rate was determined as $\text{ETR} = \Phi_{\text{PSII}} \times (\text{PFD} \times 0.84) \times 0.5$.

4.2.6 Pigment analysis and epoxidation states

Algal cells were harvested by centrifugation and pigments were extracted by breaking cells with 100% acetone at 4°C using a Mini-Beadbeater (3110BX, BioSpec). Extracts were clarified by centrifugation. The supernatant was filtered through a 0.22 µm syringe filter and samples were stored at -20°C until analysed. Pigments were separated and quantified by high-performance liquid chromatography (HPLC) as described previously (Ivanov et al. 1995). The system contained a Beckman System Gold programmable solvent module 126, diode array detector module 168 (Beckman Instruments, San Ramon, CA, USA), CSC-Spherisorb ODS-1 reverse phase column (5 µm particle size, 25 x 0.46 cm I.D.) with an Upchurch Perisorb A guard column (both columns from Chromatographic Specialties Inc., Concord, ON, Canada). Samples were injected using a Beckman 210A sample injection valve with a 20 µl sample loop. Pigments were eluted isocratically for 6 minutes with a solvent system acetonitrile:methanol: 0.1 M Tris-HCl (pH 8.0) (72:8:3.5, v/v/v), followed by a 2 minute linear gradient to 100% methanol:hexane (75:25, v/v) which continued isocratically for 4 minutes. Total run time was 12 minutes. The flow rate was 2 cm³ min⁻¹. Absorbance was detected at 440 nm, and peak areas were integrated by Beckman System Gold software. Retention times and response factors of Chl *a*, Chl *b*, lutein and β-carotene were determined by injection of known amounts of pure standards purchased from Sigma (St. Louis, MO, USA). The retention times of zeaxanthin, antheraxanthin and violaxanthin were determined by using pigments purified by thin-layer chromatography (Ivanov et al. 1995).

4.2.7 SDS-PAGE and immunoblotting

Thylakoids were isolated as described in detail by Morgan et al. (1998). Thylakoid preparations were solubilized in a 60 mM Tris (pH 7.8) buffer containing 1 mM EDTA, 12% (w/v) sucrose and 2% (w/v) SDS to attain an SDS:Chl ratio of 20:1. Samples were loaded on an equal Chl basis. Electrophoretic separation was performed with a 12.5% (w/v) polyacrylamide resolving gel containing 6 M urea, 0.66 M Tris (pH 8.8) and a 8% (w/v) polyacrylamide stacking gel containing 0.125 M Tris (pH 6.8) using the Laemmli buffer system (Laemmli 1970). Electrophoresis was performed using a Mini-Protean II apparatus (Bio-Rad).

Separated thylakoid polypeptides were either stained with Coomassie blue R, or transferred electrophoretically to nitrocellulose membranes (Bio-Rad, 0.2 μm pore size) at 5°C for 1 h at 100 V. The membranes were pre-blocked with a Tris-buffered salt (20 mM Tris, pH 7.5; 150 mM NaCl) containing 5% (w/v) milk powder and 0.01% (w/v) Tween 20. Membranes were probed with Lhcb4 (#AS06 117, Agrisera) and Lhcbm5 (#AS09 408, Agrisera) antibodies, at a dilution of 1:10000 and 1:5000, respectively. After incubation with the secondary antibody conjugated with horseradish peroxidase (Sigma, 1:20000 dilution), the antibody-protein complexes were visualized by incubation in ECL chemiluminescent detection reagents (GE Healthcare) and developed on X-ray film (Fuji Film).

4.3 Results

4.3.1 Growth temperature and cell morphology

Figure 4.1C illustrates the growth curves of *Chlamydomonas sp.* UWO 241 cells grown under steady-state temperatures of 8°C, 11°C and 16°C and a common light intensity of light intensity of 150 $\mu\text{mol photons m}^{-2} \text{s}^{-1}$. Consistent with previous studies, this Antarctic strain failed to grow at temperatures of 20°C or higher, confirming its psychrophilic nature. Figure 4.1D shows the effects of steady-state growth temperature on cell morphology, as measured by the percentage of palmelloids present in each sample using quantitative light microscopy. Measurements taken shortly after cell inoculation were highly variable and showed little difference among the 3 different growth temperatures in which palmelloids made up approximately 25% of the population for the first 200 hours of growth. Significant differences in relative palmelloid content among growth temperatures became evident after 250 hours, a time point which also corresponded to the early exponential growth stage of UWO241 cells (Fig. 4.1A). Palmelloid to single cell ratios were most pronounced between different growth temperatures following mid-exponential cell growth, which occurred at approximately 350 hours after inoculation. Between 350-400 hours, the palmelloid to single cell ratio was highest for cells grown at 16°C, where palmelloids made up 43-51% of the population. In contrast, the lowest proportion of palmelloids to single cells occurred when cells were grown at 11°C, where only 9-11% of the population consisted of palmelloids.

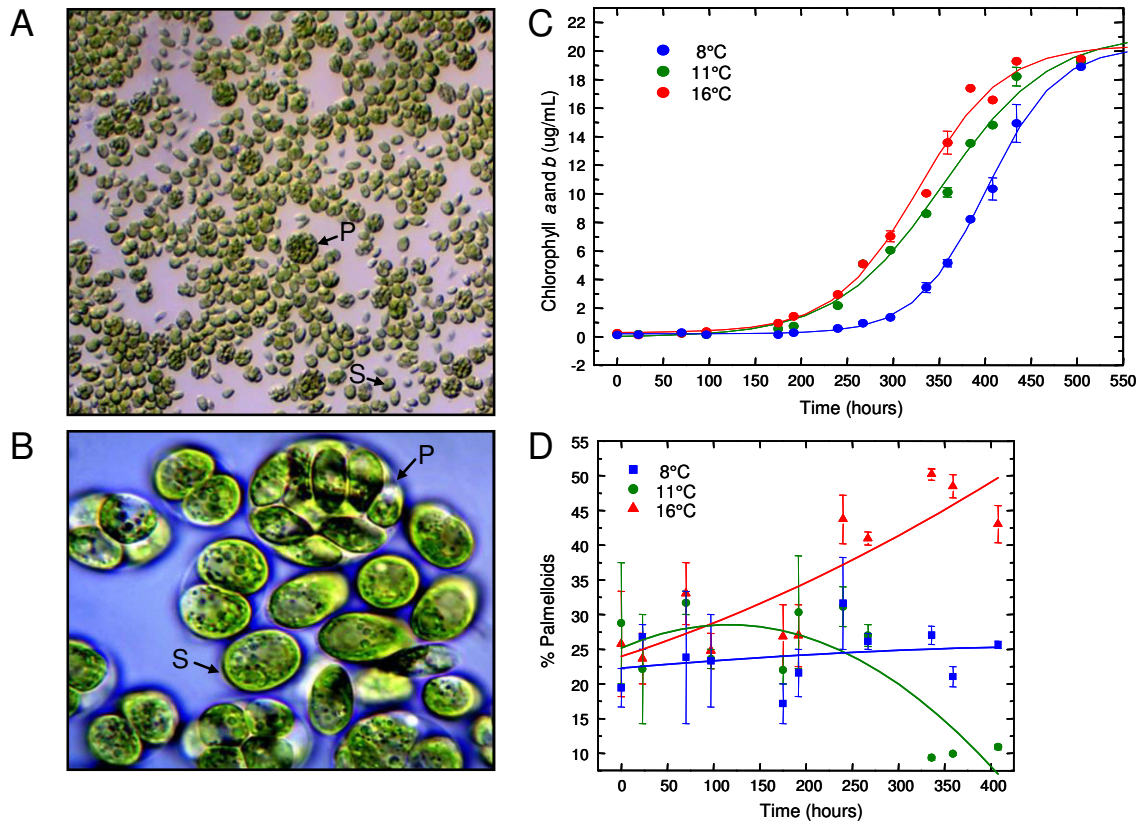


Figure 4.1: Light microscope images of *Chlamydomonas* sp. UWO241 cultures at 100x (A) and 1000x (B) magnification. Cells exist as motile, flagellated single cells (S) and multicellular palmelloids (P). Growth curves of UWO 241 cells grown under various steady-state temperatures, as measured by total chlorophyll concentrations (C). Percentage of cell units present as palmelloids was measured under the same growth temperature regimes (D).

Compared to both 11°C and 16°C, UWO241 cells grown at 8°C showed little difference in palmelloid content throughout the growth curve, with a proportion of 22-25% palmelloids at 350-400 hours (Fig. 4.1D).

Figure 4.2 shows light microscope images of the psychrophile, *Chlamydomonas sp.* UWO241 and a mesophile, *Chlamydomonas raudensis* SAG 49.72, grown under different temperature regimes. Previous studies have established the distinct optimal growth temperatures for UWO241 to be 8°C and 28°C for SAG 49.72 (Morgan et al. 1998, Szyszka et al. 2007). The highest permissive growth for the psychrophile is 16°C, whereas the lowest temperature at which the mesophile, SAG 49.72 grows is 11°C (Morgan et al. 1998, Szyszka et al. 2007). Both of these algal strains have shown to exist as motile, single cells as well as membrane-bound palmelloids.

In the psychrophilic UWO241 strain (Fig. 4.2A), the images are consistent with the quantitative light microscope data (Fig. 4.1D), and show different cell morphological compositions for each of the growth temperatures. Growth of UWO241 at 8°C resulted in the appearance of a heterogeneous mixture, consisting of single cells and small palmelloids (Fig. 4.2A, 8°C). Growth at 11°C produced nearly homogeneous cultures of single cells, whereas growth at 16°C resulted in the highest palmelloid content, where approximately half of the culture consisted of palmelloids (Fig. 4.2A, 11°C and 16°C). It should be noted that the palmelloids observed at 8°C appeared to be smaller, and made up of fewer cells than those at 16°C (Fig. 4.2A, 8°C and 16°C).

Although SAG 49.72 also shows varying cell morphology in response to growth temperature, the specific response is distinct when compared to UWO241 (Fig. 4.2B). Growth of SAG 49.72 at the optimal temperature of 28°C resulted in cell populations composed of more than 90% single cells, whereas the lower growth temperature of 16°C produced more heterogeneous cell populations, where palmelloids made up about 40% of the population (Fig. 4.2B, 28°C and 16°C). At the lowest, permissive growth temperature of 11°C for this mesophile, palmelloids comprise more than 60% of the cell population (Fig. 4.2B, 11°C). Therefore, the highest permissive temperature of 16°C for the psychrophilic UWO241 and lowest permissive temperature of 11°C for the mesophilic

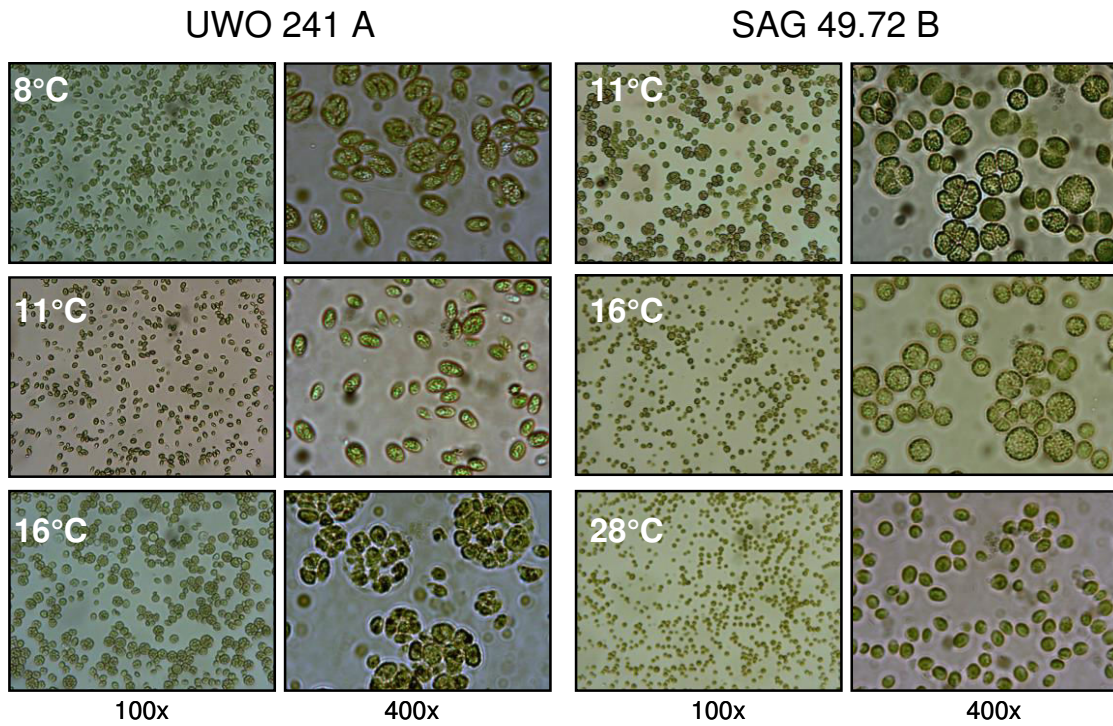


Figure 4.2: Light microscope images of both UWO 241 (A) and SAG 49.72 (B) cells grown under various steady-state temperatures, demonstrating the effects of growth temperature on cell morphology. The psychrophilic strain, UWO 241 exhibits a high ratio of palmelloids to single cells at its upper, suboptimal temperature of 16°C, whereas the mesophilic SAG 49.72 strain shows this phenotype at its lower, suboptimal temperature of 11°C.

SAG 49.72 produced the highest ratio of palmelloids to single cells (Fig. 4.2, Appendix 4S1). Furthermore, the widely used model green alga, *Chlamydomonas reinhardtii* (1690) exhibited a similar response in cell morphology to growth temperature as the mesophile, *Chlamydomonas raudensis* SAG 49.72 (Appendix 4S2).

4.3.2 Cell isolation and flow cytometry

A technique was established to physically separate the heterogeneous mixtures of *Chlamydomonas sp.* UWO241 cells, based upon cell size (Fig. 4.3). Culture filtration using microfilters with varying pore sizes allowed for the isolation of three distinct size populations, enriched with cells in the range of 8-11 μm , 5-8 μm and those smaller than 5 μm (Fig. 4.3). Microfilters with large, 11 μm pores removed any adherent cells as well as potential debris from the sample. The resulting filtrate was composed of a heterogeneous mixture of cells, designated as the control sample (Fig. 4.3A). Membranes with 8 μm pores were used to isolate the largest palmelloids in the culture (Fig. 4.3B). The filtrate from this step was passed through membrane filters with 5 μm pores, which captured small to medium sized palmelloids as well as a number of large single cells, which had a comparable diameter to that of the smallest palmelloids (Fig. 4.3D). The resulting filtrate contained a nearly homogenous suspension of single, motile cells (Fig. 4.3D).

Flow cytometry was used to confirm the cell size distribution and estimated cell sizes (Fig. 4.4). Mean forward angle light scatter (FSC) values, which are proportional to the cross-sectional area of cells, were derived from distribution curves and showed considerable differences among all 3 cell fractions (Fig. 4.4A). Control cultures exhibited mean FSC size distribution values of 1.24×10^6 . Fractions consisting predominantly of large palmelloids (8-11 μm) showed mean FSC values of 1.86×10^6 , smaller palmelloids (5-8 μm) had mean FSC values of 1.38×10^6 , while the nearly homogeneous suspension of single cells resulted in a mean of 0.70×10^6 . Thus, a 2-fold increase in the average FSC values was observed in smaller palmelloids (5-8 μm) compared to single cells (>5 μm), while larger palmelloids (8-11 μm) showed nearly 3-fold higher mean values (Fig. 4.4A). Therefore, the mean cross-sectional area of palmelloids was approximately 3 times that of single cells.

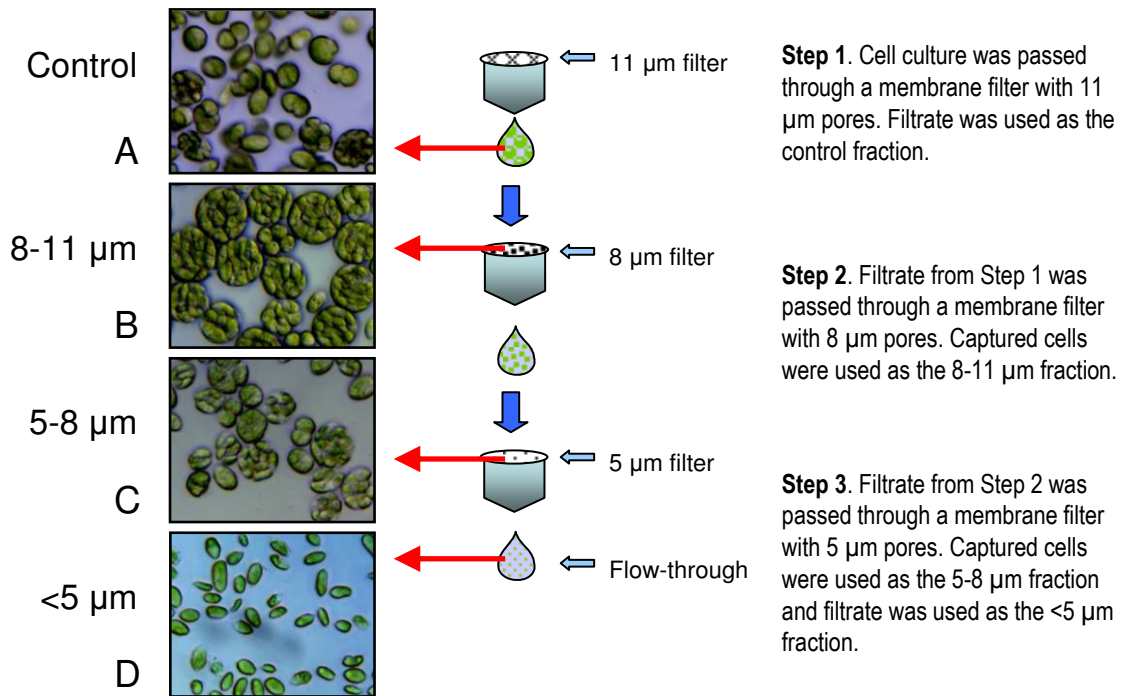


Figure 4.3: Membrane filtration procedure carried out for the separation of different sized cell units. Step 1. Dilute cell culture was passed through 11 μm hydrophilic nylon net filters by gravity flow, using a glass filter holder. Cells captured on the filter were discarded and the flow-through filtrate was utilized as the control fraction (A). This control cell suspension was passed through hydrophilic polycarbonate membrane filters with 8 μm pores with the aid of gentle vacuum aspiration. Cells retained on the filters were washed with culture medium, re-suspended and centrifuged to concentrate the cells, which were used as the 8-11 μm fraction (B). The flow-through filtrate was passed through hydrophilic polycarbonate membrane filters with 5 μm pores using gentle vacuum aspiration. Cells retained on the filters were washed, resuspended in culture medium and centrifuged as for the previous step, and used as the 5-8 μm fraction (C). The flow-through filtrate was centrifuged and used as the single cell enriched, <5 μm fraction (D). Fractions were monitored using light microscopy (A-D, left).

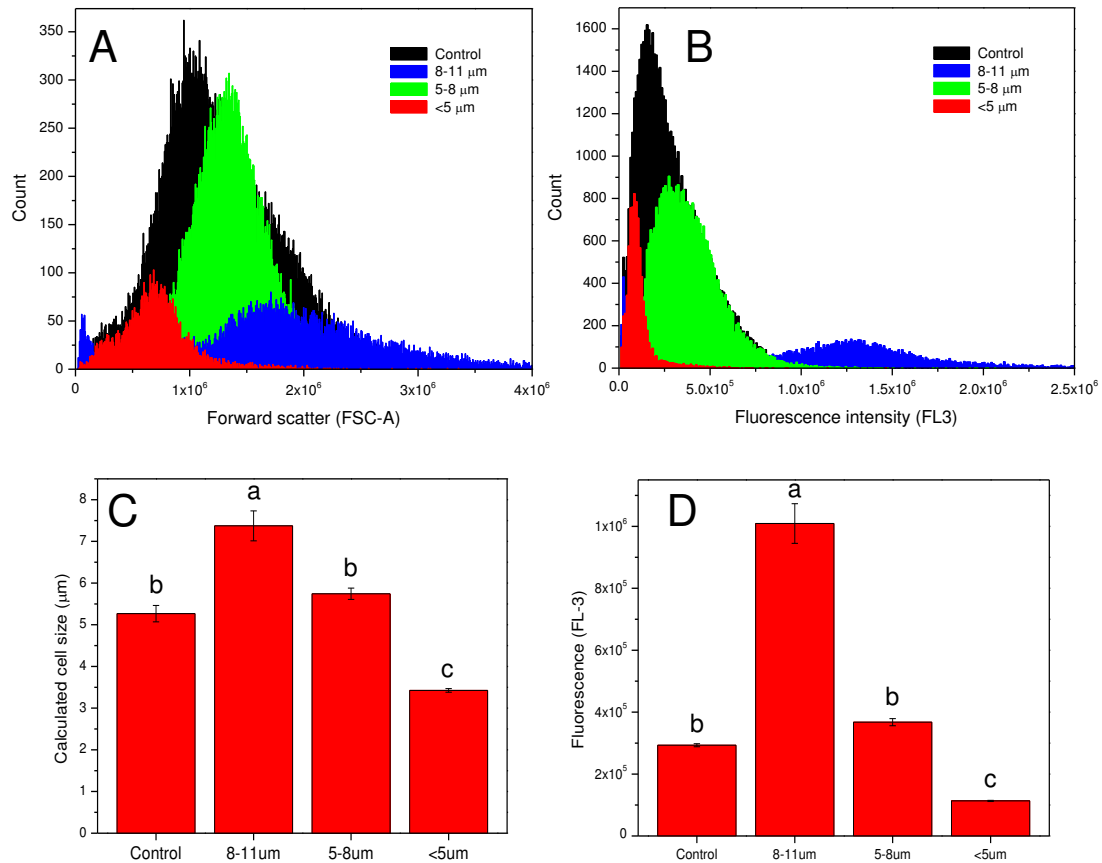


Figure 4.4: Analysis of isolated subpopulations of UWO241 cells using flow cytometry. Overlay histogram of forward scatter channel (FSC-A) analysis for all cell fractions (A). Estimation of cell size using mean FSC-A values and bead calibration (B). Mean (\pm SE, $n=3$) calculated sizes with different letters indicate significant difference, as determined by Tukey's HSD ($p<0.01$). Combined histograms of FL-3 (>670nm long-pass filter), measuring red chlorophyll fluorescence (C) and the corresponding mean FL-3 values (\pm SE) (Tukey's HSD, $p<0.01$) (D).

Estimation of absolute cell size of each fraction was performed by comparing FCS values from microspheres of known sizes through the generation of a calibration curve (Fig. 4.4B). Average cell sizes were calculated to be 5.27 μm for control cultures, 7.37 μm for the fraction containing the largest palmelloids (8-11 μm), 5.74 for the smaller palmelloids (5-8 μm) and 3.42 μm for the predominantly single-cell fraction (<5 μm). Thus, based on the filter pore sizes used for cell separation, estimated particle sizes of each fraction were within expected ranges.

Red chlorophyll fluorescence was also measured for each separated cell fraction using an FL-3 detector (>670 nm) (Fig. 4.4C and D). Mean FL-3 values were derived from fluorescence distribution curves (Fig. 4.4C). The largest palmelloids were characterized by the highest chlorophyll fluorescence (1.009×10^6), which was 2.75 times greater than that of smaller palmelloids (0.367×10^6), and 8.9 times greater than that of single cells (0.113×10^6). Control cells exhibited chlorophyll fluorescence of 0.293×10^6 (Fig. 4.4D). Therefore, the variance in chlorophyll fluorescence (FL-3) among fractionated cells demonstrated greater differences, compared to their cross-sectional area (FSC).

4.3.3 77K fluorescence

To assess differences in steady-state energy distribution between the isolated cell fractions, we collected low temperature (77K) fluorescence emission spectra for control, single cells (<5 μm) and palmelloids (8-11 μm) (Fig. 4.5A, Appendix 4S3). Control cells exhibited the typical 77K fluorescence emission for UWO241 cells, with maxima at 682 and 696 nm associated with photosystem II, but with minimal fluorescence emission in the region of 713 nm, associated with photosystem I, as previously observed for this psychrophile (Morgan et al. 1998, Morgan-Kiss et al. 2002, Szyszka et al. 2007). Although PSI-associated fluorescence (713 nm) was similar to control cells, difference spectra indicated that single cells (<5 μm) showed a higher emission at 681 nm than control cells (Fig. 4.5A and B). In contrast, palmelloids (8-11 μm) showed a higher emission at 680 nm, in addition to enhanced emission in the region of 711-713 nm (Fig. 4.5A and C). Compared to palmelloids, single cells exhibited higher emission 680 nm, and a lower emission at 713 nm (Fig. 4.5D, Appendix 3S3, Appendix 3S4). Thus,

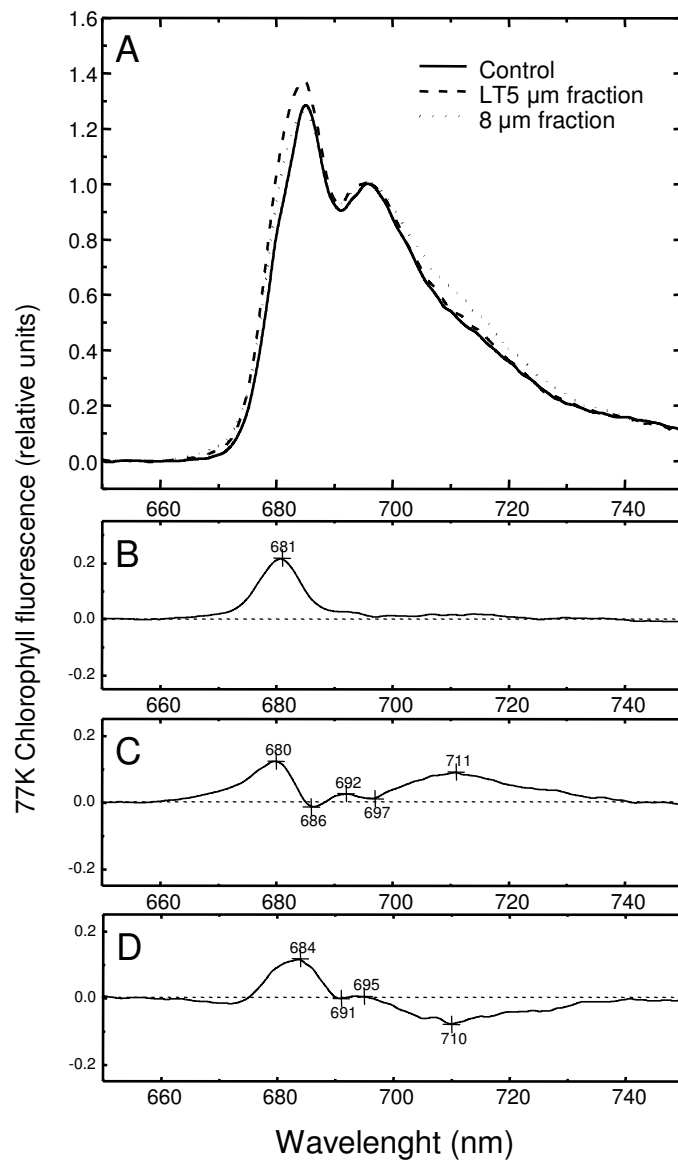


Figure 4.5: Low temperature (77K) chlorophyll fluorescence emission spectra of UWO241 control cells (solid line), LT 5 μm cell fraction (dashed line) and 8 μm cell fraction (dotted line) (A). Chl fluorescence was excited at 436 nm. The spectra were normalized at 695 nm. Corresponding difference spectrum of LT 5 μm cell fraction – control (B), 8 μm cell fraction – control (C) and LT 5 μm - 8 μm cell fraction (D).

UWO241 single cells and palmelloids exhibited differences in energy distribution between PSII and PSI.

4.3.4 Chlorophyll a fluorescence induction

To assess functional differences in photosynthetic characteristics, we compared room temperature fluorescence induction curves for control, single cells and palmelloid fractions measured at their growth temperature and irradiance (Table 4.1). Maximal PSII photochemical efficiency, measured as F_v/F_m , was minimally different between single cells (0.671 ± 0.007) and palmelloids (0.665 ± 0.020) (Table 4.1). In addition, we quantified the following photosynthetic parameters under steady-state conditions: maximum photochemical efficiency (F_v/F_m), excitation pressure, measured as $1-q_L$, yield of PSII (Φ_{PSII}), yield of non-photochemical quenching (Φ_{NPQ}), yield of non-regulated dissipation of excess energy (Φ_{NO}) and electron transport rates (ETR) (Table 4.1). Although single cells and palmelloids exhibited no significant differences in F_v/F_m , both excitation pressure ($1-q_L$) and non-photochemical quenching (Φ_{NPQ}) were higher in single cells than palmelloids. However, non-regulated dissipation (Φ_{NO}) was significantly higher in palmelloids than single cells (Table 4.1).

Figure 4.6 illustrates fluorescence induction curves for cell fractions as a response to increasing actinic light intensity, ranging from 50 to 1000 $\mu\text{mol photons m}^{-2} \text{s}^{-1}$. In contrast to the single cells, the fluorescence induction in the palmelloids (Fig. 4.6C) was similar to that observed for control samples (Fig. 4.6A). Consistent with previous studies, an irradiance greater than 200 $\mu\text{mol photons m}^{-2} \text{s}^{-1}$ almost completely quenched F_m' (Szyszka et al. 2007). In addition, the fluorescence induction curves of control, single cells and palmelloids were characterized by a fast initial decay of F_s to, or below F_o levels upon illumination (Fig. 4.6A-C, closed triangles). The extent of this initial quenching of F_s was quantified and plotted as a function of actinic irradiance (Fig. 4.7A). In all cases, the extent of initial F_s quenching increased with increasing actinic irradiance. Single cells exhibited a light-induced, transient quenching of F_s that was 31% greater than palmelloids at 1000 $\mu\text{mol photons m}^{-2} \text{s}^{-1}$. Moreover, this transient quenching was 3-fold greater at 1000 than at 50 $\mu\text{mol photons m}^{-2} \text{s}^{-1}$ (Fig. 4.7A). In single cells, F_s was

Table 4.1: Energy partitioning parameters calculated for each cell fraction from Chl fluorescence induction traces (Fig. 5). Values represent the mean relative yields (\pm SE, n=6) of Fv/Fm = maximum photochemical efficiency, 1-qL = excitation pressure, Φ PSII = efficiency of PSII, Φ NPQ = non-photochemical quenching, and Φ NO = non-regulated dissipation. Values followed by different letters are significantly different, as determined by ANOVA and Tukey's test ($p < 0.05$).

	Fv/Fm	1-qL	Φ PSII	Φ NPQ	Φ NO	Φ NO/ Φ NPQ
Control	0.732 \pm 0.02a	0.462 \pm 0.01a	0.349 \pm 0.01a	0.321 \pm 0.01a	0.329 \pm 0.00c	1.027 \pm 0.02b
Single cells	0.671 \pm 0.01b	0.470 \pm 0.02a	0.298 \pm 0.01b	0.347 \pm 0.01a	0.355 \pm 0.01b	1.021 \pm 0.02b
Palmelloids	0.665 \pm 0.02b	0.393 \pm 0.01b	0.344 \pm 0.01a	0.272 \pm 0.02b	0.384 \pm 0.01a	1.414 \pm 0.04a

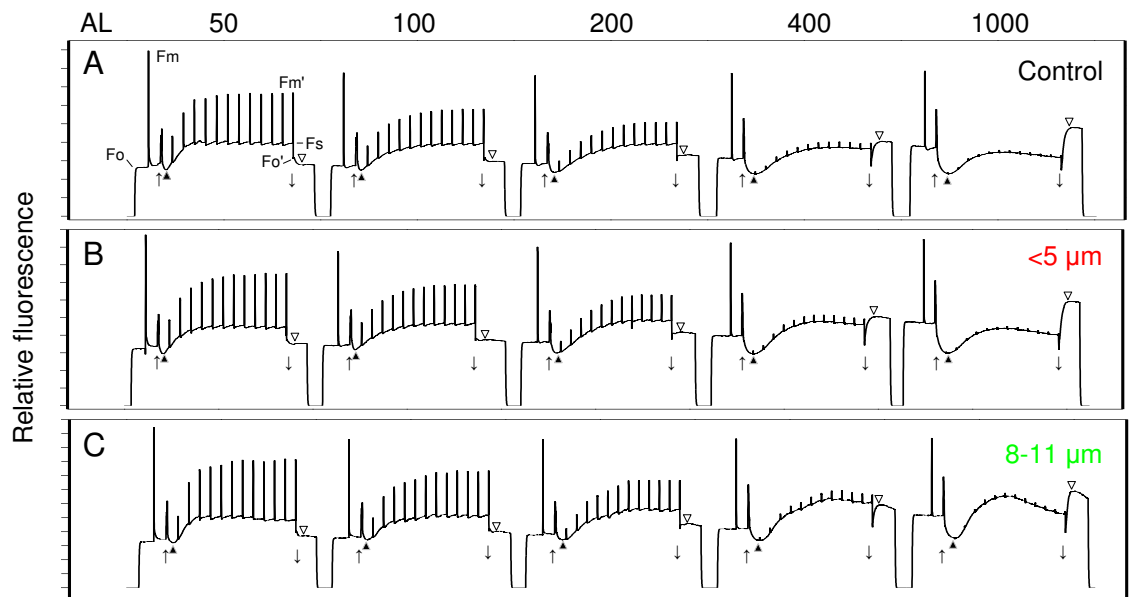


Figure 4.6: Chlorophyll fluorescence light response traces of UWO 241 control cells (A) and separated cell fractions: $<5 \mu\text{m}$ (B) and $8\text{-}11 \mu\text{m}$ (C). Cultures were measured at increasing actinic light (AL) intensities of 50, 100, 200, 400 and 1000, $\mu\text{mol photons m}^{-2} \text{s}^{-1}$. (\uparrow) Actinic light on. (\downarrow) Actinic light off. Fluorescence quenching during onset of actinic light [F_0 - \blacktriangle] (d), and post-illumination rise [\blacktriangledown - F_0']. Cells were dark adapted for 15 min prior to collection of the fluorescence traces.

lower than the initial F_o at $1000 \mu\text{mol photons m}^{-2} \text{s}^{-1}$, which was also reflected in control cells but not palmelloids (Fig. 4.6A-C).

UWO241 cells also exhibited a post-illumination rise in F_o (Fig. 4.6, open triangles), the extent of which was also light-dependent and similar in all samples (Fig. 4.7B).

Therefore, single cells of UWO241 exhibited a greater fluorescence quenching upon illumination compared to palmelloids. This is consistent with the greater inhibition of ETR in single cells versus palmelloids and control cells at an actinic irradiance greater than $200 \mu\text{mol photons m}^{-2} \text{s}^{-1}$ (Fig. 4.7C).

All cell fractions showed a similar increase in excitation pressure, measured as $1-q_L$, concomitant with a comparable decrease in PSII efficiency (Φ_{PSII}) (Fig. 4.7D and E). Although all UWO241 cells responded to increasing irradiance with an increase in non-photochemical quenching (Φ_{NPQ}), palmelloids generally exhibited lower NPQ levels than single cells (Fig. 4.7F). Furthermore, palmelloids showed the greatest, 35% increase in non-regulated dissipation (Φ_{NO}) at an irradiance of $400 \mu\text{mol photons m}^{-2} \text{s}^{-1}$ or greater (Fig. 4.7G). Therefore, UWO241 palmelloids appeared to be predisposed to dissipate a greater proportion of their energy through Φ_{NO} than through Φ_{NPQ} , compared to single cells.

4.3.5 Pigment composition

Pigment compositions were quantified on a per Chl basis for the cell fractions of UWO241 using HPLC (Fig. 4.8). Although Chl a levels remained constant in all fractions, chlorophyll b levels were 43% lower in palmelloids, than single cells (Fig. 4.8A) which resulted in more than 2-fold higher chlorophyll a/b ratios in palmelloids compared to single cells (Fig. 4.8B).

As previously reported, lutein is the most abundant carotenoid to accumulate in UWO241 cells (Morgan et al. 1998). Under the present growth conditions, zeaxanthin was present in non-detectable or trace amounts for all measured groups. Neoxanthin, violaxanthin, antheraxanthin and zeaxanthin did not show any notable differences among the different sized cell groups and consequently, no significant differences in epoxidation states

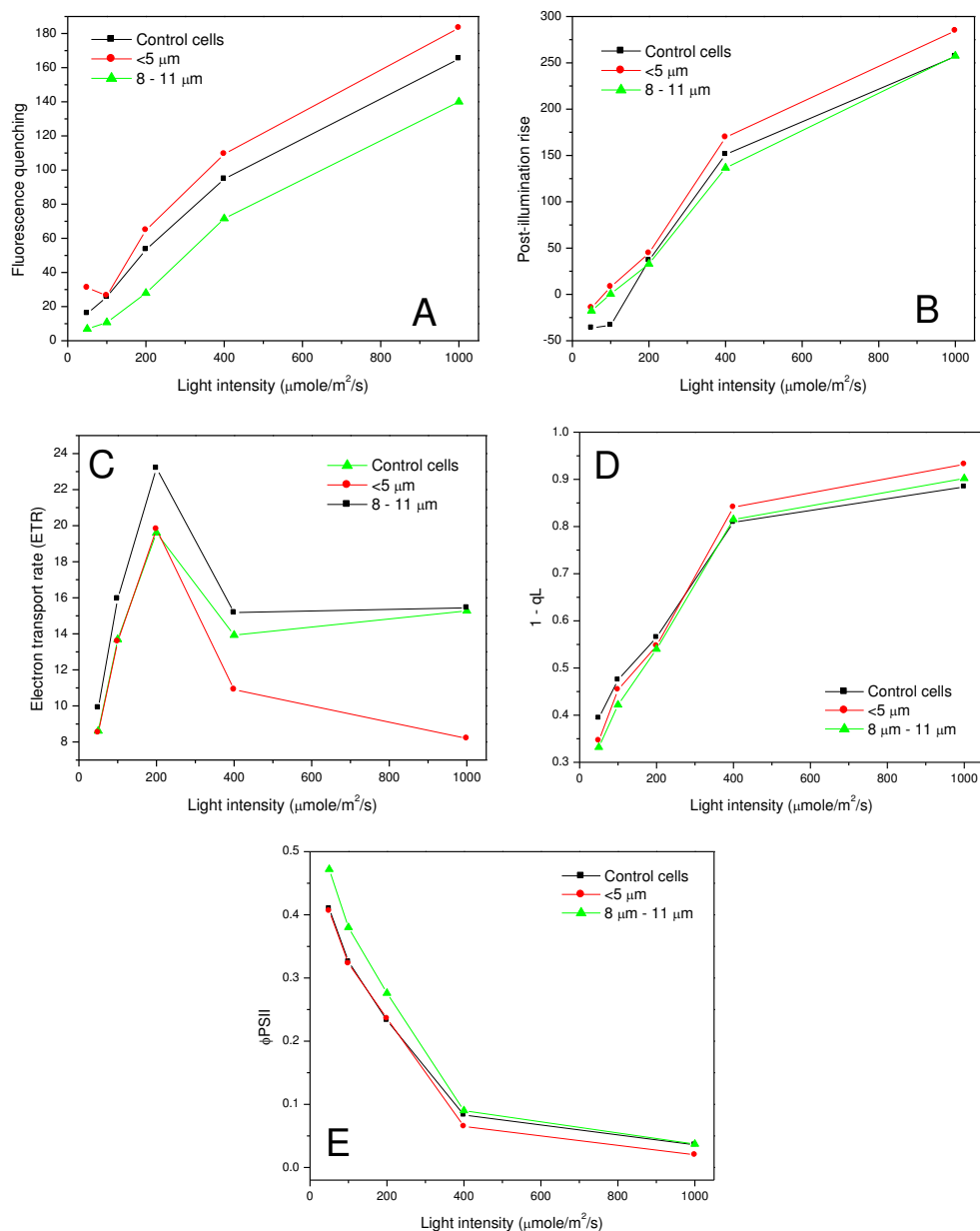


Figure 4.7: Parameters calculated from chlorophyll fluorescence light response traces of UWO 241 control cells and separated cell fractions, measured at increasing actinic light (AL) intensities of 50, 100, 200, 400 and 1000 $\mu\text{mol photons m}^{-2} \text{s}^{-1}$. Fluorescence quenching during onset of actinic light [F_0 - \blacktriangle] (A), post-illumination rise [∇ - F_0'] (B), electron transport rate (C), $1 - q_L$ = excitation pressure (D) and Φ_{PSII} = efficiency of PSII (E).

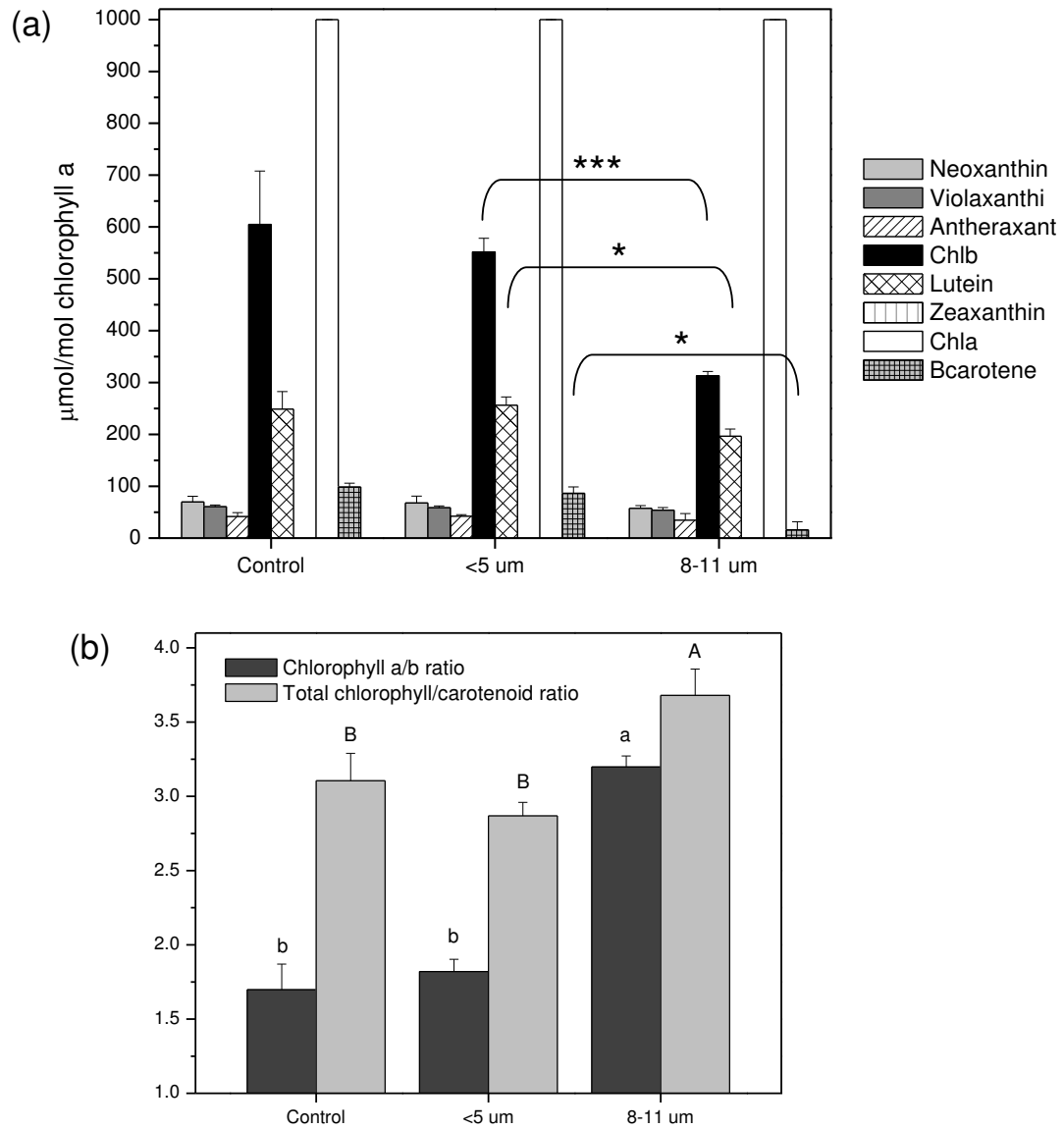


Figure 4.8: Composition of photosynthetic pigments in control and separated cell fractions based on size (A). Pigment concentrations are expressed as μmol per mole of chlorophyll a. Mean values between single cells and palmelloids were analyzed by an unpaired t-test, with the following significance levels: *significant at $p < 0.05$, **significant at $p < 0.005$ and ***significant at $p < 0.001$. No asterisk indicates no significance. Analysis of chlorophyll a/b ratios and total chlorophyll (a+b) to total carotenoid pool (mean \pm SE) (B). Different letters indicate significant difference for $n=4$, as determined by Tukey's HSD ($p < 0.05$) for both Chl a/b ratios (lower case) and Chl/carotenoid ratios (upper case).

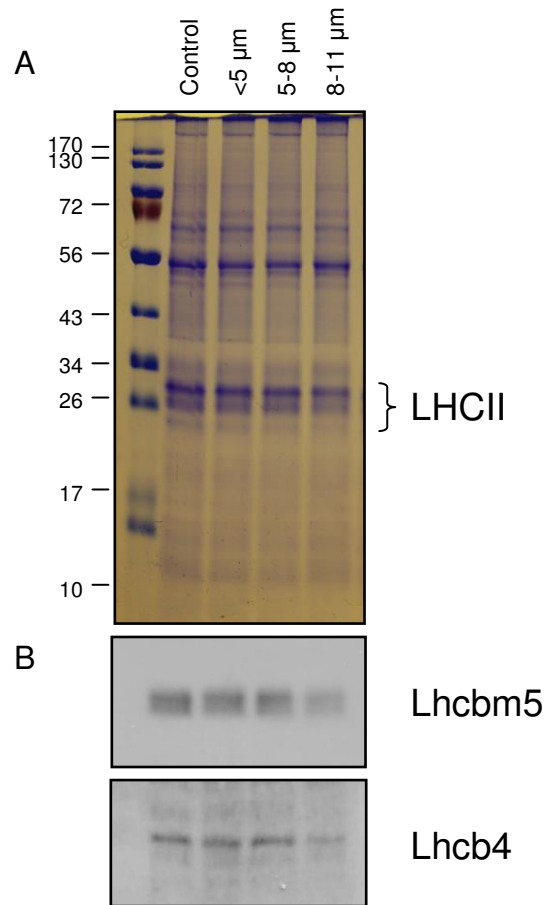


Figure 4.9: Coomassie stained SDS-PAGE analysis of thylakoid membrane proteins from control and different-sized cell fractions of UWO 241 (A). Immunoblot analysis of proteins probed with antibodies raised against Lhcbm5 and Lhcb4 (B). Lanes of SDS-PAGE were loaded on an equal Chl basis. Values on the left indicate apparent molecular mass (kDa).

occurred under the conditions used. However, compared to single cells, a significant, 82% lower β -carotene level and a 20% lower lutein content was observed in palmelloids compared to single cells (Fig. 4.8A). Thus, palmelloids exhibited the lowest total carotenoid pools, reduced by 27-29% in comparison to single cells (Fig. 4.8B).

4.3.6 SDS-PAGE and immunoblotting

Thylakoid membrane proteins from separated cell fractions were analyzed by SDS-PAGE (Fig. 4.9A). Examination of a Coomassie-stained gel containing thylakoid polypeptides from each fraction showed little difference between their protein compositions, although palmelloids (8-11 μ m) appeared to contain decreased levels of LHCII proteins (Fig. 4.9A). A reduction of LHCII in large palmelloids was confirmed by immunoblotting with antibodies raised against Lhcbm5 and Lhcb4 (Fig. 4.9B). Decreased abundance of LHCII in large palmelloids is consistent with increased Chl a/b ratios, and decreased chlorophyll fluorescence emission at 680 nm, compared to single cells (Fig. 4.5D, Appendix 3S4, 4.8B).

4.4 Discussion

Previous studies have shown that palmelloid formation in *Chlamydomonas* can be induced by altering culture media, addition of compounds which inhibit growth, malfunction in flagella and cell walls, and in the presence of grazers (Iwasa and Murakami 1968, Nakamura et al. 1975, Mikheeva and Kruchkova 1980, Olsen et al. 1983, Devine et al. 1993, Franqueira et al. 1999, Lurling and Beekman 2006). However, to our knowledge, induction of the palmelloid state in *Chlamydomonas* has not been previously reported as a response to growth temperatures. In both the Antarctic psychrophile, *Chlamydomonas* sp. UWO241 and the mesophilic *Chlamydomonas raudensis* SAG 49.72, temperature has a profound effect on cell morphology. A supra-optimal growth temperature of 16°C in the Antarctic psychrophilic strain (UWO 241) in contrast to a suboptimal growth temperature of 11°C in the mesophilic strain (SAG 49.72) induced an increased proportion of palmelloids relative to single cells (Fig. 4.1D, Fig. 4.2). Previous reports have also demonstrated that these growth temperatures also result in reduced growth rates for both species (Szyszka et al. 2007). Thus, we conclude

that a shift to either suboptimal or supraoptimal growth temperatures may induce palmelloid formation in *Chlamydomonas* species.

Pigment analysis revealed that, compared to single cells, palmelloids of UWO241 contain significantly reduced levels of chlorophyll b, resulting in higher Chl a/b ratios and reduced levels of β -carotene and lutein which are consistent with the lower abundance of the LHCII proteins, Lhcb4 and Lhcbm5 and decreased F682/F712 ratios (Fig. 4.5D, Appendix 3S4, Fig. 4.8B, Fig. 4.9).

Analysis of room temperature chlorophyll a fluorescence of single cells versus palmelloids of UWO241 demonstrated that under optimal growth conditions, maximum photochemical efficiency of PSII (Fv/Fm) did not differ between single cells and palmelloids (Table 4.1). Furthermore, single cells and palmelloids showed a comparable increase in excitation pressure (1-qL), and decrease in the yield of PSII electron transport (Φ PSII) in response to increasing irradiance (Fig. 4.7D and E).

Although fluorescence quenching was associated with an increase in NPQ for both single cells and palmelloids, palmelloids exhibited lower levels of NPQ with concomitant higher levels of non-regulated dissipation of excess absorbed energy (Φ NO) (Fig. 4.6, Table 4.1). Therefore, single cells appear to favour partitioning of excess excitation energy through typical down-regulatory processes (NPQ) associated with the xanthophyll cycle and antenna quenching whereas palmelloids favour partitioning of excess energy through other, constitutive energy dissipative processes (Φ NO). Although the mechanism for quenching through NO remains equivocal, it has been proposed to originate through PSII reaction center quenching (Weis and Berry 1987, Bukhov et al. 2001, Ivanov et al. 2008). The process of non-photochemical quenching (NPQ) involves xanthophyll cycle activity, and light harvesting proteins. Therefore, a reduction of both carotenoid pools and LHCII proteins may result in a reduction of non-photochemical (NPQ) antenna quenching in UWO241 palmelloids. It is likely that in the absence of sufficient antenna quenching, other non-regulated dissipation mechanisms, such as reaction center quenching, probably occur (Ivanov et al. 2005; Zulficarov et al. 2007; Ivanov et al. 2008). This is the case for a chlorophyll b-deficient *Chlorina F2* barley mutant, with

extensively reduced light harvesting antennae sizes. While the proportion of antenna energy dissipation through Φ_{NPQ} was 38% lower in the *F2* mutant compared to WT, this was concomitant with a 34% increase in constitutive, non-regulated dissipation (Φ_{NO}), presumed to occur via reaction center quenching (Ivanov et al. 2008). In addition, similar to the observations made for palmelloids of UWO241, *Chlorina F2* exhibited a slight increase in PSII photochemical quenching (Φ_{PSII}) and lower excitation pressure (1-qL), despite considerable LHC reductions (Ivanov et al. 2008).

In this study, large palmelloids of UWO241 maintained the highest levels of non-regulated dissipation (Φ_{NO}) and lowest levels of non-photochemical quenching (NPQ) during steady-state growth and exposure to high irradiance (Fig. 4.6, Table 4.1). Previous studies have shown that compared to growth at low temperatures, high levels of Φ_{NO} and reduced Φ_{NPQ} are also exhibited by UWO241 cultures grown at 16°C, where large palmelloids make up nearly half of the population (Fig. 4.1D, Fig. 4.2A; 16°C, Szyszka et al. 2007). Therefore, partitioning of excess light energy appears to be closely related to the morphological structure of UWO241 cells.

The post-illumination rise in fluorescence intensity was greater in single cells than palmelloids which indicates that the plastoquinone pool of single cells is more reduced in the dark compared to palmelloids (Fig. 4.7B). In addition, palmelloids maintained higher rates of electron transport in response to increased light intensity, compared to single cells (Fig. 4.7C).

4.5 Conclusion

It is well recognized that cultures of algae are formed by cells that can vary in age, size and growth rates. Our studies indicate that UWO241 cultures are also composed of different subpopulations of cells that differ in morphology, a property that can be regulated by growth temperatures. Individual morphological states of UWO241 are characterized by distinct pigment profiles, energy partitioning pathways and thus, responses to excess light. Therefore, palmelloids and single cells of UWO241 are photosynthetically distinct, and the overall state of a heterogeneous population is determined by the distribution of individual cells that coexist in the culture. Interestingly,

however, compared to single cells, palmelloids did not exhibit shade-adapted characteristics.

4.6 References

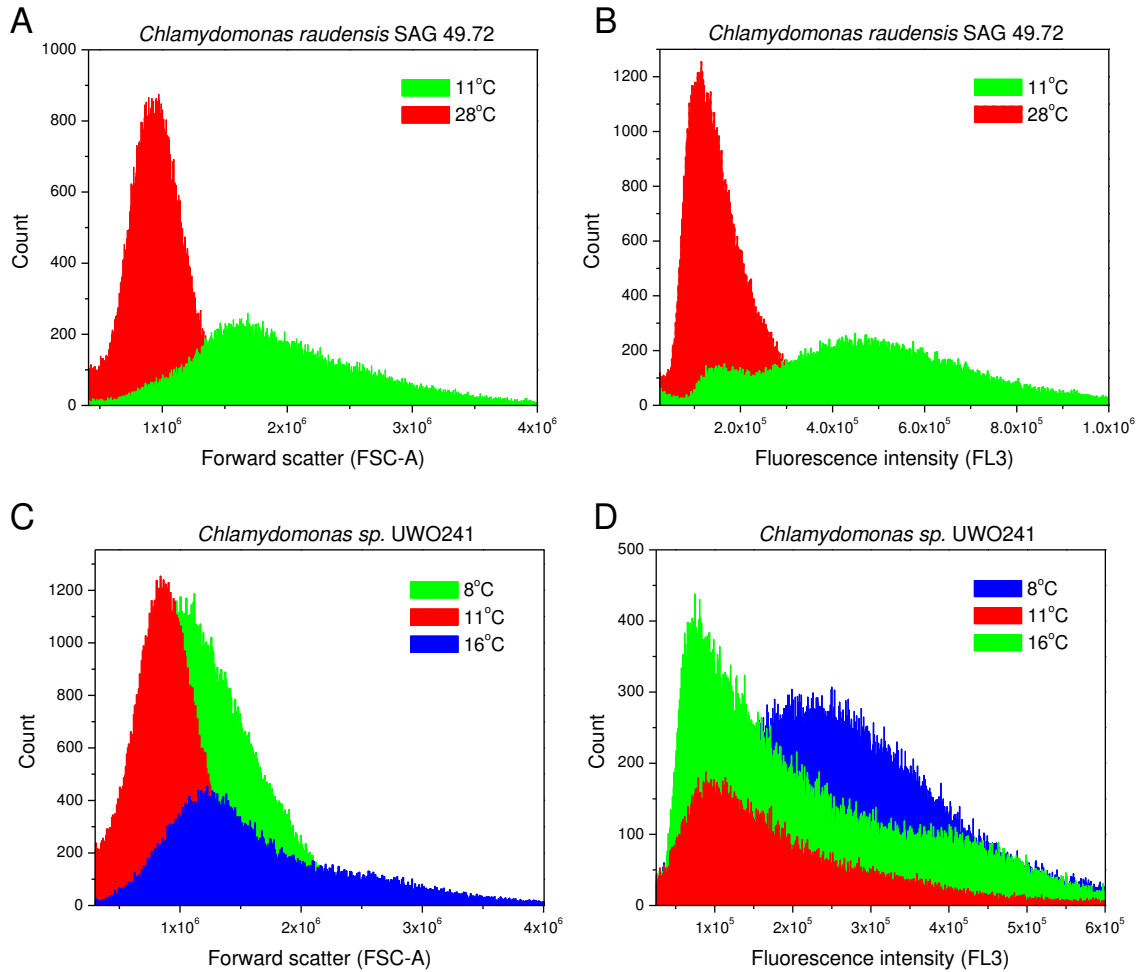
- Bassi R, Croce R, Cugini D, Sandonà D.** (1999) Mutational analysis of a higher plant antenna protein provides identification of chromophores bound into multiple sites. *Proc Natl Acad Sci USA* **96**(18):10056-61
- Bukhov NG, Heber U, Weise C, Shuvalov VA.** (2001) Energy dissipation in photosynthesis: does the quenching of chlorophyll fluorescence originate from antenna complexes of photosystem II or from the reaction center? *Planta* **212**(5-6):749-58
- Chunaev A, Mirnaya O, Maslov V, Boschetti A.** (1991) Chlorophyll b- and loroxanthin-deficient mutants of *Chlamydomonas reinhardtii*. *Photosynthetica* **25**:291–301
- Coleman AW.** (1983) The roles of resting spores and akinetes in chlorophyte survival. In Fryxell GA. [Ed.] *Survival strategies of the algae*. Cambridge University Press, Cambridge, UK, pp. 1-21
- Craigie RA, Cavalier-Smith T.** (1982) Cell volume and control of the *Chlamydomonas* cell cycle. *J Cell Sci* **54**:173-91
- Devine M, Duke SO, Fedtke C.** (1993) *Physiology of herbicide action*. PTR Prentice-Hall, Englewood Cliffs, NJ, pp. 166
- Franqueira D, Cid A, Torres E, Orosa M, Herrero C.** (1999) A comparison of the relative sensitivity of structural and functional cellular responses in the alga *Chlamydomonas eugametos* exposed to the herbicide paraquat. *Arch Environ Contam Toxicol* **36**:264-9
- Fritsch FE.** (1945) *The structure and reproduction of the algae, vol. I*. Cambridge University Press, New York, NY, pp. 39
- Fritsen CH, Prisco JC.** (1999) Seasonal change in the optical properties of the permanent ice cover on Lake Bonney, Antarctica: Consequences for lake productivity and phytoplankton dynamics. *Limnol Ocean* **44**(2):447-54
- Giuffra E, Cugini D, Croce R, Bassi R.** (1996) Reconstitution and pigment-binding properties of recombinant CP29. *Eur J Biochem* **238**(1):112-20
- Harris EH.** (2009) *The Chlamydomonas Sourcebook, Vol. 1: Introduction to Chlamydomonas and Its Laboratory Use*. Academic Press, San Diego, pp. 41-45
- Heinze I, Pfündel E, Hühn M, Dau H.** (1997) Assembly of light harvesting complexes II (LHC-II) in the absence of lutein: A study on the α -carotenoid-free mutant C-2A'-34 of the green alga *Scenedesmus obliquus*. *Biochim Biophys Acta* **1320**:188-94

- Howard-Williams C, Schwarz A, Hawes I, Priscu JC.** (1998) Optical properties of lakes of the McMurdo Dry Valley lakes, Antarctica. *In* Priscu JC. [Ed.] *Ecosystem Dynamics in a Polar Desert: The McMurdo Dry Valleys, Antarctica*. Antarctic Research Series, Vol. 72, American Geophysical Union, pp. 189-203
- Ivanov AG, Krol M, Apostolova EL, Morgan-Kiss RM, Naydenova N, Hüner NPA, Sane PV.** (2005) Oligomerization state of LHCII modulates the redox properties of the acceptor side of photosystem II in Costata-2/133 mutant of pea. *Physiol Mol Biol Plants* **11**:199-207
- Ivanov AG, Król M, Maxwell D, Hüner NPA.** (1995) Abscisic acid induced protection against photoinhibition of PS II correlates with enhanced activity of the xanthophyll cycle. *FEBS Lett* **371**: 61-4
- Ivanov AG, Hurry V, Sane PV, Öquist G, Hüner NPA.** (2008) Reaction centre quenching of excess light energy and photoprotection of Photosystem II. *J Plant Biol* **51**:85-96
- Iwasa K, Murakami S.** (1968) Palmelloid formation of *Chlamydomonas* I. Palmelloid induction by organic acids. *Physiol Plant* **21**(6):1224-33
- Iwasa K, Murakami S.** (1969) Palmelloid formation of *Chlamydomonas* II. Mechanism of palmelloid formation by organic acids. *Physiol Plant* **22**(1):43-50
- Jaenicke L, Kuhne W, Spessert R, Wahle U, Waffenschmidt S.** (1987) Cell wall lytic enzymes (autolysins) of *Chlamydomonas reinhardtii* are (hydroxy)proline specific proteases. *Eur J Biochem* **170**:485-91
- Kramer DM, Johnson G, Kiirats O, Edwards GE.** (2004) New fluorescence parameters for the determination of QA redox state and excitation energy fluxes. *Photosynth Res* **79**: 209-18
- Kubo T, Kaida S, Abe J, Saito T, Fukuzawa H, Matsuda Y.** (2009) The *Chlamydomonas* hatching enzyme, sporangin, is expressed in specific phases of the cell cycle and is localized to the flagella of daughter cells within the sporangial cell wall. *Plant Cell Physiol* **50**(3):572-83
- Laemmli UK.** (1970) Cleavage of structural proteins during the head of bacteriophage T4. *Nature* **227**:680-5
- Lizotte MP, Priscu JC.** (1994) Natural fluorescence and quantum yields in vertically stationary phytoplankton from perennially ice-covered lakes. *Limnol Ocean* **39**(6):1399-1410
- Lokstein H, Tian L, Polle JE, DellaPenna D.** (2002) Xanthophyll biosynthetic mutants of *Arabidopsis thaliana*: altered nonphotochemical quenching of chlorophyll fluorescence is due to changes in Photosystem II antenna size and stability. *Biochim Biophys Acta* **1553**(3):309-19
- Lurling M, Beekman W.** (2006) Palmelloids formation in *Chlamydomonas reinhardtii*: defence against rotifer predators? *Ann Limnol-Int J Lim* **42**(2):65-72

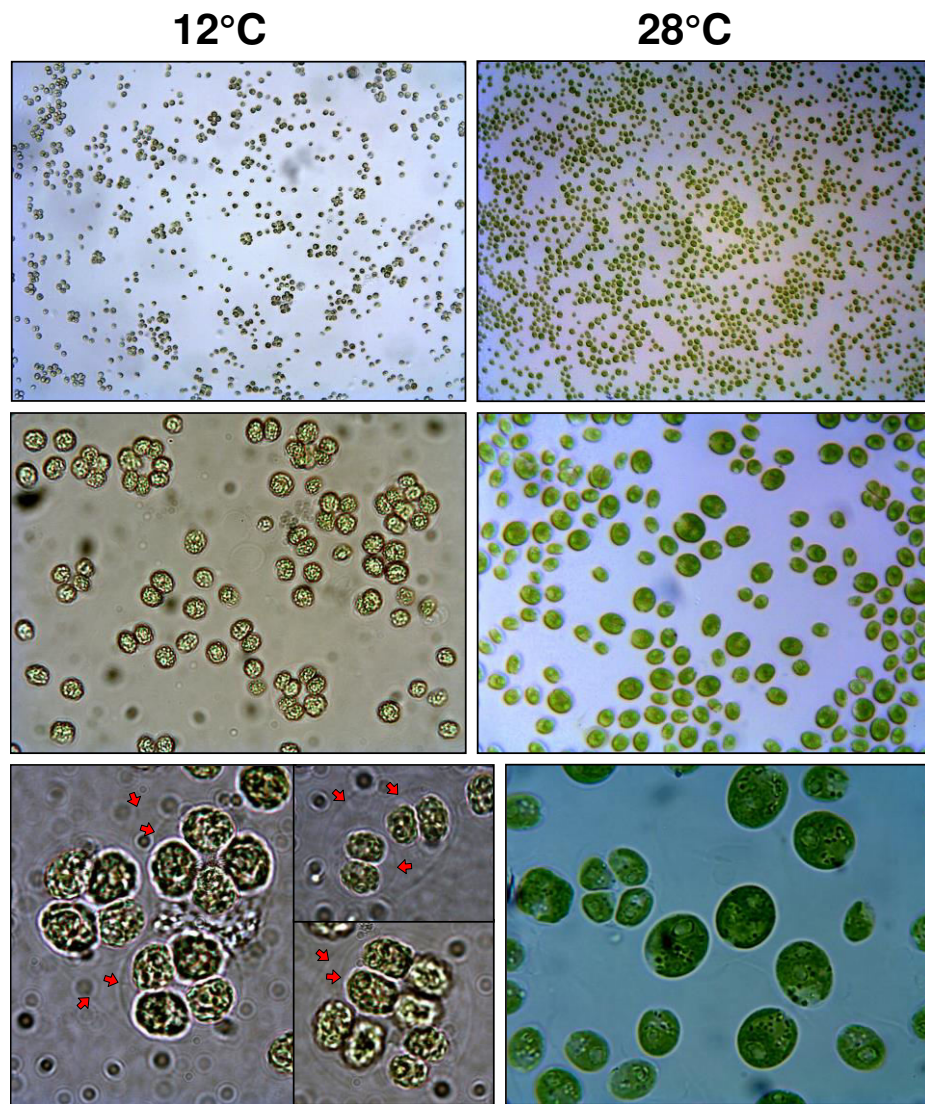
- Matsuda Y, Koseki M, Shimada T, Saito T.** (1995) Purification and characterization of a vegetative lytic enzyme responsible for liberation of daughter cells during the proliferation of *Chlamydomonas reinhardtii*. *Plant Cell Physiol* **36**:681–9
- Mergenhagen D.** (1980) Die Kinetik der Zoosporenfreisetzung bei einem Mutantenstamm von *Chlamydomonas reinhardtii*. *Mitt Staatsinst Allg Bot Hamburg* **17**:18-26
- Mikheeva TM, Kruchkova HM.** (1980) Morphological changes in *Chlamydomonas sp.* and *Scenedesmus acuminatus* in the presence of zooplankton. *Botanica* **5**:60-3
- Morgan RM, Ivanov AG, Priscu JC, Maxwell DP, Hüner NPA.** (1998) Structure and composition of the photochemical apparatus of the Antarctic green alga, *Chlamydomonas subcaudata*. *Photosynth Res* **56**:303–14
- Morgan-Kiss RM, Ivanov AG, Hüner NPA.** (2002) The Antarctic psychrophile, *Chlamydomonas subcaudata*, is deficient in state I-state II transitions. *Planta* **214**(3): 435-45
- Nakamura K, Bray DF, Wagenaar EB.** (1975) Ultrastructure of *Chlamydomonas eugametos* palmelloids induced by chloroplatinic acid treatment. *J Bacteriol* **121**(1):338-43
- Niyogi KK, Björkman O, Grossman AR.** (1997) The roles of specific xanthophylls in photoprotection. *Proc Natl Acad Sci USA* **94**:14162–7
- Oldenhof H, Zachleder V, Van den Ende H.** (2007) The cell cycle of *Chlamydomonas reinhardtii*: the role of the commitment point. *Folia Microbiol* **52**:(1) 53–60
- Olsen Y, Knutsen G, Lien T.** (1983) Characteristics of phosphorus limitation in *Chlamydomonas reinhardtii* (Chlorophyceae) and its palmelloids. *J Phycol* **19**(3):313-19
- Plumley FG, Schmidt GW.** (1987) Reconstitution of chlorophyll a/b light-harvesting complexes: Xanthophyll-dependent assembly and energy transfer. *Proc Natl Acad Sci USA* **84**:146-50
- Pocock T, Lachance MA, Pröschold T, Priscu JC, Kim SS, Hüner NPA.** (2004) Identification of a psychrophilic green alga from Lake Bonney Antarctica: *Chlamydomonas raudensis* Ettl. (UWO241) Chlorophyceae. *J Phycol* **40**(6):1138-48
- Pogson BJ, Niyogi KK, Björkman O, DellaPenna D.** (1998) Altered xanthophyll compositions adversely affect chlorophyll accumulation and nonphotochemical quenching in *Arabidopsis* mutants. *Proc Natl Acad Sci USA* **95**:13324-9
- Rosenberg B, Renshaw E, VanCamp L, Hartwick J, Drobnik J.** (1967) Platinum-induced filamentous growth in *Escherichia coli*. *J Bacteriol* **93**:716-21
- Savitch LV, Ivanov AG, Gudynaite-Savitch L, Hüner NPA, Simmonds J.** (2011) Cold stress effects on PSI photochemistry in *Zea mays*: differential increase of FQR-dependent cyclic electron flow and functional implications. *Cell Physiol* **52**(6):1042-54

- Schlösser UG.** (1966) Enzymatisch gesteuerte freisetzung von zoosporen bei *Chlamydomonas reinhardtii* Dangeard in syn-chronkultur. Arch Microbiol **54**:129-59
- Spigel RH, JC Priscu.** (1996) Evolution of temperature and salt structure of Lake Bonney, a chemically stratified Antarctic lake. Hydrobiol **321**:177-90
- Szyszka B, Ivanov A, Hüner NPA.** (2007) Psychrophily is associated with differential energy partitioning, photosystem stoichiometry and polypeptide phosphorylation in *Chlamydomonas raudensis*. Biochim Biophys Acta **1767**(6):789-800
- Tissut M, Ravanel P, Nurit F, Deslandres C, Bourguignon J.** (1987) Effects of LS 82556 on thylakoid activities and photosynthesis: A comparison with paraquat and acifluorfen. Pestic Biochem Physiol **29**(3):209-16
- Trainor FR.** (1985) Survival of algae in desiccated soil: a 25 year study. Phycologia **24**:79-82
- Voigt J, Mergenhagen D, Mfinzner P, Vogeler HP, Nagel K.** (1989) Effects of light and acetate on the liberation of zoo-spores by a mutant strain of *Chlamydomonas reinhardtii*. Planta **178**:456-62
- Voigt J, Mergenhagen D, Wachholz I, Manshard E, Mix M.** (1990) Cell-wall abnormalities of a *Chlamydomonas reinhardtii* mutant strain under suboptimal growth conditions. Planta **183**:65-8
- Weis E, Berry JA.** (1987) Quantum efficiency of photosystem II in relation to 'energy'-dependent quenching of chlorophyll fluorescence. Biochim Biophys Acta **894**:198-208
- Zulfigarov IS, Ham OK, Misra SR, Kim JY, Nath K, Koo HY, Kim HS, Lee CH.** (2007) Dependence of reaction center-type energy-dependent quenching on photosystem II antenna size. Biochim Biophys Acta **1767**:773-80

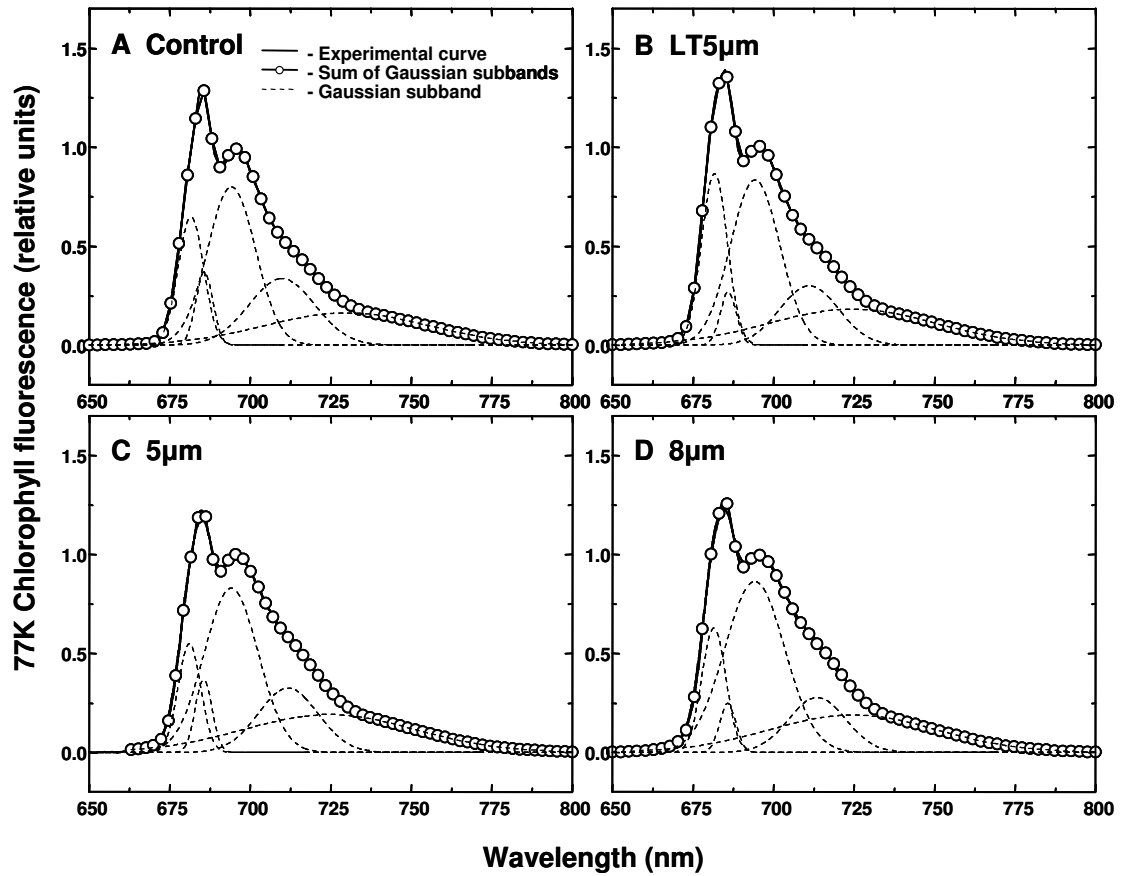
4.7 Appendices



Appendix 4S1: Analysis of *Chlamydomonas raudensis* SAG 49.72 and *Chlamydomonas* sp. UWO241 cell cultures grown at various temperatures using flow cytometry. Overlay histogram of forward scatter channel (FSC-A) (A) and red chlorophyll fluorescence (FL-3) (B) of SAG 49.72 grown at 11°C and 28°C, as well as FSC-A (C) and FL-3 (D) of UWO241 grown at 8°C, 11°C and 16°C.



Appendix 4S2: Light microscope images of *Chlamydomonas reinhardtii* (1690) grown at 12°C and 28°C. The ratio of palmelloids to single cells was greater during growth at lower temperatures. At high magnification, multiple membranes are visible (red arrows) surrounding cells grown at 12°C.



Appendix 4S3: Typical chlorophyll fluorescence emission spectra of UWO 241 control cells and separated cell fractions based on size. Cultures were grown at 5°C and 100 $\mu\text{mol photons m}^{-2} \text{s}^{-1}$. Emission spectra were obtained for Chl *a* excitation at 436 nm.

Chapter 5

5 General discussion and future perspectives

5.1 Major contributions

The majority of my PhD research was focused on the altered thylakoid protein phosphorylation pattern exhibited by the Antarctic psychrophile, *Chlamydomonas sp.* UWO241, through the identification of its unique phosphoproteins, and investigation of LHCII phosphorylation.

5.1.1 Phosphoproteins of *Chlamydomonas sp.* UWO241

Chlamydomonas sp. UWO241 phosphorylates proteins associated with a large ~1000 kDa PSI-cytochrome b_6/f supercomplex, which, most likely functions in cyclic electron flow. Separation of individual subunits of this PSI-Cyt b_6/f supercomplex by isoelectric focusing, led to the identification of 2 major phosphorylated proteins, including a 17 kDa PsbP-like protein and a 70 kDa ATP-dependent zinc metalloprotease FtsH. Since stability of the PSI-Cyt b_6/f supercomplex is dependent on the phosphorylation status of the thylakoid membrane, this supercomplex likely functions in the dynamic regulation between linear and cyclic electron transport in UWO241.

5.1.2 Reduced PSII phosphorylation in *Chlamydomonas sp.* UWO241

Investigation of the typically observed phosphorylated PSII-associated proteins demonstrated that the Antarctic psychrophile maintains reduced levels of both LHCII and PSII core complex phosphorylation. Compared to *C. reinhardtii*, *C. sp.* UWO241 exhibits a strong reduction in phosphorylation of the core proteins, CP43 and D2, as well as the minor LHCII (Lhcb4 and Lhcb5) polypeptides, which play a major role in state transitions (Fig. 5.1). Sequence analysis revealed that the N-terminal ends of Lhcb4 and Lhcb5 lack specific phosphorylation sites. Thus, a state transition deficiency in UWO241 is caused by altered amino acid sequences of minor LHCII proteins, which likely occurred as an

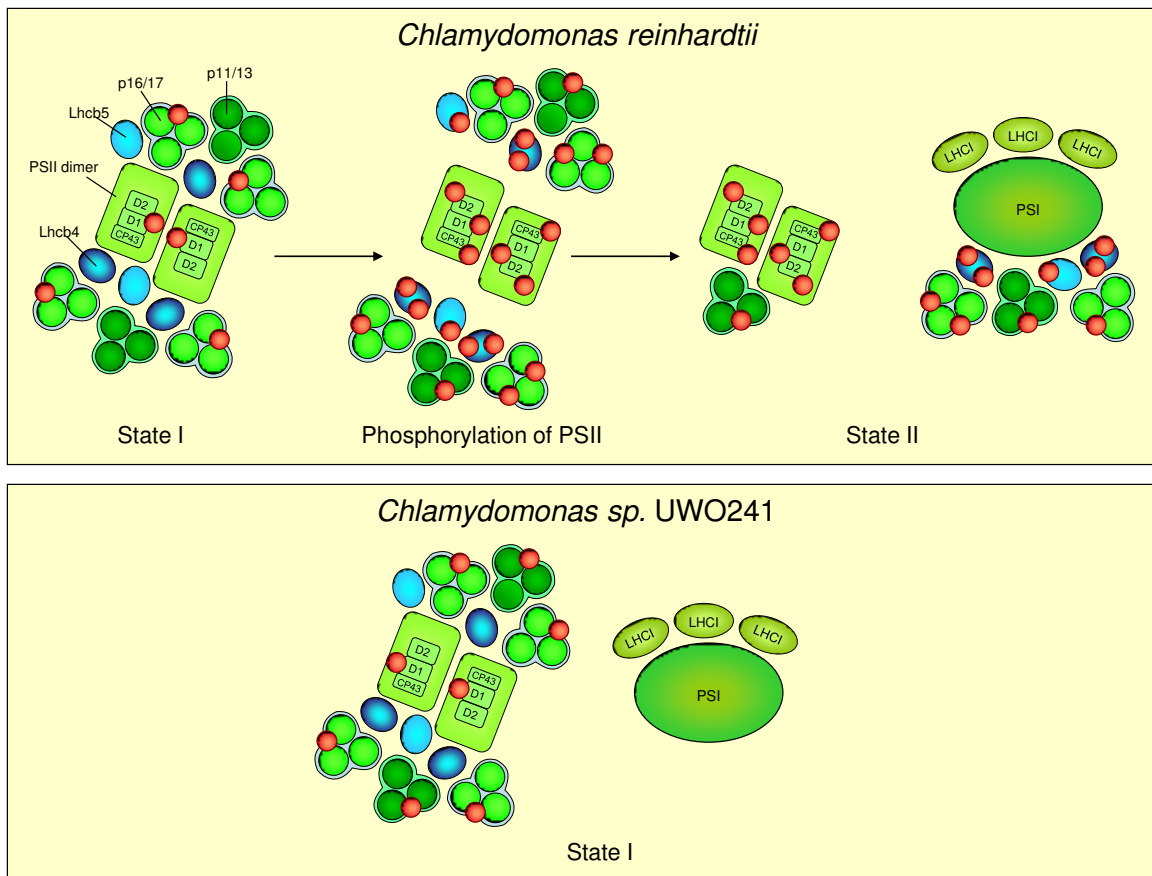


Figure 5. 1: A model of PSII phosphorylation in *C. reinhardtii* and *C. sp. UWO241*. In state I, major (p11/13, p16/17) and minor (Lhcb4, Lhcb5) LHCII proteins associate with PSII dimers. Some phosphorylation of p16/p17 occurs during state I in *C. reinhardtii*. During transition to state II, phosphorylation of PSII core proteins (D2 and CP43) as well as both major and minor LHCII proteins causes detachment of LHCII from PSII dimers. Major LHCII associate with PSI, using minor LHCII proteins (Lhcb4 and Lhcb5) as docking sites. In UWO241, reduced phosphorylation of minor LHCII proteins, Lhcb4 and Lhcb5, as well as PSII core proteins, does not result in the uncoupling of LHCII from PSII dimers, or their association with PSI.

adaptation to the unique natural environment of this Antarctic psychrophile. These studies have improved our understanding of UWO241 being locked in State I.

5.1.3 Phosphorylation profile reflects altered function in *Chlamydomonas sp.* UWO241

It has been demonstrated that successful acclimation to changing environments is associated with the capacity of chloroplasts to maintain a largely oxidized PQ pool of both short and long term durations (Bailey et al. 2004, Grieco et al. 2012). The Antarctic psychrophile, *C. sp.* UWO241, exhibits a greater dependence on cyclic electron flow (CEF), associated with a PSI-Cyt *b₆/f* complex. Therefore, an oxidized PQ pool and the balance of excitation energy between the two photosystems may be maintained through regulation of the CEF pathway, rather than regulation of state transitions in UWO241 during linear electron flow. In addition, high rates of cyclic electron transport exhibited by UWO241 may also contribute to the maintenance of photostasis by 1) protection of PSII by the generation of a proton gradient across the thylakoid membrane, thereby increasing the levels of NPQ; and 2) generation of additional ATP when energy is in high demand. Therefore, increased levels of CEF would be advantageous for UWO241 under the natural conditions of low temperatures and high salt.

During linear electron transport, the transition from state I to state II is activated in response to an over-reduced PQ pool. However, a requirement for state transitions would be reduced when cyclic electron transport occurs at a high rate. Consistently, UWO241 exhibits reduced phosphorylation of proteins associated with state transitions and increased phosphorylation levels of proteins associated with a PSI-Cyt *b₆/f* supercomplex, resulting in the unique phosphorylation pattern observed for this psychrophile.

5.1.4 A model of cyclic electron flow in *Chlamydomonas sp.* UWO241

Until recently, the composition of the thylakoid membrane-enclosed lumen has been poorly characterized. Thus, the function of this chloroplast compartment has been considered to play a limited role in electron transport and photosynthesis. A recent proteomic analysis had identified over 80 proteins in the lumen of *Arabidopsis*, for which

only approximately half have been assigned a putative function, including isomerases, m-type thioredoxins, chaperones, peroxidases and proteases (Schlichter and Soll 1996, Adam 2001, Kieselbach et al. 2000, Peltier et al. 2002). Two-dimensional isoelectrophoresis of lumenal proteins also revealed the expression of a surprising number of paralogs (Peltier et al. 2002). In addition to several plastocyanin, PsbO (OEC33) and PsbQ (OEC16) paralogs, the authors discovered seven weakly related PsbP (OEC23)-like paralogs (Peltier et al. 2002).

In addition, several reports have shown evidence for nucleotide-dependent processes in the chloroplast lumen (Spetea et al. 2004), including the presence of a nucleoside diphosphate kinase (NDPKIII), a trans-thylakoid membrane nucleotide transport system, and the capacity of lumenal PsbO (OEC33) to bind GTP (Spetea et al. 2004, Thuswaldner et al. 2007, Yin et al. 2010). Several studies have revealed the existence of a thylakoid ATP/ADP carrier (TAAC) that delivers stromal ATP to the thylakoid lumen in exchange for ADP (Spetea et al. 2004, Thuswaldner et al. 2007, Yin et al. 2010). Spetea *et al.* (2004) demonstrated the presence of a 17 kDa nucleoside diphosphate kinase III (NDPKIII) in the thylakoid lumen, which catalyzes the transfer of a phosphate group from ATP to GDP, in the synthesis of GTP, a nucleotide known to alter the conformation of a wide array of GTP-binding proteins (GTPases). These same authors demonstrated the light and DCMU sensitive high-affinity binding of GTP to the PSII-associated, lumenal PsbO (OEC33) protein, suggesting a correlation to photosynthetic electron transport as well as the additional function of PsbO as a GTPase involved in signal transduction (Spetea et al. 2004). Subsequent studies showed that GTP binding to PsbO induces changes in the structure of this protein and stimulates the dissociation of PsbO from PSII (Lundin et al. 2007). Furthermore, in *Arabidopsis*, PsbO is encoded by two isoforms, PsbO1 and PsbO2 with seemingly different functions. While PsbO1 supports oxygen evolution, PsbO2 regulates the phosphorylation state and turnover of the D1 protein (Lundin et al. 2008). Small plant GTPases act as important molecular switches in plant signaling and exhibit significant diversity in both structure and function (Yang 2002). These G-proteins are typically between 18 and 33 kDa, require Mg²⁺ ions for activity, exist as both soluble and membrane-associated forms and are activated by a guanine nucleotide exchange factor (GEF) (Leipe et al. 2002, Lundin et al. 2007).

Coincidentally, the crystal structure of authentic PsbP from *Nicotiana tabacum* also suggests a novel function for this protein in GTP-regulated metabolism, as PsbP exhibits strong structural similarity to Mog1p, (Ifuku et al. 2004). Analysis of PsbP structural homology indicated that the folding of this protein is very similar to that of Mog1p, a 24 kDa regulatory protein which interacts with a multifunctional Ran, a small GTPase of the RAS superfamily (Baker et al. 2001, Ifuku et al. 2004). Studies in *Saccharomyces cerevisiae* have shown that Mog1p is a novel factor involved in regulating the nucleotide state of Ran (Ifuku et al. 2004). Upon formation of a complex between Mog1p and a Ran GTPase, Mog1p stimulates the release of bound GDP or GTP from Ran (Ifuku et al. 2004).

Based on my studies of the PSI-Cyt *b₆/f* supercomplex, together with established functions of several related proteins, I propose a model for cyclic electron flow in *Chlamydomonas sp.* UWO241 (Fig. 5.2). The major subunits identified in this supercomplex include photosystem I proteins, cytochrome *b₆*, cytochrome *f*, a 17 kDa PsbP-like protein, an ADP-ribosylation factor associated with the ARF family of GTPases, a PSI assembly protein associated with the Ycf4 superfamily in *Chlamydomonas*, an ATP-dependent FtsH metalloprotease, heat shock protein 70 and an adenine nucleotide (ATP/ADP) translocator. Both FtsH and the PsbP-like protein appear to be the primary phosphorylated subunits of this supercomplex.

I propose that under conditions associated with increased ATP demand (i.e. low temperatures, high irradiance, high salt), phosphorylation of a luminal PsbP-like protein in UWO241 may increase its affinity towards photosystem I. Increased levels of PSI bound PsbP-like proteins may promote their interaction with membrane-associated small Ras GTPase proteins. Binding of a PsbP-like protein with an inactive GTPase-GDP could induce a conformational change to remove the GDP nucleotide group. This would facilitate the guanine nucleotide exchange of GTPase, possibly via a luminal nucleoside diphosphate kinase (NDPK) in the activation of GTPase-GTP, which in turn, would play a role in regulating GTPase effector proteins. These proteins may include some of the subunits found associated with the PSI-Cyt *b₆/f* supercomplex, including heat shock protein 70 (HSP70), ATP-dependent metalloprotease (FtsH) and Ycf4, which have

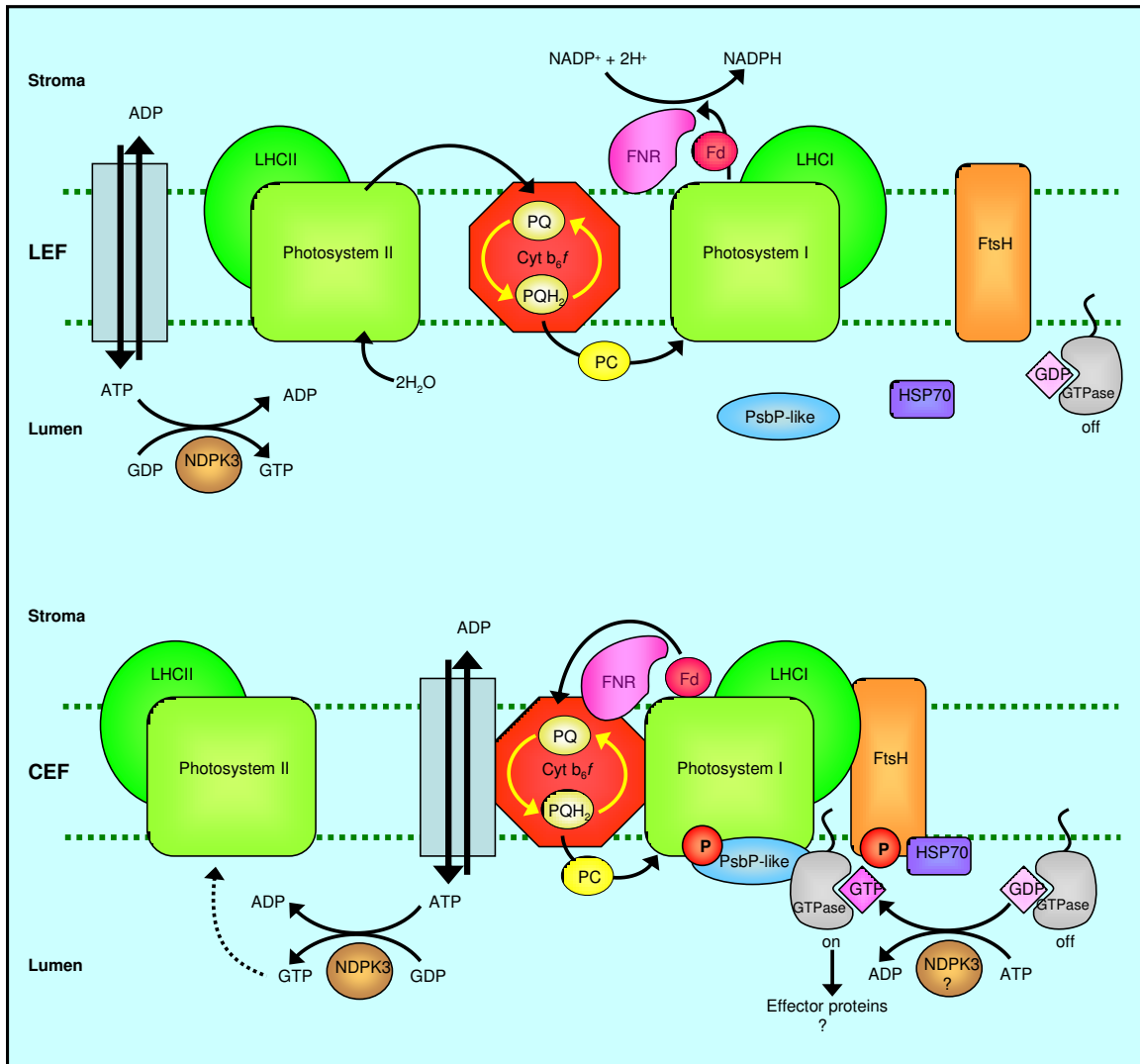


Figure 5.2: A hypothetical model of linear electron flow (top) and the PSI-Cyt b_6/f supercomplex (bottom) involved in cyclic electron flow in the psychrophilic *Chlamydomonas* sp. UWO 241.

previously been identified to function as chaperones or assembly proteins and are therefore, likely involved in maintaining the stability of this supercomplex. Thus, phosphorylation of a PsbP-like protein may subsequently activate a GTPase together with its effector proteins to ultimately assemble the structure of the PSI-Cyt *b_{6/f}* supercomplex and potentially signal other GTPase-dependent events in the lumen.

Conversely, during conditions when ATP demand is reduced (i.e. low salt, low light), dephosphorylated PsbP-like proteins may dissociate from PSI and subsequently localize to the thylakoid lumen. Decreased PsbP-like protein interaction with GTPase may result in the inactive GTPase-GDP form and favour disassembly of the PSI-Cyt *b_{6/f}* supercomplex, resulting in lower levels of CEF.

In addition, previous studies have demonstrated that a hypersaline environment can result in NaCl-induced phosphorylation of several thylakoid membrane proteins by activating the corresponding kinase (Liu and Shen 2004). Therefore, under conditions of high-salt, increased levels of phosphorylated PSI-Cyt *b_{6/f}* supercomplex subunits could further enhance CEF in UWO241.

The chloroplast ATP/ADP transporter functions to supply ATP to the lumen in exchange for ADP, which can subsequently be converted to GTP. It has been demonstrated that luminal GTP enhances D1 degradation by altering the proteolytic system (Spetea et al. 2000). Therefore, enhanced D1 photoinhibition and repair observed in UWO241 at low temperatures may be associated with increased levels of luminal GTP resulting from higher rates of CEF, in addition to increased adenylate pools.

5.2 Future directions

Phosphorylation of thylakoid proteins affects both the structure and function of photosynthetic membranes. Identification of phosphorylated proteins has been primarily achieved by immunodetection of thylakoid membrane proteins with specific antibodies. Nearly all of the phosphorylation sites have been identified by direct sequencing of complex phosphopeptide mixtures obtained through enzymatic shaving” of surface-exposed domains of thylakoid membrane proteins, without prior isolation of proteins or

their respective complexes (Vener 2008). This has resulted in a list of known phosphoproteins, which consists almost entirely of thylakoid membrane proteins. Thus, our knowledge of phosphorylated of membrane-associated proteins, as well as soluble proteins in the stroma/lumen is very limited. Future studies should be focused on identification of these phosphoproteins, as they likely play an important role in the structure and function of electron transport.

A recent study compared phosphorylation profiles of mesophyll and bundle sheath cells in *Zea mays* (Fristedt et al. 2012). Interestingly, bundle sheath cells, which primarily perform CEF, exhibited reduced phosphorylation of PSII-associated proteins, concomitant with an increase in phosphorylation of an unidentified, 15 kDa protein (Fristedt et al. 2012). Future studies should focus on the identification of the 15 kDa protein, as it may play a role in the regulation of CEF of higher plants.

The Antarctic psychrophile, *Chlamydomonas sp.* UWO241 exhibits a unique phosphorylation pattern that reflects differences in thylakoid membrane function. Phosphorylation associated with the PSI-Cyt b_6/f supercomplex results from increased cyclic electron transport (CEF) rates, while a reduction of phosphorylation associated with state transitions reflects decreased connectivity and linear electron flow between PSII and PSI. It would be interesting to examine whether an increased CEF/LEF ratio, and thus, an altered phosphorylation profile, is a common trait among cold-adapted photoautotrophs.

5.3 Conclusions

Relatively little is known about cold-adapted microorganisms that dominate the large, low-temperature portion of the Earth, in particular, the psychrophilic primary producers that depend on photoautotrophic metabolism. While UWO241 exhibits some typical cold adapted characteristics with respect to cell morphology, individual proteins and thylakoid membrane lipids and fatty acids, this psychrophile has revealed some unique photosynthetic features. The major distinguishing feature between UWO241 and mesophilic green algae is its inability to undergo state transitions. This appears to be due to be an unusual organization of the electron transport chain. Compared to similar green

algae from temperate environments, UWO241 exhibits a greater dependence on CEF which appears to be governed by the phosphorylation status of a PSI-Cyt b_6/f supercomplex. The novel protein phosphorylation of specific subunits of this supercomplex as well as the salt concentration appear to control the stability and function of this PSI-Cyt b_6/f supercomplex. Therefore, just as state transitions balance the excitation energy between PSII and PSI when these photosystems operate in concert with each other, CEF may play a prominent role in regulating energy distribution between PSII and PSI in UWO241.

With over two decades of research, *Chlamydomonas sp.* UWO241 is one of the most studied psychrophilic phytoplankton to date and can be considered the model psychrophilic photoautotroph. Consequently, we suggest that *Chlamydomonas sp.* UWO241 is an excellent candidate as the model system for the study of psychrophily and adaptation to low temperature in eukaryotic photoautotrophs. Given the recent publication of the genome sequence for *Chlamydomonas reinhardtii* (Merchant et al. 2007), comparison with genome sequence of UWO241 represents an exceptional scientific opportunity to elucidate the molecular basis of psychrophily and adaptation to low temperature in *Chlamydomonas*.

5.4 References

- Adam Z.** (2001) Chloroplast proteases and their role in photosynthetic regulation. In: Aro EM, Andersson B, Eds. *Advances in Photosynthesis and Respiration*. Dordrecht, Kluwer, pp. 265-276
- Bailey S, Horton P, Walters RG.** (2004) Acclimation of *Arabidopsis thaliana* to the light environment: the relationship between photosynthetic function and chloroplast composition. *Planta* **218**:793-802
- Baker RP, Harreman MT, Eccleston JF, Corbett AH, Stewart M.** (2001) Interaction between Ran and Mog1 is required for efficient nuclear protein import. *J Biol Chem* **276**:41255-62
- Fristedt R, Wasileska W, Romanowska E, Vener AV.** (2012) Differential phosphorylation of thylakoid proteins in mesophyll and bundle sheath chloroplasts from maize plants grown under low or high light. *Proteomics* **12**(18):2852-61

- Grieco M, Tikkanen M, Paakkanen V, Kangasjarvi S, Aro EM.** (2012) Steady-State Phosphorylation of Light-Harvesting Complex II Proteins Preserves Photosystem I under Fluctuating White Light. *Plant Physiol* **160**(4):1896-1910
- Ifuku K, Nakatsu T, Kato H, Sato F.** (2004) Crystal structure of the PsbP protein of photosystem II from *Nicotiana tabacum*. *EMBO Rep* **5**:362-7
- Kieselbach T, Bystedt M, Hynds P, Robinson C, Schröder WP.** (2000) A peroxidase homologue and novel plastocyanin located by proteomics to the *Arabidopsis* chloroplast thylakoid lumen. *FEBS Lett* **480**:271-6
- Leipe DD, Wolf YI, Koonin EV, Aravind L.** (2002) Classification and evolution of P-loop GTPases and related ATPases. *J Mol Biol* **317**:41-72
- Liu XD, Shen YG.** (2004) NaCl-induced phosphorylation of light harvesting chlorophyll *a/b* proteins in thylakoid membranes from the halotolerant green alga, *Dunaliella salina*. *FEBS Lett* **569**:337-40
- Lundin B, Nurmi M, Rojas-Stuetz M, Aro EM, Adamska I, Spetea C.** (2008) Towards understanding the functional difference between the two PsbO isoforms in *Arabidopsis thaliana* – insights from phenotypic analyses of psbo knockout mutants. *Photosyn Res* **98**:405-14
- Lundin B, Thuswaldner S, Shutova T, Eshaghi S, Samuelsson G, Barber J, Andersson B, Spetea C.** (2007) Subsequent events to GTP binding by the plant PsbO protein: structural changes, GTP hydrolysis and dissociation from the photosystem II complex. *Biochim Biophys Acta.* **1767**:500-8
- Merchant SS, Prochnik SE, Vallon O, Harris EH, Karpowicz SJ, Witman GB, et al.** (2007) The *Chlamydomonas* genome reveals the evolution of key animal and plant functions. *Science* **318**:245-50
- Peltier JB, Emanuelsson O, Kalume DE, Ytterberg J, Friso G, Rudella A, Liberles DA, Söderberg L, Roepstorff P, von Heijne G, van Wijk KJ.** (2002) Central functions of the lumenal and peripheral thylakoid proteome of *Arabidopsis* determined by experimentation and genome-wide prediction. *Plant Cell* **14**:211-36
- Schlicher T, Soll J.** (1996) Molecular chaperones are present in the thylakoid lumen of pea chloroplasts. *FEBS Lett* **379**:302-04
- Spetea C, Hundal T, Lundin B, Heddad M, Adamska I, Andersson B.** (2004) Multiple evidence for nucleotide metabolism in the chloroplast thylakoid lumen. *Proc Natl Acad Sci USA* **101**:1409-14
- Spetea C, Keren N, Hundal T, Doan JM, Ohad I, Andersson B.** (2000) GTP enhances the degradation of the photosystem II D1 protein irrespective of its conformational heterogeneity at the Q(B) site. *J Biol Chem* **275**:7205-11
- Thuswaldner S, Lagerstedt JO, Rojas-Stütz M, Bouhidel K, Der C, Leborgne-Castel N, Mishra A, Marty F, Schoefs B, Adamska I, Persson BL, Spetea C.** (2007) Identification, expression, and functional analyses of a thylakoid ATP/ADP carrier from *Arabidopsis*. *J Biol Chem* **282**:8848-59

- Vener A.** (2008) Phosphorylation of thylakoid proteins. In Demmig-Adams, B., Adams, W., & Mattoo, A. [Eds] Photoprotection photoinhibition gene regulation and environment. Springer, Dordrecht, pp.108.
- Yang Z.** (2002) Small GTPases versatile signaling switches in plants. *Plant Cell* **14**:S375-S388
- Yin L, Lundin B, Bertrand M, Nurmi M, Solymosi K, Kangasjärvi S, Aro EM, Schoefs B, Spetea C.** (2010) Role of thylakoid ATP/ADP carrier in photoinhibition and photoprotection of photosystem II in *Arabidopsis*. *Plant Physiol* **153**:666-77

Curriculum Vitae

Name: Beth Szyszka-Mroz

Post-secondary Education and Degrees: Western University
London, Ontario, Canada
2000-2004 Honours B.Sc.

Western University
London, Ontario, Canada
2005-2007 M.Sc.

Western University
London, Ontario, Canada
2008-2014 Ph.D.

Honours and Awards: Natural Sciences and Engineering Research Council Scholarship (NSERC)
2009-2013

Western Graduate Research Scholarship (WGRS)
2008-2011

Faculty of Science Graduate Student Teaching Award
Western University
2006

Related Work Experience Teaching Assistant
Western University
2005-2010

Publications:

Szyszka-Mroz B, Ivanov AG, Hüner NPA. (In press) Adaptation to low temperature in a photoautotrophic Antarctic psychrophile, *Chlamydomonas sp.* UWO 241. In: Structures, Mechanisms, and Applications of Photosynthetic Apparatus. Eds: Allakhverdiev S, Najafpour MM, Hou HJ. Bentham Science Publishers

Hüner NPA, Bode R, Dahal K, Busch FA, Possmayer M, Szyszka B, Rosso D, Ensminger I, Krol M, Ivanov AG, Maxwell DP. (2013) Shedding some light on cold acclimation, cold adaptation and phenotypic plasticity. *Botany* 91: 127-36

Chung DJ, Szyszka B, Brown JC, Hüner NPA, Staples JF. (2013) Changes in the mitochondrial phosphoproteome during mammalian hibernation. *Physiol Genomics* 45(10): 389-99

Szyszka B, Ivanov AG, Hüner NPA. (2007) Psychrophily is associated with differential energy partitioning, photosystem stoichiometry and polypeptide phosphorylation in *Chlamydomonas raudensis*. *Biochim Biophys Acta* 1767(6): 789-800